

**Mathematical Models of the Gene  
Regulatory Networks Underlying  
Mesendoderm Formation in Amphibians.**

Laura Brown, MSc.

Thesis submitted to The University of Nottingham  
for the degree of Doctor of Philosophy

November 2012

# Abstract

An early event in embryo development is the formation of mesoderm, endoderm and ectoderm, known as the primary germ layers. The gene regulatory network (GRN) consisting of the regulatory mechanisms underlying the formation of mesoderm and endoderm (the mesendoderm GRN) has been extensively studied both experimentally and using mathematical models. The *Xenopus* GRN is complex, with much of this complexity due to large numbers of Mix and Nodal genes. Mice and humans have only single Mix and Nodal genes, meaning that the *Xenopus* GRN is overly complex compared with higher vertebrates. Urodele amphibians, for example the axolotl, have single Mix and Nodal genes required for mesoderm and endoderm formation giving a model organism for the study of a simplified mesendoderm GRN.

We study the axolotl mesendoderm GRN by developing mathematical models that encompass the time evolution of transcription factors in a cell. A detailed investigation reveals that, despite differences in the axolotl mesendoderm GRN compared with the *Xenopus*, the model can qualitatively reproduce experimental observations. We obtain experimental data to estimate model parameters using a computational algorithm, then test the behaviour of the resulting mathematical model using independent data. We extend mathematical models of the *Xenopus* mesendoderm GRN to include transcription factors involved in patterning the DV axis. An investigation of this model shows that it can account for the formation of mesoderm, endoderm and anterior mesendoderm forming in regions of the embryo consistent with experimental data. In the final section of this thesis, we extend a multicellular model of the *Xenopus* mesendoderm GRN into a grid of cells.

# Acknowledgements

Thank you to my supervisors, Matt Loose and John King, for all their support and advice during this research. I appreciate all the help that others have given me along the way, members of Matt's lab past and present, especially Yi-Hsien Chen for all his time and patience in teaching me laboratory skills, starting from the basics of how to use a pipette! Also thank you to Jodie Chatfield, for providing help and support in the lab, and Andrew Johnson (AJ), for providing embryos and motivation in the lab.

To those who have helped me relax outside of my PhD work, in particular the University of Nottingham Real Ale Society and Nottingham CAMRA, thanks for giving me the opportunity to have a drink in great company.

A special thank you to Christopher Hall for being a wonderful boyfriend and for putting up with me complaining about my PhD thesis.

Finally, and most importantly, I'd like to thank my family for all their love and support during my studies. To Mum, Mamma and Sarah: thank you for putting up with me while I worked on this thesis. Also, to family members who are no longer with us, especially my Dad, I hope you would be proud of everything I have done.

# Contents

<b>1</b>	<b>Introduction</b>	<b>1</b>
1.1	Model organisms in developmental biology . . . . .	1
1.2	Stages of embryo development . . . . .	2
1.3	The primary germ layers . . . . .	3
1.4	A comparison of early development in <i>Xenopus laevis</i> and axolotl . . . . .	4
1.5	Regulation of gene expression . . . . .	6
1.5.1	Experimental techniques used in developmental biology . . . . .	6
1.5.2	Mesendoderm gene regulatory networks . . . . .	9
1.6	Morphogens in embryo development . . . . .	10
1.6.1	The TGF- $\beta$ signalling pathway . . . . .	13
1.6.2	Regulation of <i>Xenopus</i> Nodal genes . . . . .	13
1.6.3	FGF signalling . . . . .	14
1.7	Mesendodermal genes in <i>Xenopus</i> . . . . .	15
1.7.1	VegT and $\beta$ -catenin . . . . .	15
1.7.2	Mix.1 and Brachyury . . . . .	16
1.7.3	Goosecoid, Siamois and Lim1 . . . . .	16
1.8	Comparison of mesendoderm formation in axolotl and <i>Xenopus</i> . . . . .	17
1.9	Dorsal-ventral patterning in <i>Xenopus</i> . . . . .	19
1.9.1	BMP signalling . . . . .	20
1.9.2	Chordin . . . . .	20
1.9.3	Vent1/2 and Goosecoid . . . . .	21
1.10	Mathematical models of gene regulatory networks . . . . .	22
1.10.1	Overview of modelling frameworks . . . . .	23
1.11	Nonlinear ODEs of GRNs . . . . .	24

## CONTENTS

1.12	Multicellular models of GRNs . . . . .	26
1.12.1	Continuous reaction-diffusion systems . . . . .	26
1.12.2	Discrete reaction-diffusion systems . . . . .	27
1.13	Quantitative mathematical models . . . . .	28
1.13.1	Types of data used . . . . .	29
1.13.2	Parameter estimation methods . . . . .	30
1.13.3	The Genetic Algorithm . . . . .	31
1.14	Objectives . . . . .	31
1.15	Thesis overview . . . . .	32
1.15.1	Chapter 2 . . . . .	32
1.15.2	Chapter 3 . . . . .	33
1.15.3	Chapter 4 . . . . .	33
1.15.4	Chapter 5 . . . . .	33
1.15.5	Chapter 6 . . . . .	34
<b>2</b>	<b>Materials and Methods</b>	<b>35</b>
2.1	Solutions and buffers . . . . .	35
2.2	Treatment and preparation of embryos . . . . .	35
2.2.1	Micro-injection . . . . .	35
2.2.2	Axolotl embryos . . . . .	35
2.2.3	Microscopy and photography . . . . .	36
2.2.4	Morpholinos . . . . .	36
2.3	Extraction of RNA . . . . .	36
2.3.1	RNA extraction . . . . .	36
2.3.2	DNase1 treatment of RNA . . . . .	37
2.4	Analysis of gene expression by Reverse Transcriptase (RT-PCR) . . . . .	37
2.4.1	RT-PCR . . . . .	37
2.4.2	cDNA synthesis . . . . .	37
2.4.3	Real-time qPCR . . . . .	38
2.4.4	Primers and probes . . . . .	38
2.4.5	Data analysis . . . . .	38
2.5	Genome walking . . . . .	39
2.5.1	Primary PCR . . . . .	39

## CONTENTS

2.5.2	Secondary PCR . . . . .	39
2.5.3	Agarose gel electrophoresis . . . . .	39
2.5.4	Purification of DNA from agarose gels . . . . .	40
2.5.5	Ligation of DNA fragments . . . . .	40
2.5.6	Transformations . . . . .	40
2.5.7	DNA sequencing . . . . .	40
2.5.8	Sequence analysis and comparisons . . . . .	40
2.6	Developmental series . . . . .	41
<b>3</b>	<b>Single-cell Models of Mesendoderm Specification in <i>Xenopus</i> and Axolotl</b>	<b>42</b>
3.1	Introduction . . . . .	42
3.2	Mesoderm and endoderm formation in <i>Xenopus</i> . . . . .	42
3.2.1	Mathematical models of the simplified <i>Xenopus</i> mesendoderm GRN . . . . .	43
3.3	Mesendoderm formation in axolotl . . . . .	47
3.4	Model formulation . . . . .	47
3.4.1	Modelling the regulation of mesodermal and endodermal genes in axolotl . . . . .	48
3.4.2	Summary of model equations . . . . .	51
3.5	Nondimensionalisation . . . . .	52
3.6	The axolotl <i>in vitro</i> model . . . . .	54
3.6.1	Steady-state analysis . . . . .	54
3.6.2	Time dependent solutions . . . . .	58
3.6.3	Conclusions . . . . .	59
3.7	The axolotl <i>in vivo</i> model . . . . .	62
3.7.1	Steady-state equations . . . . .	63
3.7.2	Time-dependent solutions . . . . .	64
3.8	Nodal regulation in a simplified <i>Xenopus</i> mesendoderm GRN . . . . .	64
3.8.1	Biological background . . . . .	64
3.8.2	Nondimensional governing equations . . . . .	66
3.8.3	Solutions to the modified <i>Xenopus in vivo</i> model . . . . .	67
3.9	Discussion . . . . .	69
<b>4</b>	<b>Parameter Estimation in Single-cell Models of Mesendoderm Specification in Axolotl</b>	<b>73</b>
4.1	Quantitative gene expression data . . . . .	74

CONTENTS

4.1.1	The induction of mesendodermal genes in axolotl in response to <i>Activin</i> , <i>Nodal1</i> and <i>Nodal2</i> . . . . .	75
4.2	Parameter estimation in models of the axolotl mesendoderm GRN . . . . .	79
4.2.1	Mathematical model . . . . .	80
4.2.2	Preliminaries . . . . .	81
4.2.3	Parameter estimation results . . . . .	83
4.2.4	Testing model predictions . . . . .	91
4.2.5	Further parameter estimation results . . . . .	92
4.2.6	Parameter sensitivity . . . . .	95
4.3	Can a model with the <i>Xenopus</i> network topology reproduce the gene expression patterns from axolotl? . . . . .	97
4.4	Comparison of optimal parameters for the <i>Xenopus</i> and axolotl models . . . . .	102
4.5	Discussion . . . . .	104
<b>5</b>	<b>Dorsal-Ventral Patterning in a Single-cell Model of Mesendoderm Specification in <i>Xenopus</i></b> . . . . .	<b>107</b>
5.1	Introduction . . . . .	107
5.1.1	Mathematical models of DV patterning . . . . .	108
5.2	Simple ‘DV only’ model in a single cell . . . . .	112
5.2.1	Modelling the regulation of DV patterning . . . . .	112
5.2.2	Model equations . . . . .	113
5.2.3	Non-dimensional model . . . . .	114
5.2.4	Steady-state analysis . . . . .	115
5.2.5	Time-dependent solutions . . . . .	117
5.2.6	Summary . . . . .	120
5.3	A ‘DV and mesendoderm’ model in a single cell . . . . .	121
5.3.1	Model formulation . . . . .	122
5.3.2	Model equations . . . . .	122
5.3.3	Non-dimensional model . . . . .	123
5.3.4	Steady states . . . . .	125
5.3.5	Time-dependent solutions . . . . .	128
5.3.6	2D plots of the single cell model . . . . .	133
5.3.7	Summary . . . . .	134
5.4	Discussion . . . . .	134

<b>6</b>	<b>Multicellular Models of Mesendoderm Specification</b>	<b>138</b>
6.1	A multicellular model of the <i>Xenopus</i> mesendoderm GRN . . . . .	138
6.1.1	A model of Nodal signalling . . . . .	139
6.1.2	The mesendoderm GRN downstream of Nodal . . . . .	141
6.2	Multicellular models of the axolotl mesendoderm GRN . . . . .	143
6.2.1	Experimental observations . . . . .	143
6.2.2	Governing equations . . . . .	144
6.2.3	Non-dimensionalisation and parameter sizes . . . . .	146
6.2.4	Numerical solutions . . . . .	148
6.2.5	Discussion . . . . .	150
6.3	The cloning and expression of axolotl Antivin . . . . .	158
6.3.1	The axolotl <i>Antivin</i> sequence . . . . .	158
6.3.2	Expression of <i>Antivin</i> . . . . .	161
6.3.3	<i>Antivin</i> expression in <i>Nodal1</i> and <i>Antivin</i> injected animal caps. . . . .	162
6.4	Mathematical models of mesendoderm formation in a grid of cells . . . . .	162
6.4.1	Motivation . . . . .	162
6.5	The <i>Xenopus</i> mesendoderm GRN in a two-dimensional grid of cells . . . . .	163
6.6	The regulation of Nodal by VegT and $\beta$ -catenin . . . . .	165
6.6.1	Numerical solutions . . . . .	168
6.6.2	Summary . . . . .	173
6.7	A multicellular model of the <i>Xenopus</i> mesendoderm GRN . . . . .	176
6.7.1	Numerical solutions . . . . .	176
6.8	A multicellular model of the axolotl mesendoderm GRN . . . . .	183
6.8.1	Numerical solutions . . . . .	183
6.9	Discussion . . . . .	184
<b>7</b>	<b>Discussion</b>	<b>187</b>
7.1	Single cell models of the axolotl mesendoderm GRN . . . . .	187
7.2	Multicellular models of the axolotl mesendoderm GRN . . . . .	188
7.3	Modifications to the mathematical models of mesendoderm formation in <i>Xenopus</i> . . . . .	189
7.4	Comparisons of mesendoderm formation in axolotl and <i>Xenopus</i> . . . . .	190
7.5	Conclusion . . . . .	192
	<b>References</b>	<b>193</b>



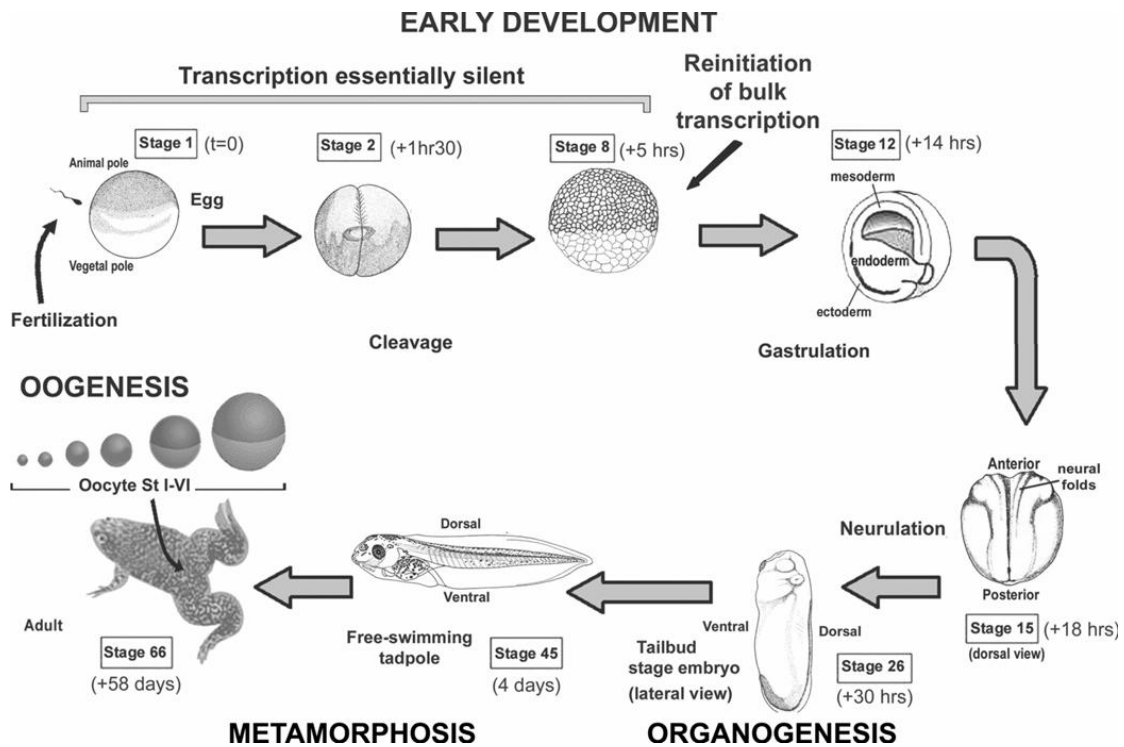
# Introduction

The development of an embryo from a single cell to a multicellular adult organism, with an established body plan consisting of numerous cell types, is a highly regulated process [41]. The field of developmental biology is concerned with uncovering the mechanisms by which this occurs. The key concepts in embryo development are **growth**, during which cells are required to both divide into the number of cells needed to form an adult organism and also increase in size, **differentiation**, where these cells become specialised for particular functions, and **morphogenesis**, where these cells organise themselves into functional structures [41]. An early event in the differentiation of cells in triploblastic embryos is the formation of the three primary germ layers; the ectoderm, mesoderm and endoderm. Each of these layers forms in different regions of the developing embryo and gives rise to different cell types. In this thesis, mathematical models of the genetic mechanisms underlying the formation of mesoderm and endoderm are explored in two model organisms, *Xenopus laevis*, an anuran amphibian, and *Ambystoma mexicanum*, a urodele amphibian.

## 1.1 Model organisms in developmental biology

The early stages of development in mammalian embryos are difficult to study since the embryo grows within the mother's body. Amphibian embryos have been historically used to study embryo development because they develop externally, meaning that they can easily be manipulated experimentally. Other features which make amphibians an excellent model system include readily available embryos and good adaptation to laboratory conditions [12, 13, 109].

Amphibians can be divided into three orders: anura (frogs and toads), urodela (salamanders and newts) and gymnophiona (limbless amphibians). In this thesis, we focus on two amphibians used as model systems in embryo development: *Ambystoma mexicanum*, a urodele amphibian, which is more commonly known as the axolotl, and *Xenopus laevis*, the African clawed frog, which is an anuran amphibian. Historically, urodeles were more commonly used as model organisms than anurans. One reason for this is that urodele embryos are larger than anuran embryos (axolotl = 2.5mm, *Xenopus*=1.5mm), making experimental intervention eas-



**Figure 1.1:** Diagram of the major events in embryo development for *Xenopus laevis*. Figure taken from [93].

ier in urodeles [106]. In 1924, Hans Spemann and Hilde Mangold used urodele embryos to demonstrate that cells transplanted from the dorsal lip into a host embryo act as an ‘organizer’, causing the surrounding cells to change fate [29]. In 1969, Nieuwkoop used the axolotl as a model organism, demonstrating that mesoderm can be induced in animal cap explants (which usually become ectoderm) by placing them on the vegetal hemisphere (which usually becomes endoderm) [105]. *Xenopus laevis* first emerged as a model organism in the 1950s. Breeding can be initiated by injecting a female *Xenopus laevis* with gonadal hormone, meaning *Xenopus* embryos are readily available throughout the year. Axolotls can be induced to breed by reducing the temperature of the aquarium [106]; however, fertilization relies on natural mating, meaning that fertilized axolotl embryos are less readily available than *Xenopus laevis* embryos. Due to the ease of obtaining embryos, *Xenopus laevis* has become a popular model organism in molecular and genetic analysis [106].

## 1.2 Stages of embryo development

An embryo progresses through a number of anatomically defined stages to become a fully developed adult organism. A summary of the main events during embryo development for *Xenopus laevis* is given in figure 1.1 and table 1.1. The single-celled fertilized egg undergoes a number of cleavages, whereby the embryo divides into a number of smaller cells (known as blastomeres) without changing its total mass. After 12 cycles of cleavage, the rate of cell

Stage	Hours from fertilization	key event
1	0	fertilized egg
2	1.5	first cleavage
8	5	zygotic transcription begins
9	7	
10	9	gastrulation begins (mesendoderm detected)
10.5	11	
11	12	mesoderm and endoderm have differentiated
15	18	neurulation
26	30	organogenesis

**Table 1.1:** A summary of key developmental stages of *Xenopus laevis* development.

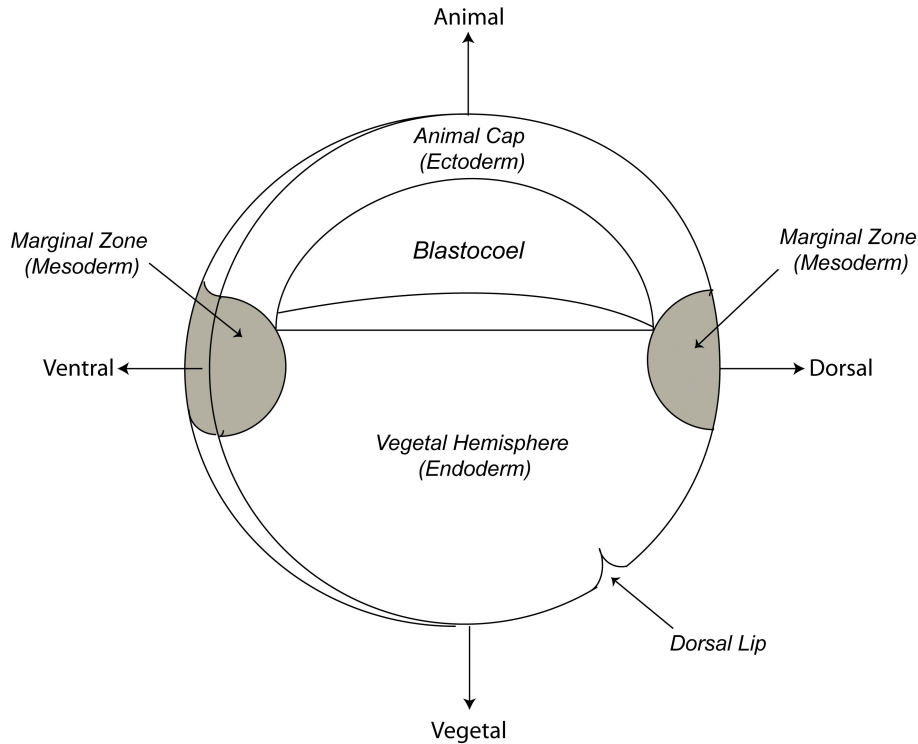
division slows and an event known as the mid-blastula transition (MBT) occurs. At the MBT zygotic transcription commences, whereby the embryo begins to transcribe its own genome [3, 51]. Prior to this the embryo relies on maternal mRNA and proteins laid down by the mother in the oocyte [51]. At stage 10, a series of morphogenic cell movements known as gastrulation begins, where cells on the outer layer of the embryo become internalised. During gastrulation the basic body plan is established and the three primary germ layers form [52, 87].

Later stages of embryo development include processes such as neurulation, where the nervous system of the organism is formed, and organogenesis, where the organs are formed. By the tadpole stages, the full body plan has been laid out and the three main body axes have been fully established: anteroposterior (running from head to tail), dorsoventral (from the back to the belly) and mediolateral (from the midline to the left or the right) [3].

### 1.3 The primary germ layers

The three germ layers (ectoderm, mesoderm and endoderm) give rise to different cell types, form in different regions of the developing embryo, and can be identified by the genes which they express (more details on the expression of these genes given in section 1.7). The ectoderm, the outer germ layer, gives rise to the epidermis and the nervous system and forms in the animal cap of the embryo (see figure 1.2). The mesoderm, the middle germ layer, gives rise to bone, muscle, heart, blood and connective tissues [41]. Initially, mesoderm forms in the marginal zone of the embryo. Key genes expressed in the mesoderm include *Brachyury*, *Gooseoid* and *eFGF*. Mesoderm (as marked by the expression of *Brachyury*) can be detected by stage 10 [85]. The endoderm, the inner germ layer, gives rise to the epithelia of the digestive and respiratory systems, and organs such as the liver, pancreas and the lungs. Endoderm forms in the vegetal pole of the embryo. Key genes expressed in the endoderm include *Mix.1*, *Mixer* and *Sox17* [56, 60, 121]. Endoderm (as marked by the expression of *Mix.1*) can be detected by stage 10 [85]. In this thesis, we will also refer to a region of the developing embryo known as the anterior mesendoderm. The anterior mesendoderm is situated on the dorsal side of the embryo and induces head structures. *Mix.1* and *Gooseoid* are coexpressed in anterior mesendoderm in stage 10 *Xenopus* embryos, and the knockdown of *Mix.1* and *Gooseoid* causes dorsoanterior defects, such as reduced head size [82].

Mesendoderm is used as a collective term to describe the mesoderm and endoderm. An al-



**Figure 1.2:** Sketch of a cross section of a stage 10 embryo. The animal pole is at the top of the embryo, and the vegetal pole is at the bottom. The marginal zone runs around the equator of the embryo. The blastocoel is an empty cavity located in the centre of the animal hemisphere. At stage 10 the dorsal lip forms on the dorsal side of the vegetal hemisphere. Cells in the animal cap are the presumptive ectoderm, and cells in the marginal zone and vegetal hemisphere are the presumptive mesoderm and endoderm, respectively.

ternative use of the term is to name a group of bipotent cells which develop to become either mesoderm or endoderm. Evidence from zebrafish, *Caenorhabditis elegans* (a nematode worm) and sea urchin indicate that a such a bipotent layer of cells exists [119]. In *Xenopus* overlapping expression domains of *Mix.1* and *Brachyury* (which mark mesoderm and endoderm, respectively) [85] can be taken as evidence that a mesendodermal population of cells exists. In this thesis we mainly use the word mesendoderm as a collective term to describe the mesoderm and endoderm. Note that studies suggest that mesendoderm may not exist in the axolotl [139].

## 1.4 A comparison of early development in *Xenopus laevis* and axolotl

In this section, we review differences in the early stages of development in anurans and urodels, as described in [64, 68], focusing on differences between axolotl and *Xenopus laevis*. In particular, we state which features are inherited from a common ancestor (an ‘ancestral trait’) and which traits have evolved.

**Pluripotency Network:** Pluripotency is the ability of a cell to form any cell type in an organism.

Given that pluripotency is an essential component of development, an assumption would be that the mechanisms governing pluripotency are conserved in chordates. However, this is not the case. In mammals the transcription factors Oct4 and Nanog are key genes in the pluripotency network which regulates pluripotency. Orthologs of these genes are also found in the axolotl genome, suggesting that pluripotency is conserved in mammals from axolotls [31, 65]. However, the pluripotency network found in mammals is not conserved in *Xenopus*, where Nanog has been deleted. This deletion is thought to have occurred after anurans and urodeles diverged from their last common ancestor [31, 65].

**Primordial Germ Cells:** Primordial germ cells (PGCs) are the cells which give rise to gametes. In vertebrates, there are two mechanisms which can give rise to these cells. In *Xenopus laevis* PGCs are predetermined by inheritance of the germ plasm and in axolotl, PGCs are induced by regulative signals [64]. Studies have shown that induced PGCs is an ancestral trait, with primitive organisms having induced PGCs [64].

**Gastrulation and the position of mesoderm cells:** During the process of gastrulation, mesodermal and endodermal cells move to the inside of the embryo, while ectodermal cells spread over the outside surface [41]. Differences in the movements associated with gastrulation arise due to differences in the locations of cells prior to gastrulation. Amphibians have a variation in the epithelial composition of the epiblast between species [130]. In anurans, the mesoderm epiblast is multilayered (stratified) with a distinct superficial epithelial layer over several layers of deep cells, and no interdigitation between the layers. In urodeles, the mesodermal epiblast becomes pseudostratified (single layered) with superficial cells which interdigitate with deep cells (see figure 1.3A,E). These differences in epithelial composition contribute to a difference in the cells from which mesoderm originate in *Xenopus* and axolotl. In *Xenopus*, mesoderm originates from deep cells underlying the surface epithelium and in axolotl the cells of the surface epithelium, along with the deep cells, contribute to mesoderm [134]. A comparative analysis suggests that the ancestral trait is the derivation of mesoderm from surface cells [64]

There are several types of cell movement associated with the internalization of the mesoderm: invagination where cells of an epithelial sheet bend inwards, involution where a sheet of cells roll inwards over an inflection point and ingression where individual cells migrate into the embryo [41, 130]. In anurans the presumptive mesoderm, in association with the supra-blastoporal endoderm, involutes around the blastoporal lip [130]. This involution occurs over the entire circumference of the blastopore and as such is referred to as an 'open blastopore' (see figure 1.3C). In urodeles, such as the axolotl, the open portion of the blastopore is restricted to the dorsal side, i.e. the blastopore is 'dorsally restricted' (see figure 1.3G). Here involution only occurs at the dorsal blastopore and ingression, via subduction, occurs ventrally and laterally [132].

In some mammals, such as humans, involution occurs at the anterior end of the primitive streak (which is homologous to the dorsal region of the blastopore in amphibians) [130]. This method of gastrulation can be described as dorsally restricted. However, in mouse and chick, the dorsally open portion of the primitive streak has been lost and cells become internalised via ingression only. This methods of gastrulation in amniotes seem to more closely resemble the

mechanisms seen in urodeles rather than anurans.

**Gene Expression Patterns:** There are also differences in gene expression profiles of early gastrula embryos in *Xenopus* and urodeles. For example, *Brachyury* is expressed in a ring shaped domain in the marginal zone at the onset of gastrulation in *Xenopus* [68]. In urodeles such as *Cynops*, *Brachyury* is not detected until the mid-gastrula stage and found in cells on the surface of the blastopore [68]. Similar to in *Cynops*, *Brachyury* expression in axolotl commences at the mid-gastrula stage [139].

**Summary:** The comparison of features of development in *Xenopus* and axolotl presented above suggests that axolotl have retained more primitive traits than *Xenopus*. Furthermore, studies of the molecular mechanisms underlying mesendoderm formation identify that the mechanisms present in axolotl are more similar to mammals than *Xenopus*. Since *Xenopus* has many derived traits, we cannot assume that features of development in *Xenopus* are the same as in higher vertebrates such as humans. However, most current genetic analyses of embryo development have been carried out in *Xenopus* and have been useful in revealing molecular mechanisms of development. In the next section, we describe how genes are expressed and regulated, give examples of experimental techniques used to investigate gene regulation and introduce the molecular mechanisms underlying mesoderm and endoderm formation as described in the mesendoderm gene regulatory network.

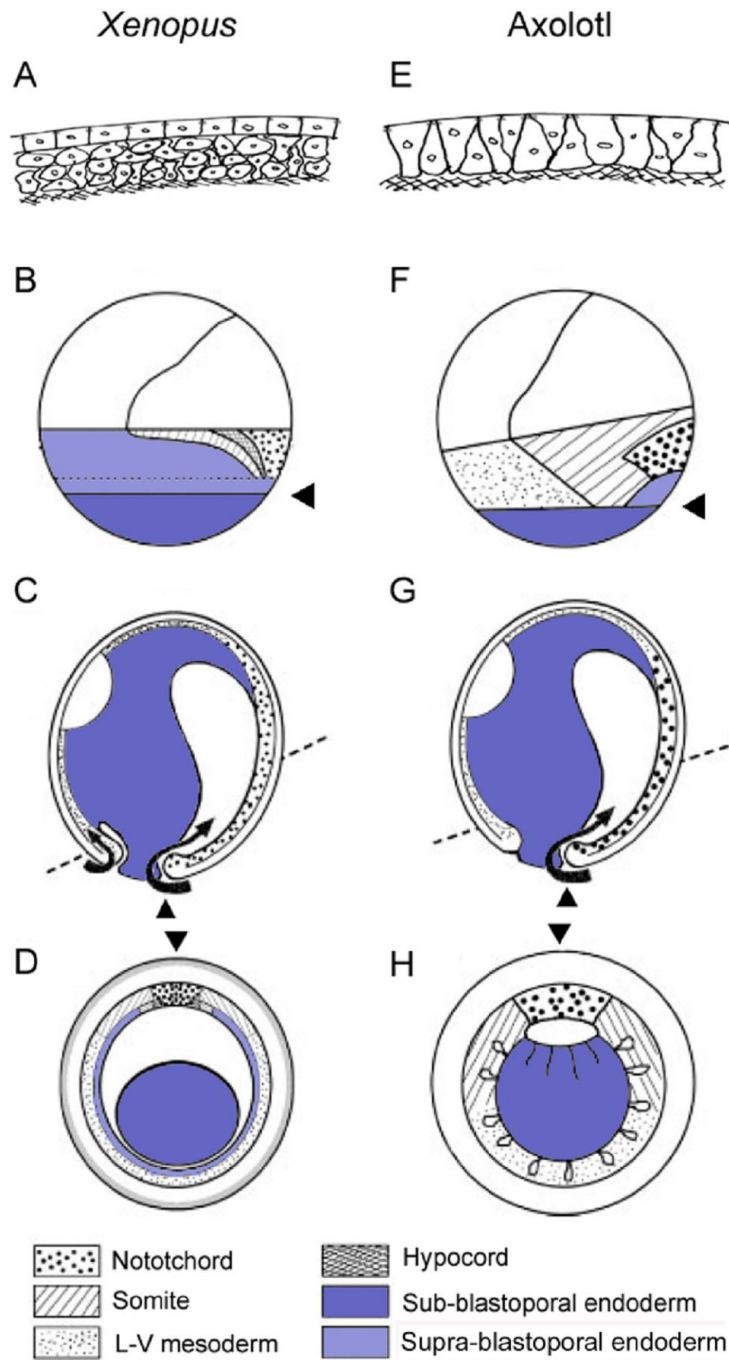
## 1.5 Regulation of gene expression

All cells of an organism contain DNA encoding every protein required by the organism. Most cells express only a subset of these proteins, with different types of cell making different proteins. The expression of genes is regulated at several levels. There are two major steps which result in the synthesis of a protein from its gene: transcription and translation (see figure 1.4A). During transcription, DNA is transcribed into RNA in the nucleus of the cell (see figure 1.4B). Once an RNA copy of the gene is produced, this can be translated into a protein. Gene expression can be regulated both at the transcription and translation levels, as well as protein modifications at the post-translational level. Proteins that bind to promoter regions of DNA and interact either to activate or to repress the transcription of a particular gene are called transcription factors. Proteins that are secreted by cells and, by activating a signalling cascade, regulate transcription in either the originating or another cell are known as signals.

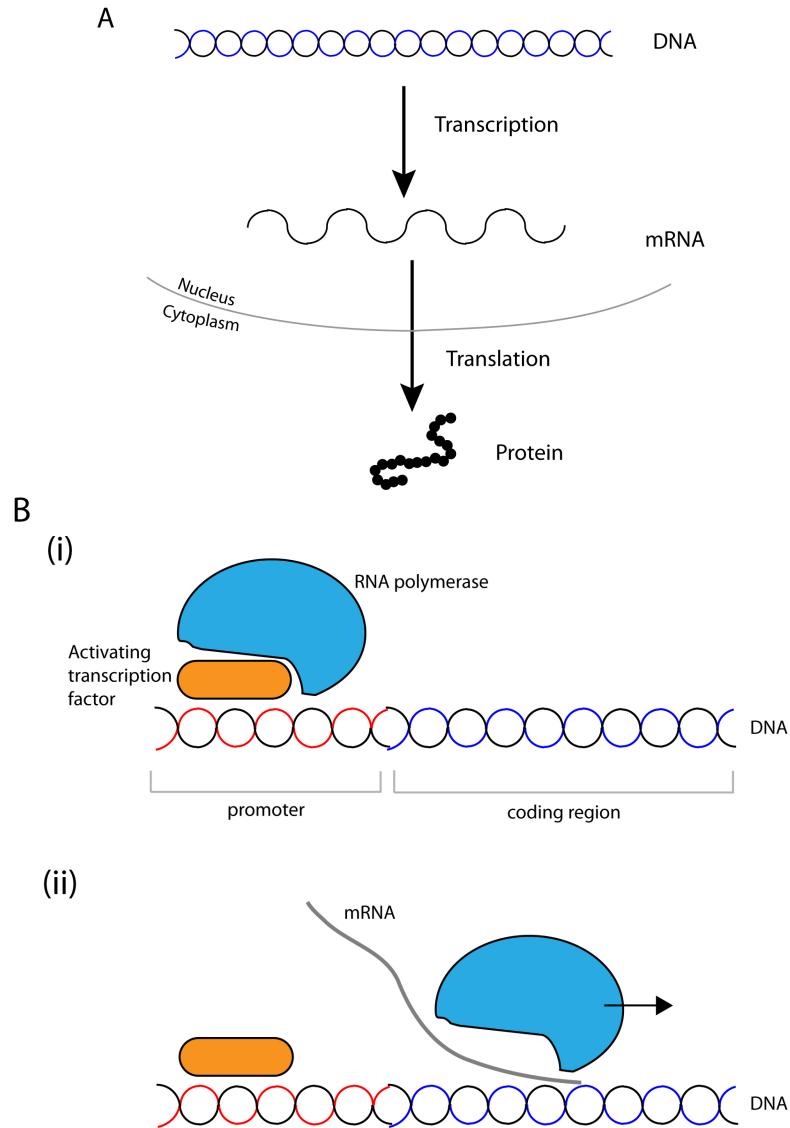
### 1.5.1 Experimental techniques used in developmental biology

Many experimental techniques are available for studying the expression and function of genes during embryo development. Here we give an overview of important techniques, with methods used to carry out experimental techniques used to obtain results in this thesis described in chapter 2.

To determine the function of a gene encoding a TF or signal and to observe the consequences of



**Figure 1.3:** A comparison of *Xenopus* (an anuran, A-D) and axolotl (a urodele, E-H) in early development. (A) *Xenopus* have a multilayered epithelium, compared with (E) the pseudostratified epithelium in axolotl. A superficial view of cell fates: (B) At the commencement of gastrulation *Xenopus* possess a smaller proportion of presumptive mesoderm (in the form of notochord precursors) than (F) axolotl whose surface mesoderm contains precursors for notochord, somite and lateral-ventral mesoderm (L-V mesoderm). (C) *Xenopus* internalize (arrows) their presumptive mesoderm by involution around the blastopore, (D) a sectional view as indicated by the dashed line in (C). (G) In axolotl, following the dorsal involution, most presumptive mesoderm ingresses laterally and ventrally, and the open portion of the blastopore is restricted to the dorsal side. (H) a sectional view as indicated by the dashed line in (G). In all figures the arrowhead marks dorsal. Figures are adapted from [130, 131]



**Figure 1.4: Gene Expression.** (A) Double stranded DNA is transcribed into a single stranded mRNA in the nucleus. The mRNA is then exported into the cytoplasm where it is translated into a protein. (B) Transcription of mRNA from DNA. (i) Transcription factors bind to the promoter of a gene to either facilitate or interfere with the assembly of a transcriptional complex comprising of transcription factors and RNA polymerase. (ii) RNA polymerase moves along the coding region of the gene, producing an mRNA copy.

gene loss on the phenotype of the organism, its spatial and temporal expression must be found, along with the affect of perturbation on downstream targets. We focus on techniques used to determine the levels of mRNA, either in a qualitative or quantitative manner. Polymerase chain reaction (PCR) is a method of cloning large quantities of a specific DNA fragment from a small amount of starting material. PCR can be used to determine if a particular gene is expressed in RNA extracted from embryos at various developmental stages. To quantify the levels of mRNA, quantitative (q)PCR, can be used to give a measure of the relative level of a gene. The regions of the embryo in which RNA transcripts are found can be determined using *in-situ*

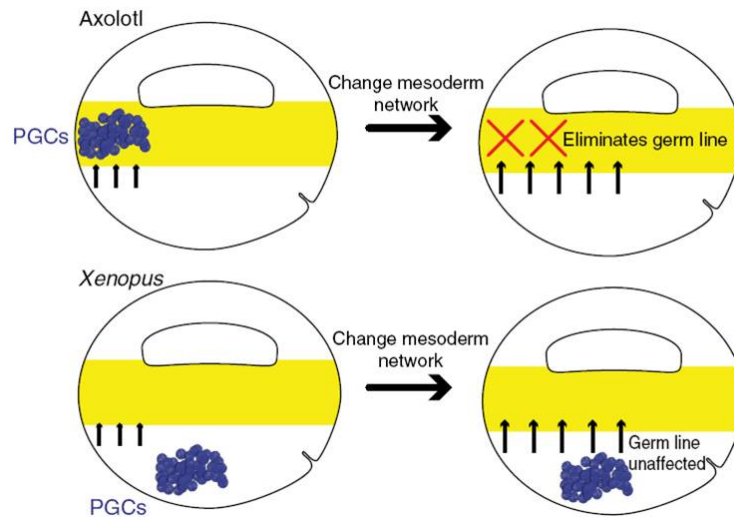


hybridisation. An anti-sense mRNA probe labeled with a dye is designed to bind to an mRNA sequence of interest to show the localisation of transcripts in whole, or sections of, embryos. A TF can act to either activate or repress the expression of downstream targets. The effects of the overexpression or knockdown of a TF show how the TF functions. If the expression of a downstream target is increased by overexpression of a TF, then the TF acts to activate the downstream gene, and if the target gene is downregulated the TF represses its target. To overexpress a gene large quantities of its mRNA can be inserted into the embryo by micro-injection, while injection of a morpholino acts to knockout the function of the gene.

## 1.5.2 Mesendoderm gene regulatory networks

The genes expressed by a cell are regulated by signals and TFs, which act either to repress or to activate the target gene. These targets may encode TFs and signals themselves, which leads to a gene regulatory network (GRN) comprising of the interactions regulating the expression of many genes. Mesendoderm specification has been extensively studied in *Xenopus laevis* by Loose and Patient [89], and also by Koide et al [75]. Figure 1.6 shows the *Xenopus laevis* mesendoderm GRN, which gives the interactions of approximately 50 transcription factors and signalling molecules. Much complexity arises in this network due to the presence of seven Mix-like genes (*Mixer*, *Mix.1-2*, *Bix.1-4*) and six Nodal-related genes (*Xnr1-6*), all of which have been shown to be functional. In addition, *Xnr5* has numerous distinct and functional copies present in the genome [140]. *Xnr3* lacks mesoderm inducing activity, and is able to induce neural tissue in animal caps, so we will not consider this any further in this thesis [50]. Other members of the Nodal family are expressed at the right time and in the correct spatial domains to be functional in mesoderm and endoderm specification [1, 66]. Mammals, such as mice and humans, possess single copies of these genes [45, 157]. Furthermore, the presence of multiple Nodal genes is not conserved in all vertebrates. Hellsten et al [53] compared the numerous Nodal genes in *Xenopus tropicalis* with the single Nodals found in chicken and humans. Both chicken and human have a single *Nodal* gene, but a synteny analysis reveals that these Nodals are present at different specific locations in the genome (known as loci). Human *Nodal* is similar to *Xnr4* in *Xenopus*, while chicken *Nodal* clusters with a separate group of six *Xenopus* Nodals. The analysis carried out in [53] suggests that two Nodal loci were present at the base of vertebrate evolution, with chicken and humans losing different copies during evolution. Other more 'ancestral' species, such as axolotl, have retained two Nodal genes. Johnson et al [65] hypothesise that the evolution of multiple Mix and Nodal genes in *Xenopus* is a consequence of predetermined PGC specification. Axolotl PGCs are induced in the mesoderm, meaning any changes to the levels of mesoderm-inducing signals caused by the expansion of a gene family can lead to the elimination of PGCs, putting a constraint on the evolution of the mesoderm GRN. However, in *Xenopus* changes to the mesoderm GRN are not constrained since PGCs are predetermined away from the mesoderm (see figure 1.5).

The fact that mammals possess single copies of *Mix* and *Nodal* genes [45, 157] leads to the prediction that a simplified GRN (sGRN) exists. A sGRN for mesendoderm in *Xenopus laevis* is



**Figure 1.5:** The localisation and methods of specification of PGCs can release constraints on evolution of the mesoderm network. In axolotl PGCs are formed within the mesoderm by induction. Changes in the levels of mesoderm inducing signals resulting from, for example, an expansion of the Nodal gene family can lead to the elimination of PGCs. In *Xenopus* PGCs are predetermined in the vegetal hemisphere, so that any changes to the mesoderm network do not affect the specification of PGCs. Figure taken from [65].

constructed, by combining the inputs of the multiple Mix-like and Nodal-related genes into a single copy for each gene family (see figure 1.7A). Recall that the axolotl has a simplified GRN for mesendoderm formation in comparison with *Xenopus laevis* [139]. In axolotl, a single Mix gene (*AxMix*) and only two Nodal genes (*AxNodal1* and *AxNodal2*) have been identified. An analysis of the roles of Nodal genes in axolotl reveal that *AxNodal1* is required for mesoderm induction, but *AxNodal2* is dispensable for this function. Initially the *Xenopus* mesendoderm sGRN was used as a prediction for the structure of the axolotl mesendoderm GRN. However, experimental testing of interactions in Axolotl embryos has revealed key differences between the axolotl and *Xenopus* networks (see section 1.8 for further details). Current knowledge on the structure of the axolotl mesendoderm GRN is summarised in figure 1.7B.

In the following sections, the signals and transcription factors involved in the mesendoderm gene regulatory network are introduced, focusing on the current knowledge in *Xenopus laevis*, since it has been studied in more detail than mesendoderm in axolotl.

## 1.6 Morphogens in embryo development

In order for a uniform field of cells to differentiate into two or more populations of cells, they must receive signals so that each cell can sense its position within the field and differentiate accordingly. A morphogen is a biochemical molecule which spreads across a field of cells, either by diffusion or some other mechanism, to determine cell fate in a concentration dependent manner [41, 133]. The existence of morphogen gradients was first proposed by Thomas Hunt

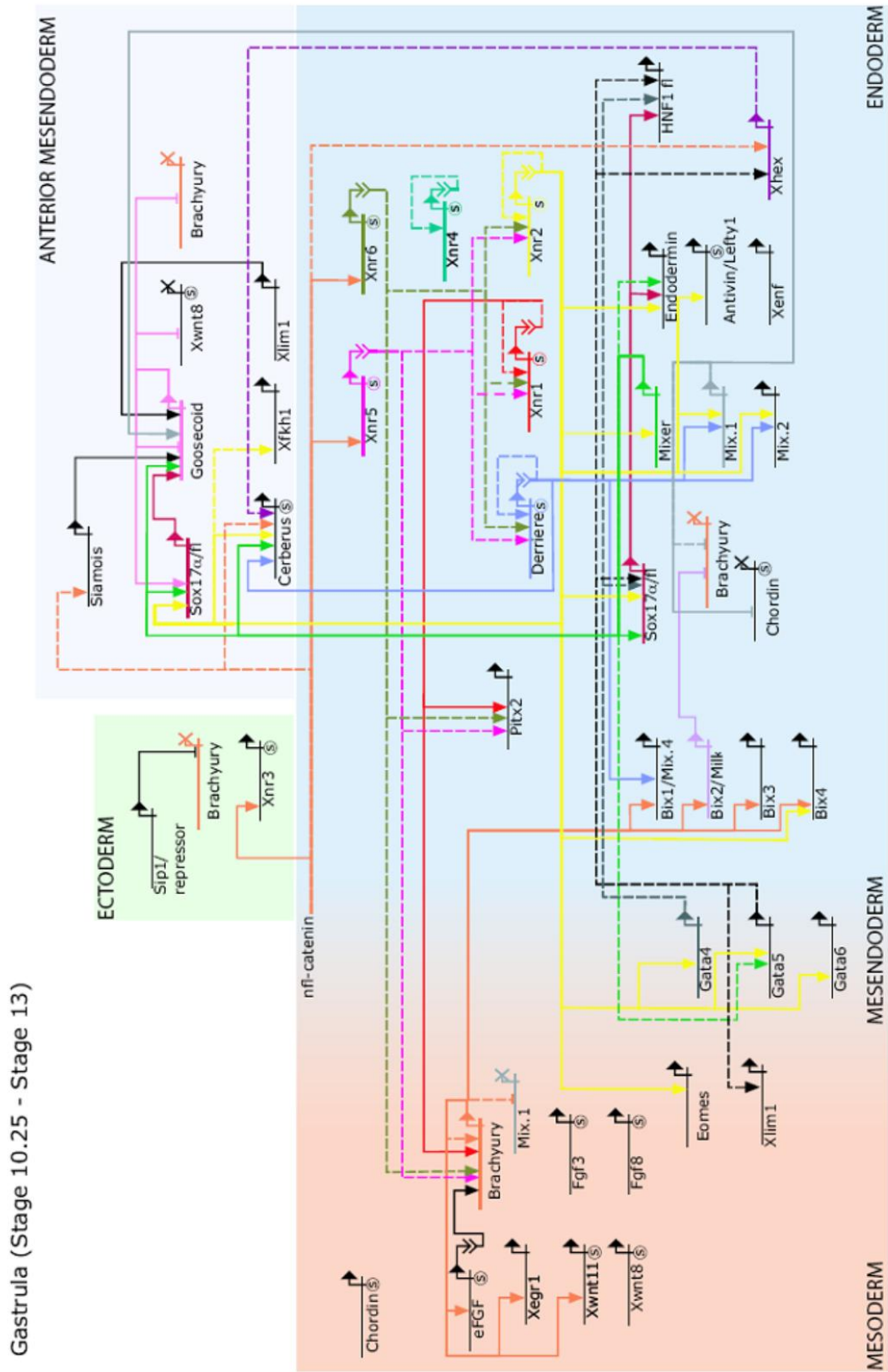
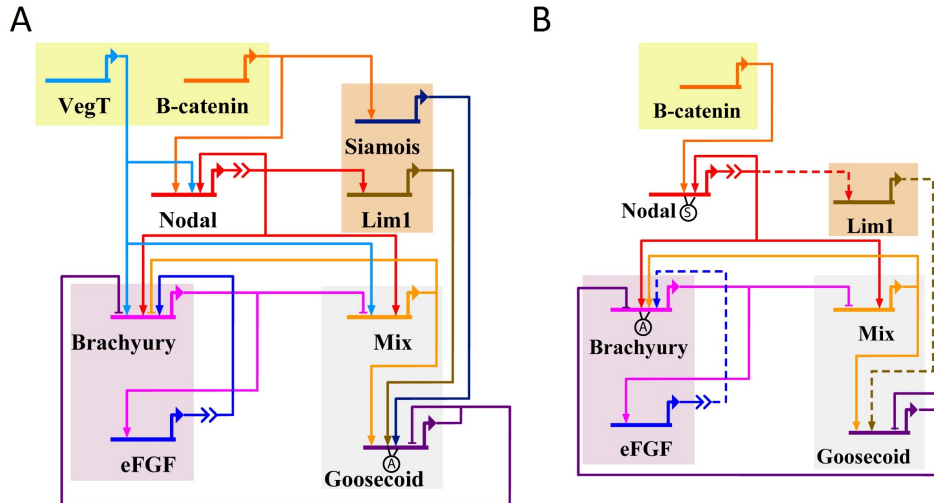


Figure 1.6: A gene regulatory network for mesoderm and endoderm formation in *Xenopus laevis*, taken from [89].



**Figure 1.7:** A comparison of the *Xenopus* and axolotl mesendoderm GRNs. **A** The simplified *Xenopus* mesendoderm GRN and **B** the axolotl mesendoderm GRN. Arrow and bar heads represent, respectively, activation and repression. The 'A' indicates that an input is, in Boolean terms, an 'AND' gate. Otherwise, multiple inputs consisting of only one type (repression or activation) correspond to an 'OR' gate. When both types are present, the repression and activation inputs are treated as two 'OR' gates coupled by an 'AND' gate. 'S' indicates genes act in synergy. In **B** solid lines indicate experimentally verified links and dashed lines indicate links which are inferred from the *Xenopus* mesendoderm GRN, which need to be verified experimentally.

Morgan [41]. Lewis Wolpert extended the concept of 'positional information' by introducing his French flag model; in this model 'flag cells' interpret their position along a morphogen gradient via the presence of expression thresholds [151]. Although the concept of morphogens was first predicted over 100 years ago, *in-vivo* candidates have only emerged within the last 25 years [42]. Morphogen gradients have now been identified in a wide variety of developmental processes [150], and have been explored using mathematical models (see section 1.12 for more details). In *Xenopus*, the first molecule identified to act as a morphogen in the induction of mesoderm was Activin, a member of the TGF- $\beta$  superfamily [136].

Cells can be induced either to become mesoderm or endoderm, dependent on the concentration of Activin-like signal it receives. Dose response experiments [43, 46–48, 112] show that at low concentrations of Activin a cell will become mesoderm (i.e. express Brachyury). As the dose of Activin increases past a threshold value, a cell will no longer express Brachyury and will express Mix.1 (i.e. endoderm). These experiments have been carried out both in single cells [43, 48, 112] and whole tissue [46, 47, 112], showing that Activin signalling does not rely on cell-cell communication. The absence of Activin mRNA expressed in the correct location and time within the embryo puzzled scientists, leading to a search for alternative Activin-like morphogens which act via the same pathway (see [42] for details). Nodal-related genes have now emerged as prime candidates for the morphogens regulating the induction of mesoderm and endoderm in *Xenopus*.

### 1.6.1 The TGF- $\beta$ signalling pathway

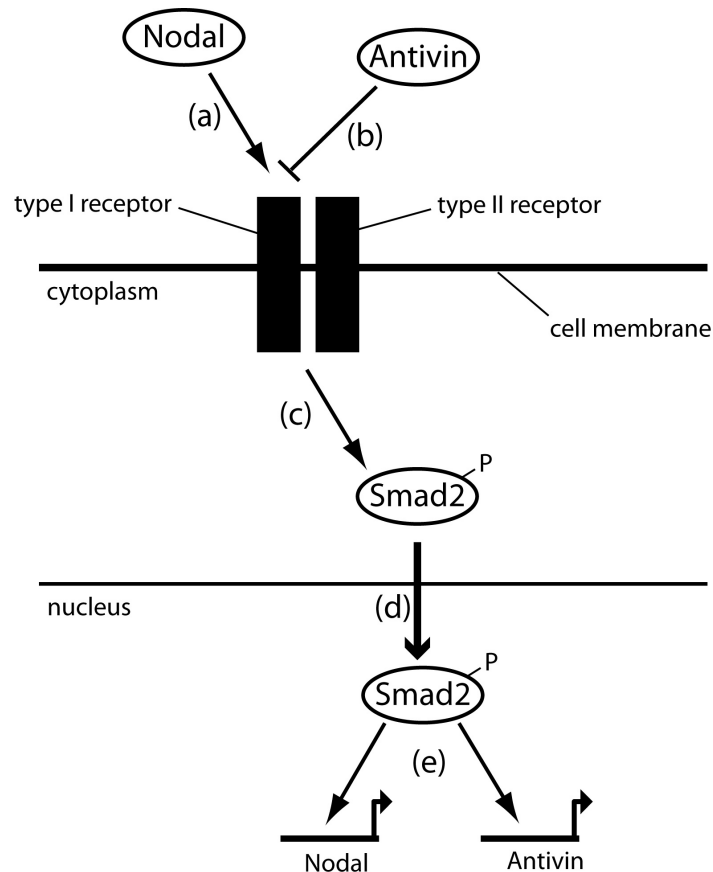
The Nodal genes (Xnr1-Xnr6) are members of the TGF- $\beta$  family of signalling molecules, which also includes BMP and Activin. The TGF- $\beta$  signalling pathway has been extensively studied (see [27, 58, 125] for reviews), here we give a brief overview of the pathway as illustrated in figure 1.8. Two receptors (type I and II) on the cell membrane are brought together by the binding of an extracellular Nodal ligand. The binding of the ligand results in the phosphorylation of the type I receptor by the constitutively active type II receptor. The activated type I receptor results in the phosphorylation of Smad2/3 inside the cell. The phosphorylated Smad (P-Smad) forms a complex with Smad-4 and then enters the nucleus. Once in the nucleus the Smad complex interacts with transcriptional co-factors, such as FoxH1 and Mixer, to regulate the ligands target genes [78]. Different targets of the Nodal signalling pathway require different transcriptional co-factors: FoxH1 is the co-factor for Nodal autoregulation, Antivin and Mix2, whereas Mixer, which is itself a target of Nodal, is the co-factor for Goosecoid expression [102].

Antivin, an antagonist of Nodal signalling activity, is induced by Nodal signaling [142]. In *Xenopus* the overexpression of Antivin has been shown to reduce the expression of Xbra and Mix1, key markers of mesendoderm [142]. Two mechanisms have been proposed for how Antivin antagonises Nodal, by binding either to its ligand [15] or to the receptor [17] or by both of these mechanisms [14].

### 1.6.2 Regulation of *Xenopus* Nodal genes

There are differences in both spatial and temporal expression of the Nodal genes in *Xenopus*, along with functional differences in early development. In this section we discuss the regulation of members of the Nodal gene family by the maternal factors VegT and  $\beta$ -catenin (as investigated by [117]). Xnr5 and Xnr6 are first detected by PCR at the MBT, with expression peaking during the blastula stages then decreasing during gastrulation, until it is no longer detected at stage 12 [141]. VegT and  $\beta$ -catenin regulate the expression of Xnr5 and Xnr6 [117, 141]. The activation of Xnr6 is also synergised by Activin-like signalling [117]. Xnr1 and Xnr2 are detected by stage 9, which is later than the first expression of Xnr5 and Xnr6 [141], and are activated either by VegT or by Activin-like signalling synergised by  $\beta$ -catenin [117]. Takahashi et al [141] hypothesize that *in-vivo* Xnr5 and 6, rather than the maternal factors, activate the expression of Xnr1 and 2. Luxardi et al [90] investigate the roles of Xnr1, Xnr2, Xnr5 and Xnr6 using antisense morpholinos (MOs) to knock down each of these genes: embryos where a single gene is knocked down show few defects whereas the double knockdown of either Xnr1 and Xnr2, or Xnr5 and Xnr6 show more severe defects. The double knockdown of Xnr5 and Xnr6 results in the repression of mesodermal markers (Brachyury, Goosecoid, Sox17), whereas the double knockdown of Xnr1 and Xnr2 prevents gastrulation, with a slight downregulation of mesendodermal genes.

The spatial distribution of phosphorylated Smad2 (P-Smad2), an extracellular component of Nodal signalling, reveals a graded and dynamic pattern [83, 126]. P-Smad2 is first detected at



**Figure 1.8:** Schematic diagram of the Nodal signalling pathway [125]. a.) Extracellular Nodal ligands bind to membrane bound receptors (type I and II), resulting in the phosphorylation of the type I receptor. b.) Extracellular Antivin can prevent the binding of Nodal to its receptor (see main text for a description of the mechanisms). c.) The activated (phosphorylated) receptor complex results in the phosphorylation of Smad2. d.) The phosphorylated Smad2 translocates to the nucleus and e.) activates downstream targets such as *Nodal* and *Antivin*.

stage 8.5 on the dorsal side of the embryo. By stage 9.75, Smad2 phosphorylation is maintained dorsally and expands to the ventral side of the embryo. At this stage P-Smad2 is present in both the mesoderm and endoderm, but the signal is stronger in the endoderm. After stage 10.5, the levels of P-Smad2 begin to decrease and by stage 14 only a weak signal is present. Lee et al [83] suggest that this downregulation could be in part due to antagonists of Nodal such as Antivin.

### 1.6.3 FGF signalling

Fibroblast growth factors (FGFs) comprise of a large family of secreted molecules that signal through FGF receptors (FGFRs), a group of tyrosine kinase receptors. FGFs have several roles in patterning the embryo including cell migration, mesendoderm formation, neural induction, midbrain-hindbrain patterning, limb induction and bone formation [32, 144]. FGF signals are transduced by three main pathways, the Ras/MAPK pathway, the PLC $\gamma$ /Ca $^{2+}$  pathway and the PI3 kinase/Akt pathway [9, 32, 144]. The Ras/MAPK pathway is the most common path-

way, which we now describe. The binding of an FGF ligand to an FGFR causes phosphorylation of the receptor and the activation of the intracellular signalling cascade. Following a complex series of interactions, which we do not describe here, Raf, MEK and MAP kinases are activated. Activated MAP kinases then enter the nucleus and act on downstream targets of FGF signalling [144].

FGF signalling is important in the induction of mesoderm. eFGF (also known as FGF4) is expressed in a ring around the blastopore in stage 10.5 *Xenopus* embryos, in a pattern similar to that of Brachyury [61]. The overexpression of eFGF induces the expression of Brachyury in *Xenopus* animal caps [62]. Similarly, Brachyury has also been shown to activate the expression of eFGF [62]. Thus these two genes form a positive feedback loop.

## 1.7 Mesendodermal genes in *Xenopus*

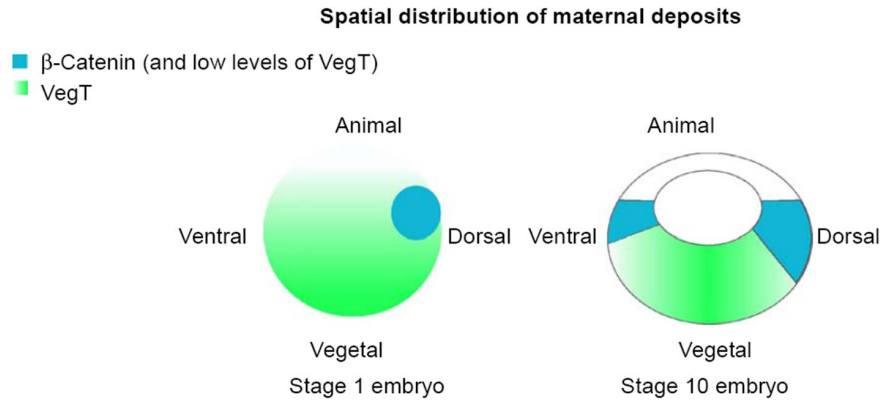
In this section, key transcription factors present in the mesendoderm gene regulatory network are introduced, along with their expression patterns in *Xenopus*. Emerging differences in the behaviour and expression patterns of these genes in axolotl are introduced in section 1.8.

### 1.7.1 VegT and $\beta$ -catenin

The localisation of maternal transcripts (i.e. transcribed by the mother and present in the embryo before zygotic transcription commences) provided important positional information for the specification of mesoderm and endoderm. Two maternal factors, VegT [89, 154] and  $\beta$ -catenin [127] have been shown to have roles in mesoderm induction.

VegT, which belongs to the T-box family of transcription factors [155], is present as a maternal transcript which has been shown to function in the induction of mesoderm and endoderm. In *Xenopus* oocytes the expression of VegT is restricted to the vegetal half (i.e. to the prospective endoderm) [155]. In embryos depleted of VegT endoderm fails to form, as shown by a reduction or absence of Sox17 and Mix1 expression, and mesoderm induction is also reduced as judged by Brachyury and Goosecoid expression [154]. The ability of VegT to induce mesoderm and endoderm is via its regulation of TGF- $\beta$  (Nodal) signalling [21, 74], and by directly activating *Mix.1* and *Brachyury* [89].

$\beta$ -catenin is a maternally expressed transcription factor which is expressed in the dorsal region of the embryo following an event known as cortical rotation. By stage 9.5, its expression has spread around an equatorial ring in the prospective mesoderm [126]. Both the knockdown and overexpression of  $\beta$ -catenin reveals that it regulates expression of mesodermal genes such as Brachyury [127].  $\beta$ -catenin also regulates Nodal signalling, affecting the temporal pattern but not the overall levels of P-Smad2 activation [83]. The spatial distribution of VegT and  $\beta$ -catenin in stage 1 and stage 10 embryos is illustrated in figure 1.9.



**Figure 1.9:** Cartoon of spatial distribution of the maternal factors VegT and  $\beta$ -catenin in *Xenopus*, taken from [95]. In a stage 1 embryo, VegT is localised vegetally and  $\beta$ -catenin is localised dorsally. By stage 10,  $\beta$ -catenin has spread round the marginal zone to ventral regions.

## 1.7.2 Mix.1 and Brachyury

*Mix.1* and *Brachyury* are genes, which encode transcription factors, expressed in the prospective endoderm and the prospective mesoderm, respectively. *Mix.1* is the founding member of the Mix-like family of homeodomain-containing genes in *Xenopus* [121], with at least six other Mix-like genes being present (*Mix.2-Mix.3*, *Bix.1-Bix.4*). *Mix.1* is expressed through out the vegetal hemisphere during early gastrulation (stage 10) [85]. *Brachyury* is a T-box transcription factor first cloned in mice, which is expressed in the primitive streak of mice [57] and in the marginal zone in *Xenopus* [135]. In *Xenopus*, the overexpression of *Brachyury* causes animal caps (the prospective ectoderm) to form ventral mesoderm [25] and embryos injected with XBra-EnR, a dominant negative construct, fail to complete gastrulation [22]. At stage 10 the expression of *Mix.1* overlaps with the expression of *Brachyury* in the marginal zone. As development proceeds, the expression domains of *Mix.1* and *Brachyury* gradually become more refined, with *Mix.1* absent from the dorsal expression domain of *Brachyury* by stage 10.5 [85].

## 1.7.3 Goosecoid, Siamois and Lim1

Goosecoid, Siamois and Lim1 are all transcription factors expressed in the dorsal regions of gastrula stage *Xenopus* embryos, in the organiser. Goosecoid, a homeobox gene, first detected just before the start of gastrulation, marks the region where the dorsal lip will form [19]. Goosecoid is a transcriptional repressor, which, in association with *Mix.1* (both genes being expressed in dorsoanterior endoderm) represses the expression of *Brachyury* [82]. The Siamois gene encodes for a homeodomain protein and is localised dorsally in *Xenopus* embryos [86]. Siamois is regulated by  $\beta$ -catenin [89], and acts in cooperation with the transcriptional activator Lim1. Siamois has been cloned in *Xenopus* only and no similar gene is found in fish or amniotes [53].

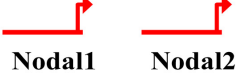
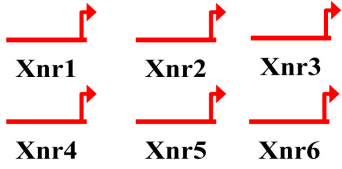
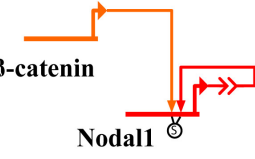
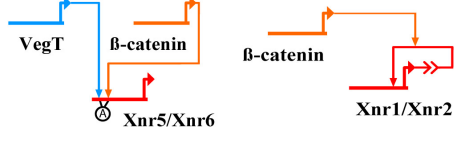

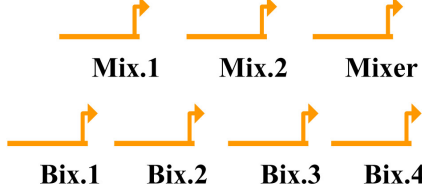
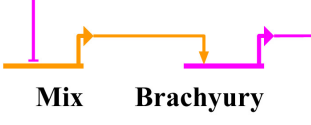
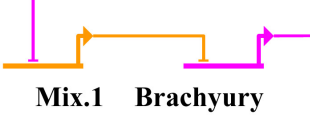
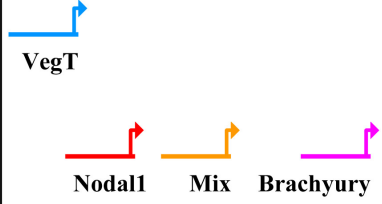
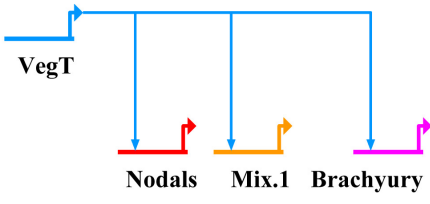



## 1.8 Comparison of mesendoderm formation in axolotl and *Xenopus*

We have identified the axolotl as an amphibian with a single *Mix* and two *Nodal* genes, making it a more suitable model organism than *Xenopus* for studying the behaviour of a simplified mesendoderm GRN [139]. Mesendoderm formation in *Xenopus* has been extensively studied, with the function of all genes present explored and collated into a GRN [75, 89]. Mesendoderm formation in axolotl has not been studied in the same detail as in *Xenopus*, but investigations to date have found several differences in the mechanisms of mesendoderm formation in axolotl and *Xenopus*. In this section, we compare the structure of the mesendoderm GRN in axolotl and *Xenopus*, addressing each of the differences illustrated in figure 1.10 in turn.

Recall that two *Nodal* genes (*AxNodal1* and *AxNodal2*) are found in axolotl [139] and that the evolutionary history of *Nodal* genes suggests that ancestral species have two *Nodal* genes [53]. Taken together with evidence presented in section 1.4, the presence of two *Nodal* genes suggest that the axolotl is an example of a species with ancestral traits. The function of the two axolotl *Nodal* genes has been investigated using morpholino oligonucleotides (MOs) [139]. MOs bind to exon/intron boundaries in DNA, thus preventing the translation of mRNA into protein, disrupting the function of the genes protein product. Embryos injected with *AxNodal1* MO fail to gastrulate, indicating that mesoderm does not form in the absence of *AxNodal1*. Furthermore, the expression of mesendodermal genes is lost in the absence of *Nodal1*, showing that *AxNodal1* is required for mesendoderm formation. Gastrulation still occurs in *AxNodal2* MO embryos and mesendodermal genes are still expressed, indicating that *AxNodal2* is not required for mesendoderm formation. Therefore the axolotl mesendoderm GRN contains a single *Nodal* gene, as is found in mammals [45, 157]. The induction of *Nodal* genes by maternal factors varies between the different *Xenopus* *Nodals* and *Nodal1* in axolotl. A systematic investigation of *Xenopus* *Nodal* gene induction in response to VegT,  $\beta$ -catenin and *Nodal* signalling has been carried out in [117]. *Xnr1,2* and 4 expression is induced by VegT, or by *Nodal* signalling in synergy with  $\beta$ -catenin. *Xnr 5* and 6 require both VegT and  $\beta$ -catenin to be present for their induction, and cannot be induced by *Nodal* signalling. In axolotl, *Nodal1* has been identified as a direct target of  $\beta$ -catenin [16].

There is one *Mix* gene in axolotl (*AxMix*) [139], compared with seven *Mix*-type genes (*Mixer*, *Mix.1-2*, *Bix.1-4*) in *Xenopus* [89]. The expansion of the *Xenopus* *Mix* family, along with the *Nodal* family, is another example of subfunctionalisation occurring in *Xenopus*. In embryos treated with an *AxMix* MO development halts at the early gastrula stages, disrupting the formation of mesoderm [139]. An analysis of gene expression in these embryos shows that the knockdown of *AxMix* results in the down-regulation of *Brachyury*. These data show that *Mix* is required for the expression of *Brachyury* in axolotl. A knockdown of all *Mix* genes has not been carried out in *Xenopus*, due to the technical difficulties in achieving this. However, mutual negative regulation of *Brachyury* and *Mix.1* drives the segregation of mesoderm and endoderm in *Xenopus* [85]. Thus it is surprising that a similar mechanism is not present in axolotl. In mice, the inhi-

	Axolotl	<i>Xenopus</i>
1	2 Nodal Genes 	6+ Nodal Genes 
2		
3	1 Mix gene 	7 Mix genes 
4		
5		
6	Siamois not present	

**Figure 1.10:** Network diagrams highlighting differences between the axolotl and *Xenopus* mesendoderm GRNs. The first column gives features of the axolotl mesendoderm GRN and the second column gives the corresponding features on the *Xenopus* mesendoderm GRN. Row 1: At least 6 Nodal genes are found in *Xenopus*, compared with 2 Nodal genes in axolotl. Row 2: In *Xenopus*,  $\beta$ -catenin acts in two different ways on Nodal;  $\beta$ -catenin enhances Nodal autoregulation of Xnr1 and Xnr2, and the expression of Xnr5 and Xnr6 is activated by  $\beta$ -catenin in the presence of VegT. In axolotl, Nodal1 can be activated by  $\beta$ -catenin alone and we also assume that it can enhance Nodal autoregulation. Row 3: There are seven Mix genes in *Xenopus* and one Mix gene in axolotl. Row 4: Mix and Brachyury mutually repress each other in *Xenopus*, but, in axolotl, Mix is required for the expression of Brachyury. Row 5: VegT acts to activate expression of Nodal, Mix and Brachyury in *Xenopus*, but in axolotl VegT does not activate these genes. Row 6: Siamois is a gene found in *Xenopus* but not axolotl.

bition of Mix11 (the mouse Mix gene) causes a decrease in Brachyury expression, meaning that Mix11 is required to activate Brachyury [139]. Thus, in both axolotl and mice, Mix is required for the expression of Brachyury. The knock down of Brachyury in axolotl results in *AxMix* being initially down-regulated, before an up-regulation at later stages, suggesting Brachyury negatively regulates *AxMix* [139], as is observed in *Xenopus* [85].

The localisation of maternal factors also varies when comparing axolotl and *Xenopus*. In *Xenopus*, the T-box protein VegT is localized to the vegetal pole of the oocyte. However, in axolotl oocytes VegT is not localised [104]. VegT is also expressed throughout the oocyte in lungfish and sturgeon, suggesting that the localisation of VegT is not an ancestral vertebrate trait [16].  $\beta$ -catenin is another maternal factor which accumulates dorsally in both *Xenopus* and axolotl embryos after cortical rotation. The roles of VegT and  $\beta$ -catenin in the axolotl are investigated in [16] with key results mentioned here. In axolotl animal caps,  $\beta$ -catenin can induce mesoderm and endoderm in a dose dependent manner and VegT does not induce mesoderm or endoderm.  $\beta$ -catenin stills induce mesoderm and endoderm in axolotl animal caps when co-injected with AxVegT-Enr, a dominant negative VegT construct, meaning that VegT is not required for inducing mesoderm in axolotl. However, a knockdown of VegT in whole embryos results in embryos which do not develop normally, which is thought to be independent of mesoderm induction. The roles of VegT and  $\beta$ -catenin in axolotl are different to their roles in *Xenopus*. In *Xenopus* animal caps, the injection of VegT or  $\beta$ -catenin mRNA alone cannot induce mesoderm and endoderm. However, co-injecting combinations of  $\beta$ -catenin and VegT in animal caps does induce mesoderm and endoderm in a manner dependent on the dose of VegT. Nodal genes, Mix.1 and Brachyury have all been identified as direct targets of VegT in *Xenopus* [89]. Experiments carried out in axolotl show that Nodal2 is a direct target of VegT, while Nodal1, Mix and Brachyury are not induced directly by VegT [16].

Another difference in mesendoderm induction between the axolotl and *Xenopus* is the organiser specific gene *Siamois*. *Siamois* appears to be specific to *Xenopus* with no similar gene found in fish or amniotes [53]. Our attempts to clone *Siamois* in axolotl using degenerate primers based on *Siamois* sequences in *Xenopus laevis* and *Xenopus tropicalis* have been unsuccessful. Given this evidence we assume that *Siamois* is absent from axolotl.

To summarise, there are several differences between the *Xenopus* and axolotl mesendoderm GRNs. Importantly, the axolotl mesendoderm GRN contains fewer Mix and Nodal genes than *Xenopus*, leading to a simpler GRN. However, the axolotl has not been studied as extensively as *Xenopus*, so some links in the axolotl mesendoderm GRN have not been verified experimentally. The *Xenopus* and axolotl mesendoderm GRNs are shown in figure 1.7.

## 1.9 Dorsal-ventral patterning in *Xenopus*

DV patterning in embryos is regulated by extracellular protein interactions. During early development, two opposing signalling centres form; the dorsal centre and the ventral centre (reviewed in [118]). Signals expressed in the dorsal centre (also called the Spemann organizer)

include Chordin and ADMP, while BMP4 and Xolloid-related (Xlr) are expressed in the ventral centre. Signals from these two centres interact to form a gradient of activity along the dorsal-ventral axis of the embryo (see figure 1.11). The earliest event in the formation of DV asymmetry is cortical rotation, resulting in the translocation of  $\beta$ -catenin to the dorsal side of the embryo [126]. After the onset of zygotic transcription (at the midblastula transition)  $\beta$ -catenin induces the expression of BMP agonists such as Chordin. A detailed description of the signals and mechanisms underlying DV axis formation is given below.

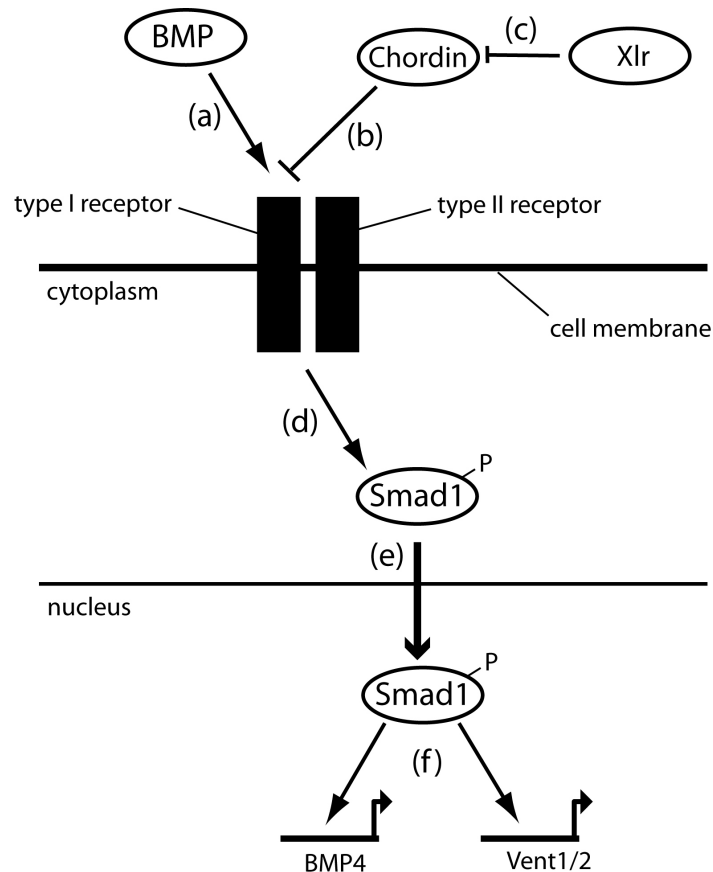
### 1.9.1 BMP signalling

Bone Morphogenic Proteins (BMPs) are members of the TGF- $\beta$  superfamily of signalling molecules [27, 58]. Most BMPs, for example BMP2, BMP4 and BMP7, are expressed in the ventral most regions of the embryo, the 'ventral centre' [27, 58]. However, Anti-dorsalizing morphogenic protein (ADMP) is a BMP signalling molecule transcribed in the Spemann organiser (i.e. the dorsal centre) [99]. BMP2 is a maternally transcribed gene, expressed throughout the embryo at early cleavage stages until blastula stages, with the signal becoming weak at gastrulation [20]. Overexpression studies show that BMP2 can trigger the BMP4 autoregulatory loop [128], meaning BMP2 is a possible candidate for activating the expression of BMP4 *in-vivo*. The knockouts of BMP2, BMP4 and BMP7, both individually and in combination, are investigated by [115]. The depletion of each BMP results in slightly dorsalised embryos with the most severe phenotype seen for BMP4 depletion and the least severe phenotype is for BMP2 depletion. A triple depletion of BMP2/BMP4/BMP7 results in a dorsalised phenotype, but still retaining a significant amount of DV patterning. Anti-dorsalising morphogenic protein (ADMP), a BMP ligand transcribed in regions of low BMP activity [99], is a candidate for maintaining DV patterning in the absence of BMP2/BMP4/BMP7 since in embryos depleted of ADMP and BMP2/4/7 DV patterning is lost [116].

The TGF- $\beta$  signalling pathway in *Xenopus* includes both BMP and Nodal. Recall that the Nodal signalling pathway is described in section 1.6.1. Here we describe the pathway for BMP [58], which is similar to the Nodal signalling pathway. A type I receptor (BMPRIA, BMPRIB) and type II receptor (BMPRII) are brought together following the binding of a BMP ligand, causing the phosphorylation of the type II receptor. The phosphorylation of the type II receptor leads to the phosphorylation of Smad1. Phosphorylated Smads (P-Smads) enter the nucleus and target genes downstream of BMP signalling, including *bmp4* and *Vent2* [58]. XVent2 is a Smad1 coactivator of BMP4 [54]. ADMP does not bind the BMPRIA (ALK3), BMPRIB (ALK6) or BMPRII receptors, instead binding to ALK2, a type I BMP receptor [116]

### 1.9.2 Chordin

Chordin, a BMP antagonist, is secreted by the organizer region of the embryo. Chordin binds to BMP ligands, forming a Chordin/BMP complex, preventing BMP from interacting with its receptors. Xolloid-related (Xlr) is a BMP-related metalloproteinase, which inactivates Chordin



**Figure 1.11:** Schematic diagram of BMP signalling. (a) Free BMP ligands bind to BMP receptors on the cell surface. (b) Chordin binds to BMP ligands preventing them from interacting with its receptor. (c) Chordin is cleaved by the protease Xlr, releasing BMP from the complex and allowing it to bind to its receptor (d) The activated (phosphorylated) receptor causes phosphorylation of Smad1. (e) Phosphorylated Smad1 translocates to the nucleus and (f) activates downstream targets such as Vent1/2 and BMP4.

by proteolytic digestion, releasing active BMP from Chordin/BMP complexes [113]. Xlr is localised to ventral and lateral sections of the marginal zone in gastrula stage embryos [26]. Chordin is a downstream target of Goosecoid, with the expression of Chordin reduced in Goosecoid depleted embryos and expanded in Goosecoid injected embryos [124].

### 1.9.3 Vent1/2 and Goosecoid

Vent1 and Vent2 are two ventrally expressed homeobox genes which function in BMP signalling [108]. The expression patterns of Vent1 and Vent2 overlap, but the extent and timing of expression differs between the two genes, as shown by *in-situ* hybridisation and RT-PCR.

At stage 10, Vent2 is present in the marginal zone and animal cap, excluding the organiser [107]. The domain of expression of Vent1 is smaller than that of Vent2. Vent2 transcripts are found throughout the animal cap [107], whilst Vent1 transcripts are only detected on the ventral side of the animal cap [38]. In the marginal zone the boundary of Vent1 expression does not extend

as far dorsally as that of Vent2 [107, 108]. The regions of Vent expression determine the fate of the mesoderm; in lateroventral regions (where both Vent genes are coexpressed) cells differentiate into mesenchyme and blood, in dorsolateral regions (where Vent2 is expressed) cells differentiate into muscle and regions with neither of the Vent genes differentiate into notochord [38]. RT-PCR analysis shows that Vent1 expression commences in late blastula, reaches maximal expression at stage 11 and is not expressed by stage 30 [38]. Vent2 is first expressed at the midblastula transition, is at its maximum during late neurula and is still expressed at stage 30 [107].

The overexpression of both Vent genes by microinjection of mRNA cause ventral phenotypes, suggesting that the Vents function in specifying ventral regions of the embryo [38, 107]. However, the effects of Vent2 overexpression are more severe than those observed for Vent1: the phenotype for high doses of Xvent1 is microcephaly (small head) [38], but high doses of Vent2 produce *Bauchstück* ('belly piece') embryos [107]. In loss of function experiments, the dorsalisation of embryos by Vent1 and Vent2 morpholinos is greatly increased when they are co-injected [124], suggesting that the Vents act in an additive manner.

BMP4 can induce the expression of Vent2, and vice versa. Smad1 and Smad4 mediate the effect of BMP4 on Vent2 [55]. The injection of Vent2 mRNA can also rescue the dorsalisation of embryos by dominant negative BMP4 receptors. Both BMP4 and Vent2 can also ventralise dorsal mesoderm in a dose dependent manner. This evidence suggests that Vent2 functions in the specification of ventral mesoderm, as part of the BMP4 signalling pathway acting downstream of BMP4 [107]. The evidence presented above suggests that while the expression patterns of Vent1 and Vent2 overlap, they function in different ways as part of the BMP pathway, with Vent2 having a role in the BMP4 positive feedback loop, while Vent1 only acts downstream of BMP4.

It has also been proposed that Goosecoid and Vent1/2 act in a cross-regulatory loop to repress each other [107]. The knock down of Vent1/2 by Vent1 and Vent2 MOs results in a dorsalised embryo, whereas a Goosecoid MO results in a ventralised embryo [124]. Interestingly, a triple knockdown of Vent1/2 and Goosecoid results in a normal, meaning that the self-regulation of the DV axis by the cross regulation of Vent1/2 and Goosecoid is not required for the specification of the DV axis. It has been suggested that in these triple knockdown embryos the extracellular molecules of the dorsal and ventral centres might be able to mediate self-regulation of the DV axis. This is shown by a knock down of BMP in Goosecoid/Vent1/2 MO embryos, which results in a dorsalised embryo [124].

## 1.10 Mathematical models of gene regulatory networks

Recall that the expression of genes is regulated by TFs, which bind to promoter regions and act either to activate or to repress transcription of the target gene. Signalling molecules bind to receptors on a cell's surface to cause changes to levels of intracellular factors which also regulate transcription of its downstream targets. These target genes may also encode TFs or signals,

leading to a gene regulatory network (GRN). We have already provided motivation for studying the GRN underlying mesendoderm formation and proceed to give an overview of types of mathematical models which are used to analyse the behaviour of a GRN. Mathematical simulations have several advantages over wet lab experiments, such as being quicker, cheaper and being able to uncover dynamics of components that are difficult to measure via experiments. In recent years GRNs have been studied by both experimental and theoretical biologists in both single cells (for example the  $\lambda$  phage switch [40]) and multicellular systems (for example the segment polarity network in *Drosophila* [91]). There are three main classes of model used to analyse GRNs in a single cell: logical models, continuous models and stochastic models [69]. Here we give an overview of each class of model, before introducing multicellular models in the next section.

### 1.10.1 Overview of modelling frameworks

In this section, an overview of the types of mathematical models available to model GRNs is provided (as reviewed in [39, 69, 129, 137]), along with a detailed description of the ordinary differential equation (ODE) approach that we will use to develop the mathematical models in this thesis

Logic-based methods provide the simplest modelling framework, focusing on the behaviour of the network topology, rather than changes in the expression levels of genes. Boolean networks were first proposed as a method for exploring the behaviour of gene networks by Kauffman [70, 71]. In a Boolean model, each gene  $x_i$  is a node in the network which is assigned a binary variable such that it is either 'ON' ( $x_i = 1$ ) or 'OFF' ( $x_i = 0$ ). Time is defined by a number of discrete time steps ( $t_1, t_2, \dots, t_n$ ) and the state of each gene is updated synchronously according to a defined set of rules. Formally, for a set of genes ( $x_1, x_2, \dots, x_n$ ) the state of each gene at  $t + 1$  is updated according to a Boolean function ( $f_i$ ), such that

$$x_i(t + 1) = f_i(\mathbf{x}_i(\mathbf{t})). \quad (1.10.1)$$

The study of Boolean networks has been applied to a range of biological networks, including the segment polarity network in *Drosophila melanogaster*, which is capable of producing patterns which are in good agreement with experimental data [2]. Advantages of Boolean networks include fast computational analysis and a requirement for only qualitative data about the structure of the network to build a model. Disadvantages include the fact that, although a Boolean network can be used to explore steady states and the robustness of a system, it does not take into account the change in levels of gene expression on a continuous scale.

Real biological systems produce continuous rather than discrete-valued data. Continuous models, based on systems of ODEs, give real-valued levels of gene expression over a continuous timescale, producing simulations which can be directly compared with experimental data. In a continuous modelling framework, a single ODE represents the rate of change of an mRNA (or protein) ( $x$ ) in the network as a nonlinear function ( $f(\mathbf{x})$ ) of the other mRNAs (or proteins) in a

network, leading to a system of coupled ODEs of the form:

$$\dot{\mathbf{x}} = f(\mathbf{x}). \quad (1.10.2)$$

The representation of activation, repression and degradation of a an mRNA (or protein) as part of  $f(\mathbf{x})$  are introduced in section 1.11. Time-delay ODEs allow for delays between the onset of transcription and the synthesis of the protein. Advantages of using a continuous approach instead of Boolean networks included the ability to give a more detailed representation of molecular mechanisms underlying gene regulation which can be analysed using dynamical systems theory e.g. bifurcation analysis. However, a large number of kinetic parameters are required to solve such models and realistic values for these parameters are not always known, meaning models are restricted to qualitative analysis or computational techniques can be used to provide estimates for parameters (see section 1.13 for more details).

The logical and continuous models described above are deterministic, i.e. they do not take into account stochastic processes. When the number of molecules in a system is small, stochastic effects can be seen. In stochastic models of gene regulation, gene expression levels are updated using a master equation. The master equation describes how the probability that the network is in a particular state changes over time. The master equation is difficult to solve, and is usually studied using stochastic simulations algorithms. The simulation of stochastic models is more computationally demanding, and requires more detailed experimental data to fit the model than do deterministic models. In developing embryos stochastic fluctuations in the levels of individual genes are not important, since the number of mRNA/protein molecules is large and degradation rates are slow [28]

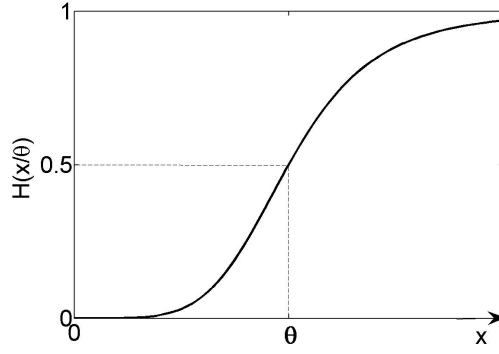
Models of mesoderm and endoderm specification currently available in the literature consist of systems of ODEs for GRNs in the *Xenopus* [95, 123] and sea urchin [76, 77]. As already mentioned, a key concept in the differentiation of the primary germ layers is the formation of two populations of cells representing mesoderm and endoderm. The two populations of cells are shown to correspond to stable steady states of the models, with mutual antagonism between mesodermal and endodermal genes determining which state dominates. These models are mentioned in more detail in chapter 3.

## 1.11 Nonlinear ODEs of GRNs

In this thesis we use a nonlinear ODE approach to modelling gene regulation. In this section, such an approach is introduced in detail. The following notation is used:  $\mathbf{X}$  is a gene, whose protein product  $\bar{\mathbf{X}}$  has a concentration  $X$ . It is assumed in these models that protein levels are proportional to mRNA levels.

Recall that gene expression is regulated by the binding of TFs to promoter regions, which either activate or repress the transcription of a target gene. A single gene is usually regulated by several TFs, but for simplicity equations are introduced for genes regulated by a single TF. For





**Figure 1.12:** Sketch of a Hill function  $\mathcal{H}(x/\theta)$  plotted against  $x$ . At  $x = 0$ ,  $\mathcal{H}(x/\theta) = 0$ . When  $x = \theta$ ,  $\mathcal{H}(x/\theta)$  is at its half-maximal value ( $1/2$ ). Finally, as  $x \rightarrow \infty$ ,  $\mathcal{H}(x/\theta)$  tends to its maximal value ( $1$ ).

a gene  $\mathbf{X}$  whose expression is activated by  $\bar{\mathbf{Y}}$ , we take the concentration  $X$  to be governed by

$$\frac{dX}{dt} = \lambda_{Y,X} \mathcal{H}\left(\frac{Y}{\theta_{Y,X}}\right) - \mu_X X \quad (1.11.1)$$

where

$$\mathcal{H}(x) = \frac{x^m}{x^m + 1} \quad (1.11.2)$$

is the Hill function with Hill coefficient  $m$ , and the positive constants  $\lambda_{Y,X}$  and  $\mu_X$  are the maximal rate of production of  $\bar{\mathbf{X}}$  induced by  $\bar{\mathbf{Y}}$  and the rate of turnover of  $\bar{\mathbf{X}}$ , respectively. As  $m$  tends towards infinity,  $\mathcal{H}(x)$  tends to  $H(x)$ , a step function defined by

$$H(x) = \begin{cases} 0 & \text{if } 0 \leq x < 1 \\ 1/2 & \text{if } x = 1 \\ 1 & \text{if } x > 1. \end{cases} \quad (1.11.3)$$

The parameter  $\theta_{Y,X}$  is therefore considered as the concentration threshold at which  $\bar{\mathbf{Y}}$  can transcriptionally regulate  $\mathbf{X}$  in the large  $m$  limit. Next consider a TF  $\bar{\mathbf{Z}}$  which acts to repress our gene  $\mathbf{X}$ . Equation (1.11.1) is extended to include this interaction such that

$$\frac{dX}{dt} = \lambda_{Y,X} \mathcal{H}\left(\frac{Y}{\theta_{Y,X}}\right) \left\{ 1 - \mathcal{H}\left(\frac{Z}{\theta_{Z,X}}\right) \right\} - \mu_X X \quad (1.11.4)$$

where  $\theta_{Z,X}$  is the threshold concentration at which  $\bar{\mathbf{Z}}$  can repress  $\bar{\mathbf{X}}$ .

Multiple inputs to a gene are modelled via nonlinearities motivated by Boolean logic. Consider a gene regulated by multiple transcription factors, which are either activators ( $y_i$ ) or repressors ( $z_i$ ). The regulation of a gene which can be activated independently by one or more transcription factors can be treated as an 'OR' gate ( $y_1 \vee y_2 \vee y_3 \vee \dots$ ). When two activators are both required to activate a gene they are treated as an 'AND' gate ( $y_1 \wedge y_2$ ). When both an activator and a repressor are present this is treated as an 'AND-NOT' gate ( $y_1 \wedge \neg z_1$ ). In the case where several activators and repressors are present, we assume the gene is only expressed if

at least one activator is present and no inhibitors are present above there threshold value, i.e. ‘OR’ gates coupled by an ‘AND-NOT’ gate  $((y_1 \vee y_2 \vee y_3 \vee \dots) \wedge \neg(z_1 \vee z_2 \vee z_3 \vee \dots))$ . For example, If  $\bar{X}$  AND  $\bar{Y}$  are required to activate  $\bar{X}$ , then the rate of production term is taken to be  $\lambda_{YZ,X} \mathcal{H}\left(\frac{Y}{\theta_{Y,X}}\right) \mathcal{H}\left(\frac{Z}{\theta_{Z,X}}\right)$ . If  $\bar{X}$  OR  $\bar{Y}$  is required to activate  $\bar{X}$ , then the rate of production term is taken to be  $\lambda_{Y,X} \mathcal{H}\left(\frac{Y}{\theta_{Y,X}}\right) + \lambda_{Z,X} \mathcal{H}\left(\frac{Z}{\theta_{Z,X}}\right)$ .

## 1.12 Multicellular models of GRNs

Recall that a morphogen gradient, whereby the fate of a cell is determined by its position along the gradient, is an important concept in developmental biology. Multicellular models have been used to explore the propagation of a signal throughout a domain, and the mechanisms which result in the formation of a gradient, using reaction-diffusion equations. Mechanisms by which a morphogen gradient can arise include ‘source-sink’ [81] and ‘activator-inhibitor’ [92]. In a ‘source-sink’ model a ‘source’, producing the signal, and a ‘sink’, absorbing the signal, are found at opposing ends of the spatial domain. In an ‘activator-inhibitor’ model, a gene and its inhibitor are both activated by a signal, the inhibitor then acts to restrict the spread of the signal. The modelling frameworks used for multicellular models of embryo development are introduced in this section, along with a review of selected models from the literature.

### 1.12.1 Continuous reaction-diffusion systems

In continuous reaction-diffusion systems the size of cells is assumed to be infinitesimal and signals are assumed to diffuse rapidly. The rate of change of a molecule ( $\mathbf{s}(x, t)$ ) at position  $x$  can then be defined by

$$\frac{\partial \mathbf{s}}{\partial t} = D \frac{\partial^2 \mathbf{s}}{\partial x^2} + \mathbf{f}(\mathbf{s}), \quad (1.12.1)$$

where  $D \frac{\partial^2 \mathbf{s}}{\partial x^2}$  is the diffusion term with diffusion coefficient  $D$  and the function  $\mathbf{f}(\mathbf{s})$  accounts for the reactions which take place.

There are conflicting views as to whether morphogen gradients arise by diffusion or by some other mechanism. Kerszberg and Wolpert [72] investigate the spread of a morphogen in a two dimensional lattice of cells, loosely basing the properties of the models on TGF- $\beta$  signalling molecules in *Xenopus*. They find that a model of simple diffusion does not produce a morphogen gradient. Instead the morphogen saturates available receptors, with a steep front profile of activated receptors propagating through a field of cells. An alternative ‘bucket brigade’ mechanism is proposed, where the ligand propagates by binding to and activating receptors, then dissociating and binding to neighbouring receptors. Lander et al [80] extend the diffusion model of Kerszberg and Wolpert to include receptor mediated ligand degradation and the internalization of ligand-receptor complexes. The addition of these terms allows morphogen gradients to form by simple diffusion in a one dimensional system, accounting for observa-

tions in the formation of the Dpp gradient in the *Drosophila* wing disc. They also investigate the ‘bucket-brigade’ mechanism, finding that it cannot account for the existing data in *Drosophila*. Chisholm et al [18] use mathematical models to investigate morphogen gradients arising due to cell proliferation. In these models a gradient forms via the dilution of morphogen mRNA: when a cell divides, the resulting daughter cells receive an equal share of the parent cell’s mRNA. Several cases are considered and give a mechanism for the formation of a gradient in the absence of diffusion.

### 1.12.2 Discrete reaction-diffusion systems

In models which include the intracellular regulation of extracellular gradients two different length scales must be considered. Intracellular protein concentrations are typically assumed to be uniform within a single cell, whereas extracellular proteins (e.g. morphogens) diffuse within the extracellular domain. Therefore a model of the regulation of a morphogen gradient must include both continuous processes (e.g. the diffusion of ligands) and discrete processes (e.g. intracellular interactions). Here we will introduce two methods for modelling this kind of system.

Let  $\mathbf{p}_i$  be intracellular protein concentrations and  $\mathbf{s}_i$  be local signal concentrations. Then

$$\frac{d\mathbf{s}_i}{dt} = \check{D}\Delta\mathbf{s}_i + \mathbf{f}(\mathbf{s}_i, \mathbf{p}_i) \quad (1.12.2a)$$

$$\frac{d\mathbf{p}_i}{dt} = \mathbf{g}(\mathbf{s}_i, \mathbf{p}_i) \quad (1.12.2b)$$

gives a suitable modelling framework, where  $\check{D}$  is a diagonal matrix of the form  $\check{D} = \text{diag}(\check{D}_1, \check{D}_2, \check{D}_3, \dots)$ , where  $\check{D}_N$  is the coupling coefficient of the  $N$ th signal and  $\Delta\mathbf{s}_i$  is the coupling term defined as

$$\Delta\mathbf{s}_i \equiv \mathbf{s}_{i-1} - 2\mathbf{s}_i + \mathbf{s}_{i+1}. \quad (1.12.3)$$

Intracellular and extracellular reactions are given by the functions  $\mathbf{f}$  and  $\mathbf{g}$ , respectively. Models of the form given in (1.12.2) can give solutions which differ from the spatially continuous version (equation (1.12.1)) [36]. In a continuous reaction-diffusion equation, travelling wave solutions will propagate throughout the medium. In the discrete case, travelling wave solutions only exist if coupling between cells is sufficiently strong: if this is not the case then waves do not propagate and appear to be ‘pinned’. In an alternative approach developed by Muratov and Shvartsman [103], space is treated as a continuous variable, incorporating cells as discrete variables. Each cell is of fixed length  $L$ , such that cell  $i$  is associated with the interval  $[iL, (i+1)L]$ . The diffusion of a signal  $s$  is governed by

$$\frac{\partial s}{\partial t} = D \left( \frac{\partial^2 s}{\partial x^2} + \frac{\partial^2 s}{\partial y^2} \right). \quad (1.12.4)$$

The intracellular protein concentration  $p_n$  is calculated as a function of the concentration of signal bound receptor ( $c$ ) on the cell, using the integral of receptor concentration along the cell

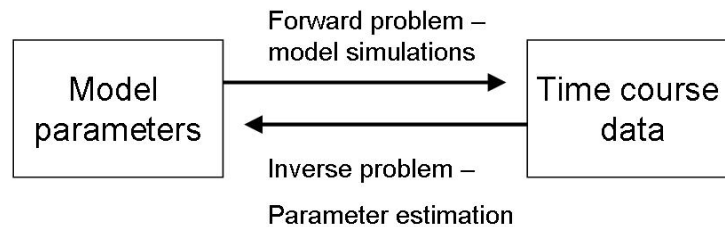
surface.

Many aspects of developmental biology have been explored using mathematical models. Here we review several examples including formation of the Bicoid gradient in *Drosophila* embryos, somite segmentation in vertebrates and primitive streak formation in chicks. Bicoid is a homeobox transcription factor present in early *Drosophila* embryos. During the early stages of development *Drosophila* embryos undergo multiple cycles of mitosis without cell division, resulting in a syncytium (a single cell with multiple nuclei). Maternal *bicoid* mRNA is localised to the anterior pole and, once Bicoid transcription commences, a morphogen gradient forms along the anterior-posterior axis. This morphogen gradient is then interpreted by target genes to form discrete patterns along the anterior-posterior axis. Grimm et al [44] review models used to describe the formation of the Bicoid gradient, each model being based on a single continuous reaction-diffusion equation. Differences in the models, such as the presence/absence of degradation, nucleocytoplasmic shuttling or parameter choices, can result in different characteristics of the model solutions. None of the models described can fully account for quantitative experimental observations, but raise questions that can be answered by further experimental work to give a fuller understanding of the mechanisms underlying the formation of the Bicoid gradient. A second example is that of somite segmentation. Somites are groups of cells which form along the anterior-posterior axis and later give rise to structures such as vertebrae. Models of the mechanisms underlying the formation of somites are reviewed in [30]. A key hypothesis for the mechanism of somite formation is that of the clock and wavefront model, first proposed by Cooke and Zeeman [24]. The model consists of a 'wavefront', or a morphogen gradient, which moves posteriorly and a cellular oscillator which acts as a 'clock'. As cells at the correct stage in the oscillatory cycle are passed by the wavefront they undergo a state transition and become somites. Mathematical models of this process have been formulated as reaction-diffusion equations, which are able to reproduce key experimental observations [5, 6]. The last example is that of primitive streak formation. During the development of a chick embryo the primitive streak is the first axial structure to form. During the initiation of the streak cells migrate and a thickening of cells marks the primitive streak. Page et al [110] develop both continuous and discrete models of this process. In these models marginal zone cells produce a streak-activating chemical. Once the activator reaches a threshold level cells become committed to become part of the streak and produce an inhibitor to prevent other cells adopting this fate. The models explored in [110] are able to account for the key features of primitive streak formation.

### 1.13 Quantitative mathematical models

Mathematical models, such as the non-linear ODE models (see section 1.11) and the reaction-diffusion equations described in the previous section, require information on biological values of kinetic parameters in order to be solved. Where such information is not available qualitative analysis of the models, for example bifurcation analysis, can give insights into the behaviour of the model for several different parameter regimes. However to obtain a quantitative model

which is capable of reproducing experimental data, biological obtained measurements are required. For simple systems which contain only a few genes and no feedback loops, the required parameters can be measured directly. Since GRNs often consist of many genes, each being regulated by multiple TFs and signals, along with the presence of feedback loops, some model parameters can be difficult to measure directly. In these cases, the task of inferring parameter values from experimental data is known as the inverse problem (see figure 1.13). Solving the inverse problem for a given experimental time course is not a trivial task. In many cases only limited data are available, for only a subset of the genes in the network. Once parameter values have been inferred the model can be solved using an ODE solver to give quantitative time courses for each gene in the network. In this section, types of data which can be used to obtain parameter values in GRNs are introduced, together with a brief overview of methods used to estimate parameters and the genetic algorithm, which we will use to estimate parameters in this thesis, is introduced in detail. We consider only the case where information on the structure of the GRN is already known.



**Figure 1.13:** Given a mathematical model (in our case a system of ODEs), the forward problem consists of solving the model using a given set of parameters to give time course simulations. In the inverse problem, experimentally obtained time courses are used to estimate model parameters which can reproduce the experimentally observed data.

### 1.13.1 Types of data used

The first step towards estimating parameters of a mathematical model is to obtain quantitative experimental data. Both mRNA and protein levels can be measured to give quantitative data for gene regulation, using a variety of established experimental techniques. Here we focus our attention to methods used to quantify mRNA levels. Quantitative real time PCR (qPCR) can be used to measure the levels of a gene's mRNA, relative to a 'house-keeping' gene.

Measurements can be taken on a number of different scales; in a single cell, a uniform population of cells, or in a heterogeneous population of cells (e.g. a whole embryo). Monitoring mRNA levels in whole embryos can give important information about the developmental stages at which a gene is expressed but does not show the regions in which this occurs. The spatial distribution of gene transcripts can be found using *in-situ* hybridisation on whole embryos or sections of embryos, however these data are qualitative as they do not give information of the levels of genes in these regions. Observations in whole embryos can still give key insights into

the behaviour of the mesendoderm GRN and formulating mathematical models such as how the overexpression or knock down of a gene affects the region in which other genes in the GRN are expressed and the overall expression levels.

Measuring mRNA levels in a uniform population of cells overcomes the problem of having non-uniform distribution of mRNA in a sample. The animal cap system has been utilised to explore mesoderm and endoderm formation in both *Xenopus* [66, 79] and axolotl [139]. Animal caps, the region of the embryo which usually form ectoderm, can be induced to become mesoderm or endoderm by injecting mRNA.

High throughput techniques such as deep sequencing and microarrays are increasingly being used to give expression data on large numbers of genes in a system.

### 1.13.2 Parameter estimation methods

Numerous parameter estimation methods are available to solve the inverse problem, with many of these methods based on optimization algorithms. These algorithms involve searching parameter space either randomly or in ‘intelligent’ directions to minimise the error between the experimental data and the corresponding mathematical simulation, with the error being measured using a fitness function. A common form used for the fitness function is the sum of the least squares

$$F(X_i^{\text{data}}, X_i^{\text{model}}) = \sum_{i=1}^N \left( X_i^{\text{data}} - X_i^{\text{model}} \right)^2 \quad (1.13.1)$$

where  $X_i^{\text{data}}$  are the experimental data,  $X_i^{\text{model}}$  is the output of the model simulation, for  $N$  experimental data points. A fitness function of the form given in (1.13.1) assigns a greater error to data points that are large in magnitude compared with small data points. To overcome this issue a weighted fitness function can be used;

$$F(X_i^{\text{data}}, X_i^{\text{model}}) = \sum_{i=1}^N \omega_i \left( X_i^{\text{data}} - X_i^{\text{model}} \right)^2 \quad (1.13.2)$$

where we define  $\omega_i = 1 / (X_i^{\text{data}})^2$  to be the weighting function.

Algorithms used to estimate parameters can be divided into two main classes, namely local and global methods. Local methods start from an initial guess then search parameter space in the neighbourhood of this guess to find the minimum. Although a local search method usually converges fast to its minimum it often only finds a local, rather than the global, minimum. When applied to finding parameters for a mathematical model of a biological process, finding a local instead of a global minimum would correspond to a parameter set which is different to the true biological parameters. Global search methods overcome this problem by searching the whole parameter space, incorporating a stochastic element. These search methods can start from a random guess of parameters. However, a disadvantage of using a global method is that the algorithm takes more computational time to converge to a minimum. Hybrid methods combine the search of the entire parameter space using a global search, with the fast conver-

gence of a local search. First a global search identifies a 'good' region of parameter space which is then explored further by a local method to find the minimum.

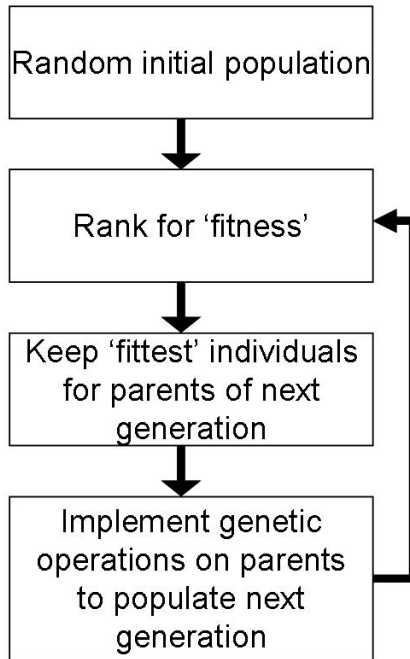
### 1.13.3 The Genetic Algorithm

The genetic algorithm (GA) is a global method which uses an evolutionary search strategy which was developed in 1975 by Holland [59]. The GA has been applied successfully to many biological problems such as a model of glucose metabolism [100] and G-protein signalling [84, 96]. Furthermore evolutionary strategies have been shown to be more successful at solving the inverse problem than other global search techniques [97]. The GA is based on biological evolution, combining a stochastic search with local improvement. Additionally, an initial guess of the parameters is not required since a random initial population is generated. Due to the stochastic nature of the GA many runs of the algorithm are usually carried out to ensure the global minimum is found.

An overview of the concepts used in the GA is now given [148]. An initial population of vectors known as a 'chromosome', containing a value for each model parameter, is generated either randomly or as defined by the user. These chromosomes are then evaluated using a fitness function, then ranked according to their fitness function value. The fittest chromosomes (i.e. those that minimise the fitness function) are retained as "parents" for the next generation. A number of genetic operations are then applied to the parent chromosomes to populate the next generation. Genetic operations include crossovers, mutation and immigration. In a crossover sections of a chromosome (an 'allele') are exchanged between the parent chromosomes to produce two children. A crossover can be simple, where the length of the allele is chosen randomly, or arithmetic, where two randomly generated numbers are used to produce linear combinations of the two parents. A mutation replaces a single element of a chromosome by a randomly generated variable. Finally randomly generated chromosomes (or 'immigrants') enter the population, adding a stochastic element to the algorithm. This new generation is then evaluated and ranked for fitness, and the process repeated for  $N$  iterations (see figure 1.13.3). After  $N$  iterations the final generation is evaluated and the chromosome that minimises the fitness function is selected.

## 1.14 Objectives

Middleton et al. [95] propose mathematical models of a simplified *Xenopus laevis* mesendoderm GRN (figure 1.7A), where multiple members of the Nodal and Mix gene families are combined into a single gene for Nodal and a single gene for Mix. The models consist of systems of non-linear ordinary differential equations, whose solutions give TF concentrations in a single cell. Key features of the mesendoderm GRN are given in the mathematical model, which qualitatively reproduces the observations of Activin dose response experiments [112]. Multicellular models, mimicking the spatial structure of embryos in a line of cells have also been formulated



**Figure 1.14:** Schematic diagram of Genetic Algorithm, this procedure is repeated for  $N$  iterations.

[94]. The aim of this thesis is to provide quantitative mathematical models of mesendoderm formation. To quantify the models, parameter values need to be inferred from experimental data. Gene expression data in the *Xenopus* mesendoderm GRN are difficult to obtain due to multiple genes in both the Mix-like and Nodal-related gene families. However, the axolotl provides a model system of a simplified mesendoderm GRN compared with that of the *Xenopus*, containing only one Mix and two Nodal genes. We therefore choose to explore mathematical models of the mesendoderm GRN using the axolotl as a model system. Initially this will be a qualitative analysis of the network in a single cell. Gene expression data will be obtained and used to seek values for the model parameters. These model parameters will then be used to explore a quantitative model, and make testable predictions about the behaviour of the network. In addition to developing a quantitative model of the axolotl mesendoderm GRN, we extend the mathematical models of the simplified *Xenopus* mesendoderm network to include recent experimental observations about the regulation of Nodal genes, and extra interactions to account for the formation of mesoderm, endoderm and anterior mesendoderm.

## 1.15 Thesis overview

### 1.15.1 Chapter 2

This chapter gives the biological materials and methods used to obtain the experimental data presented in this thesis.



### 1.15.2 Chapter 3

The main aim of this chapter is to give an overview of the differences between the axolotl and *Xenopus* mesendoderm GRNs and to ask how these changes affect the behaviour of the mesendoderm GRN in a single cell using mathematical models. We formulate mathematical model similar to those given for *Xenopus* in [95], but for the axolotl topology. The first model considered is an *in vitro* model, which includes interactions in a single cell downstream of Activin. Analysis of this model finds that bistability is obtainable, with steady states corresponding to mesoderm and anterior mesendoderm. A second model, an *in vivo* model, considers the network downstream of the maternal factors VegT and  $\beta$ -catenin. We find that in the axolotl *in vivo*, a cell can become mesoderm or anterior mesendoderm dependent on the dose of  $\beta$ -catenin it receives. We cite a recent paper about the regulation on Nodal genes by maternal factors in *Xenopus*, motivating a modification to the *Xenopus in vivo* model of [95] and explore how this changes the model behaviour. The models in this chapter are analysed qualitatively, motivated by current biological understanding of the mesendoderm GRN.

### 1.15.3 Chapter 4

The aim of this chapter is to obtain realistic biological values for the parameters in the mathematical models of the axolotl mesendoderm GRN given in chapter 3. We estimate values for these parameters using a computational algorithm which aims to minimise the error between the output of the model and corresponding quantitative biological data. First, we use the animal cap assay to explore the ability of Activin, Nodal1 and Nodal2 to induce mesoderm and endoderm in axolotl animal caps. We find that Activin can induce mesoderm and endoderm in a dose dependent manner, Nodal1 can induce only mesoderm and Nodal2 does not induce mesoderm or endoderm. Since Activin can induce both mesoderm and endoderm, we use qPCR data for the expression of Mix, Brachyury and Goosecoid in Activin injected caps to estimate parameters of a mathematical model. To validate the behaviour of the model, data is obtained for caps treated with Activin and Brachyury morpholino, showing that the model is not consistent with experimental data when Brachyury is removed from the system. This highlights the need for repeated rounds of modelling and experimental testing of predictions to refine the parameters of the mathematical model.

### 1.15.4 Chapter 5

In this chapter mathematical models of the *Xenopus* mesendoderm GRN formulated by Middleton et al [95] are extended to include Vent and BMP. The addition of these factors, which are also involved in dorsal-ventral (DV) patterning, allows the model to account for the formation of mesoderm, endoderm and anterior mesendoderm. The models formulated encompass the time evolution of transcription factors in a single cell and are shown to have steady states corresponding to dorsal and ventral cell fates. Both ‘DV only’ and ‘DV and mesendoderm’ versions of the model are developed and analysed. The ‘DV only’ model shows that the mutual negative

regulation of Vent and Goosecoid allows the formation of dorsal and ventral cells. Numerical results of the ‘DV and mesendoderm’ model shows that cells can become mesoderm, endoderm or anterior mesendoderm dependent on initial levels of VegT and  $\beta$ -catenin, with results comparing favourably with experimental data.

### 1.15.5 Chapter 6

In the final chapter, we explore multicellular models of the *Xenopus* and axolotl mesendoderm GRNs. We give a summary of the model of the *Xenopus* mesendoderm GRN in a line of cells from [94], then formulate a comparable model for the axolotl mesendoderm GRN. The solutions to this model uncover potential mechanisms for the formation of the germ layers in a population of cells. The models are then extended into a grid of hexagonal cells. We explore the models of Nodal regulation introduced in chapter 3 in a full model of Nodal signalling and the resulting patterns of P-Smad2 in a grid of cells representing the embryo. We find that the patterns of P-Smad2 compare favourably with experimental data in *Xenopus*. Furthermore the models give a testable prediction for the localisation of P-Smad2 in axolotl. Models are also explored downstream of Nodal, where the expression patterns of Mix and Brachyury are similar to those observed experimentally. In order to explore the Nodal signalling pathway in axolotl experimentally, and to obtain data that can be used in developing the multicellular model further, we also clone axolotl Antivin and measure its expression in whole embryos and *Nodal*-injected animal caps.

## CHAPTER 2

# Materials and Methods

## 2.1 Solutions and buffers

1x Modified Barth's Solution (MBS)	88 mM NaCl; 1 mM KCl, 2.4mM NaHCO <sub>3</sub> ; 15 mM Hepes; 0.3 mM CaNO <sub>3</sub> ; 0.41 mM CaCl <sub>2</sub> ; 0.82 mM MgSO <sub>4</sub> . pH 7.8 with NaOH and autoclave
10x MMR	1 M NaCl, 20 mM KCl, 20 mM CaCl <sub>2</sub> .6H <sub>2</sub> O, 10mM MgCl <sub>2</sub> , 50 mM Hepes to pH 7.5
Axolotl antibiotics	10 mg/ml penicillin/streptomycin; 10 mg/ml fungizone; 10 mg/ml kanamycin
Agarose plates	2% agarose in dH <sub>2</sub> O + 0.1% Tris-HCl pH8
SOC	20 g Bacto Tryptone; 5 g Bacto Yeast; 10 mM NaCl; 2.5 mM KCl; 10 mM MgCl <sub>2</sub> ; 10 mM MgSO <sub>4</sub> ; 20 mM Glucose
RNA-gel loading dye	95% formamide; 0.025% xylene cyanol; 0.025% bromophenol blue; 18 mM EDTA; 0.025% SDS
DNA-gel loading dye	0.1% Bromophenol blue, 0.1% Xylene Cyanol FF, 30% glycerol
Mu Agar	Mu Broth containing 15 g Bacto Agar /litre
Elution buffer	10 mM Tris-HCl, pH 7.5; 1 mM EDTA; 50 mM NaCl
TE buffer	10 mM Tris-HCl (pH 7.5); 1 mM EDTA
50X TAE	2M Tris-acetate, 0.05 M EDTA

## 2.2 Treatment and preparation of embryos

### 2.2.1 Micro-injection

Injections were done using micromanipulation and needles pulled using a micropipette puller. Injections were carried out in injection plates; petridishes with a well for stability under 1x MBS + 4% Ficoll<sub>400</sub> (Sigma) with appropriate antibiotics as described in section 2.1.

### 2.2.2 Axolotl embryos

Male and female axolotls were housed separately. Natural matings were set up by co-housing a male and female. Fertilised embryos were manually dejellied using forceps and maintained at 10°C in 1xMBS + antibiotics until required. One or two cell embryos were injected in the animal hemisphere with 2x 4nl injections (one per blastomere) in 1x MBS + 4% Ficoll + antibiotics. Injected embryos were cultured at 18°C in 1x MBS + 4% Ficoll + antibiotics until stage 9 when

they were washed down to 0.2x MBS + antibiotics and cultured until they had reached the required stage. Embryos were staged according to [4].

### 2.2.3 Microscopy and photography

Embryos were visualised under Nikon SMZ 1500 microscopes. Photographs were taken using a Nikon DXM 1200F camera. Embryos/caps were photographed on agarose plates to allow orientation of embryos/caps.

### 2.2.4 Morpholinos

Morpholinos were hydrated in non-DEPC treated nuclease-free water (Ambion) to 40 ng/nl and resuspended by heating to 65°C and cooling to 4°C twice. Hydrated morpholinos were stored at 4°C until required. Before injection, morpholinos were heated to 65°C, centrifuged and aliquots taken and stored at 37°C until they were mixed with the appropriate mRNA and injected. The morpholinos used in this thesis are:

AxBra Sp1 Morpholino 5'-TGATCTGTAGAGAGAGAAGGACAGT-3'

AxBra Sp2 Morpholino 5'-TCCCCCACCACCACTCACCGCTCCT-3'.

## 2.3 Extraction of RNA

### 2.3.1 RNA extraction

Axolotl embryos or animal caps were collected and placed in autoclaved 1.5ml eppendorf tubes with a minimal amount of liquid and were snap-frozen at -80°C and stored at -80°C until required.

Five frozen axolotl embryos (up to stage 20) were homogenised in 500µl TRI-REAGENT™ (Sigma) using homogenising sticks. A further 750µl of TRI-REAGENT™ was added to bring the final volume to 1.25 ml before spinning in a bench-top centrifuge at 13,000 rpm for 5 minutes at room temperature. The supernatant was decanted into a fresh 2.0ml tube and made up to 1.5ml with fresh TRI-REAGENT™ and left to stand for 5 minutes at room temperature. 0.2x volume of chloroform was added to the supernatant which was vortexed briefly and left to stand for 5 minutes at room temperature before spinning at 13,000 rpm for 10 minutes at room temperature. The aqueous colourless phase containing RNA was decanted and phenol:chloroform extracted. 0.5x volume of isopropanol was added to the aqueous phase collected after phenol:chloroform extraction, vortexed and precipitated at 4°C for 15 minutes and spun for 10 minutes at 13,000 rpm at room temperature. The pellet, containing RNA, was resuspended fully in 250 µl non-DEPC treated nuclease free water (Ambion) and an equal volume of 8M lithium chloride was added to precipitate the RNA. Eppendorfs were vortexed to mix and precipitation took place at 4°C for 24 hours. After precipitation samples were spun at

13,000rpm for 15 minutes at room temperature. The supernatant was carefully removed (the pellet is transparent) and the pellet washed with 70% ethanol at room temperature, vortexed, and spun for 5 minutes at 13,000rpm at room temperature. Ethanol was removed and the pellet allowed to briefly air dry before being resuspended in 10 $\mu$ l non-DEPC treated nuclease free water (Ambion) per embryo extracted.

### **2.3.2 DNase1 treatment of RNA**

The extracted RNA was treated with recombinant (r) DNase1 (Ambion), to remove genomic contamination. rDNase1 was removed with DNase inactivation reagent (Ambion) according to manufacturer's guidelines. Concentrations were determined and quality checked on 1.2% agarose gels. Samples were stored at -80°C until required.

## **2.4 Analysis of gene expression by Reverse Transcriptase (RT-PCR)**

### **2.4.1 RT-PCR**

PCR reactions were carried out in a final volume of 20 $\mu$ l and consisted of 1 $\mu$ l REDTaq Ready Mix<sup>TM</sup> PCR reaction mix (Sigma), 7 $\mu$ l dH<sub>2</sub>O, 1 $\mu$ l cDNA and forward and reverse primers at a final concentration of 1mM. RT-PCRs were run in Techne thermal cyclers according to the following programme; after an initial denature of 95°C for 5 minutes the PCR consisted of 20 cycles with denaturing at 94°C for 45 seconds, annealing at T<sub>m</sub> -5°C for 45 seconds and the extension at 72°C for 90 seconds. Samples were then run on a 1.2% agarose gel for virtual Northern analysis. 30 cycle PCRs were carried out to visualise DNA by ethidium bromide staining.

### **2.4.2 cDNA synthesis**

cDNA synthesis was carried out using SuperScript<sup>TM</sup> III (Invitrogen) as described by the manufacturer. In a 20 $\mu$ l reaction, 500ng total RNA was used to make cDNA from animal caps and 1 $\mu$ g RNA was used to make cDNA from whole embryos in the presence of 200ng of random hexamer primers. Reverse transcriptase reactions took place at 50°C for 60 minutes with the synthesised cDNA stored at -20°C until required. For qRT-PCR, cDNA synthesis reactions were set up as described and mixed together and diluted with 30 $\mu$ l non-DEPC treated nuclease free water (Ambion) per reaction. cDNA samples were then stored at -20°C.

### 2.4.3 Real-time qPCR

For relative quantification of gene expression in morpholino assays and on developmental series, qRT-PCR was performed using the ABI 7500 Sequence Detection System (Applied Biosystems) with TaqMan fluorescence resonance energy transfer (FRET) technology. qRT-PCRs were carried out in triplicate on 96 well Fast plates (Applied Biosystems) in 25 $\mu$ l reactions. All tubes were vortexed briefly and spun down prior to use. Reactions contained 1 $\mu$ l cDNA; 1x qPCR mix with ROX (ABgene), 200 nM final concentration of both forward and reverse primers, 5 pmol of probe. Reactions were made up to 25 $\mu$ l with non-DEPC treated nuclease free water (Ambion). Plates were sealed with optical adhesive film (Applied Biosystems) briefly spun to remove air bubbles and run on an AB 7500 sequence detection system. The program followed is: 50°C for 2 minutes, 94°C for 15 minutes followed by 40 cycles of 94°C for 15 seconds and 60°C for 1 minute.

### 2.4.4 Primers and probes

Primers and probes were designed using Primer Express version 3.0 software (Applied Biosystems) according to manufacturer's instructions. Primers (Invitrogen) were resuspended to a final concentration of 10 $\mu$ M, aliquoted and stored at -80°C. Probes (Sigma) are dual-labelled fluorogenic probes (5' FAM; 3' TAMRA) and HPLC purified. Probes were aliquoted and stored at -80°C until required. Working stocks were stored at -20°C. Primer and probe sequences are shown below:

	Forward (5'-3')	Reverse (5'-3')
AxNodal1	CCCAGTGGATGAAACGTTTCAG	GGGTCGGGTGGTACAGCTT
AxNodal2	CATACCGCTGTGATGGAAAGTG	CCCGCTCTGGAATGTACAATT
AxBrachyury	CATTGACCACATGTACCAATTGC	GATCAAGGGTCAATCGTGAGTTC
AxMix	GTCCAGGATCCAGGTCTGGTT	GCTTCTGGGTGGATTGATTATAA
AxFGF8	TGCAGGTCCTTGGAACAA	AAGGTGTCCGTTTCCACAATTAA
AxSox17	TGGATACGACGCTCCACAGA	CTCCCTGTAGTGGCCGATGT
AxGsc	GCCTCTTCCAGGAGACCAAGT	TGGCTCTGCGGTTCTTGAAC
AxODC	ATGCCCGTCATGAGTAGTACCA	CCCGGACCCAGGTTTACG
	Probe (5'-3')	
AxNodal1	CGACGAATCATGCCTACATGCAGAGC	
AxNodal2	AGCATTTCCAGCCCACCAACCATG	
AxBrachyury	TACCCATAGTTCTTTGTGCAGCATCCACG	
AxMix	AATAGGCGTGCCAAGTCCCGCC	
AxFGF8	ACGGCGACTCGCACGCCA	
AxSox17	CATGAGCAGCAGTCCAGCAGGACAAC	
AxGsc	CACCCGAGAGCAGCTGGCCC	
AxODC	GACAGTCCAAGTTTCATTCAATTGCTG	

### 2.4.5 Data analysis

qRT-PCR data were analysed by the comparative CT method [88]. Validation experiments were carried out on a 4-fold dilution series of cDNAs from 1 to 1/256 to ensure the PCR efficiencies of the target and endogenous reference, (ODC), were approximately equal. The data were analysed in excel (Microsoft) and graphs were plotted of the ratio of gene expression relative

to uninjected for morpholino-injected embryos, and relative to stage 12 for the developmental series. Error bars are one standard deviation of the sample.

## 2.5 Genome walking

The GenomeWalker™ Universal kit (Clontech) was used according to manufacturer's guidelines to produce 4 GenomeWalker libraries from axolotl DNA (prepared by Yi-Hsien Chen). The primary and secondary round of PCR were carried out as described below:

### 2.5.1 Primary PCR

The PCR reactions were carried out in a final volume of 25 $\mu$ l, consisting of 12.5 $\mu$ l master mix1 (Thermo Scientific), 9.5 $\mu$ l dH<sub>2</sub>O, 1 $\mu$ l AP1 (Clontech), 1 $\mu$ l GSP1 (10 $\mu$ M) and 1 $\mu$ l of cDNA library. PCRs were run in Techne thermal cyclers according to the following program; 7 cycles of 94°C for 25 seconds and 72°C for 5 minutes, followed by 32 cycles at 94°C for 25 seconds and 67°C for 5 minutes, then held at 67°C for an additional 7 minutes. 5 $\mu$ l of the primary PCR product was then run on a 1.2% agarose gel for visualisation.

### 2.5.2 Secondary PCR

The PCR reactions were carried out in a final volume of 25 $\mu$ l, consisting of 12.5 $\mu$ l master mix1 (Thermo Scientific), 9.5 $\mu$ l dH<sub>2</sub>O, 1 $\mu$ l AP2 (Clontech), 1 $\mu$ l GSP2 (10 $\mu$ M) and 1 $\mu$ l of dilute (1 in 20) primary PCR product. PCRs were run in Techne thermal cyclers according to the following program; 7 cycles of 94°C for 25 seconds and 72°C for 5 minutes, followed by 25 cycles at 94°C for 25 seconds and 67°C for 5 minutes, then held at 67°C for an additional 7 minutes. The secondary PCR product was then run on a 1.2% agarose gel for visualisation. The PCR product was then extracted, cloned and sequenced as described in sections 2.5.4– 2.5.7.

### 2.5.3 Agarose gel electrophoresis

Digested DNA and transcribed RNA both for probes and embryo injections were analysed on 1.2–2.0% (w/v) agarose in 1x TAE gels and were run in 1x TAE. Ethidium bromide was added to gels, to intercalate with nucleic acids, at a final concentration of 1 $\mu$ g/ml. For electrophoresis, DNA samples were mixed to give 1x DNA-loading buffer. 100bp and 1Kb DNA ladders (NEB) were run alongside samples to identify sizes. Pictures were taken by placing gels in a MultiMage™ light cabinet and photographed using an AlphaImager™ 1220 Documentation & Analysis System (Alpha Innotech Corporation).

### **2.5.4 Purification of DNA from agarose gels**

DNA run on agarose gels was visualised using a low intensity UV transilluminator and excised from the gel using a scalpel. DNA fragments were extracted from agarose gels using Spin columns from QIAquick gel extraction Kit (QIAGEN) according to manufacturer's guidelines.

### **2.5.5 Ligation of DNA fragments**

Insert and vector were mixed together at a ratio of approximately 3:1. 1 $\mu$ l T4-DNA ligase and buffer to 1x (NEB) were added to 10 $\mu$ l reactions and incubated for 5 hours at room temperature or overnight at 14°C.

### **2.5.6 Transformations**

70 $\mu$ l of competent E. coli (strain DH5 $\alpha$ ) were incubated on ice with 50-100 ng of plasmid DNA for 30 minutes. The cells were heat shocked at 42°C for 45 seconds to allow plasmid uptake and then cooled on ice for 90 seconds. 250 $\mu$ l of SOC media was added and the cells were incubated at 37°C for 1 hour. 50 $\mu$ l to 100 $\mu$ l of the transformation mixture were spread onto Mu agar plates containing the appropriate antibiotic which were incubated at 37°C overnight. For blue/white selection, 30 $\mu$ l of 20mg/ml X-GAL and 30 $\mu$ l 100 mM IPTG were spread onto the agar prior to plating the transformation.

### **2.5.7 DNA sequencing**

DNA sequencing was carried out entirely by GeneService. PCR reactions contained 50 ng of DNA, 5 $\mu$ M of primer (T3/T7/SP6), 1 $\mu$ l sequencing buffer (Applied Biosystems) and 1  $\mu$ l Big Dye Mix (Applied Biosystems) made up to final 10 $\mu$ l volume with dH<sub>2</sub>O. PCR program was: 25 cycles at 96°C for 30 seconds, 50°C for 15 seconds and 60°C for 4 minutes. DNA was precipitated in 50 $\mu$ l ethanol and Sodium Acetate (pH5.6) to a final concentration of 0.1 M for 15 minutes at room temperature. Tubes were spun at 13,000 rpm for 5 minutes at room temperature in a bench top microfuge and the supernatant removed. The pellet was washed with 150 $\mu$ l of 80% ethanol and spun at 13000 rpm for 5 minutes at room temperature in a benchtop microfuge. The supernatant was removed and pellet air dried at room temperature and sent to GeneService for sequencing using ABI 3730 DNA sequencing technology.

### **2.5.8 Sequence analysis and comparisons**

NCBI BLAST (version 2.2.18) was used to determine sequence comparisons. All sequences were analysed in BioEdit [49]. Alignments were carried out using the ClustalW Multiple alignment application built in to BioEdit [145].



## 2.6 Developmental series

Total RNA was isolated by TRI reagent (sigma) and RT-PCR was according to RedTaq readyMix PCR reaction (sigma). Axolotl development series contains 13 different samples: (EC) early cleavage: 4-8 cells, (LC) late cleavage: 8-16 cells, stage 8, 9, 10.5, 12, 16, 20, 25, 30, 35, 40 and ÚRT (negative control). PCR primers used for gene expression are: AxAntivin forward primer: 5' CAAGCAGAGCAACGTCTGCTG 3' and AxAntivin reverse primer; 5' TCACACCACGGA-GATGTTGTC 3'.

# Single-cell Models of Mesendoderm Specification in *Xenopus* and Axolotl

## 3.1 Introduction

In the previous chapter we introduced the axolotl as a model organism with a simpler mesendoderm GRN than *Xenopus*. However the genetic regulation of mesoderm and endoderm has been extensively studied in *Xenopus* (see [89, 149] and references therein), while studies in axolotl are rather limited in comparison [139]. We begin this chapter by giving a review of the mathematical models developed by Middleton et al [95] based on a simplified version of the mesendoderm GRN in *Xenopus*. We then develop mathematical models of mesendoderm formation based on current knowledge of the mesendoderm GRN in the axolotl. The time evolution of transcription factors in a single cell are described in the model, which is shown to have stable steady states corresponding to mesoderm and anterior mesendoderm cell types. We consider two versions of the model; an *in vitro* model showing how the dose of Activin a cell is subjected to determines cell fate, and an *in vivo* model which explores the behaviour of the GRN in response to doses of  $\beta$ -catenin. Numerical investigations show that the models qualitatively reproduce experimental data, and can be used to motivate further experiments. We then modify the *Xenopus in vivo* model formulated in [95] based on recent experimental evidence, showing that the resulting numerical results are consistent with experimental observations.

## 3.2 Mesoderm and endoderm formation in *Xenopus*

The GRN underlying the formation of mesoderm and endoderm in *Xenopus laevis* contains around 50 TFs and signals and is described in [75, 89]. Important genes within the network include the maternal factors VegT and  $\beta$ -catenin and zygotic factors *Mix.1*, *Brachyury*, *Goosecooid* and the *Nodal* family. The maternal factors VegT and  $\beta$ -catenin are expressed in specific regions of a developing *Xenopus* embryo; VegT is localised to vegetal regions [155] and  $\beta$ -catenin is ex-

pressed in dorsal regions [126]. VegT and  $\beta$ -catenin initiate the expression of zygotic genes, such as members of the *Nodal* family, *Mix.1* and *Brachyury*, providing initial positional information in the embryo. Mesoderm and endoderm cell types can be identified by the genes expressed; *Brachyury* expressing cells form mesoderm and *Mix.1* expressing cells form endoderm. Competition between the formation of mesodermal and endodermal cell types is created by mutual negative regulation of *Mix.1* and *Brachyury*. The mutual repression of two transcription factors is a common mechanism in GRNs underlying the specification of two different cell fates, for example in the *Drosophila* gap gene network [111] and hematopoietic stem cell differentiation [120].

*Xenopus Nodal* genes (*Xnr1-Xnr6*) are expressed in response to VegT and  $\beta$ -catenin and act as morphogens during development, activating Activin-like signals. Since multiple *Nodal* genes are required to induce mesoderm and endoderm in *Xenopus*, Activin (a protein which activates the same signalling pathway as Nodals) can be used to investigate the induction of mesoderm. Activin dose response experiments have been carried out in both single cells [43, 48, 112] and whole tissues [46, 47, 112], showing that *Brachyury* is expressed in cells treated with a low dose of Activin and *Mix.1* and *Goosecoid* are co-expressed in cells treated with a high dose of Activin.

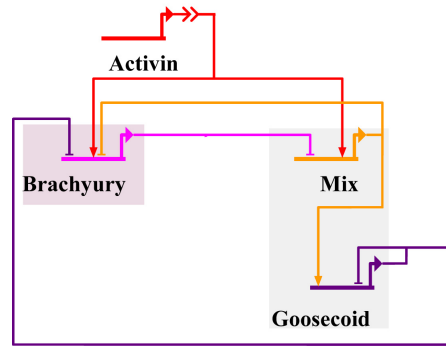
Much of the complexity of the *Xenopus* mesoderm GRN arises due to the presence of seven *Mix-like* genes (*Mixer*, *Mix.1-2*, *Bix.1-4*) and six *Nodal-related* genes (*Xnr.1-6*). Motivated by the presence of single copies of *Mix* and *Nodal* in mammals [45, 157], a simplified version of the *Xenopus* mesoderm GRN with single nodes representing *Mix* and *Nodal* is proposed in [95]. The behaviour of this simplified network is explored using mathematical models in [95], which we give a detailed review of in section 3.2.1. Saka and Smith [123] formulate a mathematical model of mesoderm formation in *Xenopus*, focusing on the mutual negative regulation of *Brachyury* and *Goosecoid*, showing that a simple negative feedback loop is able to account for the formation of different cell types. ODE models of the Sea Urchin mesoderm GRN are formulated and explored in [76, 77]. These models explore subnetworks of the full GRN comparing simulation results to experimental data, motivating the need for further experimental investigation.

### 3.2.1 Mathematical models of the simplified *Xenopus* mesoderm GRN

We now describe the mathematical models of the simplified mesoderm GRN formulated by Middleton et al [95] and give a summary of key model findings. Two versions of the model are considered, namely the *in vitro* model and the *in vivo* model.

#### The *in vitro* model of Middleton et al [95]

The *in vitro* model aims to reproduce qualitatively *Xenopus* animal cap experiments whereby *Brachyury* is expressed at low Activin concentrations and *Goosecoid* is expressed at high Activin concentrations [48, 112]. An ODE model is formulated based on the interactions of *Brachyury*

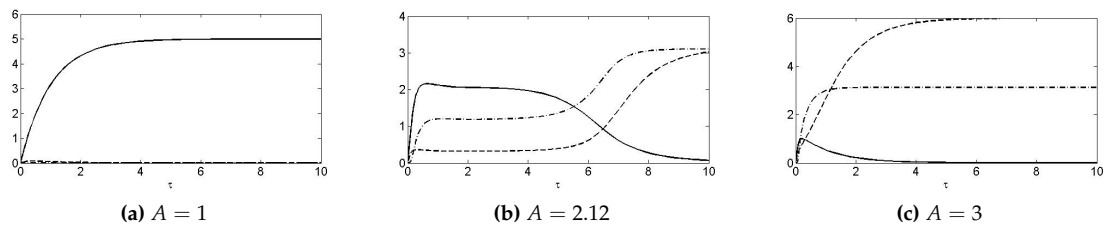


**Figure 3.1:** The simplified *Xenopus* mesenteroderm GRN downstream of Activin, upon which the *Xenopus in vitro* is based [95]. Arrow heads and bar heads represent activation and repression, respectively. The purple and blue boxes show the two competing gene subgroups which arise due to the mutual repression between Brachyury and Mix (together with Goosecoid).

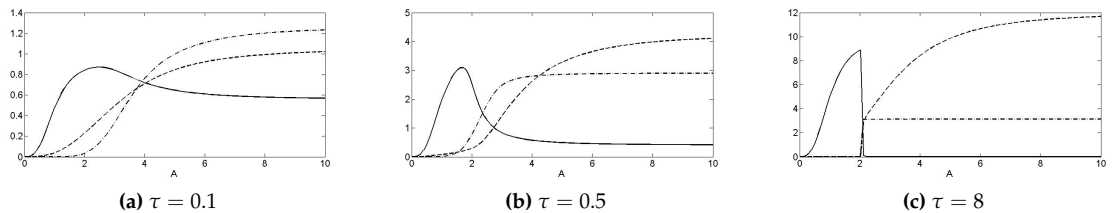
(B), Mix (*M*) and Goosecoid (*G*) downstream of Activin (*A*) shown in figure 3.1. Activin induces the expression of Mix and Brachyury, which negatively regulate each other. Mix also activates Goosecoid which acts to repress both its own expression and that of Brachyury. Both steady state and time-dependent solutions are explored in detail in [95]. Here we give a brief summary of important findings. For an appropriate choice of parameters the *in vitro* model is bistable, with stable steady states corresponding to mesoderm (Brachyury expressing cells) and anterior mesenteroderm (cells co-expressing Mix and Goosecoid). Furthermore, time-dependent solutions show that the concentration of Activin a cell is treated with determines which steady state the system reaches. At low concentrations of Activin, the system evolves to the stable steady state corresponding to mesoderm (figure 3.2(a)), while for high concentrations of Activin, the system evolves to the anterior mesenteroderm stable steady state (figure 3.2(c)). At an intermediate concentration of Activin the system passes through a ‘mesenteroderm’ phase, where Mix, Goosecoid and Brachyury are all co-expressed for a period of time, before the system ultimately evolves to one of two stable steady states (in the case shown in figure 3.2(b), the anterior mesenteroderm steady state). The ‘mesenteroderm’ phase corresponds to the solution passing close to the unstable steady state of the system. Figure 3.3 plots concentrations of Mix, Goosecoid and Brachyury as functions of Activin concentration at three time points,  $\tau = 0.1$ ,  $\tau = 0.5$  and  $\tau = 8$ . Initially all three transcription factors are co-expressed for all doses of Activin (see  $\tau = 0.1$ , figure 3.3(a)). As time proceeds the expression domains of Mix, Brachyury and Goosecoid become more refined, until Brachyury alone is expressed for low doses of Activin and Mix and Goosecoid are co-expressed at high doses of Activin (see figure 3.3(b), (c)). The qualitative numerical results of the *in vitro* model are consistent with quantitative experimental data.

#### The *in vivo* model of Middleton et al [95]

The *in vivo* model describes the simplified mesenteroderm GRN downstream of the maternal factors VegT and  $\beta$ -catenin, based on the interactions illustrated in figure 3.4. The model gives the network in a single cell within a uniform population of cells, such that signals (Nodal and



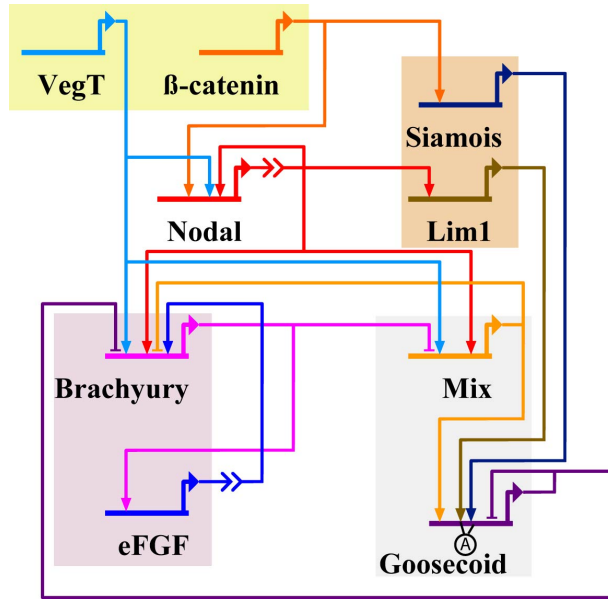
**Figure 3.2:** Plots showing the time evolution of Brachyury (solid line), Mix (dashed line) and Goosecoid (dot-dashed line) for various doses of Activin ( $A$ ). **(a)** For small  $A$  the system evolves to the mesoderm (i.e. Brachyury expressing) stable steady state. **(b)** For  $A$  close to some critical value  $A^c$ , solutions pass close to the unstable steady state (marked by the co-expression of all three transcription factors) before evolving to one of the stable steady states (in this case anterior mesendoderm). **(c)** For values of  $A$  greater than the critical value ( $A > A^c$ ) the system evolves to the anterior mesendoderm (Mix and Goosecoid co-expressing) steady state. Solutions are computed by the `ode15s` solver in `Matlab`, using the equations and parameters as given in [95].



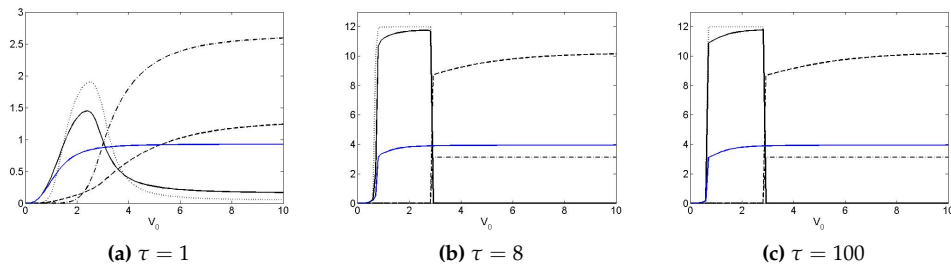
**Figure 3.3:** Numerical solutions of the *Xenopus in vitro* model as functions of Activin concentration ( $A$ ). The response of Brachyury (thin solid line), Mix (dashed line) and Goosecoid (dot-dashed line) are shown. Solutions are computed by the `ode15s` solver in `Matlab`, using equations and parameters as given in [95].

eFGF) are assumed to be strong enough to act on downstream targets. The model is shown to have stable steady states corresponding to mesoderm and anterior mesendoderm which can be reached dependent on the initial concentration of VegT present in the cell, reproducing experimental observations. Solutions to the *in vivo* model are plotted as functions of initial VegT concentration ( $V_0$ ) in figure 3.5. If  $V_0$  is too small, the system evolves to the trivial steady state. For small  $V_0$ , the system will evolve to the mesoderm branch. Increasing  $V_0$  through some critical value ( $V_0^C$ ) causes the system to evolve to the anterior mesendoderm branch. A further investigation shows that in the presence of  $\beta$ -catenin, the range of values of VegT for which mesoderm is induced increases (see [95]).

In constructing the simplified mesendoderm GRN from the full GRN, assumptions are made about how the single representative nodes for Mix and Nodal genes function in the network. The *Xenopus* Nodal genes (*Xnr1-Xnr6*) all have slightly different functions and modes of regulation. The assumptions underlying the mode of action of the single Nodal are discussed in further in section 3.8.



**Figure 3.4:** The *in vivo* simplified *Xenopus* mesendoderm GRN, upon which the *in vivo* model of [95] is based. Arrow heads and bar heads represent activation and repression, respectively. Maternal factors are shown in the yellow box and all other transcription factors and signals are zygotic. Nodal and eFGF genes encode signals while all other genes encode transcription factors. An 'A' indicates that an input is, in Boolean terms an 'AND' gate. Otherwise multiple inputs to a gene correspond to an 'OR' gate.



**Figure 3.5:** Numerical solutions to the *Xenopus in vivo* model as functions of initial VegT concentration ( $V_0$ ) at various times ( $\tau$ ). The response of Brachyury (thin solid line), eFGF (dotted line), Mix (dashed line), Goosecoid (dot-dashed line) and Nodal (blue solid line) are shown in response to an initial concentration of VegT. Solutions are computed by the `ode15s` solver in `Matlab`, using equations and parameters as given in [95].

### Summary

Both the *in vitro* and *in vivo* models of the simplified *Xenopus* mesendoderm GRN qualitatively reproduce experimental observations, with stable steady states representative of mesoderm and anterior mesendoderm being reached dependent on the initial dose of Activin (the *in vitro* case) or VegT (the *in vivo* case). Since no information is available about the biological values for model parameters, such as turnover rates of proteins and rates of production of a protein in response to a TF, the analysis of the models is qualitative. The mesendoderm GRN consists of several genes, many which are regulated by multiple TFs and signals, making some model

parameters difficult to measure directly. Instead parameter values can be inferred by fitting the output of model simulations to experimental data. Recall that, in the mathematical models of the *Xenopus* mesendoderm GRN, the inputs of multiple Mix and Nodal genes were combined to give a single representative gene for each family, meaning that data for these representative genes is difficult to obtain. To overcome this problem, we propose using axolotl as a model system for a simplified mesendoderm GRN. Axolotl possess one Mix gene and two Nodal genes giving a model system with a simplified mesendoderm GRN. In the remainder of this chapter we formulate and analyse models of the axolotl mesendoderm GRN.

### 3.3 Mesendoderm formation in axolotl

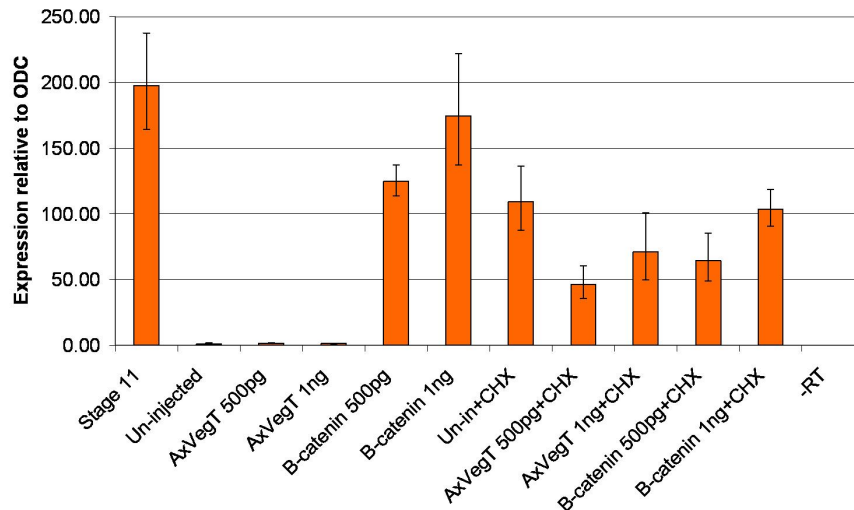
Recall from section 1.8 that there are several differences in mesendoderm formation between axolotl and *Xenopus*. Most importantly, the axolotl mesendoderm GRN contains only one Mix gene and one Nodal gene, giving a simpler network to study than the *Xenopus* mesendoderm GRN. Other differences include a change in the regulation of Brachyury by Mix, and the role of maternal factors. In this section we test whether Goosecoid is a direct target of  $\beta$ -catenin in axolotl.

#### Is Goosecoid a directly regulated by $\beta$ -catenin?

If Siamois is removed from figure 1.7(b), then the maternal factor  $\beta$ -catenin functions only via Nodal signalling in the axolotl mesendoderm network. However it is not know if Goosecoid is directly or indirectly regulated by  $\beta$ -catenin. To determine this, we measured the expression of Goosecoid in caps overexpressing  $\beta$ -catenin and treated with cycloheximide (CHX) to prevent protein synthesis (see figure 3.6). Goosecoid has been shown to be expressed downstream of  $\beta$ -catenin, but not VegT, in axolotl. In uninjected caps treated with CHX, Goosecoid is upregulated, suggesting that CHX alone can induce Goosecoid expression. Caps injected with  $\beta$ -catenin and treated with CHX show lower levels of Goosecoid than caps injected with  $\beta$ -catenin in the absence of CHX. This suggests that Goosecoid is not a directly regulated by  $\beta$ -catenin and that acts via an intermediate transcription factor.

### 3.4 Model formulation

In this section we formulate mathematical models of the axolotl mesendoderm GRN based on the network topology shown in figure 3.7. Note that not all of the links in the GRN have been verified experimentally, so some links (marked by dashed lines) are inferred from the *Xenopus* mesendoderm GRN. We write an equation governing the time evolution of each gene in the axolotl mesendoderm GRN, using an approach similar to that of Middleton et al [95]. Two versions of the model are developed representing the GRN in a single cell; the *in vitro* model giving the mesendoderm GRN downstream of Activin in a single dissociated cell, and the *in vivo* model which describes the mesendoderm GRN downstream of  $\beta$ -catenin in a single



**Figure 3.6: Determining if Goosecoid is a directly regulated  $\beta$ -catenin.** Embryos were injected with either VegT or  $\beta$ -catenin at the single cell stage. By stage 7, embryos were cultured either with or without cycloheximide and caps cut at stage 9. The injection and treatment of caps was carried out by Yi-Hsien Chen and qPCR measurements were carried out by myself (Laura Brown). The expression of Goosecoid was measured relative to ODC by qPCR. The data shown is normalised to Goosecoid expression in uninjected caps.

Protein	Signal or TF	Protein Concentration
$\beta$ -catenin	signal	$C$
Nodal	signal	$N$
Activin	signal	$A$
Mix	TF	$M$
Brachyury	TF	$B$
Goosecoid	TF	$G$
FGF	signal	$E$
Lim1	TF	$L$

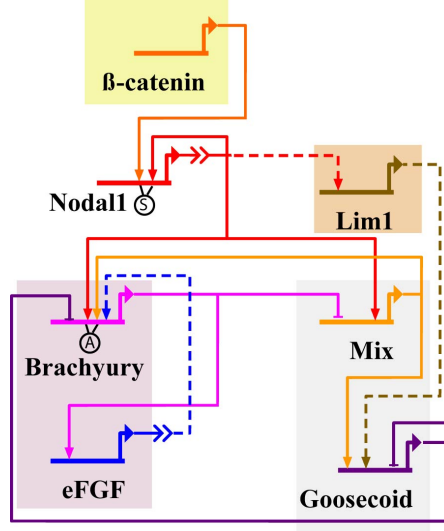
**Table 3.1:** Summary of genes present in the axolotl mesendoderm network, with the notation used in the mathematical models for the concentration of each protein.

cell embedded in a uniform population of cells. A summary of the terms, and a definition of parameters, used to formulate our equations was given in section 1.11, and notation used to describe the concentration of each protein in the mesendoderm GRN is given in table 3.1.

### 3.4.1 Modelling the regulation of mesodermal and endodermal genes in axolotl

The regulation of each gene present in the axolotl mesendoderm GRN is now described, stating which interactions are known from experimental knowledge in axolotl and which interactions are inferred from knowledge of gene regulation in *Xenopus*. Terms that are different from those in the *Xenopus* models of [95] are highlighted in red.





**Figure 3.7:** The axolotl mesendoderm GRN. Solid lines indicate experimentally verified links and dashed lines indicate links which are inferred from the *Xenopus* mesendoderm network, which need to be verified experimentally.

### The time evolution of $\beta$ -catenin

$\beta$ -catenin is deposited as a maternal factor in the embryo. In the model this is represented by an initial concentration  $\beta$ -catenin. The initial deposit of  $\beta$ -catenin is turned over at a constant rate  $\mu_C$ . The concentration of  $\beta$ -catenin is governed by the equation

$$\frac{dC}{dt} = -\mu_C C. \quad (3.4.1)$$

Note that (3.4.1) can be solved to give the concentration of  $\beta$ -catenin at time  $t$  as

$$C(t) = C_0 e^{-\mu_C t}, \quad (3.4.2)$$

where  $C_0$  is the initial concentration of  $\beta$ -catenin.

### The time evolution of Nodal1

Nodal1 is a direct target of  $\beta$ -catenin ( $C$ ), with  $\beta$ -catenin activating the expression of Nodal1 [16]. We assume, as occurs for the *Xenopus* Nodals *Xnr1,2,4*, that axolotl Nodal1 autoregulates its own production enhanced by the presence of  $\beta$ -catenin. The time evolution of Nodal1 is governed by

$$\frac{dN}{dt} = \lambda_{C,N} \mathcal{H}\left(\frac{C}{\theta_{C,N}}\right) + \lambda_{N,N} \mathcal{H}\left(\frac{N}{\theta_{N,N}}\right) \left\{ 1 + \lambda_{C,N2} \mathcal{H}\left(\frac{C}{\theta_{C2,N}}\right) \right\} - \mu_N N. \quad (3.4.3)$$

Note that the equation for the time evolution of Nodal1 appears only in the *in vivo* model.

### The time evolution of Activin

Activin appears in the *in vitro* model, and not the *in vivo* model. In the *Xenopus in vitro* model, it was assumed that the input of Activin is a constant parameter, rather than a variable. This is supported by biological evidence whereby a cell can remember the concentration of Activin it is initially exposed to via the maintenance of a pool of phosphorylated Smad2 [10]. We assume that this memory of the level of Activin is a general feature of Activin signalling, and set Activin to be a constant parameter in our models.

### The time evolution of Mix

Nodal1 or Activin is required to activate the expression of Mix, with these signals being the only factors in our model which induce Mix. Brachyury acts to repress the expression of Mix. These interactions have been experimentally verified in axolotl [139], leading to the following equation for the time evolution of Mix

$$\frac{dM}{dt} = \lambda_{X,M} \mathcal{H} \left( \frac{X}{\theta_{X,M}} \right) \left\{ 1 - \mathcal{H} \left( \frac{B}{\theta_{B,M}} \right) \right\} - \mu_M M, \quad (3.4.4)$$

where  $X = A$  in the *in vitro* model and  $X = N$  in the *in vivo* model.

### The time evolution of Goosecoid

The expression of Goosecoid can be activated by Mix. In the *Xenopus* mesendoderm GRN, both Siamois and Lim1 are required to be present to activate Goosecoid in the absence of Mix. Since Siamois is not present in axolotl, we assume that Lim1 ( $L$ ) alone can activate Goosecoid in the absence of Mix. We also assume that Goosecoid negatively autoregulates its own production. The time evolution of Goosecoid is therefore given by

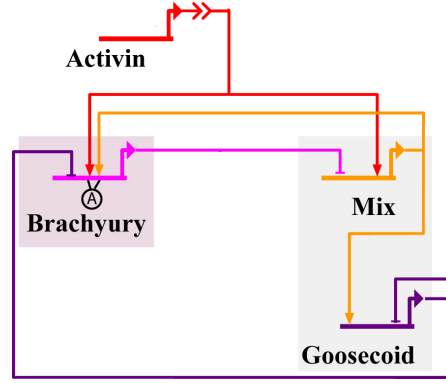
$$\frac{dG}{dt} = \left\{ \lambda_{L,G} \mathcal{H} \left( \frac{L}{\theta_{L,G}} \right) + \lambda_{M,G} \mathcal{H} \left( \frac{M}{\theta_{M,G}} \right) \right\} \left\{ 1 - \mathcal{H} \left( \frac{G}{\theta_{G,G}} \right) \right\} - \mu_G G. \quad (3.4.5)$$

### The time evolution of Brachyury

Brachyury ( $B$ ) has been shown to require Mix ( $M$ ) to be activated in axolotl [139]. In our model we have that both Mix and Activin-like signals (i.e. Activin ( $A$ ) or Nodal ( $N$ )) are required to induce Brachyury expression. We also assume that eFGF ( $E$ ) can activate Brachyury, as inferred from the *Xenopus* mesendoderm GRN, and that this can occur in the absence of Mix and Activin-like signals. Goosecoid ( $G$ ) is assumed to repress Brachyury, as occurs in the *Xenopus* mesendoderm GRN. Taking all of the above into account, the equation governing the time evolution of Brachyury is

$$\frac{dB}{dt} = \left\{ \lambda_{E,B} \mathcal{H} \left( \frac{E}{\theta_{E,B}} \right) + \lambda_{X,M,B} \mathcal{H} \left( \frac{X}{\theta_{X,B}} \right) \mathcal{H} \left( \frac{M}{\theta_{M,B}} \right) \right\} \left\{ 1 - \mathcal{H} \left( \frac{G}{\theta_{G,B}} \right) \right\} - \mu_B B, \quad (3.4.6)$$

where  $X = A$  in the *in vitro* model and  $X = N$  in the *in vivo* model.



**Figure 3.8:** The axolotl *in vitro* network: the Nodal signal is stimulated by Activin. Note that this network is identical to the simplified *Xenopus in vitro* network, with the exception that in the axolotl network Mix is required for the expression of Brachyury.

### The time evolution of Lim1 and eFGF

The regulation of Lim1 and eFGF have not been studied in axolotl, we therefore assume that these factors are regulated in the same way as in the *Xenopus*, such that Lim1 is activated by Nodal

$$\frac{dL}{dt} = \lambda_{N,L} \mathcal{H} \left( \frac{N}{\theta_{N,L}} \right) - \mu_L L, \quad (3.4.7)$$

and eFGF is activated by Brachyury

$$\frac{dE}{dt} = \lambda_{B,E} \mathcal{H} \left( \frac{B}{\theta_{B,E}} \right) - \mu_E E. \quad (3.4.8)$$

## 3.4.2 Summary of model equations

### The axolotl *in vitro* model

The axolotl *in vitro* model governs the time evolution of Brachyury ( $B$ ), Mix ( $M$ ) and Goosecoid ( $G$ ) downstream of Activin ( $A$ ) in a single dissociated cell. The network upon which we base the model is shown in figure 3.8. As we are considering a single dissociated cell, it is assumed that the eFGF signal is too weak to act on downstream target so set  $E = 0$ . To simplify the model further, we do not include Lim1, as it was not included in the *Xenopus in vitro* model. The governing equations of the model are defined to be

$$\frac{dB}{dt} = \lambda_{A,M,B} \mathcal{H} \left( \frac{A}{\theta_{A,B}} \right) \mathcal{H} \left( \frac{M}{\theta_{M,B}} \right) \left\{ 1 - \mathcal{H} \left( \frac{G}{\theta_{G,B}} \right) \right\} - \mu_B B, \quad (3.4.9a)$$

$$\frac{dG}{dt} = \lambda_{M,G} \mathcal{H} \left( \frac{M}{\theta_{M,G}} \right) \left\{ 1 - \mathcal{H} \left( \frac{G}{\theta_{G,G}} \right) \right\} - \mu_G G, \quad (3.4.9b)$$

$$\frac{dM}{dt} = \lambda_{A,M} \mathcal{H} \left( \frac{A}{\theta_{A,M}} \right) \left\{ 1 - \mathcal{H} \left( \frac{B}{\theta_{B,M}} \right) \right\} - \mu_M M. \quad (3.4.9c)$$

In the absence of Activin, none of the factors in the *in vitro* model are present in an animal cap cell. We choose initial conditions to reflect this

$$M(0) = B(0) = G(0) = 0. \quad (3.4.10)$$

Mix, Brachyury and Goosecoid can then only be expressed once the cell is treated with Activin, i.e. when  $A > 0$ .

### The axolotl *in vivo* model

The axolotl *in vivo* model includes the time evolution of the maternal factor  $\beta$ -catenin ( $C$ ), as well as the zygotic factors Nodal ( $N$ ), Mix ( $M$ ), Brachyury ( $B$ ), eFGF ( $E$ ), Goosecoid ( $G$ ) and Lim1 ( $L$ ). The network upon which we base the model is shown in figure 3.7, and the resulting governing equations are

$$\frac{dC}{dt} = -\mu_C C, \quad (3.4.11a)$$

$$\frac{dN}{dt} = \lambda_{C,N} \mathcal{H}\left(\frac{C}{\theta_{C,N}}\right) + \lambda_{N,N} \mathcal{H}\left(\frac{N}{\theta_{N,N}}\right) \left\{1 + \lambda_{C,N2} \mathcal{H}\left(\frac{C}{\theta_{C2,N}}\right)\right\} - \mu_N N, \quad (3.4.11b)$$

$$\frac{dL}{dt} = \lambda_{N,L} \mathcal{H}\left(\frac{N}{\theta_{N,L}}\right) - \mu_L L, \quad (3.4.11c)$$

$$\frac{dE}{dt} = \lambda_{B,E} \mathcal{H}\left(\frac{B}{\theta_{B,E}}\right) - \mu_E E, \quad (3.4.11d)$$

$$\frac{dB}{dt} = \left\{ \lambda_{E,B} \mathcal{H}\left(\frac{E}{\theta_{E,B}}\right) + \lambda_{NM,B} \mathcal{H}\left(\frac{N}{\theta_{N,B}}\right) \mathcal{H}\left(\frac{M}{\theta_{M,B}}\right) \right\} \left\{1 - \mathcal{H}\left(\frac{G}{\theta_{G,B}}\right)\right\} - \mu_B B, \quad (3.4.11e)$$

$$\frac{dG}{dt} = \left\{ \lambda_{L,G} \mathcal{H}\left(\frac{L}{\theta_{L,G}}\right) + \lambda_{M,G} \mathcal{H}\left(\frac{M}{\theta_{M,G}}\right) \right\} \left\{1 - \mathcal{H}\left(\frac{G}{\theta_{G,G}}\right)\right\} - \mu_G G, \quad (3.4.11f)$$

$$\frac{dM}{dt} = \lambda_{N,M} \mathcal{H}\left(\frac{N}{\theta_{N,M}}\right) \left\{1 - \mathcal{H}\left(\frac{B}{\theta_{B,M}}\right)\right\} - \mu_M M. \quad (3.4.11g)$$

An initial concentration of  $\beta$ -catenin is required for the mesoderm and anterior mesendoderm to form, such that  $C(0) = C_0$ , where  $C_0$  is a positive constant. All other TFs and signals are initially absent from the cell, such that

$$C(0) = C_0, \quad N(0) = 0, \quad L(0) = 0, \quad E(0) = 0, \quad B(0) = 0, \quad G(0) = 0, \quad M(0) = 0. \quad (3.4.12)$$

## 3.5 Nondimensionalisation

To reduce the number of parameters in the model, it is nondimensionalised using the timescale of Brachyury turnover,  $\tau = \mu_B t$ . Concentrations,  $Z$ , are scaled  $\hat{Z} = Z/\theta_Z$ , and the dimensionless parameters are defined as follows:

$$\hat{\theta}_{Z,X} \equiv \theta_{Z,X}/\theta_Z, \quad \hat{\lambda}_{Y,Z} \equiv \lambda_{Y,Z}/\theta_Z \mu_B, \quad \hat{\lambda}_{XM,B} \equiv \lambda_{XM,B}/\theta_B \mu_B, \quad \hat{\mu}_Z \equiv \mu_Z/\mu_B.$$

The following notation is used for parameters of the form  $\theta_Z$  for notational simplicity:

$$\theta_X \equiv \theta_{X,B}, \quad \theta_G \equiv \theta_{G,B}, \quad \theta_B \equiv \theta_{B,E}, \quad \theta_E \equiv \theta_{E,B}, \quad \theta_L \equiv \theta_{L,G}, \quad \theta_M \equiv \theta_{M,B}, \quad \theta_C \equiv \theta_{C,N},$$

where  $X = A$  in the *in vitro* model and  $X = N$  in the *in vivo* model. After applying the non-dimensional scalings (and dropping the hats for notational simplicity) the nondimensional equations governing the systems are given as below.

### The axolotl *in vitro* model

The axolotl *in vitro* model is governed by the following nondimensional equations

$$\frac{dB}{dt} = \lambda_{AM,B} \mathcal{H}(A) \mathcal{H}(M) \{1 - \mathcal{H}(G)\} - B, \quad (3.5.1a)$$

$$\frac{dG}{dt} = \lambda_{M,G} \mathcal{H}\left(\frac{M}{\theta_{M,G}}\right) \left\{1 - \mathcal{H}\left(\frac{G}{\theta_{G,G}}\right)\right\} - \mu_G G, \quad (3.5.1b)$$

$$\frac{dM}{dt} = \lambda_{A,M} \mathcal{H}\left(\frac{A}{\theta_{A,M}}\right) \left\{1 - \mathcal{H}\left(\frac{B}{\theta_{B,M}}\right)\right\} - \mu_M M, \quad (3.5.1c)$$

subject to

$$M(0) = B(0) = G(0) = 0. \quad (3.5.2)$$

### The *in vivo* model

The nondimensional equations governing the *in vivo* model are

$$\frac{dC}{d\tau} = -\mu_C C, \quad (3.5.3a)$$

$$\frac{dN}{d\tau} = \lambda_{C,N} \mathcal{H}(C) + \lambda_{N,N} \mathcal{H}\left(\frac{N}{\theta_{N,N}}\right) \left\{1 + \lambda_{C,N} \mathcal{H}\left(\frac{C}{\theta_{C,N2}}\right)\right\} - \mu_N N, \quad (3.5.3b)$$

$$\frac{dL}{d\tau} = \lambda_{N,L} \mathcal{H}\left(\frac{N}{\theta_{N,L}}\right) - \mu_L L, \quad (3.5.3c)$$

$$\frac{dE}{d\tau} = \lambda_{B,E} \mathcal{H}(B) - \mu_E E, \quad (3.5.3d)$$

$$\frac{dB}{d\tau} = \{\lambda_{E,B} \mathcal{H}(E) + \lambda_{NM,B} \mathcal{H}(N) \mathcal{H}(M)\} \{1 - \mathcal{H}(G)\} - B, \quad (3.5.3e)$$

$$\frac{dG}{d\tau} = \left\{ \lambda_{L,G} \mathcal{H}(L) + \lambda_{M,G} \mathcal{H}\left(\frac{M}{\theta_{M,G}}\right) \right\} \left\{ 1 - \mathcal{H}\left(\frac{G}{\theta_{G,G}}\right) \right\} - \mu_G G, \quad (3.5.3f)$$

$$\frac{dM}{d\tau} = \lambda_{N,M} \mathcal{H}\left(\frac{N}{\theta_{N,M}}\right) \left\{ 1 - \mathcal{H}\left(\frac{B}{\theta_{B,M}}\right) \right\} - \mu_M M, \quad (3.5.3g)$$

subject to initial conditions

$$C(0) = C_0, \quad N(0) = 0, \quad L(0) = 0, \quad E(0) = 0, \quad B(0) = 0, \quad G(0) = 0, \quad M(0) = 0, \quad (3.5.4)$$

where  $C_0$  is a positive constant.

Variable	Parameter	Value	Variable	Parameter	Value
$M$	$\lambda_{A,M}$	11	$B$	$\lambda_{AM,B}$	40
	$\theta_{A,M}$	3	$G$	$\lambda_{M,G}$	8
	$\theta_{B,M}$	1		$\theta_{M,G}$	1
	All $\mu$	1		$\theta_{G,G}$	4

**Table 3.2:** Dimensionless parameter values used to solve the axolotl *in vitro* model given in (3.5.1). Parameters were selected such that (3.5.1) is bistable with steady states corresponding to mesoderm and anterior mesendoderm, and so that the system evolves to these steady states dependent on the concentration of Activin ( $A > 0$ ).

### 3.6 The axolotl *in vitro* model

In this section we consider solutions to the *in vitro* model of the axolotl mesendoderm GRN defined in (3.5.1) subject to initial conditions (3.5.2). Recall that the *in vitro* model governs the concentrations of Mix ( $M$ ), Brachyury ( $B$ ) and Goosecoid ( $G$ ) downstream of Activin ( $A$ ). The only difference between the axolotl *in vitro* model and the *Xenopus in vitro* model is the action of Mix on *Brachyury*. In the *Xenopus* model Mix negatively regulates the expression of *Brachyury*, whereas in the axolotl model Mix is required for *Brachyury* expression. The mutual negative regulation of Mix and Brachyury is thought to be an important mechanism in driving the differentiation of mesoderm and anterior mesendoderm in *Xenopus*. Given that this mutual regulation is not present in axolotl, we investigate solutions to the axolotl *in vitro* model to ask if, for a suitable choice of parameter values, the model is bistable with steady states corresponding to mesoderm and anterior mesendoderm. Experimental data obtained from axolotl animal caps show that Activin induces Mix and Brachyury in a dose dependent manner, with Brachyury expressed at low concentrations of Activin and Mix expressed in cells with a high concentration of Activin (Personal communication, Yi-Hsien Chen, also see section 4.1.1). Given this experimental evidence, we expect that we should find solutions to the model corresponding to mesoderm and anterior mesendoderm which are reached dependent on the dose of Activin a cell is treated with. Unless otherwise stated time dependent solutions are computed using the `ode15s` routine in `Matlab` and steady state solutions are computed using `Xppaut` [34], subject to the parameters given in table 3.2.

#### 3.6.1 Steady-state analysis

We now proceed to explore steady state solutions of (3.5.1). These are found by setting  $d/dt = 0$  in (3.5.1) such that the steady states are defined by

$$B^* = \lambda_{AM,B} \mathcal{H}(A) \mathcal{H}(M^*) \{1 - \mathcal{H}(G^*)\}, \quad (3.6.1a)$$

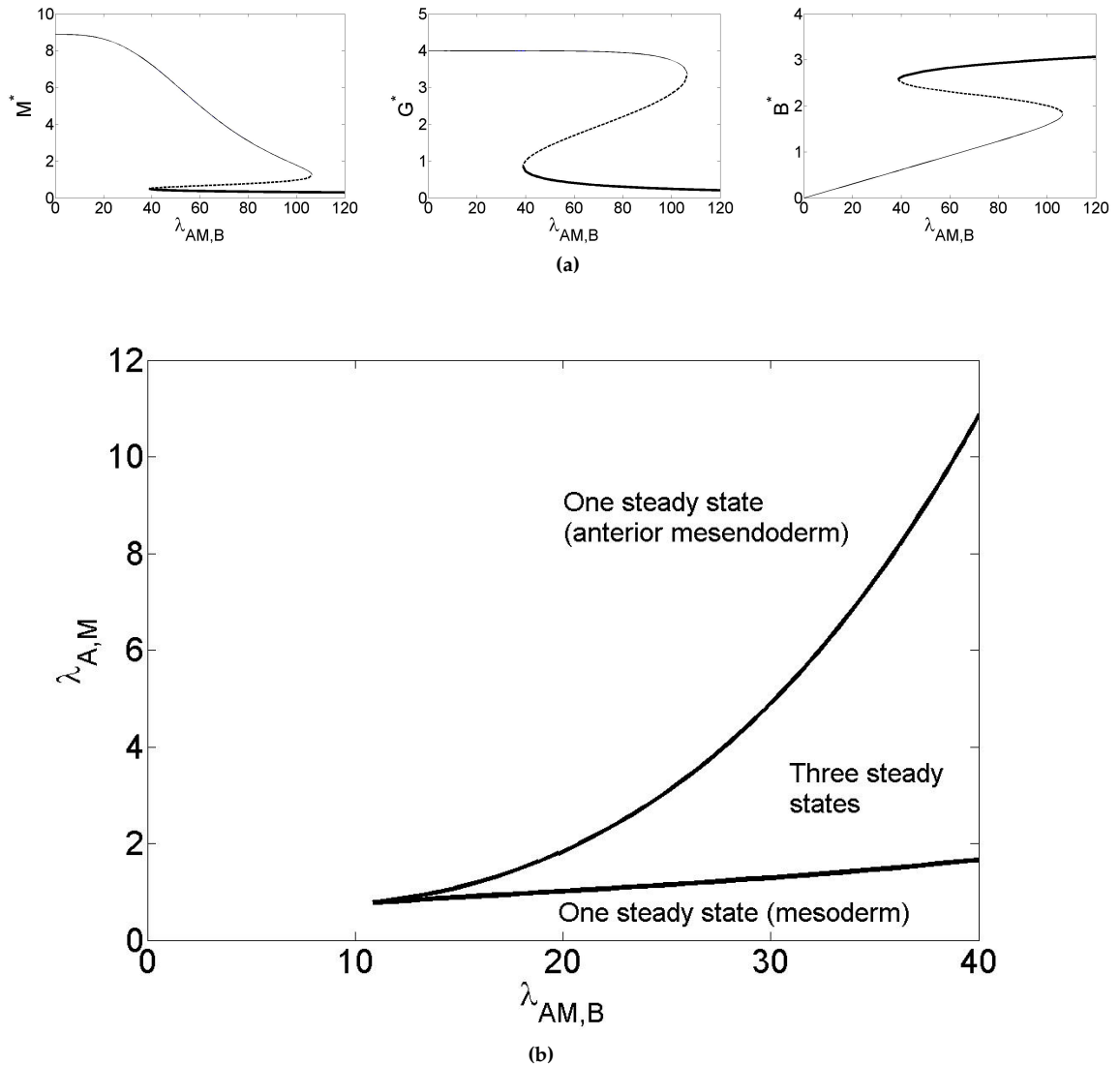
$$G^* = \frac{\lambda_{M,G}}{\mu_G} \mathcal{H}\left(\frac{M^*}{\theta_{M,G}}\right) \left\{1 - \mathcal{H}\left(\frac{G^*}{\theta_{G,G}}\right)\right\}, \quad (3.6.1b)$$

$$M^* = \frac{\lambda_{A,M}}{\mu_M} \mathcal{H}\left(\frac{A}{\theta_{A,M}}\right) \left\{1 - \mathcal{H}\left(\frac{B^*}{\theta_{B,M}}\right)\right\}. \quad (3.6.1c)$$

As discussed above, we seek solutions to (3.6.1) such that it is bistable with steady states corresponding to mesoderm and anterior mesendoderm. It has been shown in other biological systems that for bistability to occur in a model consisting of two mutually repressing factors the Hill coefficient must satisfy  $m > 1$  [37, 95]. Furthermore Middleton et al [95] select  $m = 3$  in solutions to the *Xenopus* mesendoderm models, therefore we choose  $m = 3$  to solve the axolotl models. We find that the parameter values which yield bistability in the *Xenopus in vitro* model do not give bistability in the axolotl *in vitro* model. However, bistability can still be obtained in the axolotl model with a different choice of parameter values. Unless otherwise stated the parameters in table 3.2 are used to produce all numerical results in this section.

In axolotl, Mix is required for the expression of *Brachyury*. However, experimental observations show that, dependent on the dose of Activin a cell is treated with, either *Mix* is upregulated (which when co-expressed with *Goosecoid* corresponds to anterior mesendoderm) or *Brachyury* is upregulated (corresponding to mesoderm). We choose  $\lambda_{A,M}$  and  $\lambda_{AM,B}$  (parameters representing the rate of production of Mix in response to Activin and the rate of production of Brachyury in response to Mix and Activin, respectively) such that both these fates are available to a cell. Steady state solutions of (3.5.1) are plotted as functions of  $\lambda_{AM,B}$  in figure 3.9(a). The system is bistable with stable steady states associated with mesoderm and anterior mesendoderm. For small  $\lambda_{AM,B}$  the system is monostable with the steady state representing the anterior mesendoderm. As  $\lambda_{AM,B}$  increases, a fold bifurcation marks the onset of bistability and the appearance of the mesoderm stable steady state. For further increases of  $\lambda_{AM,B}$ , another fold bifurcation occurs and the system is monostable with only the only stable steady state representing the mesoderm. We find that the concentrations of Mix and Brachyury at the anterior mesendoderm steady state are rather sensitive to changes in  $\lambda_{AM,B}$ , with Mix decreasing and Brachyury increasing as  $\lambda_{AM,B}$  is increased. However at the mesoderm steady state Mix and Brachyury concentrations are in comparison insensitive to changes in  $\lambda_{AM,B}$  and levels of *Goosecoid* are insensitive to changes in this parameter at both stable steady states. In the  $M^*$  plot in figure 3.9(a) the unstable steady state is closest to the mesoderm steady state suggesting that when  $A = 5$ , and for  $\lambda_{AM,B}$  within the bistable region, the system is more likely to evolve to the anterior mesendoderm state, as confirmed in the time-dependent solutions in figure 3.14. In figure 3.9(b) folds are plotted in  $(\lambda_{AM,B}, \lambda_{A,M})$  space. The positions of these folds represent the maximum and minimum rates of production for which both the mesoderm and anterior mesendoderm fate are available to the cell. Bistability occurs only for both  $\lambda_{AM,B}$  and  $\lambda_{A,M}$  sufficiently large. If the rate of production of Mix in response to Activin ( $\lambda_{A,M}$ ) is too large then only the anterior mesendoderm steady state is available to a cell, and similarly if it is too small then only the mesoderm steady state is available.

*Goosecoid* is the only factor in our model which can repress *Brachyury*. In figure 3.10(a) steady state solutions are plotted against  $\lambda_{M,G}$  (the rate of production of *Goosecoid* in response to Mix). Note that compared with the range of  $\lambda_{M,G}$  for which bistability is obtained in the *Xenopus* model, bistability occurs only for a small range of  $\lambda_{M,G}$  in our axolotl model. For values of  $\lambda_{M,G}$  too small mesoderm is the only steady state available. As  $\lambda_{M,G}$  increases through some critical value, a fold bifurcation occurs and the system becomes bistable. As  $\lambda_{M,G}$  increases

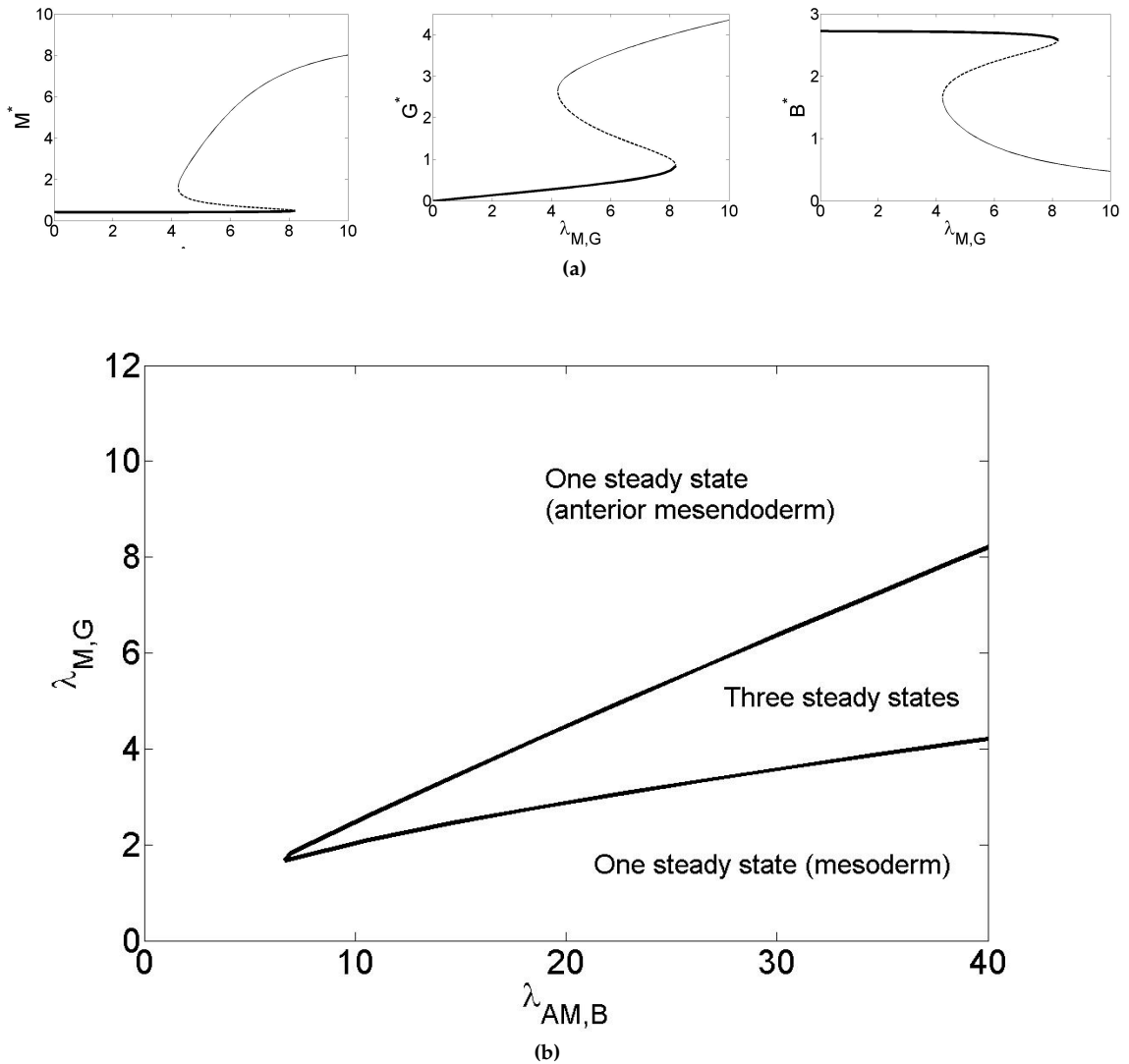


**Figure 3.9:** (a) Steady state solutions to (3.5.1) plotted against  $\lambda_{AM,B}$  for  $A = 5$ . Thick solid lines represent the mesoderm steady state, thin solid lines represent the anterior mesendoderm steady state and dashed lines represent the unstable steady state. Fold bifurcations mark the appearance and disappearance of the steady states. (b) Solution structure in terms of the bifurcation parameters  $\lambda_{AM,B}$  and  $\lambda_{A,M}$ , these representing the folds that determine the maximum rates of production of Brachyury and Mix in response to activation by Activin. The two folds meet at a cusp point. Unless otherwise states parameters are as given in table 3.2.

through another critical value a second fold bifurcation marks the disappearance of the mesoderm steady state. In figure 3.10(b) folds are plotted in  $(\lambda_{M,G}, \lambda_{AM,B})$  space. The positions of these folds represent the maximum and minimum rates of production for which both the mesoderm and the anterior mesendoderm fate are available to the cell.

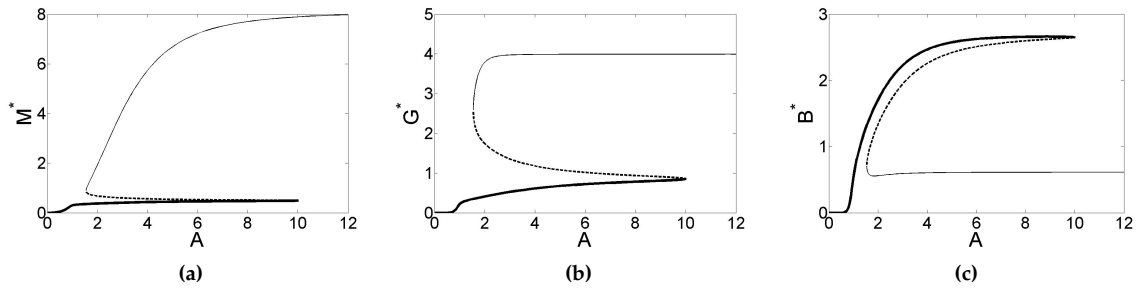
Steady state solutions in response to varying the dose of Activin ( $A$ ) are shown in figure 3.11. For small values of  $A$ , Mix, Brachyury and Goosecoid are all at the trivial steady state. As  $A$  increases, the expression of these factors also increases. For a further increase to  $A$ , a fold bifurcation occurs and the system is bistable. For further increases to  $A$  a fold bifurcation marks





**Figure 3.10:** (a) Steady state solutions to (3.5.1) plotted against  $\lambda_{M,G}$  for  $A = 5$ . Thick solid lines represent the mesoderm steady state, Thin solid lines represent the anterior mesendoderm steady state and dashed lines represent the unstable steady state. Fold bifurcations mark the appearance and disappearance of the stable steady states. (b) Solution structure in terms of the bifurcation parameters  $\lambda_{AM,B}$  and  $\lambda_{M,G}$ , these representing the folds that determine the maximum rates of production of Brachyury in response to activation by Activin and Goosecoid in response to Mix. The two folds meet at a cusp point. Unless otherwise stated parameters in table 3.2 are used to calculate solutions.

the disappearance of the mesoderm stable steady state. Note that as  $A$  increases the levels of Brachyury on the mesoderm steady state branch increase, while Brachyury levels on the anterior mesendoderm branch are insensitive to changes in  $A$ . Similarly Mix levels at the anterior mesendoderm stable steady state increase as  $A$  increases, but Mix levels on the mesoderm branch are insensitive to changes in  $A$ .

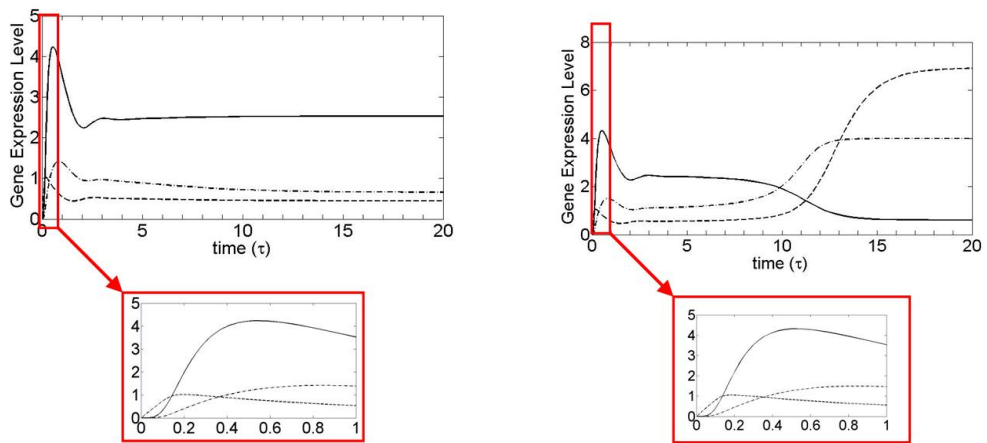


**Figure 3.11:** Steady state solutions to (3.5.1) plotted against  $A$ . Thick solid lines represent the mesoderm steady state, Thin solid lines represent the anterior mesendoderm steady state and dashed lines represent the unstable steady state. Fold bifurcations mark the appearance and disappearance of the stable steady states. All other parameters are given in table 3.2.

### 3.6.2 Time dependent solutions

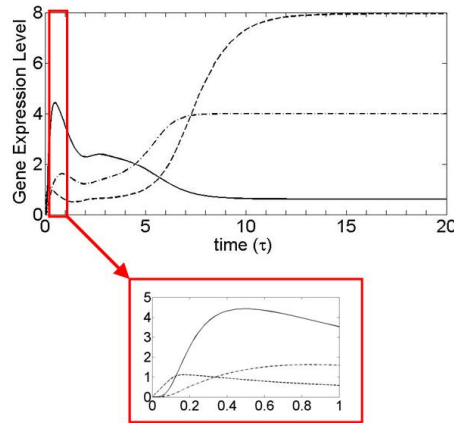
The steady state analysis of the axolotl *in vitro* model shows that, for an appropriate choice of parameter values, the system is bistable. We now seek time dependent solutions to the model, aiming to reproduce qualitatively Activin dose response experiments whereby Brachyury is up-regulated at low doses of Activin and Mix is up-regulated at high doses of Activin. Time-course solutions for the concentrations of Mix, Brachyury and Goosecoid in response to three different levels of Activin are plotted in figure 3.12. These levels of Activin were selected to illustrate that both mesoderm and anterior mesendoderm cell fates are solutions to the model. For a low dose of Activin the system evolves to the mesoderm stable steady state, where Brachyury is up regulated and Mix and Goosecoid are expressed at a low level, as shown in figure 3.12(a). At a high dose of Activin the system evolves to the anterior mesendoderm steady state, where Mix and Goosecoid are up regulated and Brachyury is expressed at a low level, as shown in figure 3.12(c). For an intermediate dose of Activin, the concentrations of Mix, Goosecoid and Brachyury initially resemble the mesoderm steady state, before an increase in the levels of Mix and Goosecoid cause the system to evolve to the anterior mesendoderm steady state, as shown in figure 3.12(b). Note that for all doses of Activin, the initial behaviour of the system is similar, as illustrated in figure 3.13. Mix expression precedes that of Brachyury, followed by a peak in Brachyury expression. The level of Brachyury then either reaches its up regulated steady state value, or becomes down regulated due to an increase in the levels of Mix and Goosecoid. Solutions to (3.5.1) are plotted as functions of Activin dose ( $A$ ) in figure 3.14. For  $A = 0$  the system remains at the trivial steady state. For  $A$  large enough, the system evolves to the mesoderm steady state and, as  $A$  is increased further, the system passes through some critical value ( $A^C$ ) and for  $A > A^C$  evolves to the anterior mesoderm stable steady state.

In the axolotl *in vitro* model, Goosecoid is an important factor as its negative regulation of Brachyury creating competition between Brachyury-expressing and Mix-expressing cells. In the *Xenopus in vitro* model, Goosecoid is not required for the formation of two opposing populations of cells. Figure 3.15(a),(c),(e) plots solutions to the *Xenopus in vitro* model in the absence of Goosecoid. Two distinct cell types form corresponding to mesoderm and endoderm, with



(a)  $A = 4$

(b)  $A = 4.5$



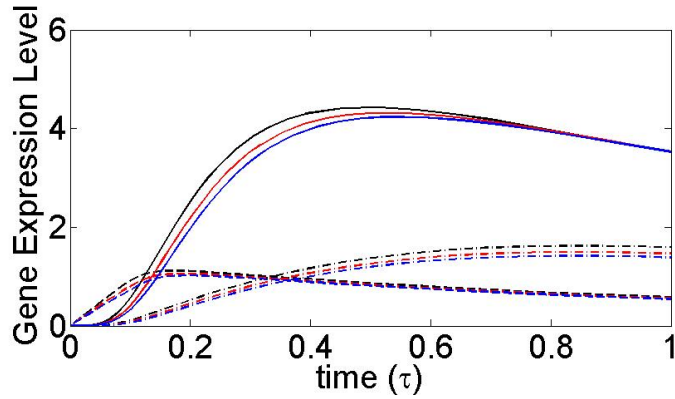
(c)  $A = 6$

**Figure 3.12:** Numerical solutions of the axolotl *in vitro* model (3.5.1). The response of Brachyury (thin solid line), Mix (dashed line) and Goosecooid (dot-dashed line) are shown. Parameters used are given in table 3.2.

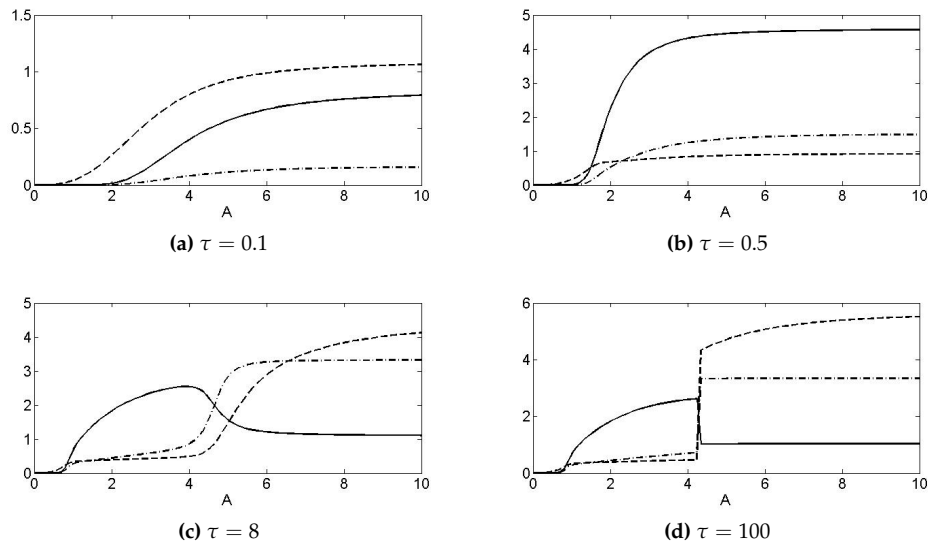
these fates being reached dependent on the dose of Activin. Solutions to the axolotl *in vitro* model in the absence of Goosecooid are plotted as functions of Activin concentration in figure 3.15(b),(d),(f). For all concentrations of Activin, the system evolves to the mesoderm steady state, showing that Goosecooid is essential for the formation of a Mix up-regulated steady state.

### 3.6.3 Conclusions

In this section we have explored solutions to the *in vitro* mathematical model of the axolotl mesendoderm GRN. The *in vitro* model describes the mesendoderm GRN downstream of Activin in a single dissociated cell. Numerical solutions were sought to reproduce qualitatively



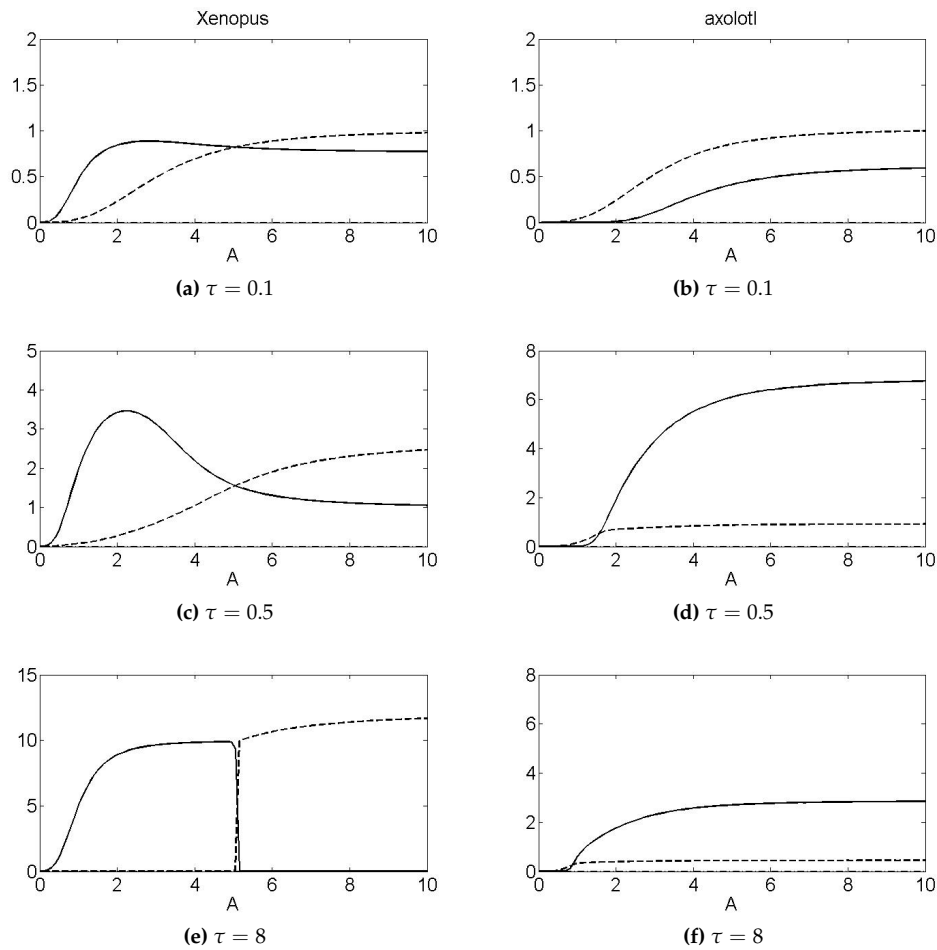
**Figure 3.13:** Numerical solutions of the axolotl *in vitro* model (3.5.1). The response of Brachyury (thin solid line), Mix (dashed line) and Goosecoid (dot-dashed line) are shown for  $A = 4$  (blue lines),  $A = 4.5$  (red lines) and  $A = 6$  (black lines). Parameters used are given in table 3.2.



**Figure 3.14:** Numerical solutions of the axolotl *in vitro* model (3.5.1) as functions of  $A$ . The response of Brachyury (thin solid line), Mix (dashed line) and Goosecoid (dot-dashed line) are shown. Parameters used are given in table 3.2.

experimental observations in axolotl animal caps treated with Activin, such that low doses of Activin induce mesoderm and high doses of Activin induce anterior mesendoderm. A steady state investigation of the model reveals that, for a suitable choice of parameters, the model is bistable with steady states corresponding to mesoderm and anterior mesendoderm. Time dependent solutions show that these stable steady states can be reached dependent on the dose of Activin. For low doses of Activin the model reaches the stable steady state corresponding to mesoderm and for high doses the model reaches the anterior mesendoderm steady state, thus reproducing experimental data qualitatively.

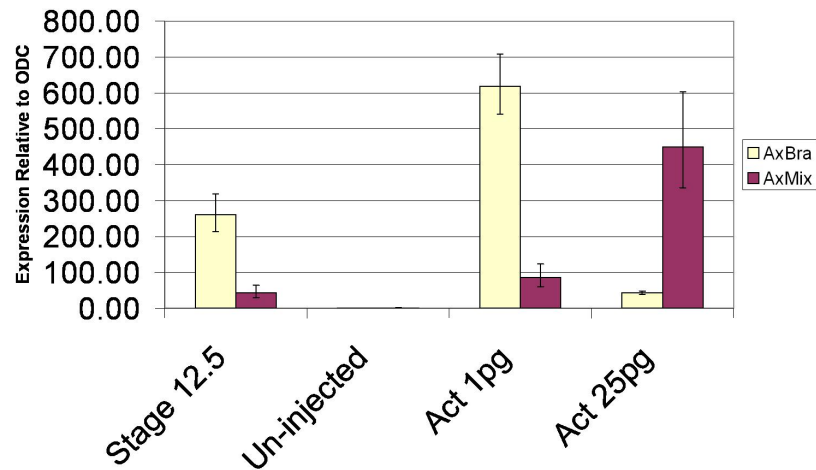
Plots of time dependent solutions showed that for all doses of Activin there is an initial peak in Brachyury expression, before evolving to one of the stable steady states. This was unexpected



**Figure 3.15:** Numerical solutions of the *Xenopus in vitro* model [95] and *axolotl in vitro* model (3.5.1), in the absence of Goosecoid, as functions of  $A$ . The response of Brachyury (thin solid line), Mix (dashed line) and Goosecoid (dot-dashed line) are shown. Parameters used are given in table 3.2 for the *axolotl* model and as given in [95] for the *Xenopus*.

since in whole embryos Mix expression precedes Brachyury, with Mix expressed from stage 8 and Brachyury expression commencing at stage 11 [139]. However the only parameter sets we have found that yield bistability give this early peak of Brachyury expression. This gives a prediction from our model, which can be tested by obtaining time course expression data in Activin treated animal caps, such data are presented in section 4.1.1.

The main difference between the *axolotl in vitro* model and the *Xenopus in vitro* model in [95] is the regulation of Brachyury by Mix. In *Xenopus* Mix negatively regulates Brachyury, but in *axolotl* Mix is required for the expression of Brachyury. Changing the sign of this interaction leads to different parameter values being required to give bistability. Comparing the Activin dose response curve in the *Xenopus in vitro* model (figure 3.3) and the *axolotl in vitro* model (figure 3.14) we see qualitative differences in the solutions of the models. Both models are bistable with steady states which can be interpreted as corresponding to mesoderm and anterior mesoderm cell fates. In the *Xenopus* model, Mix and Goosecoid are not expressed



**Figure 3.16:** qPCR analysis of gene expression induced by Activin in axolotl animal caps. Cap explants were collected when sibling embryos reached stage 12.5 and qPCR analysis was performed to examine gene expression levels. Data obtained by Yi-Hsien Chen.

at the mesoderm steady state, and Brachyury is not expressed at the endoderm steady state. In the axolotl model, although Brachyury is expressed at lower levels than Mix or Goosecoid at the anterior mesendoderm steady state, it is expressed at a non-zero level. Similarly, at the mesoderm steady state Mix and Goosecoid levels are non zero, but at lower concentrations than Brachyury. Experimental data from axolotl show that in mesodermal cells Brachyury is upregulated and Mix is expressed at low levels (figure 3.16)f. Similarly, in anterior mesendoderm cells Mix is upregulated and Brachyury is expressed at low levels (figure 3.16). The steady states of the mathematical model are therefore in qualitative agreement with experimental observations.

Another difference between the *Xenopus* and axolotl *in vitro* models is the requirement of Goosecoid for bistability. In *Xenopus* both Mix and Goosecoid can suppress the expression of Brachyury. Therefore the *Xenopus in vitro* model still shows bistable behaviour in the absence of Goosecoid. However, Goosecoid is the only factor that can repress Brachyury, making it essential for bistability in the axolotl *in vitro* model. This gives an interesting testable prediction that mesoderm and endoderm will still form in *Xenopus* embryos lacking Goosecoid in the axolotl, while a knockdown of Goosecoid will result in embryos not forming endoderm. The prediction that mesoderm and endoderm will still form in *Xenopus* embryos lacking Goosecoid is consistent with experimental observations whereby the knockdown of Goosecoid results in the disruption of patterning of the dorsal-ventral and anterior-posterior axis, but no disruption to mesoderm and endoderm formation is reported [124].

### 3.7 The axolotl *in vivo* model

In this section we explore solutions to the axolotl *in vivo* model (3.5.3). Recall that the *in vivo* model describes the concentrations of Nodal1 ( $N$ ), Lim1 ( $L$ ), eFGF ( $E$ ), Brachyury ( $B$ ), Mix ( $M$ )

and Goosecoid ( $G$ ) downstream of the maternal factor  $\beta$ -catenin ( $C$ ).

### 3.7.1 Steady-state equations

Steady states of the *in vivo* are found by setting  $d/d\tau = 0$  in (3.5.3), then solving the resulting equations which are given by

$$C^* = 0, \quad N^* = \psi \mathcal{H} \left( \frac{N^*}{\theta_{N,N}} \right), \quad (3.7.1a)$$

$$L^* = \frac{\lambda_{N,L}}{\mu_L} \mathcal{H} (N^*), \quad E^* = \frac{\lambda_{B,E}}{\mu_E} \mathcal{H} (B^*), \quad (3.7.1b)$$

$$B^* = \{ \lambda_{E,B} \mathcal{H} (E^*) + \lambda_{NM,B} \mathcal{H} (N^*) \mathcal{H} (M^*) \} \{ 1 - \mathcal{H} (G^*) \}, \quad (3.7.1c)$$

$$G^* = \frac{1}{\mu_G} \left\{ \lambda_{M,G} \mathcal{H} \left( \frac{M^*}{\theta_{M,G}} \right) + \lambda_{L,G} \mathcal{H} \left( \frac{L^*}{\theta_{L,G}} \right) \right\} \left\{ 1 - \mathcal{H} \left( \frac{G^*}{\theta_{G,G}} \right) \right\}, \quad (3.7.1d)$$

$$M^* = \frac{\lambda_{X,M}}{\mu_M} \mathcal{H} \left( \frac{N^*}{\theta_{X,M}} \right) \left\{ 1 - \mathcal{H} \left( \frac{B^*}{\theta_{B,M}} \right) \right\}. \quad (3.7.1e)$$

As in the *Xenopus in vivo* model, the steady state equations are independent of the levels of  $\beta$ -catenin. Equation (3.7.1a) has two solutions, the trivial steady state  $N = 0$  and a non-trivial steady state  $N = N^* > 0$ , corresponding to down-regulated and up-regulated Nodal1, respectively. Solving the remaining equations for the trivial steady state of Nodal ( $N = 0$ ) we obtain

$$E^* = \frac{\lambda_{B,E}}{\mu_E} \mathcal{H} (B^*), \quad B^* = \lambda_{E,B} \mathcal{H} (E^*), \quad G^* = M^* = 0. \quad (3.7.2)$$

(3.7.2) is a bistable system, with steady states corresponding to FGF and Brachyury upregulating each other (i.e mesoderm) and the trivial steady state. When Nodal1 is expressed at its non-trivial steady state,  $N = N^* > 0$ , steady states of TFs downstream of Nodal1 are

$$E^* = \frac{\lambda_{B,E}}{\mu_E} \mathcal{H} (B^*), \quad (3.7.3a)$$

$$B^* = \{ \lambda_{E,B} \mathcal{H} (E^*) + \lambda_{NM,B} \mathcal{H} (N^*) \mathcal{H} (M^*) \} \{ 1 - \mathcal{H} (G^*) \}, \quad (3.7.3b)$$

$$G^* = \frac{1}{\mu_G} \left\{ \lambda_{M,G} \mathcal{H} \left( \frac{M^*}{\theta_{M,G}} \right) + \lambda_{L,G} \mathcal{H} \left( \frac{L^*}{\theta_{L,G}} \right) \right\} \left\{ 1 - \mathcal{H} \left( \frac{G^*}{\theta_{G,G}} \right) \right\}, \quad (3.7.3c)$$

$$M^* = \frac{\lambda_{X,M}}{\mu_M} \mathcal{H} \left( \frac{N^*}{\theta_{X,M}} \right) \left\{ 1 - \mathcal{H} \left( \frac{B^*}{\theta_{B,M}} \right) \right\}. \quad (3.7.3d)$$

Note that if we set  $L^* = E^* = 0$  in (3.7.3) and replace  $N^*$  with  $A$ , then these steady state equations are identical to those for the axolotl *in vitro* model (3.6.1). Therefore, (3.7.3) is bistable, with stable steady states corresponding to mesoderm and anterior mesendoderm. Thus, for a suitable choice of parameters, the axolotl has four stable steady states; one corresponding to anterior mesendoderm, two to mesoderm and one to the trivial steady state (ectoderm).

Variable	Parameter	Value	Variable	Parameter	Value
C	$\mu_C$	0.01	M	$\lambda_{X,M}$	12
N	$\lambda_{N,N}$	3		$\theta_{X,M}$	3
	$\theta_{N,N}$	1		$\theta_{B,M}$	1
	$\lambda_{C,N}$	1	G	$\lambda_{M,G}$	8
	$\lambda_{C,N2}$	1		$\theta_{M,G}$	1
B	$\lambda_{X,B}$	6		$\lambda_{L,G}$	1
	$\lambda_{E,B}$	12	$\theta_{G,G}$	3	
E	$\lambda_{B,E}$	12	L	$\lambda_{N,L}$	1
	All other $\mu$	1		$\theta_{N,L}$	1

**Table 3.3:** Dimensionless parameter values used to obtain numerical results in the axolotl *in vivo* model. Parameters were selected such that (3.5.3) is bistable with steady states corresponding to mesoderm and anterior mesendoderm, and so that the system evolves to these steady states dependent on the concentration of  $\beta$ -catenin ( $C > 0$ ).

### 3.7.2 Time-dependent solutions

Recall from section 1.8 that  $\beta$ -catenin can induce mesoderm and endoderm in a dose dependent manner in axolotl. In this section, we obtain numerical solutions to the axolotl *in vivo* model aiming to reproduce these observations. Solutions to (3.5.3) are plotted as functions of initial  $\beta$ -catenin concentration ( $C_0$ ) in figure 3.17. For  $C_0$  small enough the system evolves to the mesoderm branch. As  $C_0$  is increased beyond some critical value, the system will evolve to the anterior mesendoderm branch. For  $C_0$  too small the system evolves to the trivial steady state where neither Mix nor Brachyury are expressed. These numerical results are in qualitative agreement with qPCR data collected from axolotl animal caps injected with  $\beta$ -catenin: At low doses of  $\beta$ -catenin animal caps will become mesoderm (expressing Brachyury) and at higher doses cells become anterior mesendoderm (expressing Mix and Goosecoid).

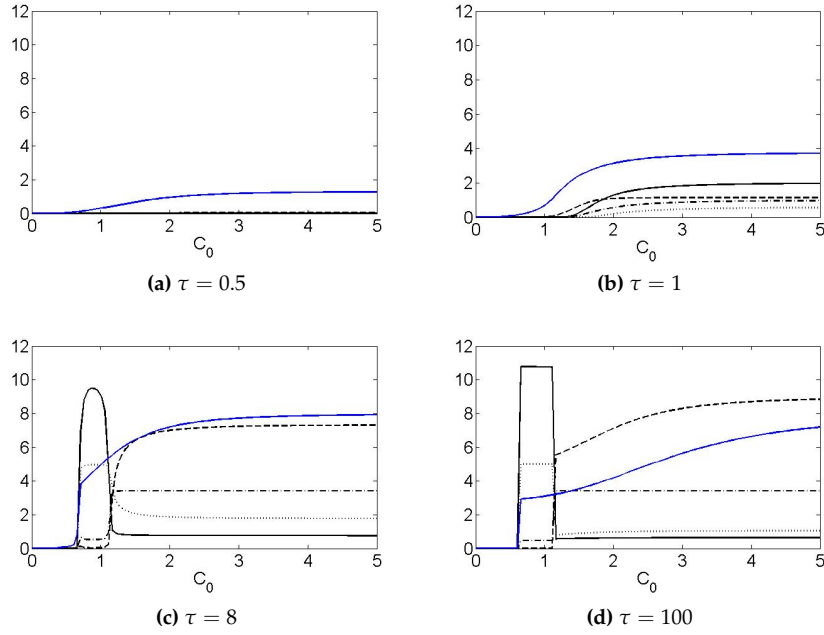
## 3.8 Nodal regulation in a simplified *Xenopus* mesendoderm GRN

In this section we discuss assumptions made when combining the multiple Nodal genes present in *Xenopus* into a single representative node in the simplified mesendoderm GRN. In particular we highlight differences in the mechanisms of induction of the *Xenopus* Nodals by VegT and  $\beta$ -catenin, and the importance of these Nodals in mesendoderm specification. We present evidence published since the formulation of the simplified mesendoderm GRN and *Xenopus in vivo* model of [95], and modify the model based on this data. The modified *in vivo* model is then used to investigate how changing the way in which VegT and  $\beta$ -catenin act on a single Nodal gene alters downstream solution of the model.

### 3.8.1 Biological background

Recall that there are six members of the Nodal gene family in *Xenopus*, *Xnr1-Xnr6*. *Xnr3* does not induce mesoderm [50], thus we do not consider this gene any further in this section. There are differences in the timing, function and induction of the remaining Nodal genes, which we now describe. *Xnr5* and *Xnr6* are the first Nodal genes to be expressed in *Xenopus* embryos with

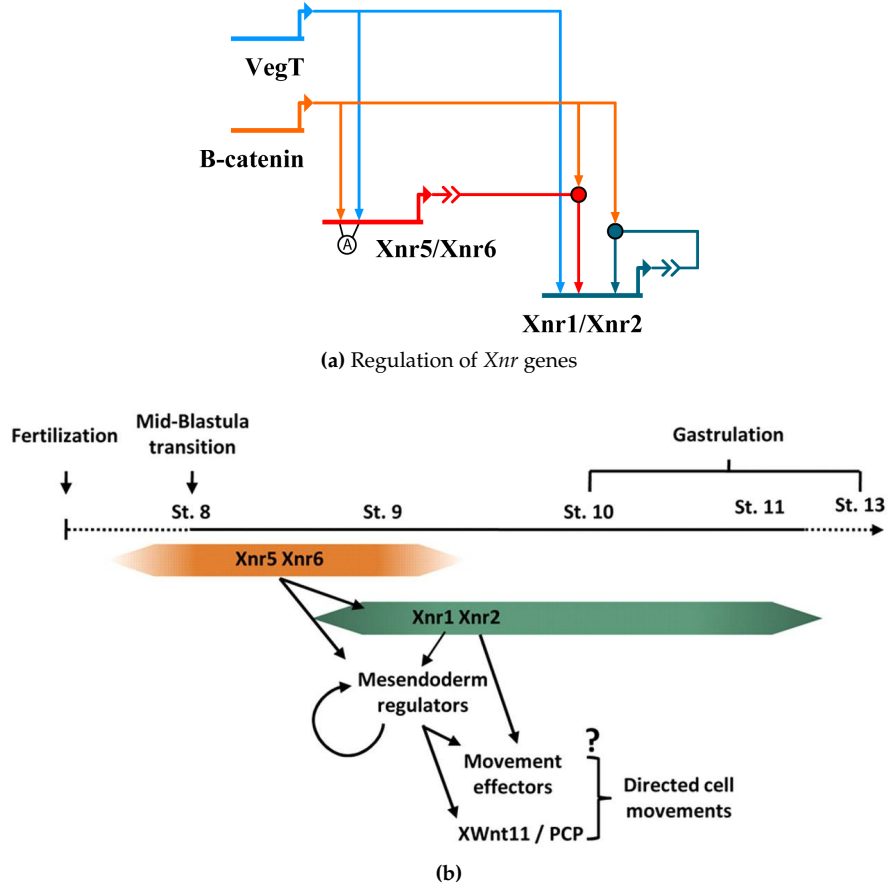




**Figure 3.17:** Numerical solutions of the axolotl *in vivo* model (3.5.3) as functions of  $C_0$ , for various values of  $\tau$ . The response of Brachyury (thin solid line), eFGF (dotted line), Mix (dashed line), Goosecoid (dot-dashed line) and Nodal (blue solid line) are shown in response to an initial concentration of  $\beta$ -catenin. Parameters used are given in table 3.3.

expression first detected at the onset of zygotic transcription (stage 8 - 8.5). *Xnr5* and *Xnr6* expression peaks during blastula and decreases at the onset of gastrulation [141]. *Xnr1* and *Xnr2* are expressed from stage 9 and are maintained throughout gastrulation [141]. A targeted knock-down of Nodal genes carried out in [90] shows that *Xnr5/Xnr6* are required for mesendoderm induction and *Xnr1/Xnr2* are required for gastrulation movements. While a single knockdown of *Xnr5* or *Xnr6* does not disrupt mesendoderm formation, a double knockdown results in a downregulation of mesendodermal genes. Similarly, embryos develop normally when *Xnr1* or *Xnr2* are knocked down individually, but a double knockdown prevents gastrulation. A systematic study of the induction of Nodal expression by combinations of VegT,  $\beta$ -catenin and Activin-like signalling shows Nodal genes require different combinations of these factors to be induced [117]. *Xnr1*, *Xnr2* and *Xnr4* are induced in the presence of VegT, or by Activin-like signalling synergised by  $\beta$ -catenin. *Xnr5* and *Xnr6* are induced by VegT and  $\beta$ -catenin with both factors essential for this induction. A summary of the regulation and timing of *Xnr* gene expression from [90] is shown in figure 3.18.

In the *in-vivo* mathematical model of Middleton et al [95], Nodal is activated either by VegT alone, or by Nodal autoregulation enhanced by  $\beta$ -catenin (figure 3.19A). This method of regulation is as observed experimentally for *Xnr1* and *Xnr2* [117]. However *Xnr5* and *Xnr6* have been shown to be key regulators of mesendoderm induction, while *Xnr1* and *Xnr2* are secondary to this process [90]. We propose a modified version of the equation for the rate of change of Nodal in the *Xenopus in vivo* model representing the regulation of *Xnr5* and *Xnr6* rather than *Xnr1* and



**Figure 3.18:** (a) Regulation of *Xnr* genes by VegT and  $\beta$ -catenin. (b) The timing of *Xnr* gene expression and a model for the control of gastrulation and the regulation of mesenteroderm regulators. *Xnr5* and *Xnr6* can activate both the mesenteroderm programme and *Xnr1* and *Xnr2*. *Xnr1* and *Xnr2* activate movement effectors and may also contribute to the mesenteroderm programme. Figure taken from [90].

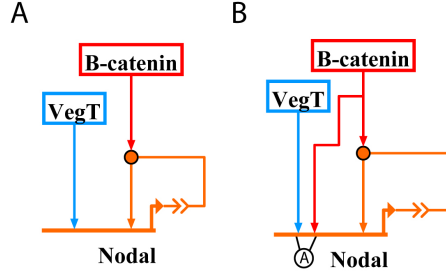
*Xnr2*. This single Nodal gene requires both VegT and  $\beta$ -catenin to be present for its activation (figure 3.19B). Although *Xnr5* and *Xnr6* cannot autoregulate, we still include a term for Nodal autoregulation which is enhanced by  $\beta$ -catenin. Our justification for this is that *Xnr1* and *Xnr2* may still play a small role in mesenteroderm induction. The equation for the rate of change of Nodal based upon figure 3.19B is

$$\frac{dN}{dt} = \lambda_{V,N} \mathcal{H}\left(\frac{V}{\theta_{V,N}}\right) \mathcal{H}\left(\frac{C}{\theta_{C,N}}\right) + \lambda_{N,N} \mathcal{H}\left(\frac{N}{\theta_{N,N}}\right) \left\{ \left(1 + \lambda_{C,N} \mathcal{H}\left(\frac{C}{\theta_{C,N2}}\right)\right) \right\} - \mu_N N. \quad (3.8.1)$$

The equations for the time evolution of the other genes in the network remain as in the *Xenopus in-vivo* model of [95].

### 3.8.2 Nondimensional governing equations

The equations governing the modified *Xenopus in vivo* model are given below. For a detailed description of the evidence used to construct this model and the non-dimensional scalings refer



**Figure 3.19:** Ways of modelling VegT and  $\beta$ -catenin acting on a single representative Nodal gene in *Xenopus*. **(A)** Nodal is activated by VegT alone, with  $\beta$ -catenin enhancing Nodal autoregulation. **(B)** Both VegT and  $\beta$ -catenin are required to activate Nodal, with  $\beta$ -catenin enhancing Nodal autoregulation.

to [94].

$$\frac{dV}{d\tau} = -\mu_V V, \quad (3.8.2a)$$

$$\frac{dC}{d\tau} = -\mu_C C, \quad (3.8.2b)$$

$$\frac{dN}{d\tau} = \lambda_{V,N} \mathcal{H}(V) \mathcal{H}\left(\frac{C}{\theta_{C,N}}\right) + \lambda_{N,N} \mathcal{H}\left(\frac{N}{\theta_{N,N}}\right) \left\{1 + \lambda_{C,N} \mathcal{H}\left(\frac{C}{\theta_{C,N}}\right)\right\} - \mu_N N, \quad (3.8.2c)$$

$$\frac{dL}{d\tau} = \lambda_{N,L} \mathcal{H}\left(\frac{N}{\theta_{N,L}}\right) - \mu_L L, \quad (3.8.2d)$$

$$\frac{dI}{d\tau} = \lambda_{C,I} \mathcal{H}\left(\frac{C}{\theta_{C,I}}\right) - \mu_I I, \quad (3.8.2e)$$

$$\frac{dE}{d\tau} = \lambda_{B,E} \mathcal{H}(B) - \mu_E E, \quad (3.8.2f)$$

$$\frac{dB}{d\tau} = \left\{ \lambda_{V,B} \mathcal{H}\left(\frac{V}{\theta_{V,B}}\right) + \lambda_{E,B} \mathcal{H}(E) + \lambda_{NM,B} \mathcal{H}(N) \right\} \{1 - \mathcal{H}(G + M)\} - B, \quad (3.8.2g)$$

$$\frac{dG}{d\tau} = \left\{ \lambda_{LL,G} \mathcal{H}(L) \mathcal{H}(I) + \lambda_{M,G} \mathcal{H}\left(\frac{M}{\theta_{M,G}}\right) \right\} \left\{1 - \mathcal{H}\left(\frac{G}{\theta_{G,G}}\right)\right\} - \mu_G G, \quad (3.8.2h)$$

$$\frac{dM}{d\tau} = \left\{ \lambda_{V,M} \mathcal{H}\left(\frac{V}{\theta_{V,M}}\right) + \lambda_{N,M} \mathcal{H}\left(\frac{N}{\theta_{N,M}}\right) \right\} \left\{1 - \mathcal{H}\left(\frac{B}{\theta_{B,M}}\right)\right\} - \mu_M M, \quad (3.8.2i)$$

subject to initial conditions

$$V(0) = V_0, \quad C(0) = C_0, \quad N(0) = 0, \quad L(0) = 0, \quad I(0) = 0, \quad E(0) = 0, \\ B(0) = 0, \quad G(0) = 0, \quad M(0) = 0,$$

where  $V_0, C_0$  are positive constants.

### 3.8.3 Solutions to the modified *Xenopus in vivo* model

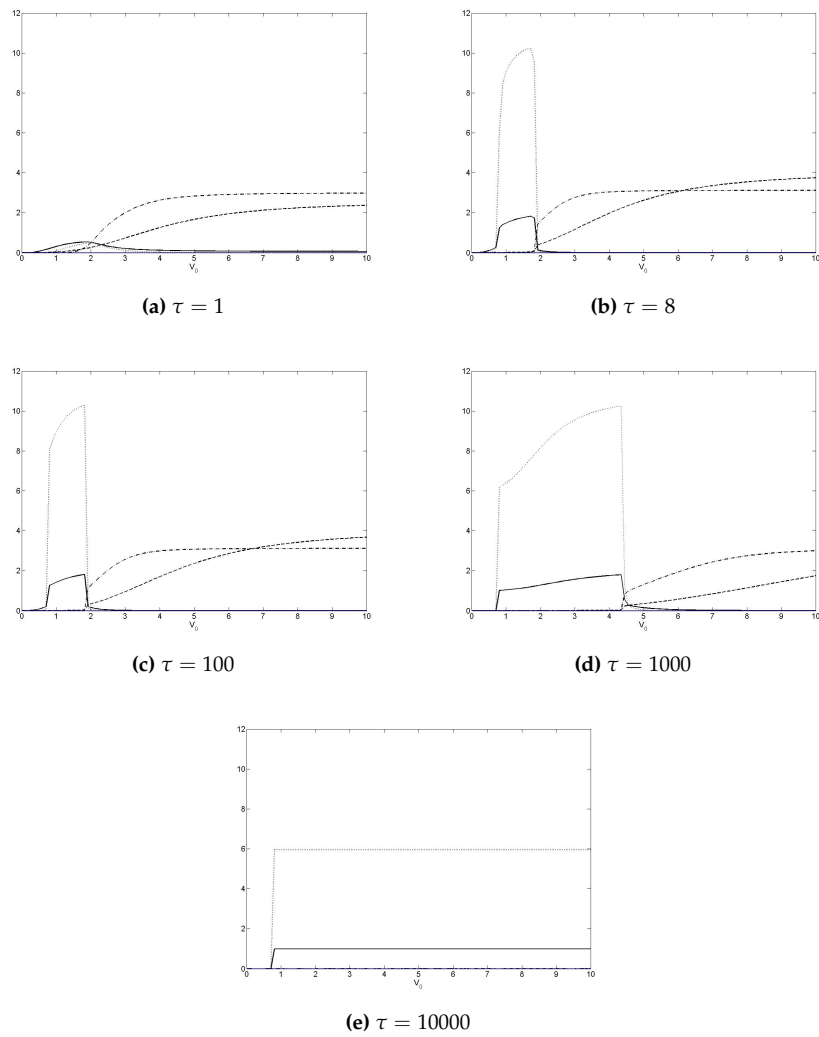
We now analyse solutions to the modified *Xenopus in vivo* model and compare these solutions with the original *Xenopus in vivo* model of [95]. Remember that the sole difference between the original and modified equations is the role of VegT and  $\beta$ -catenin in inducing Nodal. The steady state solutions to (3.8.2) are identical to those for the original *Xenopus in vivo* model

shown in [95], since the steady states are independent of VegT and  $\beta$ -catenin. Therefore the system (3.8.2) has three non-trivial steady states, one corresponding to endoderm (requiring a non-trivial steady state concentration of Nodal) and two to mesoderm (in the presence and absence of Nodal). We seek time-dependent solutions to (3.8.2) to show how initial levels of VegT and  $\beta$ -catenin determine the steady states the systems reaches. As in [95], we explored the effects of initial VegT and  $\beta$ -catenin concentrations on the dynamics of the *in vivo* model.

Solutions to (3.8.2) are plotted as functions of initial VegT concentration ( $V_0$ ) in figure 3.20. In this case  $\beta$ -catenin is not present such that  $C(0) = 0$  for all values of  $V_0$ . Initially we find that Mix and Brachyury are induced by VegT in a dose dependent manner, with Brachyury expressed for small  $V_0$  and Mix expressed for large  $V_0$ . As time proceeds, Brachyury becomes expressed for an increasing range of  $V_0$ . The system ultimately evolves to a steady state with upregulated eFGF and Brachyury for  $V_0$  large enough (for small  $V_0$  the system evolves to the trivial steady state). This steady state corresponds to eFGF and Brachyury upregulating each other (i.e. mesoderm). Note that Nodal is not expressed with these initial conditions, since VegT and  $\beta$ -catenin are both required for the expression of Nodal. Solutions to the mathematical model with  $\beta$ -catenin in the absence of VegT show no expression of Mix or Brachyury genes, since no factors upstream of these genes are induced by  $\beta$ -catenin alone.

We define an initial condition of  $\beta$ -catenin ( $C(0) = C_0$ ) as follows:  $C_0 = a - bV_0$  for  $V_0 < a/b$  and  $C_0 = 0$  for  $V_0 \geq a/b$ . Numerical solutions of (3.8.2) in the presence of both VegT and  $\beta$ -catenin are plotted in figure 3.21. In cells where VegT and  $\beta$ -catenin are co-expressed ( $V_0 > 5$ ), Nodal is expressed at non-trivial levels. In this region, Brachyury and eFGF are expressed for initial conditions of high  $\beta$ -catenin and low VegT, and Mix and Goosecoid are expressed for high VegT and low  $\beta$ -catenin. These two steady states correspond to mesoderm and anterior mesoderm, respectively. For  $V_0 \geq 5$ , the model simulation is identical to that given in figure 3.20.

The results of the mathematical model show that in a single cell model, which neglects spatial effects, VegT and  $\beta$ -catenin are both required for the model to evolve to steady states corresponding to mesoderm ( $N = N^* > 0$ ) and anterior mesoderm, dependent of the dose of VegT. In the absence of VegT,  $\beta$ -catenin does not induce mesoderm markers. For concentrations of VegT in the absence of  $\beta$ -catenin, the system does not evolve to mesoderm and anterior mesoderm in a dose dependent manner. Instead, Mix and Brachyury are initially induced by VegT in a dose dependent manner, but with expression levels lower than those obtained in a model with both VegT and  $\beta$ -catenin in combination. These theoretical observations qualitatively agree with experimental data obtained by Yi-Hsien Chen (see figure 3.22) [16]. Axolotl animal caps injected with concentrations of VegT (10pg and 50pg) fail to induce mesoderm. An analysis of gene expression in these caps reveals that 10pg VegT weakly induces Brachyury, but not Mix.1 or Mixer. A higher dose of VegT (50pg) induces both Mix and Brachyury. Axolotl animal caps co-injected with  $\beta$ -catenin and VegT cause an exaggerated dorsal mesoderm response, with a low dose of VegT inducing mesoderm markers such as Brachyury and higher doses of VegT inducing endodermal markers such as Mix.1 and Mixer (a member of the *Xenopus* Mix family).

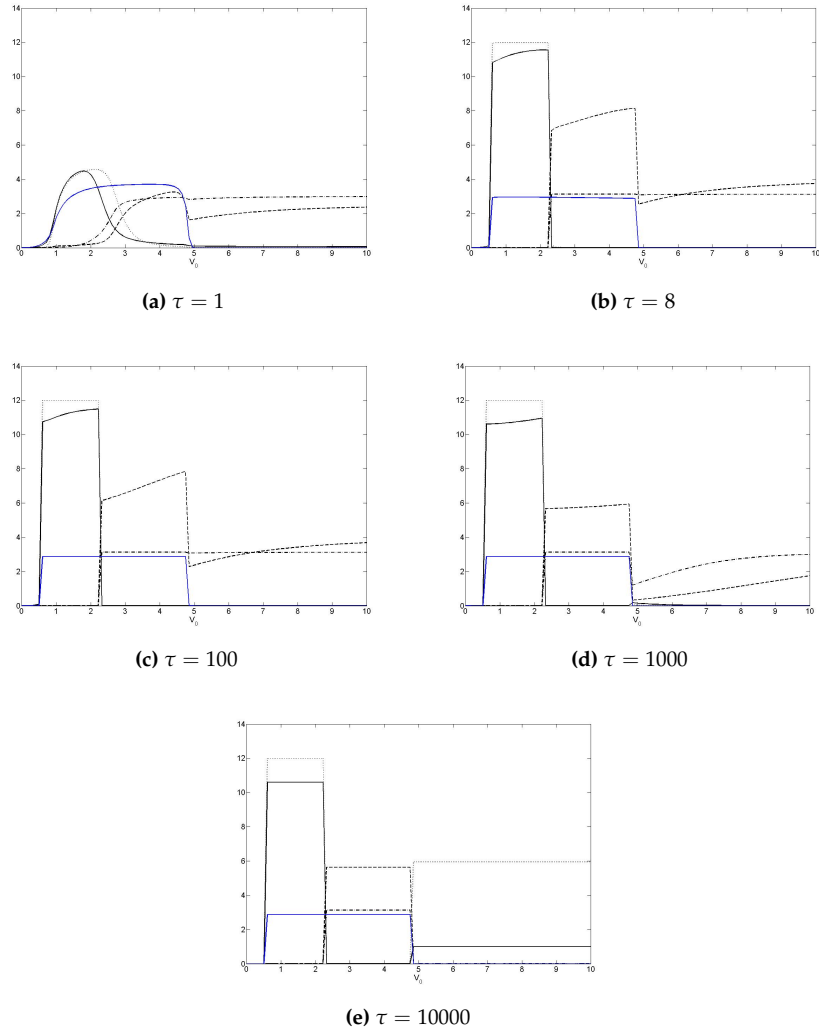


**Figure 3.20:** Numerical solutions to the *Xenopus in-vivo* model as a function of initial VegT concentration. The mathematical model is as given in [95], with the modified equation for  $\frac{dN}{dt}$  as defined in (3.8.1), where  $V(0) = V_0$  and  $C(0) = 0$ . The response of the following genes are shown: Brachyury (thin solid line), eFGF (dotted line), Mix (dashed line), Goosecoid (dash-dotted line) and Nodal (blue solid line). Parameter values used are given in [95], with the addition of  $\theta_{C,N2} = 1$ .

### 3.9 Discussion

In this chapter single cell models of mesendoderm specification in *Xenopus* and axolotl were considered. We reviewed mathematical models of [95] which are based on a simplified version of the full mesendoderm GRN in *Xenopus*. The axolotl was then introduced as a more suitable model organism than *Xenopus* for studying a simplified mesendoderm GRN. A single Mix and a single Nodal are required for mesendoderm formation in axolotl, compared with multiple Mix and Nodal genes in the *Xenopus* mesendoderm GRN.

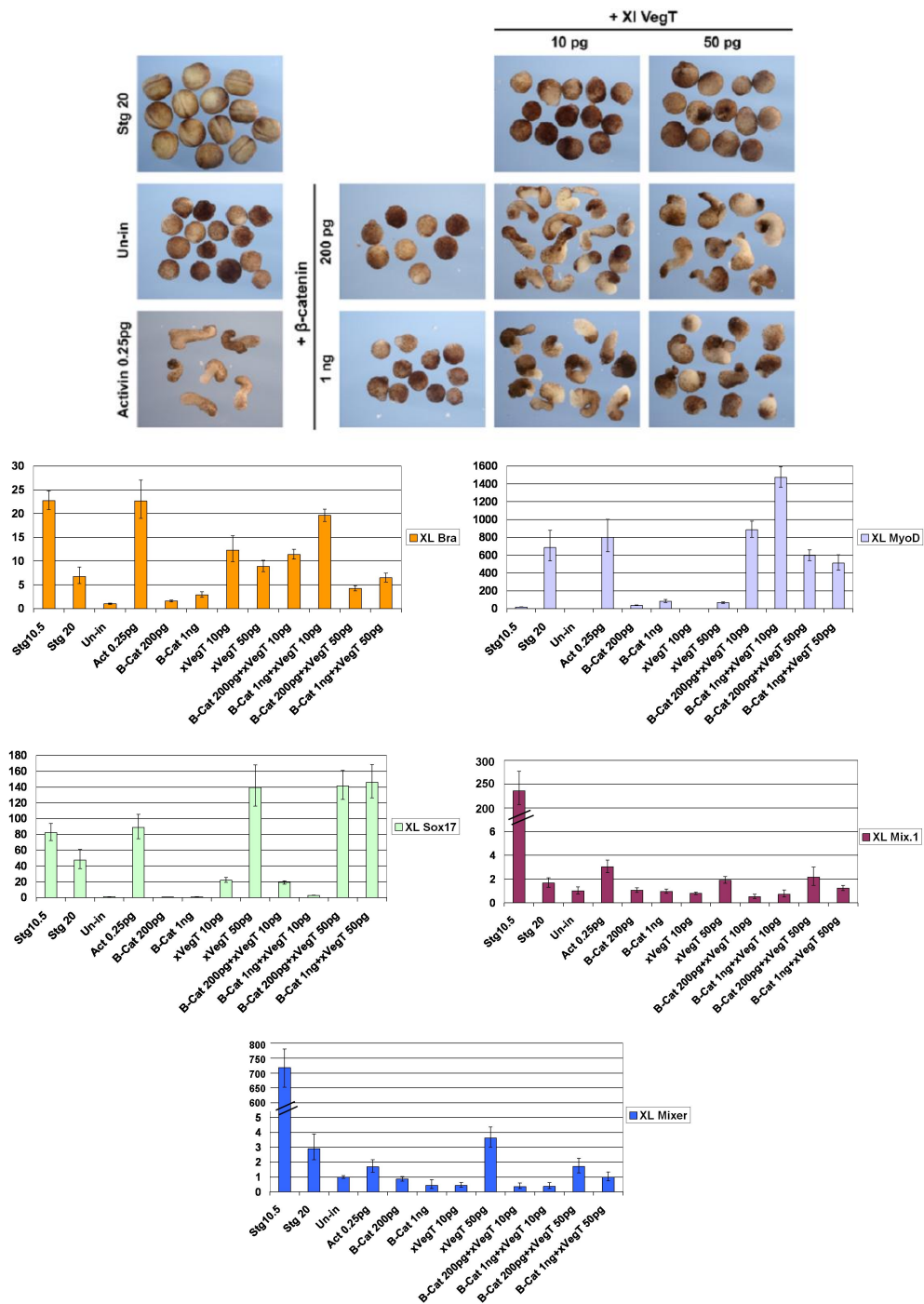
There are several differences in the topology of the axolotl and *Xenopus* mesendoderm GRNs which were described in this chapter such as the role of the maternal factors and the regulation



**Figure 3.21:** Numerical solutions to the *Xenopus in-vivo* model as a function of initial VegT concentration. The mathematical model is as given in [95], with the modified equation for  $\frac{dN}{dt}$  as defined in (3.8.1), where  $V(0) = V_0$  and  $C(0) = a - bV_0$ ,  $a = 50$ ,  $b = 10$ . The response of the following genes are shown: Brachyury (thin solid line), eFGF (dotted line), Mix (dashed line), Goosecoid (dash-dotted line) and Nodal (blue solid line). Parameter values used are given in [95], with the addition of  $\theta_{C,N2} = 1$ .

of Brachyury by Mix (see figure 1.7). Given these differences between the axolotl and *Xenopus* networks, we modified the equations of the simplified *Xenopus* mesendoderm models given in [95] to account for the axolotl mesendoderm GRN. Two models were formulated giving the time evolution of transcription factors in a single cell. Both models were found to be bistable, with steady states corresponding to mesoderm and anterior mesendoderm.

The axolotl *in vitro* model, which considered the time evolution of Mix, Brachyury and Goosecoid in response to Activin (figure 3.8), is able to reproduce qualitatively experimental observations in axolotl animal caps, where Brachyury is upregulated at low doses of Activin and Mix is upregulated at high doses of Activin (Yi-Hsien Chen, personal communication). The model was found to be bistable, with the steady states corresponding to mesoderm and ante-



**Figure 3.22:** *Xenopus* animal caps overexpressing XIvegT,  $\beta$ -catenin and in combination. Animal caps were cut from stage 9 embryos injected with various combinations of activin, XIvegT and  $\beta$ -catenin. The amounts of RNA injected are indicated. Animal cap explants were collected at stage 20. Animal caps treated with activin elongate. Dramatic elongation is caused by co-injection of XIvegT and  $\beta$ -catenin mRNAs. XIvegT or  $\beta$ -catenin alone injected samples show no elongation. qPCR analysis shows gene expression levels relative to ODC and then normalised to uninjected samples (Un-in). Data obtained by Yi-Hsien Chen.

rior mesendoderm. These two states can be reached dependent on the dose of Activin. For low doses of Activin a cell evolves to the mesoderm steady state. As the dose of Activin is increased there exists a critical dose of Activin ( $A^C$ ), such that for  $A > A^C$  the system evolves to anterior mesendoderm. The solutions to the model give predictions for a time course for expression of Mix, Brachyury and Goosecoid in response to Activin. To test the validity of the model, we will treat axolotl animal caps with doses of Activin and measure gene expression at several time points to see if experimental and model time courses are qualitatively in agreement. The only difference between the axolotl *in vitro* model (based on the GRN in figure 3.8) and the *Xenopus in vitro* model (based on the GRN in figure 3.1) is the regulation of *Brachyury* by Mix. In *Xenopus* there is a mutual antagonism of Mix.1 and *Brachyury*, which is thought to drive the formation of mesoderm and endoderm. In axolotl, where this mutual antagonism is not found, Mix is required for the expression of *Brachyury*. The only factor that creates competition between mesoderm and anterior mesendoderm is the repression of *Brachyury* by *Goosecoid*.

The axolotl *in vivo* model investigates the mesendoderm GRN downstream of  $\beta$ -catenin based on the GRN given in figure 3.7. Analysis of the model shows that  $\beta$ -catenin, in a similar manner to Activin, can induce mesoderm and anterior mesendoderm in a dose dependent manner. In this model  $\beta$ -catenin acts to induce Nodal signalling and there are no maternal factors present which act directly on Mix/*Brachyury*. In contrast, in the *Xenopus in vivo* model VegT and  $\beta$ -catenin induce Nodal signalling and VegT can also directly activate Mix and *Brachyury* (see figure 3.4).

Modifications to the *Xenopus in vivo* model were considered using recent experimental evidence. In the *in vivo* model of [95], it was assumed that VegT alone could induce the expression of the single representative Nodal. However a recent paper reveals that both VegT and  $\beta$ -catenin are required for the expression of the earliest expressed Nodal genes, so we modified the *in vivo* mathematical model to reflect this. This modified model, as with the original *in vivo* model, has four steady states, two corresponding to mesoderm, one to endoderm and one to the trivial steady state (i.e. ectoderm). Our numerical investigations showed that for all initial concentrations of VegT in the absence of  $\beta$ -catenin, solutions evolve to a mesoderm steady state, where *Brachyury* and FGF are maintained via a positive feedback loop. For cells exposed to both VegT and  $\beta$ -catenin, the mesoderm and endoderm steady states are both available. These results are consistent with experimental data.

The analysis of the mathematical models presented in this chapter is qualitative, since values for the model parameters are not available in the literature. Although the axolotl provides a model system in which to study a more simplified mesendoderm network than the *Xenopus*, obtaining parameter values for our model parameters is still a non-trivial task. Due to the many interactions between the genes in the network, including feedback loops, it is difficult to measure individual parameters directly. However techniques exist whereby time course expression of genes can be used to estimate many parameters at a time, and fit the model to the time course expression data. In the next chapter, we introduce such parameter estimation techniques and we obtain data and present preliminary findings of our model fits.



# Parameter Estimation in Single-cell Models of Mesendoderm Specification in Axolotl

In chapter 3 we identified the axolotl as a suitable model system for studying the mesendoderm GRN. The axolotl mesendoderm GRN contains one Mix and one Nodal gene which, when compared with the large Mix and Nodal gene families in *Xenopus*, provides a simpler GRN to study. We formulated and analysed qualitatively two versions of a single cell model of the axolotl mesendoderm GRN, namely the *in vitro* and *in vivo* models. The *in vitro* model gives the interactions of Mix, Brachyury and Goosecoid downstream of Activin, based on the network in figure 3.8, and in the *in vivo* model  $\beta$ -catenin activates *Nodal*, which then activates downstream genes (i.e. *Mix*, *Brachyury*, *Goosecoid* and *FGF*) based on the network in figure 3.7. Both models were found to be bistable with stable steady states corresponding to mesoderm and anterior mesendoderm. The *in vitro* model reached these steady states dependent on the dose of Activin and the *in vivo* model reached the steady states dependent on the dose of  $\beta$ -catenin consistent with experimental data given in [16]. In this chapter, we estimate parameter values in the *in vitro* model using a computational algorithm which minimises the error between experimental data and the output of the model. We select the animal cap system as a suitable experimental assay for obtaining data for use in the algorithm, since it gives gene expression data in a uniform population of cells. We investigate the ability of Nodal1 and Activin to induce mesendoderm in axolotl, we also confirm that, as shown in [139], Nodal2 is not involved in the induction of mesendoderm in axolotl. We then use these data to estimate parameters in the axolotl *in vitro* model. The behaviour of the model subject to the resulting parameter set is then tested against independent gene knockout data, which suggests that further rounds of model refinement and parameter estimation are required. Finally, we fit our data from axolotl animal caps to the *Xenopus in vitro* model and compare this to the axolotl *in vitro* model to show differences in the behaviour of the two models.

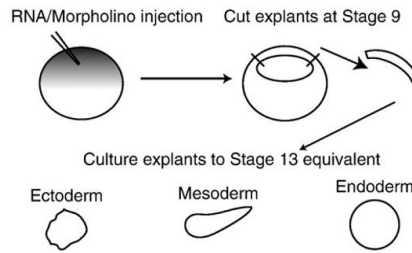


Figure 4.1: Schematic illustrating the animal cap assay as taken from [139].

## 4.1 Quantitative gene expression data

Numerous molecular biology techniques are available for obtaining information on the expression of genes in the developing embryo, as reviewed in section 1.13.1. These data can be qualitative, showing if a particular gene is expressed, or quantitative, giving absolute or relative levels of mRNA or protein in a sample. Recall that the output of the mathematical models formulated in chapter 3 produces a time course for the level of each gene in the mesendoderm GRN. Thus we require quantitative gene expression data to fit the model to. The models give the mesendoderm GRN in a single cell. Therefore we do not require information on the spatial distribution of genes or the spatial gradients which give rise to this expression. Directly measuring quantitative gene expression data for an individual cell is not currently possible, so we consider approaches for obtaining expression data in a single cell.

The animal cap assay is a well established experimental technique used to study the induction of mesendoderm in axolotl [139] and *Xenopus* [66, 79]. Animal caps are the region of the embryo which normally form ectoderm, and consist of a uniform population of cells. By treating animal caps with mesendoderm inducing factors they will form either mesoderm and endoderm. In the assay, embryos are injected with RNA at the single cell stage and left to develop until stage 9. At stage 9 animal cap explants are cut from the embryo and cultured until a time point of interest. The phenotype of the caps show the type of cells it consists of: mesoderm is marked by an elongated animal caps and endoderm is marked by a rounded phenotype (see figure 4.1). To measure the expression of genes in the animal cap samples, RNA can be extracted and used as a template for real-time quantitative PCR (qPCR), confirming the phenotype by measuring levels of mesendoderm-specific genes. qPCR gives the expression of genes relative to ODC, a ‘house keeping’ gene whose expression is constant in all animal cap samples.

Kühn et al [76] investigate a single cell mathematical model of the mesendoderm GRN in sea urchin, using time course gene expression data from whole embryos. Since the available data give gene expression across the whole embryo rather than in a single cell, they recalculate the whole embryo data as follows to give gene expression in a single cell

$$\text{Cellular expression} = \frac{\text{Whole embryo expression}}{\text{Number of cells expressing each gene.}}$$

Regions where a gene is expressed is determined using in-situ hybridization data, and the num-

ber of cells in these regions are inferred from fate maps. Recalculating quantitative data using this method makes numerous assumptions such as the number of cells in a region of the embryo and the uniform expression of the gene in regions where it is expressed and no expression in regions where WISH cannot detect expression. In comparison, Animal caps consist of a uniform population of cells thus overcoming the need to adjust data from whole embryos. However, there are still issues with using the animal cap assay data to estimate parameter values in mathematical models, which are discussed later in this chapter.

Next we need to select a gene which induces mesoderm and endoderm in axolotl animal caps to investigate models of the mesendoderm network. From our knowledge of the *Xenopus* mesendoderm network, we know that VegT and  $\beta$ -catenin are maternal factors involved in the induction of mesoderm and endoderm which act to induce Nodal genes [21, 74, 83, 117, 127, 154]. It has previously been shown that VegT is not required to induce mesoderm and endoderm in the axolotl [16], so we do not consider VegT any further.  $\beta$ -catenin regulates the specification of mesoderm and endoderm via the induction of Nodal signals. Activin can also induce mesoderm and endoderm in *Xenopus* animal caps [46, 47, 112]. Note that Activin is not a candidate for inducing mesendoderm in wild-type embryos, as it is not expressed in the early embryo and specific Activin blocking reagents do not affect normal development (see [42] for a review). This gives us four candidate genes which may be able to induce mesoderm and endoderm in animal caps:  $\beta$ -catenin (a maternal factor), Nodal-1 and Nodal-2 (which are induced by maternal factors) and Activin. Initially we choose to investigate the induction of mesoderm and endoderm by Activin, Nodal-1 and Nodal-2. Once this has been fully explored we will add upstream factors such as  $\beta$ -catenin to our model at a later date.

#### 4.1.1 The induction of mesendodermal genes in axolotl in response to *Activin, Nodal1* and *Nodal2*

In this section we investigate the induction of mesoderm and endoderm by Activin, Nodal1 and Nodal2. Activin can induce mesoderm and endoderm in a dose dependent manner in *Xenopus* [43, 46–48, 112] and 1pg of Activin has been shown to induce mesoderm in axolotl animal caps [139]. Nodal1 is required for gastrulation to occur in axolotl, as shown by a knockout using antisense morpholino oligos (MO) in whole embryos [139]. In embryos treated with a Nodal1 MO mesendodermal genes (for example Mix and Brachyury) are downregulated. In the absence of Nodal2 embryos still gastrulate, and mesendodermal genes are still expressed [139]. Given these existing data we predict that Activin and Nodal1 will induce mesoderm and endoderm in a dose dependent manner, and Nodal2 will not induce mesoderm and endoderm, when over-expressed in axolotl animal caps.

To test the ability of Activin, Nodal1 and Nodal2 to induce mesendoderm we use the animal cap assay as shown in the schematic in figure 4.1. Embryos were injected with the levels of mRNA shown in table 4.1, and uninjected caps which form ectoderm were used as a control. Uninjected whole embryos were also used as a timing control. Since we wish to use the data obtained for fitting our mathematical models, we collect animal cap samples at four time points.

mRNA	Amounts		
Activin	1pg	25pg	-
Nodal1	100pg	500pg	1ng
Nodal2	100pg	500pg	1ng

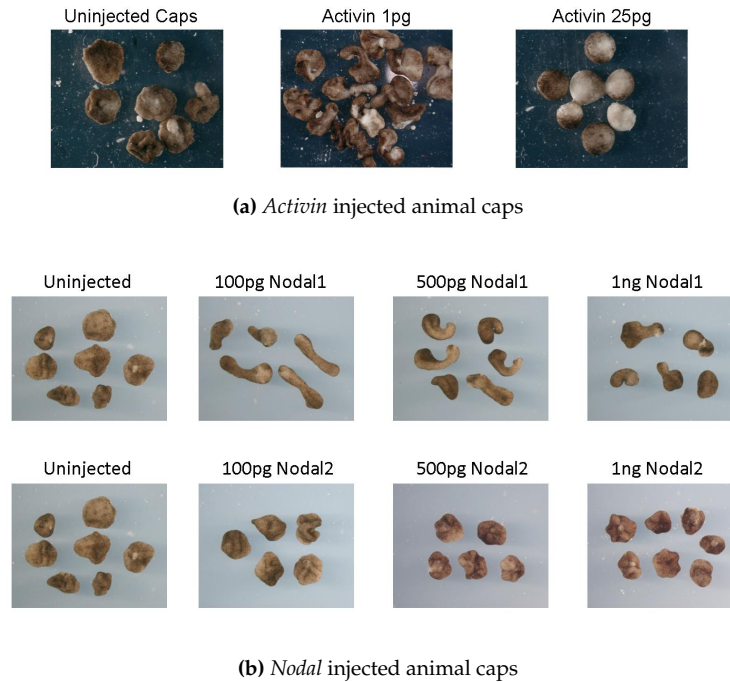
**Table 4.1:** Amounts of Activin, Nodal1 and Nodal2 injected into single cell embryos in the animal cap assay.

The first time point corresponds to when the caps were cut at stage 9 ('0 hours'), caps are then collected at 12, 24 and 48 hours later. Each sample was assayed using qPCR for the expression of several genetic markers of mesoderm and endoderm: *Brachyury* (a marker of mesoderm), *Mix*, *Sox17* (a marker of endoderm), *FGF8*, *Goosecoid*, *Nodal1* and *Nodal2*. The phenotype of the animal cap samples were noted at either 24 or 48 hours.

The phenotypes of animal caps overexpressing Activin, Nodal1 and Nodal2 are shown in figure 4.2. As expected, uninjected caps form ectoderm. At a low dose (1pg) of Activin the caps elongate forming mesoderm, and at a higher dose (25pg) caps become endoderm (figure 4.2a). Caps injected with doses of AxNodal1 form mesoderm; elongation of caps is greatest at 100pg AxNodal1, increasing the dose to 500pg the caps still elongate, reduces the extent of this elongation. At 1ng of AxNodal1, the caps resemble neither mesoderm, endoderm or ectoderm. Caps injected with doses of AxNodal2 do not form mesoderm or endoderm. This result suggests that AxNodal2 does not function in mesendoderm induction, which is consistent with previous observations that embryos still form mesoderm in the absence of AxNodal2 [139].

To confirm the phenotypes of the animal cap samples, the expression of mesendodermal genes was measured by qPCR. Gene expression in Activin injected caps is shown in figure 4.3. *Brachyury* is upregulated in 1pg Activin caps and not expressed in 25pg Activin caps. *Mix* is induced at both doses of Activin, with strongest expression in 25pg Activin caps. The induction of *Goosecoid* by Activin follows a similar pattern to the induction of *Mix*, with *Goosecoid* induced at both 1pg and 25pg Activin, with the greatest expression at the 25pg dose. Also note that the expression of *Goosecoid* in Activin caps is much stronger than expression in uninjected whole embryos. An analysis of the induction of *Sox17* by Activin confirms that endoderm forms at 25pg Activin, as marked by strong expression of *Sox17*. Conversely, *Sox17* is not induced at 1pg Activin.

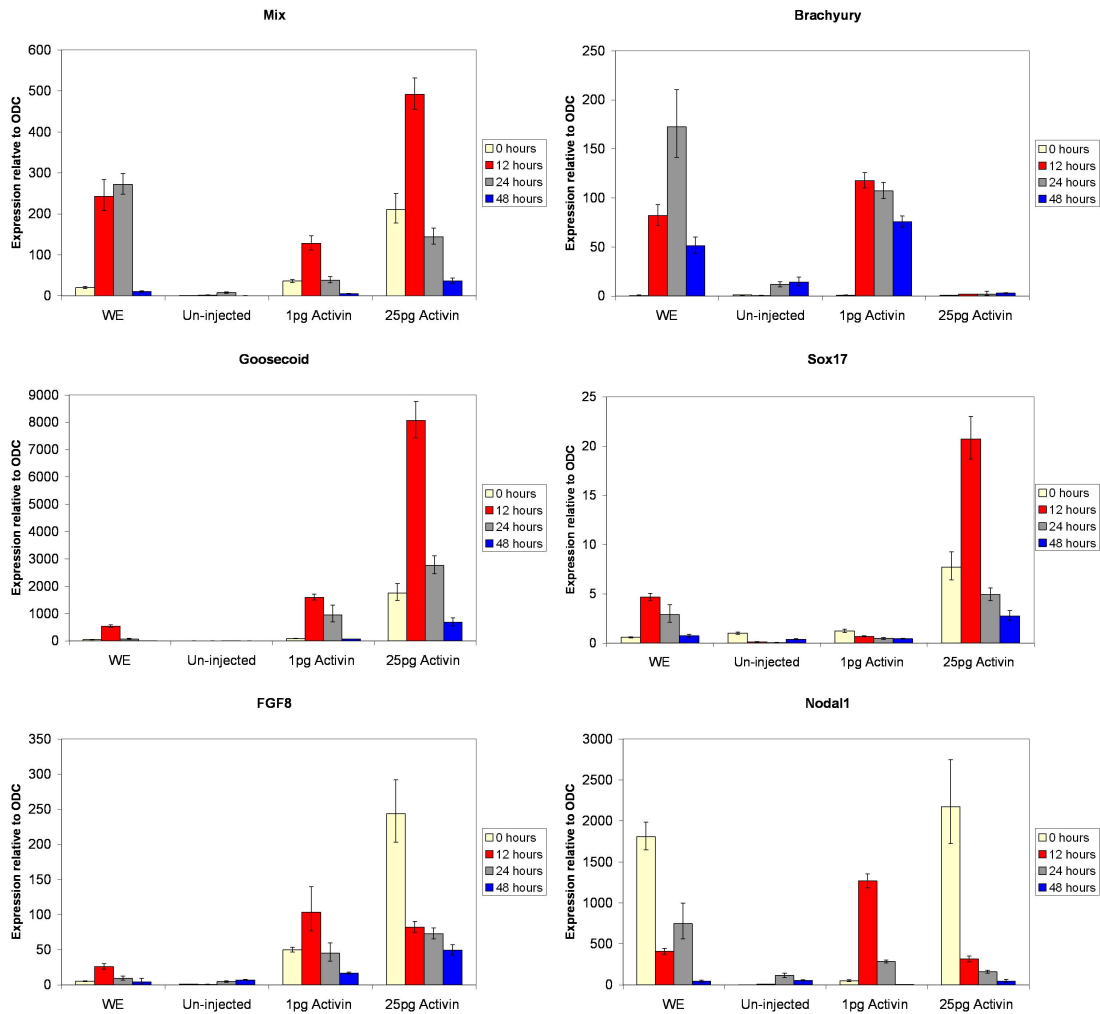
The induction of key mesendodermal genes by Nodal1 is shown in figure 4.4. *Brachyury* is induced strongly by 100pg Nodal1 and at higher doses (500pg and 1ng Nodal1) the induction of *Brachyury* is weaker than that for 100pg, but still greater than the levels in uninjected caps. Note that, at all three doses of Nodal1, *Brachyury* is not upregulated until 24 hours (corresponding to stage 12 whole embryos). This is similar to that seen in whole embryos, where *Brachyury* expression does not commence until the midblastula stages [64, 139]. The levels of *Mix* induced by Nodal1 are low compared with expression in whole embryos. The induction of *Mix* is strongest at 100pg Nodal1 and at 500pg and 1ng Nodal1 levels of *Mix* are similar to those found in uninjected caps. All three doses of Nodal1 fail to induce *Goosecoid* or *Sox17*. The lack of induction of *Sox17* suggests that endoderm is not induced by Nodal1 in axolotl



**Figure 4.2: Axolotl animal caps overexpressing (a) *Activin*, (b) *Nodal1* and *Nodal2*.** Animal caps were photographed at (a) 48 hours (stage 15 whole embryo control) and (b) 24 hours (stage 12 whole embryo control). Animal caps were cut from stage 9 embryos injected with *Activin*, *Nodal1* or *Nodal2* RNA into the animal pole at the one or two cell stage. Amounts injected per embryo are stated above each set of caps. **(a)** At a low dose (1pg) of *Activin*, caps show an elongation phenotype and at a higher dose (25pg *Activin*) caps form an endodermal-like tissue. **(b)** Animal caps elongated in response to Ax*Nodal1*, with the most extensive elongation occurring in response to the lowest dose (100pg) of Ax*Nodal1*. Animal caps did not differ from the uninjected phenotype in response to Ax*Nodal2*.

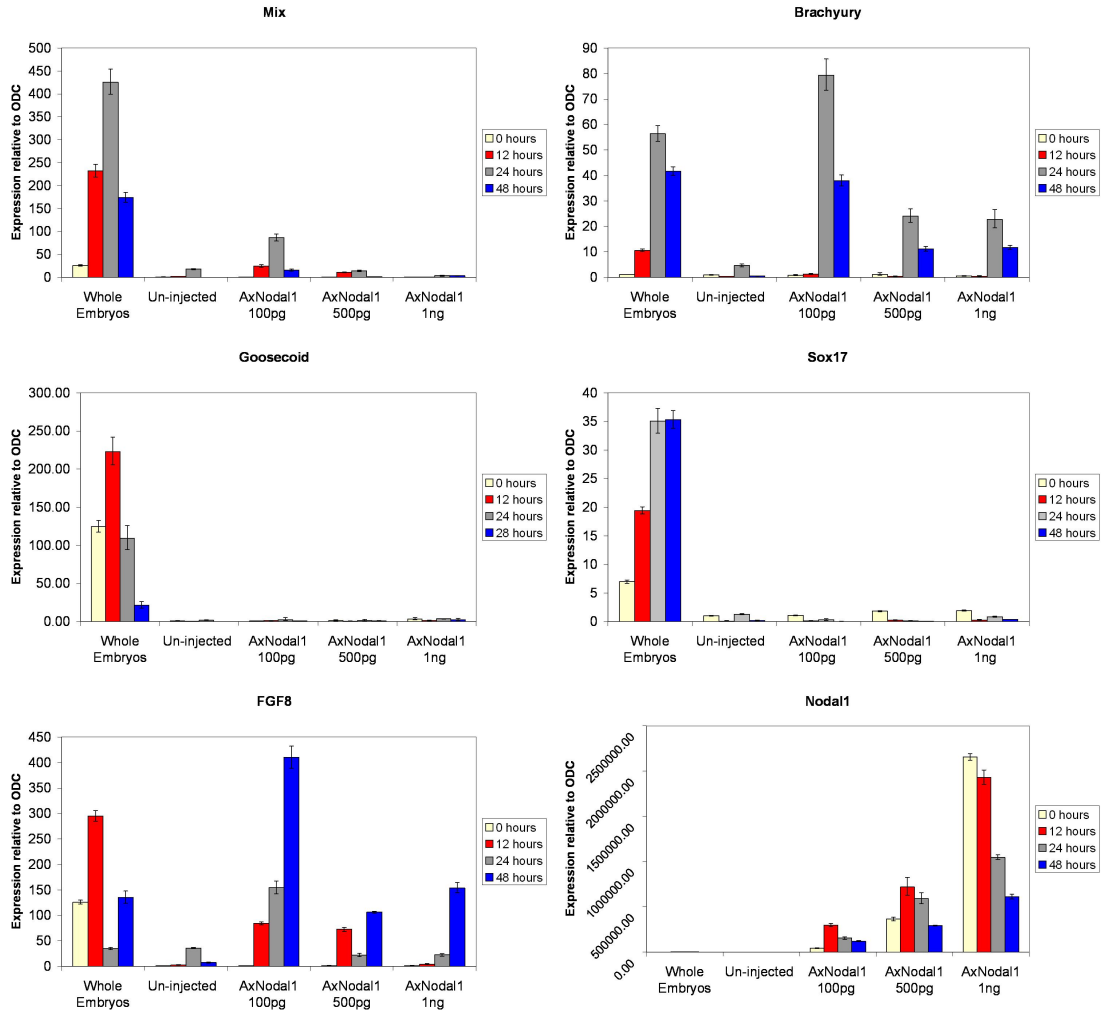
animal caps. FGF8 is expressed at all three levels of *Nodal1*, with expression being highest at 100pg *Nodal1* and decreasing as the dose of *Nodal1* increases. The levels of *Nodal1* measured in animal caps from embryos injected with *Nodal1* are much higher than the levels in whole embryos or uninjected caps. This is expected since a whole embryo contains only 1.78pg of *Nodal1* (Yi-Hsien Chen, personal communication) and we injected doses of 100pg, 500pg and 1ng. At the two lower doses (100pg and 500pg) of *Nodal1*, the levels of *Nodal* present increases between 0 and 12 hours before decreasing at later time points. At the highest dose (1ng) of *Nodal1*, the expression of *Nodal1* is highest at 0 hours and decreases as time proceeds. *Nodal2* is not capable of inducing the expression of mesendodermal genes at doses of 100pg, 500pg or 1ng as shown in figure 4.5.

The data presented in this section shows differences in mesendoderm induction by *Activin*, *Nodal1* and *Nodal2*. *Activin* is able to induce mesoderm and endoderm in a dose dependent manner in axolotl animal caps. Mesoderm is induced at a low dose (1pg *Activin*) and endoderm is induced at a high dose (25pg *Activin*). Mesoderm, but not endoderm, is induced by *Nodal1* and neither mesoderm or endoderm are induced by *Nodal2*. The differences in the ability of *Activin*, *Nodal1* and *Nodal2* to induce mesoderm and endoderm are shown in the expression



**Figure 4.3: qPCR analysis of gene expression in response to Activin.** Caps were collected at the equivalent to stage 9 (0 hours), then 12, 24 and 48 hours later. Gene expression levels are relative to ODC, then normalised to each gene in uninjected caps at 0 hours.

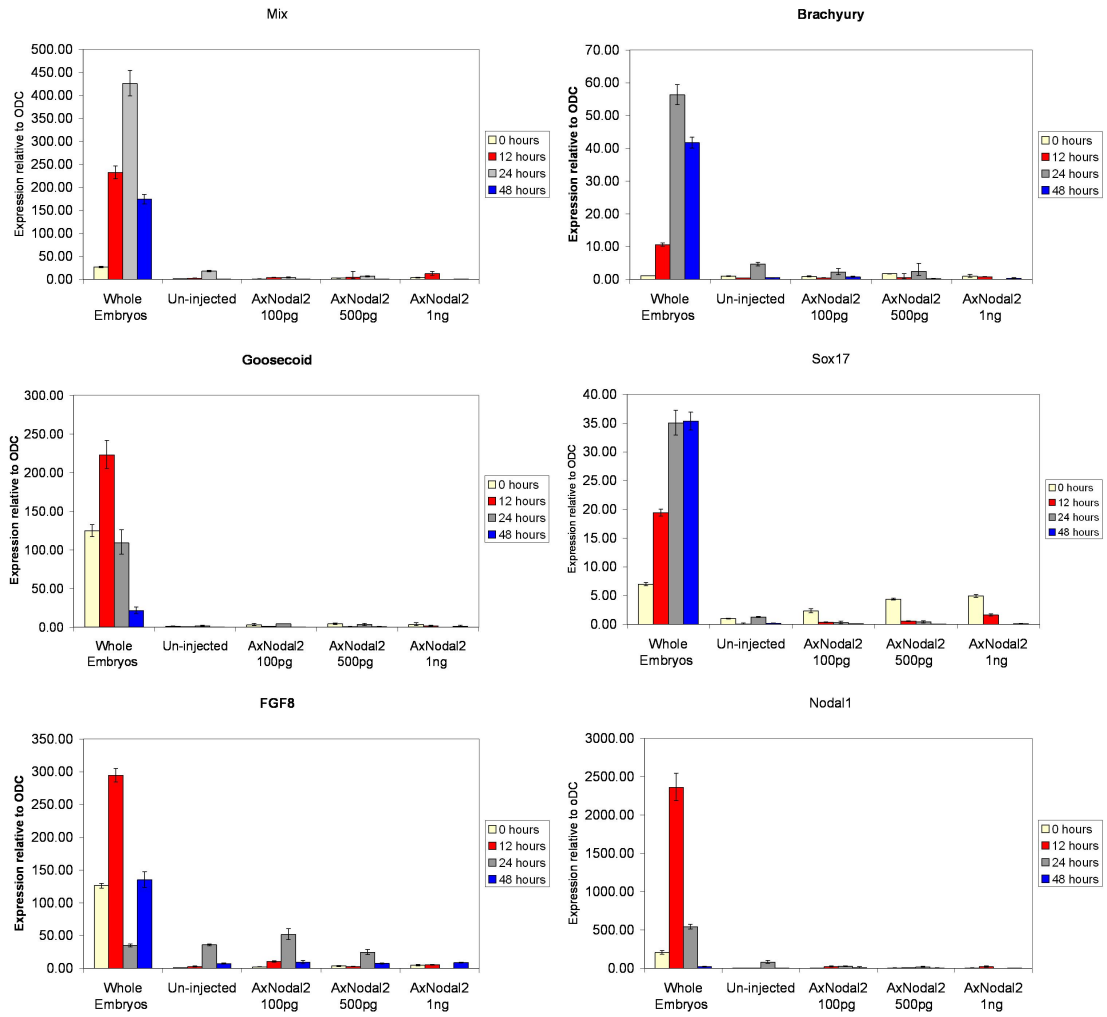
of genes. A key difference in the genes induced by Nodal1 and Activin is the expression of Mix. In caps which form mesoderm (100pg Nodal1 and 1pg Activin caps) levels of Mix are approximately 100 times the level found in uninjected caps. When the level of Activin is increased to a dose capable of inducing endoderm, Mix expression is approximately 500 times the uninjected cap level. However as the dose of Nodal1 is increased Mix levels decrease. Genes downstream of Mix, such as Goosecoid and Sox17 are also not induced by any level of Nodal1, but are strongly induced at high levels of Activin. This suggests that Nodal1 and Activin induce Mix in different ways. This is surprising since Nodal and Activin are thought to act through the same signalling pathway. The differences in the induction of Mix by Nodal1 and Activin warrants further investigation, which is beyond the scope of this thesis. Nodal2 does not induce any mesendodermal genes, consistent with it not having a role in mesendoderm induction [139].



**Figure 4.4:** qPCR analysis of gene expression in response to AxNodal1. Caps were collected at the equivalent to stage 9 (0 hours), then 12, 24 and 48 hours later. Gene expression levels are relative to ODC, then normalised to each gene in uninjected caps at 0 hours.

## 4.2 Parameter estimation in models of the axolotl mesendoderm GRN

In this section we use the experimental data presented in section 4.1 to estimate parameters in a mathematical model of the axolotl mesendoderm GRN. Our experimental findings indicate that Activin can induce both mesoderm and endoderm, whilst Nodal1 only induces mesoderm. Since mesendoderm induction by Nodal1 requires further experimental investigation, we choose to estimate parameter values in a model of the axolotl mesendoderm GRN downstream of Activin. As described in section 1.13, many computational algorithms are available that search parameter space to minimise the error between a mathematical model and experimental data. Here we choose to use a hybrid algorithm which combines the genetic algorithm (GA) with a local parameter search. The algorithm is implemented in MATLAB, using the ga



**Figure 4.5: qPCR analysis of gene expression in response to Nodal2.** Caps were collected at the equivalent to stage 9 (0 hours), then 12, 24 and 48 hours later. Gene expression levels are relative to ODC, then normalised to each gene in uninjected caps at 0 hours.

function from the global optimization toolbox for the GA and the `fmincon` function from the optimization toolbox for the local search.

#### 4.2.1 Mathematical model

The axolotl *in vitro* model developed in chapter 3 describes the axolotl mesendoderm GRN downstream of Activin in a single dissociated cell. However the animal caps used to obtain our experimental data consist of a uniform population of cells. As such we modify the axolotl *in vitro* model to describe the mesendoderm GRN in a single cell embedded in a uniform population of cells. In a single dissociated cell we assumed that the eFGF signal secreted was too weak to act on its downstream targets. Therefore eFGF was not included in the *in vitro* model developed in chapter 3. In a uniform population of cells, such as an animal cap, we assume



that the eFGF signal secreted is strong enough to act on its downstream targets. As such we include terms in our model representing the action of eFGF. Recall that eFGF is activated by Brachyury and also acts to positively regulate Brachyury, forming an eFGF/Brachyury positive feedback loop. To keep our model as simple as possible, and to reduce the number of unknown parameters, we represent the eFGF/Brachyury feedback loop as the positive autoregulation of Brachyury. The governing equations of the axolotl *in vitro* model we will use for estimating parameter values are

$$\frac{dM}{dt} = \lambda_{A,M} \mathcal{H} \left( \frac{A}{\theta_{A,M}}, m_1 \right) \left\{ 1 - \mathcal{H} \left( \frac{B}{\theta_{B,M}}, m_2 \right) \right\} - \mu_M M, \quad (4.2.1a)$$

$$\frac{dG}{dt} = \lambda_{M,G} \mathcal{H} \left( \frac{M}{\theta_{M,G}}, m_3 \right) \left\{ 1 - \mathcal{H} \left( \frac{G}{\theta_{G,G}}, m_4 \right) \right\} - \mu_G G, \quad (4.2.1b)$$

$$\frac{dB}{dt} = \left[ \lambda_{A,B} \mathcal{H} \left( \frac{A}{\theta_{A,B}}, m_5 \right) \mathcal{H} \left( \frac{M}{\theta_{M,B}}, m_6 \right) + \lambda_{B,B} \mathcal{H} \left( \frac{B}{\theta_{B,B}}, m_8 \right) \right] \left\{ 1 - \mathcal{H} \left( \frac{G}{\theta_{G,B}}, m_7 \right) \right\} - \mu_B B, \quad (4.2.1c)$$

where  $\mathcal{H}(x, m) = \frac{x^m}{x^m + 1}$  is the Hill function with Hill coefficient  $m$ . Note that (4.2.1) is the same as (3.4.9) with the addition of the  $\lambda_{B,B} \mathcal{H} \left( \frac{B}{\theta_{B,B}} \right)$  term representing Brachyury positive autoregulation. The model has 23 unknown parameters, consisting of 4 rates of production parameters ( $\lambda$ ), 8 threshold parameters ( $\theta$ ), 3 rates of turnover ( $\mu$ ) and 8 hill coefficients ( $m$ ). To estimate values of these parameters we will use data on the expression of Mix, Brachyury and Goosecoid in caps injected with two doses (1pg and 25pg) of Activin, as shown in figure 4.3. There are 24 experimental data points which we use to estimate 23 parameters. Note that this data is rather limited given the number of unknown parameters in the model, since there is a limit on the number of embryos available to carry out any single experiment and hence a limit on the resulting number of data points.

## 4.2.2 Preliminaries

We now consider how to use the qPCR data from Activin injected animal caps to parameterise the axolotl *in vitro* model. The mathematical model describes the time evolution of transcription factors (i.e. proteins), however our data gives the level of mRNA in a sample. We assume that the concentration of protein translated from mRNA is proportional to the concentration of mRNA transcript, and fit the model to mRNA data.

The first time point at which we collect data in the experiments of section 4.1 is at stage 9 (which we call 0 hours) corresponding to when animal cap explants are removed from the embryo. However, transcription of zygotic genes commences at the mid-blastula transition (MBT) which occurs at stage 8 [41]. By stage 9 genes in the mesendoderm GRN may already be expressed. From figure 4.3 it can be seen that at 0 hours Mix and Goosecoid are upregulated in Activin injected caps compared with uninjected caps, suggesting that transcription of these genes has commenced at this time point. Stage 9 is the earliest stage at which caps can be cut from the embryo. To overcome this problem we to set the model time such that  $t = 0$

Model time $t$	Experimental Time $T$ (hours)
0	N/A
6	0
18	12
30	24
54	48

**Table 4.2:** Rescaling of experimental time scale for the mathematical model

corresponds the MBT at stage 8. Here, we assume that MBT occurs 6 hours before stage 9 and rescale time accordingly, such that  $t = T + 6$ , where  $t$  is time in the mathematical model and  $T$  is experimental time (see table 4.2).

Another issue is that the qPCR data we use are normalised to some reference concentration (see Materials and Methods, chapter 2 for more details). For example, in the gene expression data in section 4.1.1 the expression level of each gene is normalised to the genes expression in uninjected caps at 0 hours (stage 9). To ensure consistency between the experimental data and the mathematical model, we normalise the mathematical model in the same way as experimental data before comparing the model output with experimental data. For evaluating how well our *in vitro* model (4.2.1) fits to the data, we normalise all mRNA concentrations to the level of *Mix* in 1pg Activin injected caps at stage 9 (0 hours). The output of the mathematical model is then defined as:

$$\bar{X}_{i,j}^{\text{model}} = \frac{X_{i,j}^{\text{model}}}{Y_{1,6}^{\text{model}}} \quad (4.2.2)$$

where  $\bar{X}_{i,j}^{\text{model}}$  is the normalised model output for Activin dose  $i$  at time  $j$ ,  $X_{i,j}^{\text{model}}$  is the unscaled model output for Activin dose  $i$  at time  $j$  and  $Y_{1,6}^{\text{model}}$  is the unscaled model output for *Mix* at  $t = 6$  in 1pg injected caps.

In the hybrid parameter estimation algorithm the fitness function ( $F$ ) gives a measure of the error between the mathematical model and the experimental data.  $F$  is defined by

$$F(N_{i,j}^{\text{data}}, N_{i,j}^{\text{model}}) = \sum_{i=1}^m \sum_{j=1}^m \omega_i \left( N_{i,j}^{\text{data}} - N_{i,j}^{\text{model}} \right)^2, \quad (4.2.3)$$

where  $N_{i,j}^{\text{model}}$  is the normalised model output as defined in (4.2.2) and  $N_{i,j}^{\text{data}}$  is the corresponding experimental data point and  $\omega_{i,j}$  is a weighting of the fitness function. For each gene at each data point we define  $\omega_{i,j} = \frac{1}{X_{i,T}^{\text{data}}}$ , where  $X_{i,T}^{\text{data}}$  is the concentration of the gene  $X$  at  $t = T$ .

As in chapter 3, we assume that a cell can remember the concentration of Activin it receives (via the maintenance of a pool of phosphorylated Smad2), meaning that the concentration of Activin is a constant parameter in the model. To simulate a 1pg dose of Activin, we set  $A = 1$  and for a 25pg dose of Activin we set  $A = 25$ . After rescaling time as discussed above, so that  $t = T + 6$ , where  $t$  is time in the mathematical model and  $T$  is the experimental time where  $T = 0$  is the time when the caps are cut, we set initial conditions such that no factors are present in the cap at  $t = 0$  so that

$$M(0) = B(0) = G(0) = 0. \quad (4.2.4)$$

We use a hybrid algorithm, consisting of several generations of a global search method (the Genetic Algorithm [59]), followed by a local search. Since there is a stochastic element to the algorithm, we run our algorithm several times in order to minimise the error between the mathematical model and the experimental data. A measure of this error is given by the fitness function  $F$  which we define as:

$$\begin{aligned}
 F_1(\mathbf{X}_{\text{model}}, \mathbf{X}_{\text{data}}) = & \\
 & \sum_{t=6,18,30,54} \frac{(B_{\text{data}}(1,t) - B_{\text{model}}(1,t))^2}{B_{\text{data}}(1,6)^2} + 0.024 * \sum_{t=6,18,30,54} \frac{(B_{\text{data}}(25,t) - B_{\text{model}}(25,t))^2}{B_{\text{data}}(25,6)^2} \\
 & + \sum_{t=6,18,30,54} \frac{(G_{\text{data}}(1,t) - G_{\text{model}}(1,t))^2}{G_{\text{data}}(1,6)^2} + 2 * \sum_{t=6,18,30,54} \frac{(G_{\text{data}}(25,t) - G_{\text{model}}(25,t))^2}{G_{\text{data}}(25,6)^2} \\
 & + \sum_{i=1,25} \sum_{t=6,18,30,54} \frac{(M_{\text{data}}(i,t) - M_{\text{model}}(i,t))^2}{M_{\text{data}}(i,6)^2}, \quad (4.2.5)
 \end{aligned}$$

where  $B_{\text{data}}(i,t)$  ( $M_{\text{data}}(i,t)$ ,  $G_{\text{data}}(i,t)$ ) is the gene expression data for *Brachyury* (*Mix*, *Gooseoid*) for an Activin dose  $ipg$  at time  $t$  and  $B_{\text{model}}(i,t)$  ( $M_{\text{model}}(i,t)$ ,  $G_{\text{model}}(i,t)$ ) is the expression of *Brachyury* (*Mix*, *Gooseoid*) predicted by the mathematical model for an Activin dose  $ipg$  at time  $t$ .

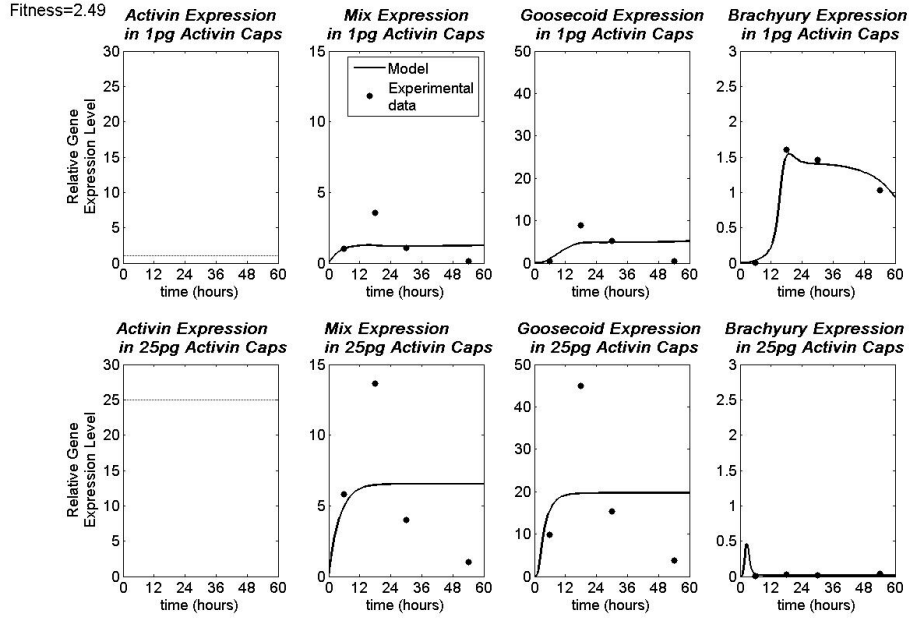
### 4.2.3 Parameter estimation results

Results of the parameter estimation algorithm are now presented. Since there is a stochastic element to the algorithm, it is not guaranteed that the model converges to the optimum solution. With this in mind we carry out numerous runs of the algorithm, presenting here the best resulting fits of the model to the experimental data. The best fit for the model (4.2.1) to experimental data is shown in figure 4.6. The model simulation is in good agreement with qPCR expression data for *Brachyury*, but does not capture the behaviour of *Mix* and *Gooseoid*. For example, the model does not show the decrease in *Mix* and *Gooseoid* after 18 hours seen in the data. To obtain a more satisfactory fit of the model to experimental data, we need to modify the mathematical model. Examples of possible modifications to the model are including extra TFs or more links between existing TFs. The decrease in levels of *Mix* and *Gooseoid* seen between 18 and 52 hours looks as if it could be due to degradation of TFs. We therefore choose to explore adding the turnover of Activin to the model.

We proceed to modify the axolotl *in vitro* model to include the turnover of Activin. In the previous model we assumed that a cell ‘remembers’ the highest dose of Activin it receives and  $A$  was set to be a constant parameter. We change the model such that Activin is turned over at a rate  $\mu_A$ , governed by the equation

$$\frac{dA}{dt} = -\mu_A A. \quad (4.2.6)$$

Initial conditions of  $A$  are defined as follows; for a 1pg dose of Activin, we set  $A(0) = 1$  and for



**Figure 4.6:** Experimental data (dots) and simulation results (lines) for the axolotl *in vitro* model (4.2.1). Model parameters were sought using a parameter estimation algorithm as described in the main text, and are as given in the ‘axolotl A’ table 4.3.

a 25pg dose of Activin we set  $A(0) = 25$ . All other equations and initial conditions remain as defined in (4.2.1) and (4.2.4).

The best fit for the model given in (4.2.1) and (4.2.6) is shown in figure 4.7. This model is able to reproduce experimental data better than the previous model which assumed a fixed concentration of Activin. The model simulations in figure 4.7 qualitatively capture the behaviour of the experimental time-course data, such as the initial increase in *Mix* and *Goosecoid*, their peak between 12 and 24 hours, and their subsequent degradation. The model simulation also reproduces the experimental data for *Brachyury*, with *Brachyury* upregulated at a 1pg dose of Activin and downregulated at 25pg Activin. The model shows a small initial peak in *Brachyury* levels between 0 and 6 hours in 25pg Activin caps, which corresponds to between stages 8 and 9 in whole embryos. We hypothesize that this is unlikely to occur *in-vivo* since in whole embryos *Brachyury* is not detected until stage 10.5 [63, 139]. However, previous studies of *Brachyury* expression do not measure the levels of *Brachyury* between key developmental stages. Therefore to determine whether this peak in expression occurs *in vivo*, *Brachyury* levels would need to be measured at hourly intervals between stages 8 and 9, although this would be a complex experiment.

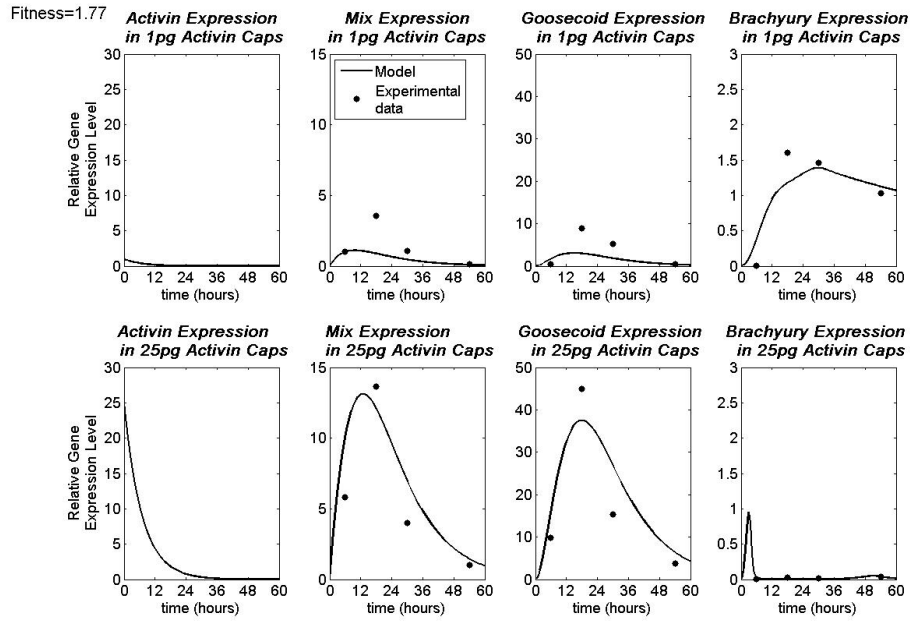
We now explore the dynamics of the model used to produce the simulations in figure 4.7 subject to various conditions to give predictions about the behaviour of the mesendoderm GRN in axolotl. To show the long term behaviour of the system, time-dependent solutions are plotted from 0 to 200 hours in figure 4.8. Activin levels decay over time, this is expected since the equation for the rate of change of Activin (4.2.6) contains only a term for its turnover. By 50

Variable	Parameter	Axolotl A	Xenopus A	Axolotl B	Xenopus B
A M	$\mu_A$	-	-	0.15	0.12
	$\lambda_{A,M}$	0.33	0.75	0.01	0.046
	$\theta_{A,M}$	5.00	1.16	9.99	5.19
	$m_1$	1.00	3.76	1.00	1.00
	$\theta_{B,M}$	0.53	1.20	0.53	1.51
	$m_2$	3.12	4.00	2.61	2.72
	$\mu_M$	0.24	0.078	0.072	0.066
G	$\lambda_{M,G}$	3.36	11.96	32.85	29.55
	$\theta_{M,G}$	0.66	3.38	45.89	24.42
	$m_3$	2.68	4.00	1.00	1.00
	$\theta_{G,G}$	1.87	23.09	100	0.78
	$m_4$	2.52	4.00	4.00	1.38
	$\mu_G$	0.14	0.13	0.23	0.18
	B	$\lambda_{A,B}$	0.16	0.03	0.09
$\theta_{A,B}$		0.53	0.28	0.013	0.032
$m_5$		2.31	3.67	3.86	2.74
$\theta_{M,B}$		0.47	997.21	<b>0.55</b>	<b>0.22</b>
$m_6$		2.87	-	1.08	-
$\theta_{G,B}$		0.97	670.09	0.032	101.01
$m_7$		2.86	1.12	4.00	3.29
$\lambda_{B,B}$		1.81	2.05	108.37	0.75
$\theta_{B,B}$		0.30	0.18	11.89	0.095
$m_8$		1.41	3.30	1.00	1.13
$\mu_B$		1.95	1.12	9.11	5.21

**Table 4.3:** Parameter values used to solve the mathematical model of the axolotl and *Xenopus* mesendoderm networks. These parameter sets are the best fits obtained using our parameter estimation algorithm.

hours after the onset of zygotic transcription Activin has reached negligible levels. After peaks in *Mix* and *Goosecooid* which occur at around 12 hours, there is a decay in mRNA levels and by 100 hours the levels are negligible. Whilst the dynamics of *Mix* and *Goosecooid* are qualitatively the same for both 1pg and 25pg Activin, the behaviour of *Brachyury* is different for the two doses of Activin. In 25pg Activin caps there is a ‘spike’ in *Brachyury* at  $t = 3$  followed by a smaller peak in expression at  $t = 50$ , apart from these two peaks in expression *Brachyury* is very weak at this dose of Activin. In 1pg Activin caps *Brachyury* peaks at approximately 30 hours then decays, note that *Brachyury* is still upregulated at 200 hours, likely a consequence of *Brachyury* positively regulating its own production (representing the eFGF/*Brachyury* feedback loop). Figure 4.9 shows model simulations for several dosed Activin. As the dose of Activin increases, the quantitative behaviour of *Mix* and *Goosecooid* remains the same; the expression of each gene increases to a maximum concentration between 12 and 24 hours before decaying to negligible levels. The maximum levels of *Mix* and *Goosecooid* increase as the dose of Activin increases. The qualitative behaviour of the time course of *Brachyury* expression changes as the dose of Activin increases. At 1pg of Activin, *Brachyury* reaches its maximum expression level at 30 hours, followed by a decrease in its expression. For Activin doses greater than 5pg there is an initial ‘spike’ in *Brachyury* levels followed by a period of downregulation and a later, smaller peak in *Brachyury* levels.

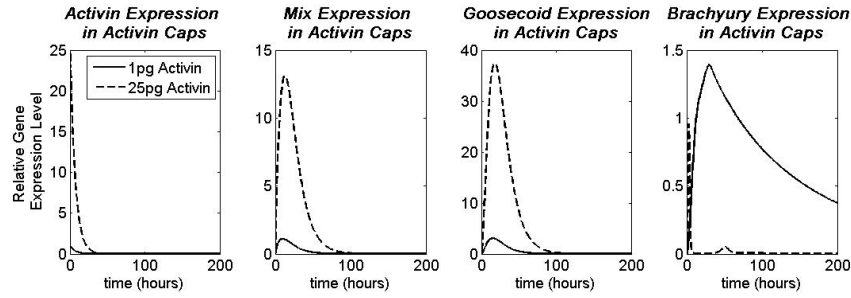
Next we investigate the role of Activin turnover on the behaviour of *Mix*, *Brachyury* and *Goosecooid* in the model. Model simulations are compared in the presence and absence of Activin turnover (corresponding to  $\mu_A = \tilde{\mu}_A$  where  $\tilde{\mu}_A$  is the value from parameter estimation and  $\mu_A = 0$ , respectively) in figure 4.10. When Activin turns over, the solutions of the model



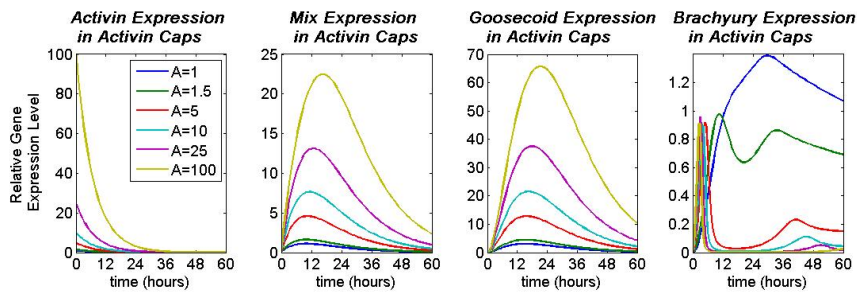
**Figure 4.7: Model simulation for the axolotl *in vitro* model including the turnover of Activin** Experimental data (dots) and simulation results (lines) for the axolotl *in vitro* model (4.2.1) and (4.2.6). Model parameters were sought using a parameter estimation algorithm as described in the main text, with the resulting parameter set given in the ‘axolotl B’ column of table 4.3.

are as described above, with Mix and Goosecoid decaying to negligible levels after reaching a maximal level between 12 and 24 hours. When Activin levels remain constant Mix and Goosecoid continue to increase until they reach a steady state value. The steady state value reached is dependent on the dose of Activin. The increase in levels of Goosecoid causes Brachyury to be down regulated in 1pg Activin caps compared with the ‘wild type’ behaviour.

In what follows we make use of existing data on the knockdown and overexpression of Mix from [139] to test our model using an independent data set from that used in parameter estimation. A knockdown of Mix in whole embryos causes a down regulation of Brachyury compared to its wild-type expression level. In the *in vitro* model (4.2.1), Mix is required for the induction of Goosecoid and Brachyury. The knockdown of Mix, by setting  $\lambda_{A,M} = 0$  in the model, results in no expression of Brachyury and Goosecoid (figure 4.11). This feature of the model results from the topology of the mesendoderm GRN rather than the parameter values used to obtain numerical solutions, meaning that this result gives no information on the validity of estimated parameter values. A further experiment carried out in [139] investigates the role of Mix in rescuing the mesoderm phenotype in caps depleted of Mix. Elongation of caps (i.e. mesoderm) is induced by 1pg Activin in animal caps, this induction is blocked by the co-injection of a Mix MO. In these samples mesoderm is rescued by Mix RNA; A low dose of Mix (20pg) causes the morphant caps to become mesoderm and a higher dose (200pg) induces endoderm. To test that Mix is able to rescue mesoderm in our mathematical model we set  $A(0) = 1$  (an initial condition of 1pg Activin),  $\lambda_{A,M} = 0$  (a Mix MO) and  $M(0) = M_{low}$  or  $M_{high}$  to simulate a low



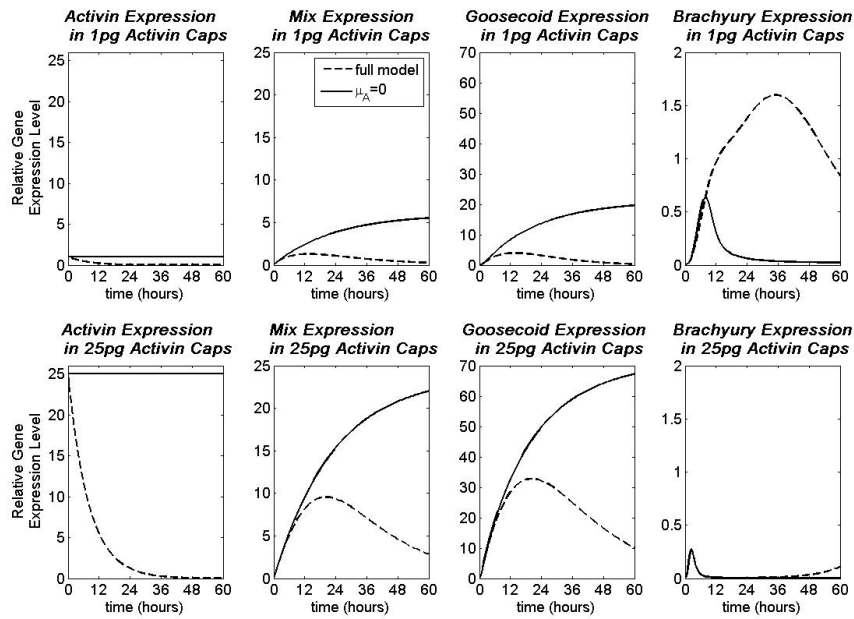
**Figure 4.8: Model simulation for the axolotl *invitro* model as given by (4.2.1) and (4.2.6), including the turnover of Activin Model parameters were sought using a parameter estimation algorithm as described in the main text, with the resulting parameter set given in the ‘axolotl B’ column of table 4.3.**



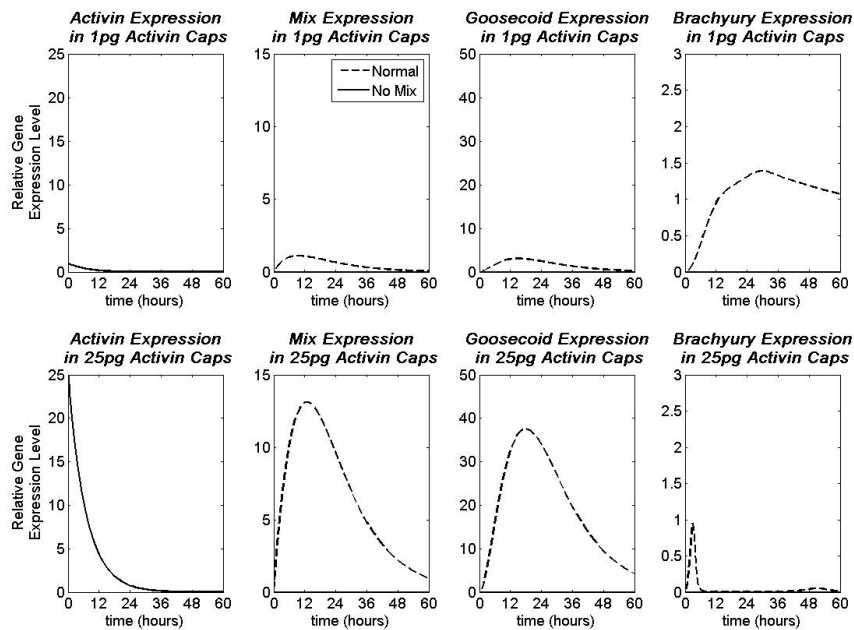
**Figure 4.9: Investigation of the level of gene expression in response to Activin. The model is as given in equations (4.2.1) and (4.2.6) solved subject to parameters given in the ‘axolotl B’ column of table 4.3.**

or high dose of Mix. In these cases the model is in qualitative agreement with experimental observations, such that a low dose of Mix rescues mesoderm, but endoderm forms at a high dose of Mix (figure 4.12).

We investigate the behaviour of our model when Brachyury and Goosecoid are either removed or overexpressed. The knockout and overexpression of Brachyury and Goosecoid have not been tested experimentally, meaning the model will give predictions that can be tested experimentally. When Brachyury is removed from the model, there is no change in the expression levels of Mix and Goosecoid (figure 4.13). This is surprising since in the mesendoderm GRN Brachyury negatively regulates Mix. When Brachyury is overexpressed there is a slight decrease in the maximum levels of Mix and Goosecoid reached, but the qualitative behaviour does not change (figure 4.14). A knockdown of Goosecoid results in an approximately two fold increase in the level of Brachyury in 1pg Activin caps and in 25pg Activin caps Brachyury is strongly upregulated when compared with the full *invitro* model. The knockdown of Goosecoid does not affect levels of Mix (figure 4.15). The overexpression of Goosecoid does not affect the expression of Mix, as expected since Mix is not downstream of Goosecoid in the mesendoderm GRN. However an overexpression of Goosecoid causes a downregulation of Brachyury. In particular the ‘spike’ of Brachyury seen in the full model does not occur when excess Goosecoid is present (figure 4.16).

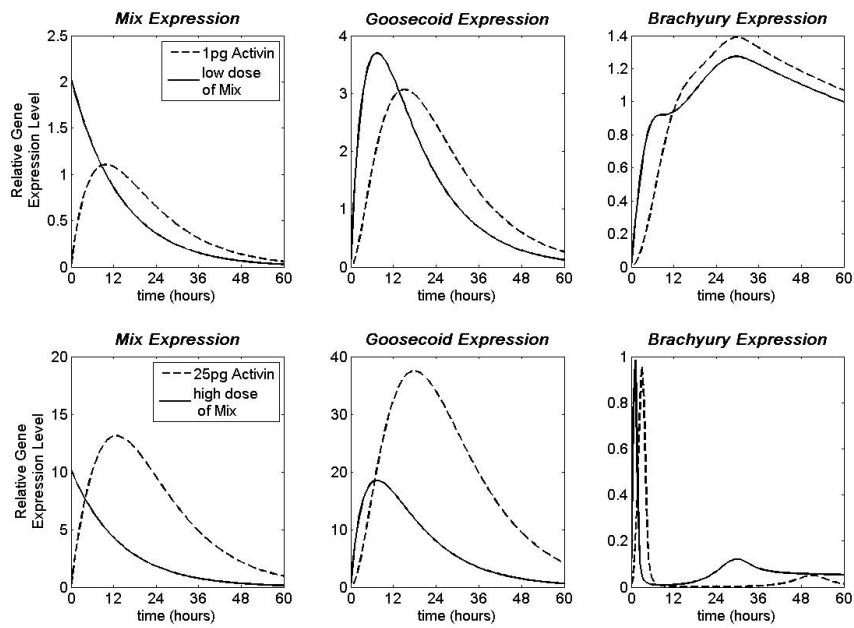


**Figure 4.10: Investigating the role of Activin turnover.** The model is solved in the presence (dashed line) and absence (solid line) of Activin turnover. The model is as given in equations (4.2.1) and (4.2.6) solved subject to parameters given in the ‘axolotl B’ column of table 4.3.

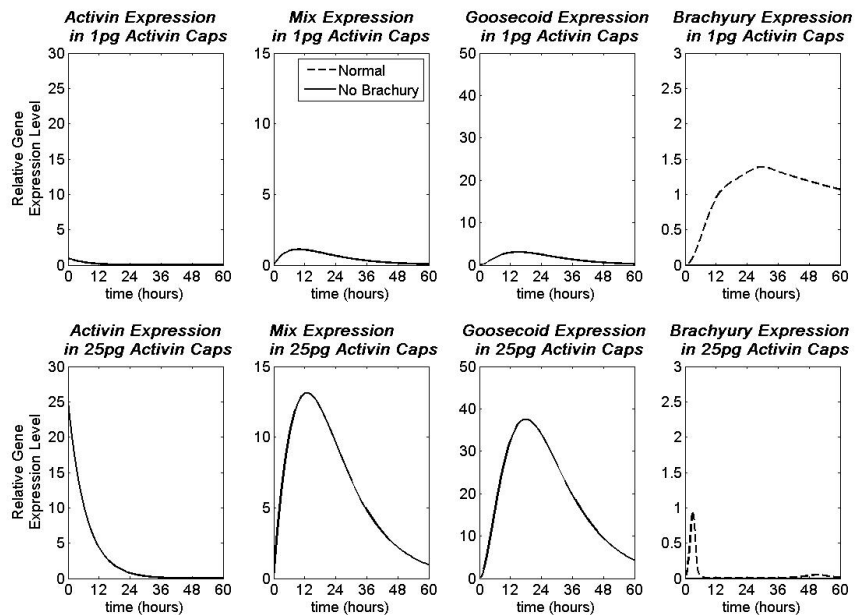


**Figure 4.11: Investigating the action of Mix.** The model is solved in the presence (dashed line) and absence (solid line) of Mix. The model is as given in equations (4.2.1) and (4.2.6) solved subject to parameters given in the ‘axolotl B’ column of table 4.3.

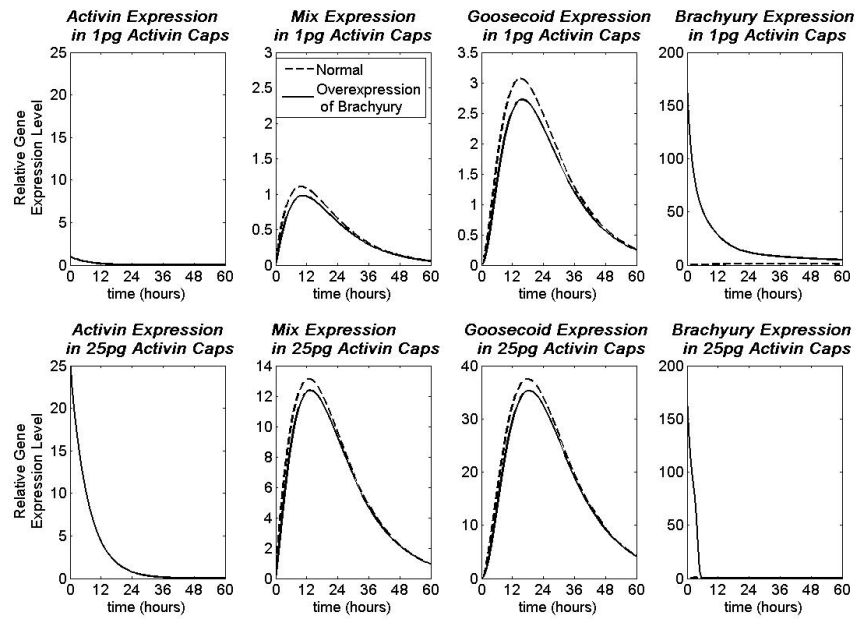




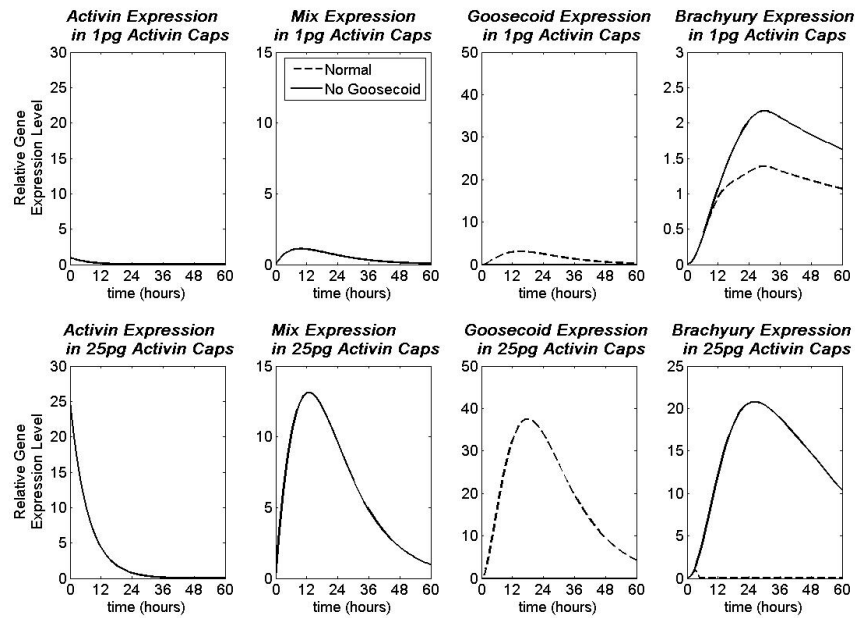
**Figure 4.12: Investigating the action of Mix** The rescue of mesoderm in Mix MO caps by the injection of a low dose Mix. Higher doses cause the caps to be endoderm. The model is as given in equations (4.2.1) and (4.2.6) solved subject to parameters given in the ‘axolotl B’ column of table 4.3.



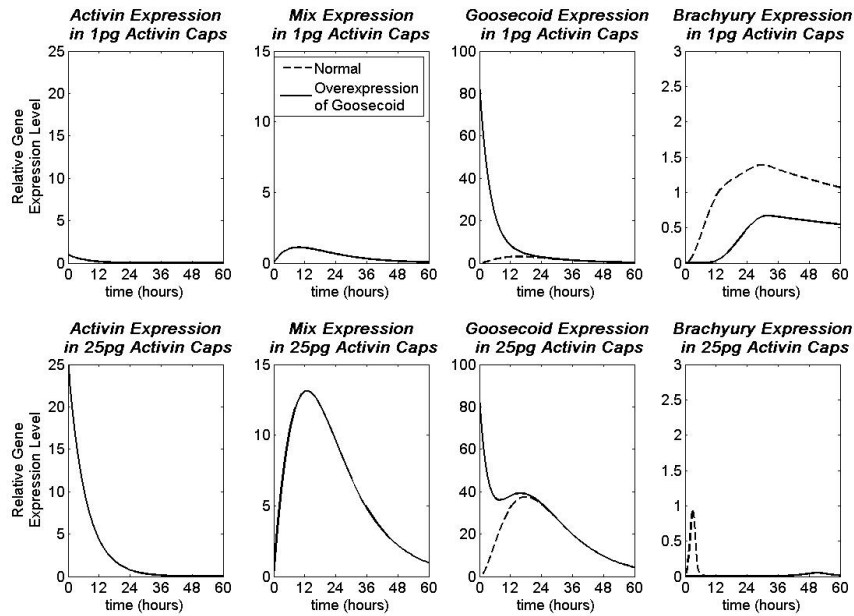
**Figure 4.13: Investigating the action of Brachyury.** The model is solved in the presence (dashed line) and absence (solid line) of Brachyury. The model is as given in equations (4.2.1) and (4.2.6) solved subject to parameters given in the ‘axolotl B’ column of table 4.3.



**Figure 4.14: Investigating the action of Brachyury.** The model is as given in equations (4.2.1) and (4.2.6) solved subject to parameters given in the 'axolotl B' column of table 4.3.



**Figure 4.15: Investigating the action of Goosecoid.** The model is solved in the presence (dashed line) and absence (solid line) of Goosecoid. The model is as given in equations (4.2.1) and (4.2.6) solved subject to parameters given in the 'axolotl B' column of table 4.3.

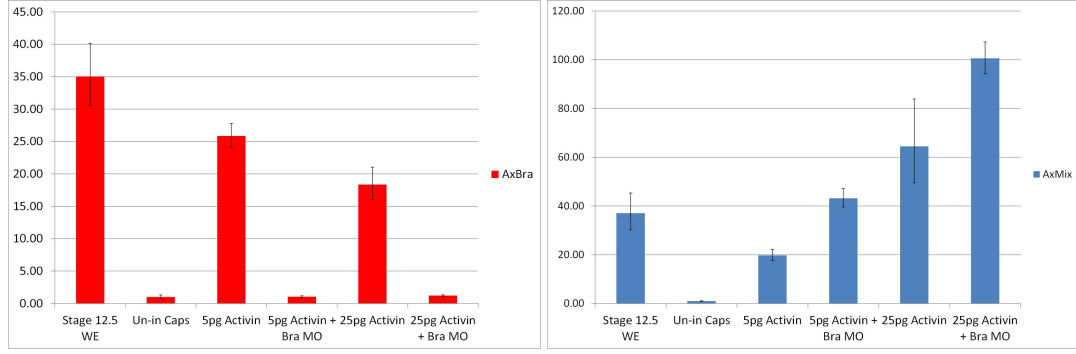


**Figure 4.16: Investigating the action of Goosecoid.** The model is as given in equations (4.2.1) and (4.2.6) solved subject to parameters given in the ‘axolotl B’ column of table 4.3.

#### 4.2.4 Testing model predictions

To verify that the model reproduces successfully the behaviour of the biological system, experimental data is obtained to test independently the predictions of the mathematical model. Here we choose to test model behaviour in the case of a Brachyury knockout. Recall from figure 4.13 that the mathematical model predicts that *Mix* and *Goosecoid* levels are unaltered when Brachyury is removed from the model. This is due to the parameter estimation algorithm selecting a high threshold concentration for the repression of *Mix* by Brachyury. To test this prediction, we knockout the function of Brachyury in *Activin* injected animal caps by co-injecting a Brachyury morpholino (MO).

We measure the expression of *Mix* in six samples, as described below. The expression of *Brachyury* is also measured as a control to show that the Brachyury MO is functioning correctly. The six samples we obtain data for are: (1) whole embryos (as a timing control), (2) uninjected caps, (3) 5pg Activin caps, (4) 5pg Activin caps with Brachyury MO, (5) 25pg Activin caps and (6) 25pg Activin with Brachyury MO. The expression of *Mix* and *Brachyury* in these samples is shown in figure 4.17. The Brachyury MO is designed such that it targets splice functions resulting in a mis-spliced mRNA. The efficiency of the MO was then measured using qPCR primers targeted at the mis-spliced region, showing that the Brachyury MO results in the knock down of functional *Brachyury* mRNA. By comparing the expression of *Mix* in the cap samples, we find that the knock down of Brachyury results in an upregulation of *Mix* at both doses of Activin. Therefore, the prediction of the mathematical model is not consistent with the experimentally obtained data.



**Figure 4.17:** The knockdown of Brachyury in Activin-injected animal caps using a Brachyury MO. The Brachyury MO causes levels of *Brachyury* to decrease to levels found in uninjected caps. The concentration of *Mix* is upregulated in the absence of Brachyury.

#### 4.2.5 Further parameter estimation results

As the mathematical model does not reproduce the behaviour of a Brachyury knockout experiment, we carry out further runs of the parameter estimation algorithm with a modified fitness function. In section 4.2.3, parameters were sought to minimise the error between the model and the expression of *Mix*, *Brachyury* and *Gooseoid* in *Activin* injected caps at four time points (using the fitness function defined in (4.2.5)). We add a term for the behaviour of a Brachyury knockout: At  $t = 18$ , we define the fitness function such that in 1pg Activin caps, *Mix* is expressed at twice the ‘wild-type’ level in a Brachyury knockout and in 25pg Activin caps with Brachyury MO, *Mix* is expressed at 1.5 times its ‘wild-type’ level, i.e.

$$F_2(\mathbf{X}_{\text{model}}, \mathbf{X}_{\text{data}}) = \frac{(2M_{\text{model}}(1, 18) - M_{\text{model}}^{\text{KO}}(1, 18))^2}{M_{\text{model}}(1, 18)^2} + \frac{(1.5M_{\text{model}}(25, 18) - M_{\text{model}}^{\text{KO}}(25, 18))^2}{M_{\text{model}}(25, 18)^2}. \quad (4.2.7)$$

The new fitness function,  $F_3$ , is

$$F_3(\mathbf{X}_{\text{model}}, \mathbf{X}_{\text{data}}) = F_1(\mathbf{X}_{\text{model}}, \mathbf{X}_{\text{data}}) + F_2(\mathbf{X}_{\text{model}}, \mathbf{X}_{\text{data}}), \quad (4.2.8)$$

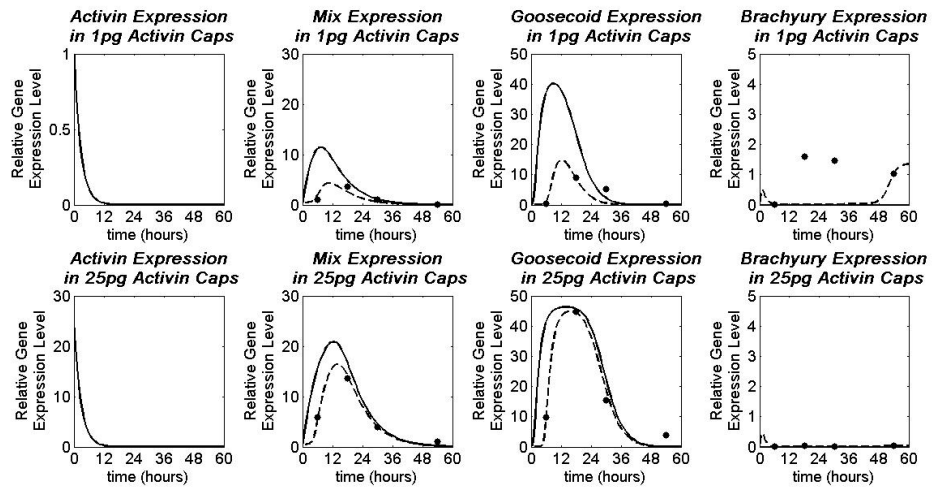
where  $F_1$  and  $F_2$  are as defined in (4.2.5) and (4.2.7), respectively.

The expression of *Mix*, *Brachyury* and *Gooseoid* for three parameter sets obtained using our parameter estimation with a fitness function defined by (4.2.8) are shown in figures 4.18, 4.19 and 4.20. In figure 4.18, the model is in good agreement with the experimental data, except for the expression of Brachyury in 1pg Activin caps. In the model Brachyury levels do not increase until  $t \approx 48$  hours, whilst in the experimental data Brachyury levels increase at  $t = 18$  hours. However we see that *Mix* is upregulated in the absence of Brachyury, as expected from Brachyury MO experiments. Figure 4.19 gives an example of a parameter set where the model gives a reasonable fit to Brachyury in both 1pg Activin caps and 25pg Activin caps. In this case the model does not fit well to the data for *Gooseoid* expression in 1pg Activin caps, but does give the correct behaviour of *Mix* in a Brachyury knockout. Figure 4.20 gives an example of a model which is in good agreement with experimental data, but does not give the correct

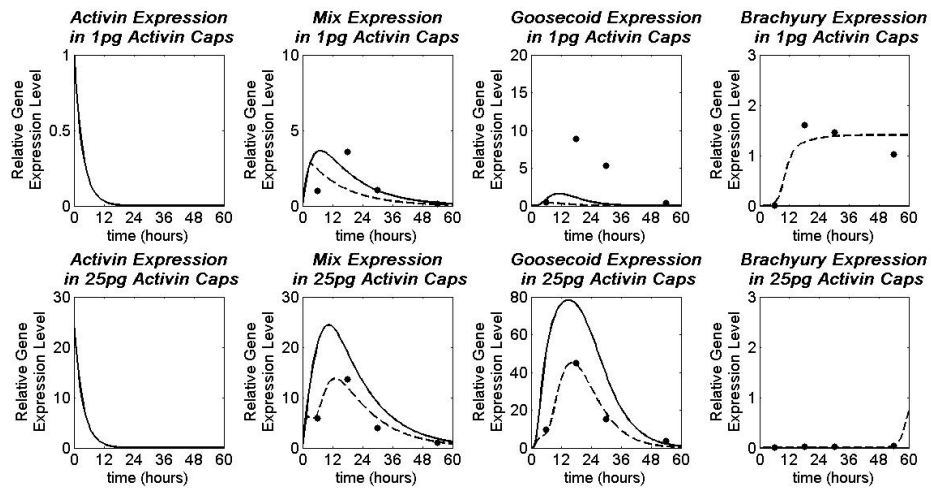
Variable	Parameter	A	B	C	Variable	Parameter	A	B	C
A	$\mu_A$	0.38	0.29	0.24	B	$\lambda_{A,B}$	1.08	0.01	0.001
M	$\lambda_{A,M}$	3.72	5.37	0.99		$\theta_{A,B}$	0.21	0.54	0.54
	$\theta_{A,M}$	0.11	2.78	0.43		$m_5$	3	3	3
	$m_1$	1	1	3		$\theta_{M,B}$	0.27	5	100
	$\theta_{B,M}$	0.01	0.01	0.5		$m_6$	4	3	4
	$m_2$	1	4	1		$\theta_{G,B}$	0.03	7.69	25
	$\mu_M$	0.12	0.07	0.05		$m_7$	1	1	1
G	$\lambda_{M,G}$	144.93	200	8.22		$\lambda_{B,B}$	45.95	16.86	6.12
	$\theta_{M,G}$	7.69	16.67	4.55	$\theta_{B,B}$	8.33	4.35	1.43	
	$m_3$	3	4	3	$m_8$	1	1	4	
	$\theta_{G,G}$	7.14	6.67	16.67	$\mu_B$	4.75	2.93	2.18	
	$m_4$	1	1	1					
	$\mu_G$	0.39	0.15	0.07					

**Table 4.4:** Parameter values used to solve the mathematical model of the axolotl mesendoderm network. These parameter sets are the best fits obtained using our parameter estimation algorithm.

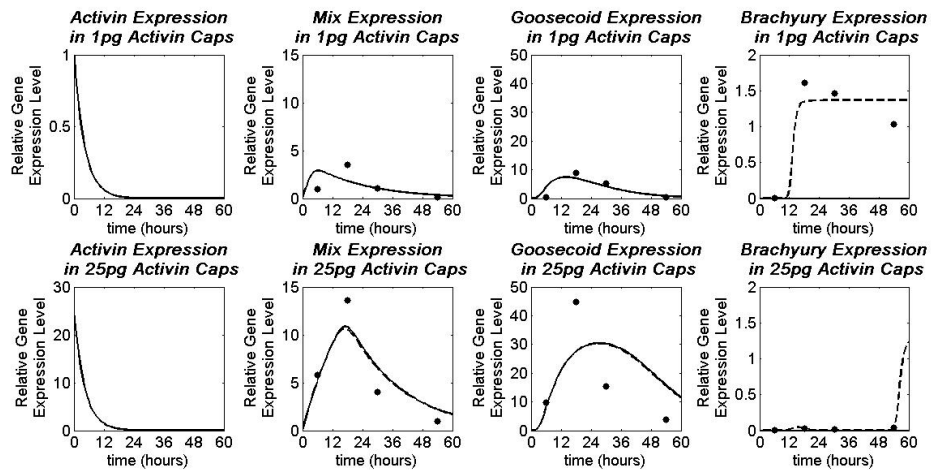
behaviour for a Brachyury knockout.



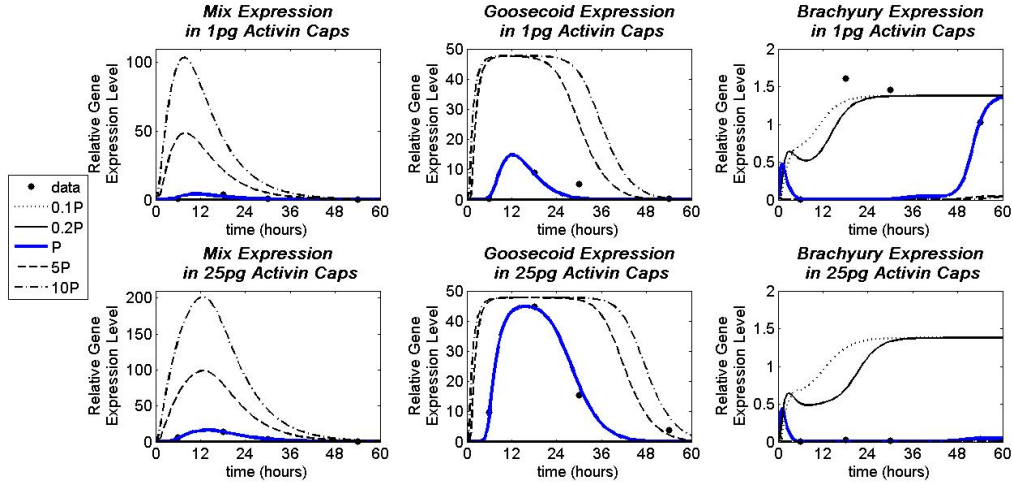
**Figure 4.18:** Model simulation for the axolotl *in vitro* model including the turnover of Activin. Experimental data (dots) and simulation results (lines) for the *in vitro* mathematical model of the axolotl mesendoderm network as given in equations (4.2.1) and (4.2.6). Dashed lines represent the full model and solid lines are for the Brachyury knockout. Model parameters were sought using a parameter estimation algorithm as described in the main text, with the resulting parameter set given in column A of table 4.4.



**Figure 4.19: Model simulation for the axolotl *in vitro* model including the turnover of Activin** Experimental data (dots) and simulation results (lines) for the *in vitro* mathematical model of the axolotl mesendoderm network as given in equations (4.2.1) and (4.2.6). Dashed lines represent the full model and solid lines are for the Brachyury knockout. Model parameters were sought using a parameter estimation algorithm as described in the main text, with the resulting parameter set given in column B of table 4.4.



**Figure 4.20: Model simulation for the axolotl *in vitro* model including the turnover of Activin** Experimental data (dots) and simulation results (lines) for the *in vitro* mathematical model of the axolotl mesendoderm network as given in equations (4.2.1) and (4.2.6). Dashed lines represent the full model and solid lines are for the Brachyury knockout. Model parameters were sought using a parameter estimation algorithm as described in the main text, with the resulting parameter set given in column C of table 4.4.



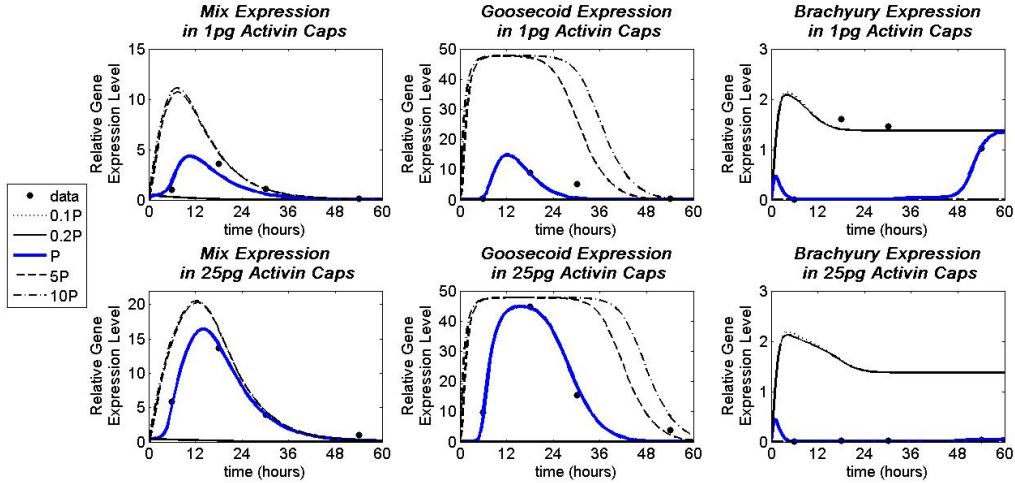
**Figure 4.21:** Numerical solutions to (4.2.1) and (4.2.6) showing the effect of varying  $\lambda_{A,M}$ . In the figure legend  $\lambda_{A,M} = P$ . All other parameters are as defined in column A of table 4.4.

#### 4.2.6 Parameter sensitivity

To explore further the behaviour of the mathematical models subject to the parameters found in this section, we investigate how changing single parameters affects the model behaviour. Figure 4.21 shows the effect of varying  $\lambda_{A,M}$  (for the model given in figure 4.18).  $\lambda_{A,M}$  is the maximal rate of production of Mix in response to Activin. All other parameters used are as defined in column A of table 4.4. Increasing the optimum value of  $\lambda_{A,M}$  causes the maximum concentration of Mix (which occurs at time  $\approx 12$  hours) to increase. The maximum value of Goosecoid does not increase above 48 in response to increases in  $\lambda_{A,M}$ . This is due to Goosecoid being able to negatively regulate its own production, limiting the maximum amount of Goosecoid which can be produced in the system. Increases in  $\lambda_{A,M}$  cause a downregulation in Brachyury, due to increased levels of Goosecoid which acts to repress Brachyury. Decreases in  $\lambda_{A,M}$  from its optimal value, cause the levels of Brachyury to reach its maximal value at an earlier time, and Mix and Goosecoid to not be expressed.

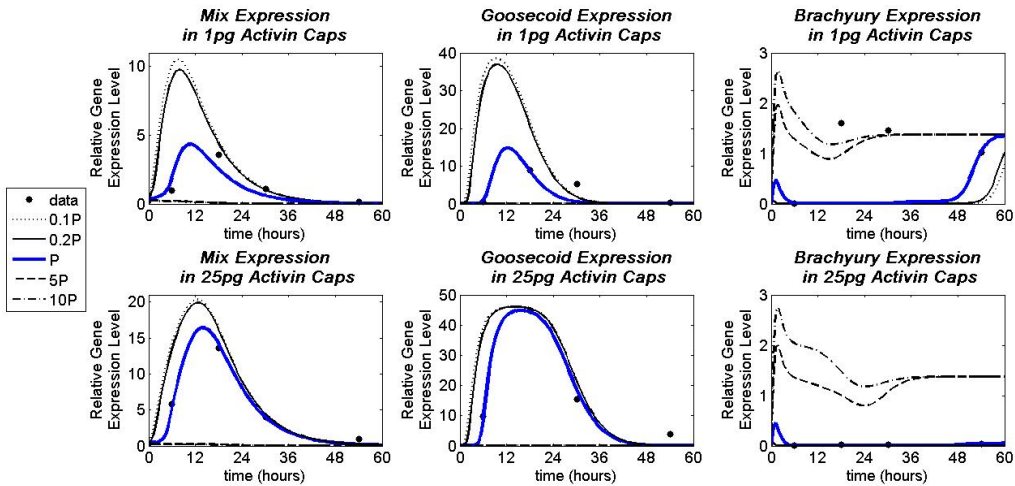
Figure 4.22 shows how varying  $\lambda_{M,G}$  affects the concentration of Mix, Brachyury and Goosecoid in the system.  $\lambda_{M,G}$  is the maximal rate of production of Goosecoid in response to Mix. As expected, increases to  $\lambda_{M,G}$  causes levels of Goosecoid to increase. However, as we found when investigating  $\lambda_{A,M}$ , the maximum Goosecoid concentration is limited due to Goosecoid negative autoregulation. The increase in Goosecoid results in Brachyury being downregulated, which in turn causes the levels of Mix to increase. When the rate of production of Goosecoid in response to Mix is low, Mix and Goosecoid are not expressed and Brachyury is upregulated.

Our investigations of the sensitivity of the model to changes in the rate of production parameters ( $\lambda$ ) show that the system is sensitive to changes in these parameters. Notably, we find that changing the rate of production of one gene has an effect on the levels of the other two genes in the network. For example, an increase of the rate of production of Mix by Antivin increases the



**Figure 4.22:** Numerical solutions to (4.2.1) and (4.2.6) showing the effect of varying  $\lambda_{M,G}$ . In the figure legend  $\lambda_{M,G} = P$ . All other parameters are as defined in column A of table 4.4.

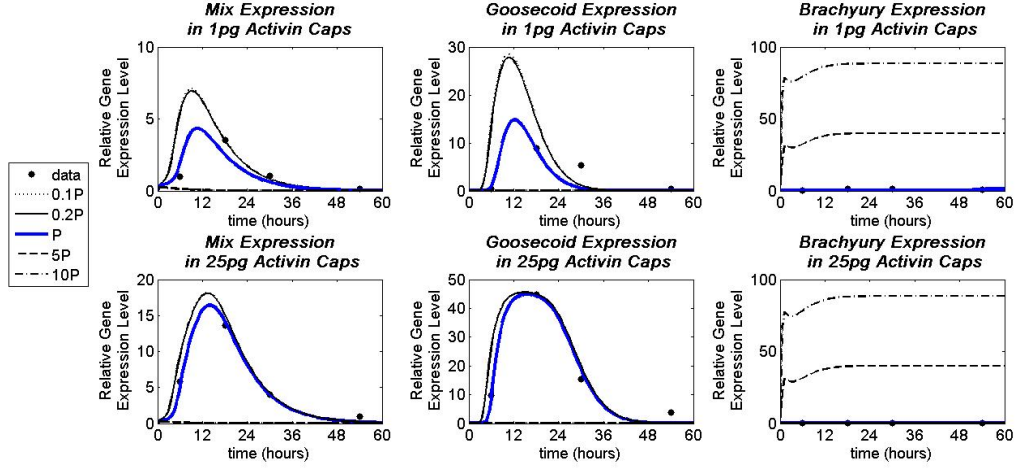
levels of Mix and this increased level of Mix means that the level of Goosecoid increases and Brachyury decreases.



**Figure 4.23:** Numerical solutions to (4.2.1) and (4.2.6) showing the effect of varying  $\lambda_{A,B}$ . In the figure legend  $\lambda_{A,B} = P$ . All other parameters are as defined in column A of table 4.4.

In figures 4.23 and 4.24, numerical results are plotted for various values of  $\lambda_{A,B}$  and  $\lambda_{B,B}$ , respectively. Increases to both these parameters causes the levels of Brachyury to increase and the levels of Mix and Goosecoid to decrease. Conversely for small values of these parameters, the expression levels of Mix and Goosecoid are increased and Brachyury expression is decreased.





**Figure 4.24:** Numerical solutions to (4.2.1) and (4.2.6) showing the effect of varying  $\lambda_{B,B}$ . In the figure legend  $\lambda_{B,B} = P$ . All other parameters are as defined in column A of table 4.4.

### 4.3 Can a model with the *Xenopus* network topology reproduce the gene expression patterns from axolotl?

Recall from chapter 3 that the key difference between the axolotl and *Xenopus* mesendoderm network downstream of Activin is the action of Mix on Brachyury (compare figures 3.8 and 3.1). In axolotl Mix is required for the expression of Brachyury, but in *Xenopus* Mix represses Brachyury. We found that both the *Xenopus* and axolotl *in vitro* models are bistable with steady states corresponding to mesoderm and anterior mesendoderm but with qualitative differences in the time course expression of genes. In this section we ask if a mathematical model with the *Xenopus* network topology (i.e. Mix repressing Brachyury) can reproduce experimental data from axolotl animal caps. To do this we use our hybrid parameter estimation algorithm to minimise the error between the model simulation and experimental data. As in the previous section (for axolotl models) we do this in two models; in the first model the level of Activin remains fixed and in the second model Activin is allowed to turn over.

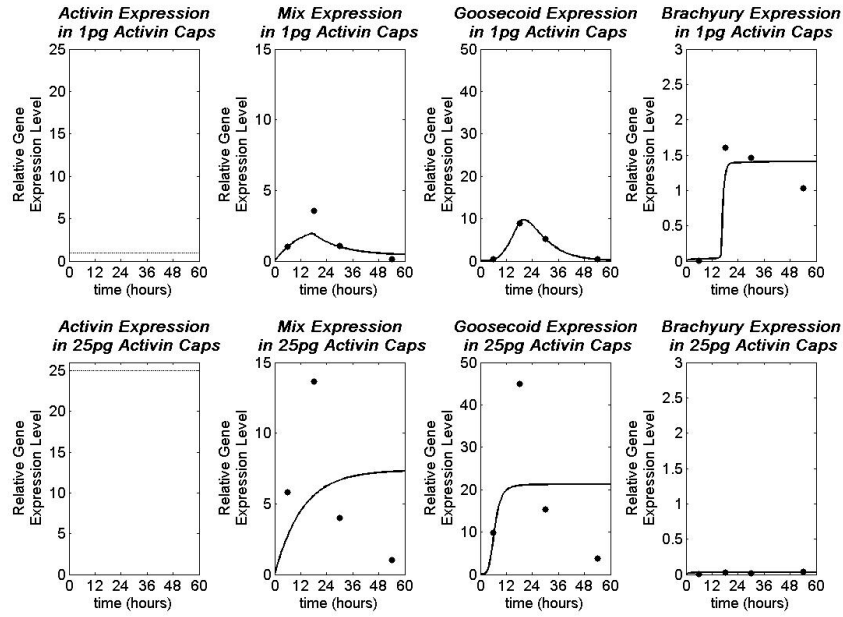
Recall that the *Xenopus in vitro* model is given by

$$\frac{dM}{dt} = \lambda_{A,M} \mathcal{H} \left( \frac{A}{\theta_{A,M}}, m_1 \right) \left\{ 1 - \mathcal{H} \left( \frac{B}{\theta_{B,M}}, m_2 \right) \right\} - \mu_M M, \quad (4.3.1a)$$

$$\frac{dG}{dt} = \lambda_{M,G} \mathcal{H} \left( \frac{M}{\theta_{M,G}}, m_3 \right) \left\{ 1 - \mathcal{H} \left( \frac{G}{\theta_{G,G}}, m_4 \right) \right\} - \mu_G G, \quad (4.3.1b)$$

$$\frac{dB}{dt} = \left[ \lambda_{A,B} \mathcal{H} \left( \frac{A}{\theta_{A,B}}, m_5 \right) + \lambda_{B,B} \mathcal{H} \left( \frac{B}{\theta_{B,B}}, m_8 \right) \right] \left\{ 1 - \mathcal{H} \left( \frac{G}{\theta_{G,B}} + \frac{M}{\theta_{M,B}}, m_7 \right) \right\} - \mu_B B, \quad (4.3.1c)$$

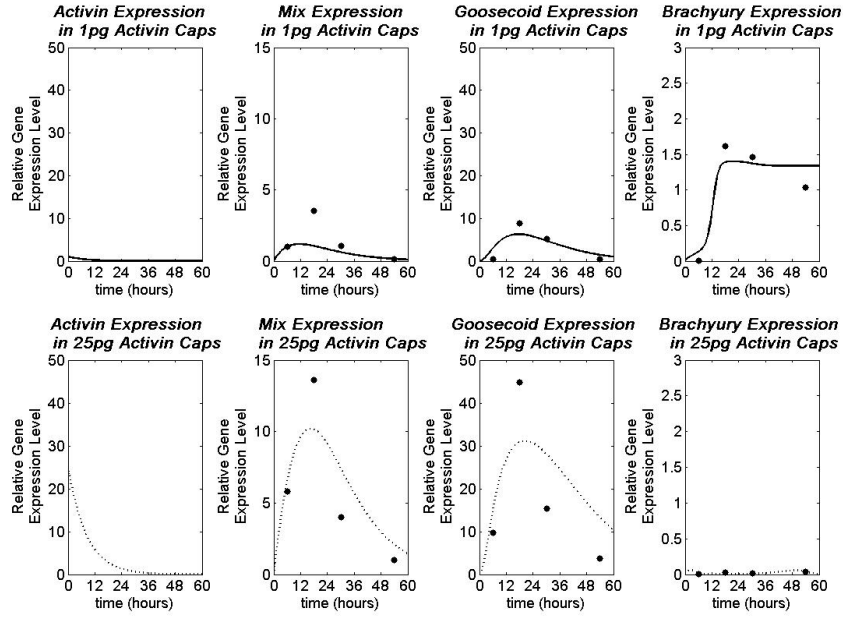
In the model where Activin can turn over we have the rate of change of Activin over time defined in equation (4.2.6).



**Figure 4.25: Model simulation for the *Xenopus in vitro* model.** Experimental data (dots) and simulation results (lines) for the *in vitro* mathematical model of the axolotl mesendoderm network as given in equation (4.3.1). Model parameters were sought using a parameter estimation algorithm as described in the main text, with the resulting parameters given in the ‘*Xenopus A*’ column of table 4.3.

Figure 4.25 gives a fit to the *Xenopus in vitro* model without the turnover of Activin. The value of the fitness function is 2.16 compared with 2.49 for the equivalent axolotl model, meaning that the parameters found for the *Xenopus in vitro* model provide a closer fit to the experimental data than the axolotl model. However, the model does not qualitatively reproduce key behaviour of the experimental data.

A solution to the *Xenopus in vitro* model with Activin degradation is given in figure 4.26. This model qualitatively reproduces the experimental gene expression data from the Activin dose response experimental in axolotl. The behaviour of the model beyond  $t = 60$  is shown in figure 4.27, Mix and Goosecoid decay to zero, but in 1pg Activin caps Brachyury reaches a non-trivial steady state. The model prediction for different doses of Activin is given in figure 4.28. As the dose of Activin increases, the quantitative behaviour of Mix and Goosecoid remains the same; the expression of each gene increases to a maximum concentration before decaying, with maximum level of Mix/Goosecoid increasing with the dose of Activin. The mathematical model is bistable, with either no Brachyury in the system (the trivial steady state) or up regulated Brachyury. At low dose of Activin Brachyury evolves to the upregulated steady state and at high doses Brachyury evolves to the trivial steady state. For intermediate concentrations (such as  $A = 5$ ) Brachyury is expressed at low levels for a time period before being upregulated and evolving to an upregulated steady state. Note that there is no ‘spike’ in Brachyury expression at high levels of Activin in the *Xenopus* model. In figure 4.29 the model is solved both in the presence and absence of Activin turnover. In the presence of Activin turnover the levels of Mix



**Figure 4.26: Model simulation for the *Xenopus in vitro* model with Activin degradation.** Experimental data (dots) and simulation results (lines) for the *in vitro* mathematical model of the axolotl mesendoderm network as given in equations (4.3.1) and (4.2.6). Model parameters were sought using a parameter estimation algorithm as described in the main text, with the resulting parameter set given in the ‘*Xenopus B*’ column of table 4.3. The fitness function is 1.89.

and Goosecoid decrease until they reach a steady state value, but in the system where Activin does not turnover the levels continue to increase until they reach a steady state value. The increase in levels of Mix and Goosecoid causes Brachyury to be down regulated in 1pg Activin caps. A knock out of Mix, Brachyury and Goosecoid is carried out to compare the behaviour of the *Xenopus in vitro* model with the axolotl *in vitro* model. A knock out of Mix in the *Xenopus in vitro* model results in the upregulation of Brachyury at both 1pg and 25pg of Activin, i.e. the caps will become mesoderm. In the absence of Mix, Goosecoid is also not expressed (figure 4.30). This is different to what is seen in the axolotl model simulations where a knockdown of Mix results in no Brachyury or Goosecoid expression, i.e. caps remain as ectoderm (figure 4.11). In the *Xenopus* model a knock out of Goosecoid does not change the levels of Mix or Brachyury (figure 4.31), but in the axolotl model Goosecoid is required for the repression of Brachyury (figure 4.15). Both in the *Xenopus* model and the axolotl model (figure 4.32 and figure 4.15, respectively) a knock down of Brachyury results in no change in the levels of Mix and Goosecoid.

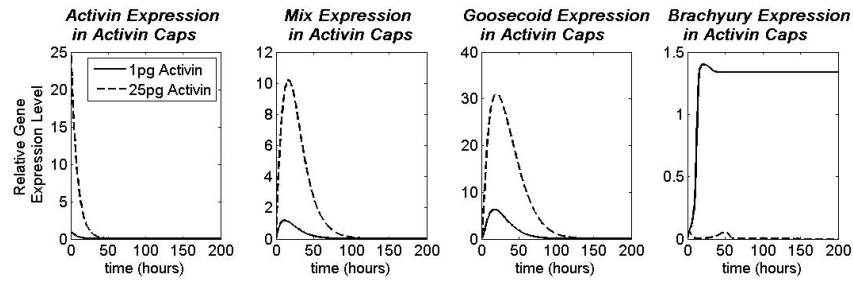


Figure 4.27: Model simulation for the *Xenopus in vitro* model as given in equations (4.3.1) and (4.2.6), including the turnover of Activin. Model parameters are given in the 'Xenopus B' column of table 4.3.

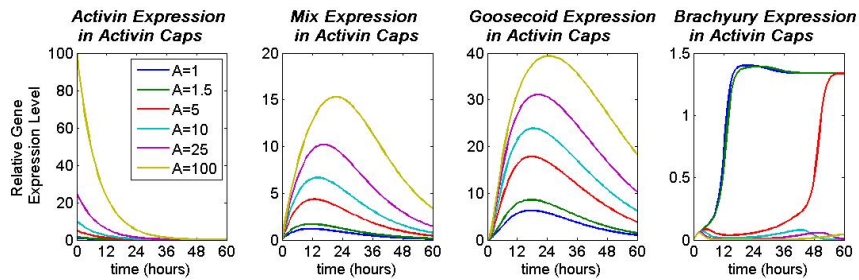


Figure 4.28: Investigating the level of gene expression in response to Activin. The *Xenopus in vitro* model is as given in equations (4.3.1) and (4.2.6) solved subject to parameters given in the 'Xenopus B' column of table 4.3.

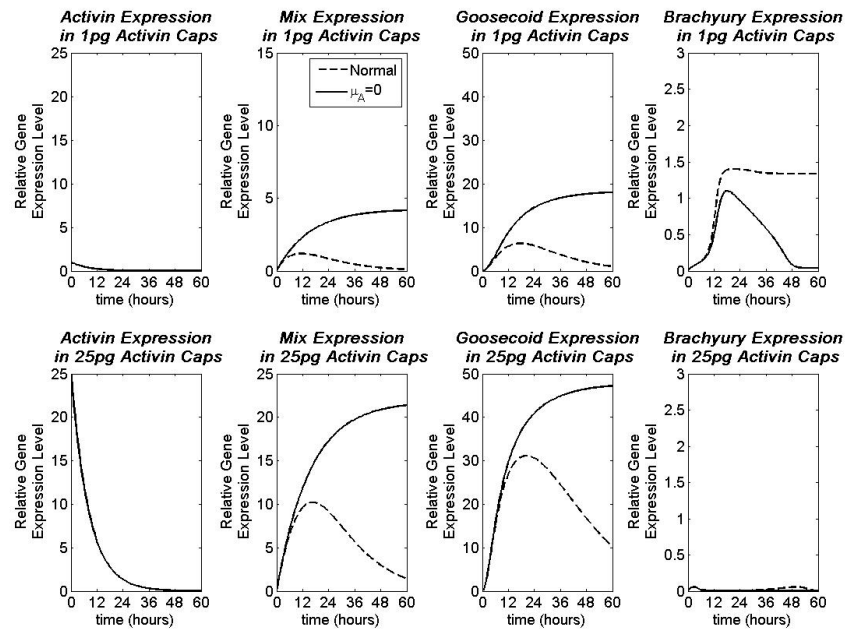
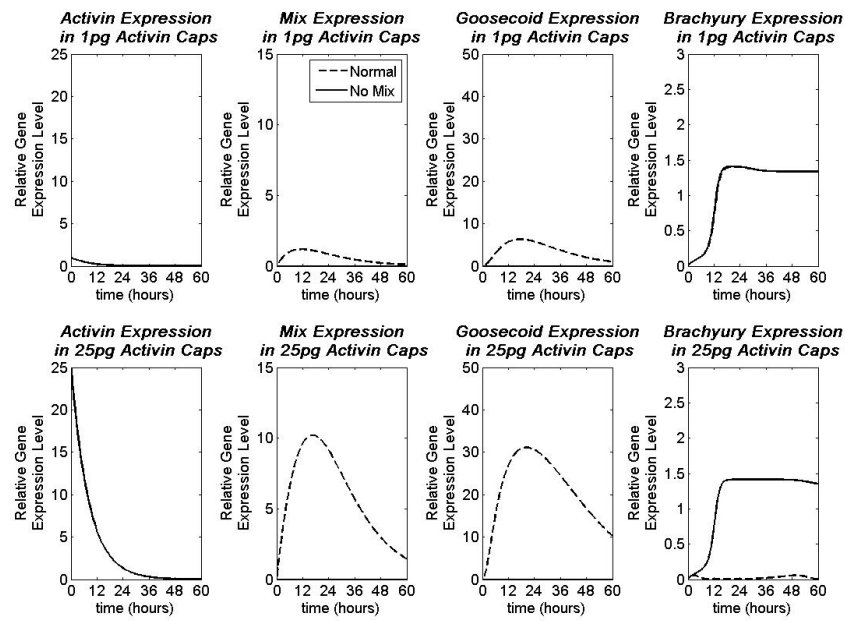
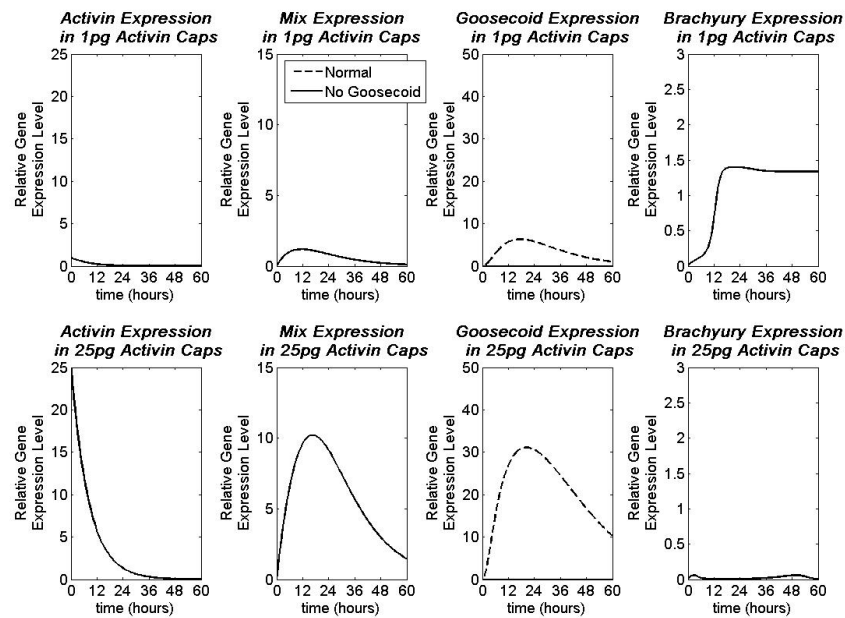


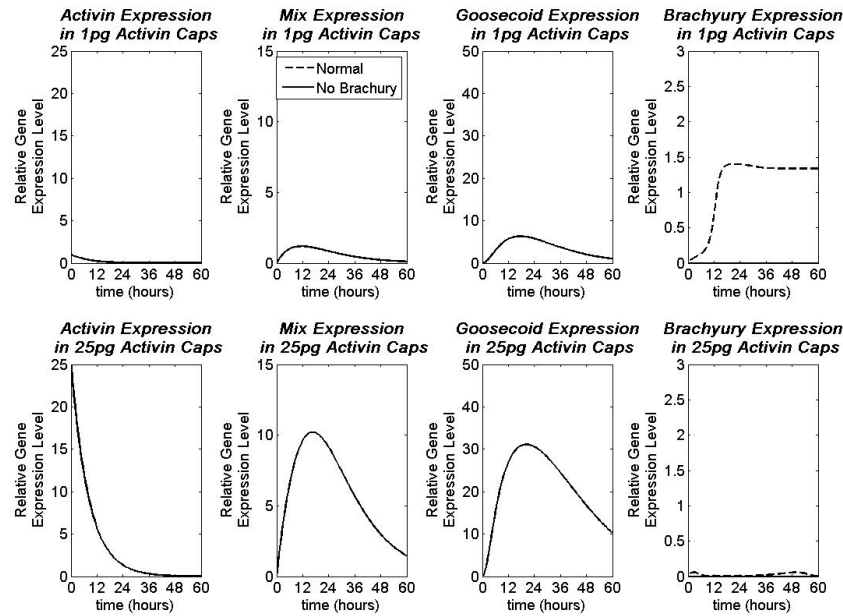
Figure 4.29: Investigating the role of Activin turnover. The model is solved in the presence (dashed line) and absence (solid line) of Activin turnover. The *Xenopus in vitro* model is as given in equations (4.3.1) and (4.2.6) solved subject to parameters given in the 'Xenopus B' column of table 4.3.



**Figure 4.30: Investigating the action of Mix.** The model is solved in the presence (dashed line) and absence (solid line) of Mix. The *Xenopus in vitro* model is as given in equations (4.3.1) and (4.2.6) solved subject to parameters given in the 'Xenopus B' column of table 4.3.



**Figure 4.31: Investigating the action of Goosecoid.** The model is solved in the presence (dashed line) and absence (solid line) of Goosecoid. The *Xenopus in vitro* model is as given in equations (4.3.1) and (4.2.6) solved subject to parameters given in the 'Xenopus B' column of table 4.3.



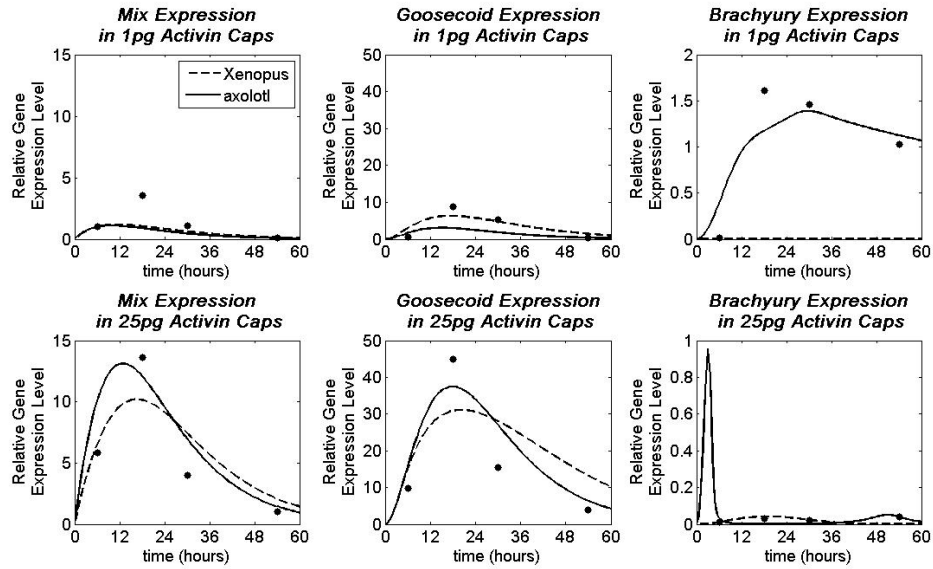
**Figure 4.32: Investigating the action of Brachyury.** The model is solved in the presence (dashed line) and absence (solid line) of Brachyury. The *Xenopus in vitro* model is as given in equations (4.3.1) and (4.2.6) solved subject to parameters given in the ‘*Xenopus B*’ column of table 4.3.

## 4.4 Comparison of optimal parameters for the *Xenopus* and axolotl models

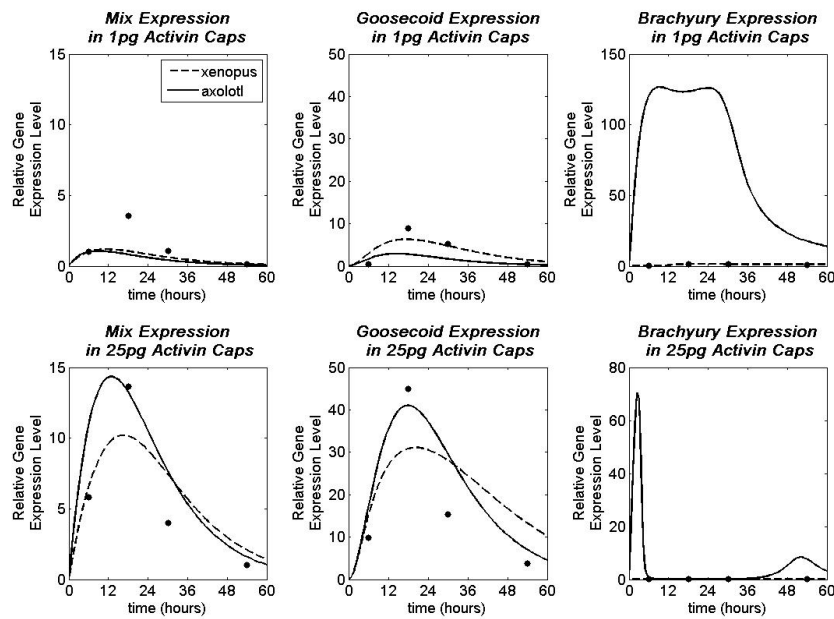
A comparison of the parameters found using the genetic algorithm for the axolotl and *Xenopus* mesendoderm networks is given in table 4.3. Many parameters have comparable values in the two models. For example, the turnover rates ( $\mu_A$ ,  $\mu_M$ ,  $\mu_G$ ,  $\mu_B$ ) have similar values in both models. However, some parameters have significantly different values between the two models:

- The threshold for Goosecoid negative autoregulation is higher in axolotl than in *Xenopus*.
- The threshold for repression of Brachyury by Goosecoid is lower in axolotl than in *Xenopus*.
- The rate of Brachyury autoregulation is much higher in axolotl than in *Xenopus*.

The parameters associated with the action of Goosecoid are those that have different values in the two models, an explanation for this is that in the axolotl model the action of Goosecoid is ‘more important’ than in the *Xenopus* model, since in the axolotl topology of the network Goosecoid is the only TF which can act to repress Brachyury, where as in the *Xenopus* network



**Figure 4.33:** Comparison of optimum parameters found for the *Xenopus* (dashed line) and axolotl (solid line) models, as applied to solve the axolotl model.



**Figure 4.34:** Comparison of optimum parameters found for the *Xenopus* (dashed line) and axolotl (solid line) models, as applied to solve the *Xenopus* model.

both Mix and Goosecoid can act to repress Mix, the weak action of Goosecoid on Brachyury can be compensated by Mix.

To explore the differences in parameters, we solve the axolotl model using the optimum parameters found for the *Xenopus* model (see figure 4.33). We find that solving the axolotl model using the *Xenopus* parameters gives the same qualitative behaviour for the expression of Mix

and Goosecoid as solving the model using the axolotl parameters. The axolotl parameters give a closer fit to the data at 25pg Activin, while the *Xenopus* parameters give a closer fit at 1pg Activin. The main difference between using the two parameters to solve the axolotl model is the expression of Brachyury: the *Xenopus* parameters do not give a close fit between the model and the data. We also solve the *Xenopus* model using both sets of parameters as shown in figure 4.34. Again we find that the main difference between the two parameter sets is the expression of Brachyury.

## 4.5 Discussion

In this chapter we used experimental data to estimate parameter values in mathematical models of the axolotl mesenteroderm GRN. The first stage in this process was to obtain suitable gene expression data using the animal cap assay. Doses of Activin, Nodal1 and Nodal2 were applied to animal caps, showing differences in their capabilities to induce mesoderm and endoderm. Activin can induce both mesoderm and endoderm in a dose dependent manner but, surprisingly, Nodal1 can induce mesoderm but not endoderm. Nodal1 and Activin are thought to act via the same TGF- $\beta$  signalling pathway. The difference in their ability to induce mesoderm and endoderm suggest these factors do not function in the same way in axolotl animal caps. For example, there may be a difference in the way Nodal1 and Activin induce the signalling pathway, or the presence of a novel pathway which has not been described previously. Work to uncover these differences in the function of Activin and Nodal1 is on-going in the lab. Nodal2 induces neither mesoderm nor endoderm, confirming previous work from Swiers et al [139] that Nodal2 does not have a role in the induction of mesoderm or endoderm.

The ability of Nodal1 to induce mesoderm but not endoderm in axolotl animal caps also warrants further investigation. Nanog, a gene involved in maintaining pluripotency [31], is a candidate for preventing endoderm forming in Nodal1 treated animal caps, based on evidence we now present. Studies into the role of Nanog in humans and mice show that Nanog blocks the expression of endoderm markers such as Sox17, but induces factors such as Mixl1, Brachyury and Goosecoid [11, 143, 147]. Furthermore, Smad2, a downstream component of Activin/Nodal signalling, directly controls the expression of Nanog [147, 153] and also forms a complex with Nanog proteins [147]. The binding of Nanog to Smad2 leads to a variation in effects on Smad2 target genes. For example, pluripotency genes are maintained in the presence of the Nanog/Smad2 complex, whereas the complex binds to, but does not activate, expression of endodermal genes [11]. In axolotl, Nanog is expressed in the animal cap from stage 9 until the completion of gastrulation [31]. Taken together, these studies of Nanog suggest that in axolotl animal caps Nanog may block the induction of endoderm by controlling the transcriptional activity of Nodal signalling. This warrants further investigation both experimentally and using mathematical models.

Quantitative PCR data expression downstream of Activin was used to estimate parameters in the mathematical model. We used a hybrid algorithm consisting of the genetic algorithm



followed by a local search to minimise the error between the model and the data. Due to the stochastic nature of the algorithm it was used several times to ensure that the best possible parameter set is found. A model which includes Activin degradation fits to the experimental data better than a model where Activin is assumed to be fixed.

The resulting model is used to make predictions about the behaviour of the mesendoderm GRN under experimental perturbations. The axolotl mesendoderm model was solved, using the best parameters from parameter estimation, to give a prediction about Mix and Goosecoid expression in cells where Brachyury is knocked out. Whilst the mathematical model predicted that this knockout would result in no change in the levels of Mix and Goosecoid, our experimental data showed that Mix is upregulated when Brachyury is removed. Since the model does not reproduce experimental knockout data, we carried out parameter estimation using a modified fitness function to include knockout data.

The axolotl animal cap data were also used to estimate parameters in the *Xenopus in vitro* model, to investigate if a different network topology can still reproduce the experimental observations. The results of parameter estimation show that despite differences in the topology of the axolotl and *Xenopus* mesendoderm networks downstream of Activin, both the axolotl and *Xenopus in vitro* models can qualitatively reproduce the expression of Mix, Brachyury and Goosecoid in Activin injected axolotl animal caps. This shows that changes in the topology of a network do not necessarily result in changes in the output of the model (such as biological phenotype). Differences in the behaviour of the two models are found by an *in silico* investigation of removing each gene from the network, giving predictions which can be tested using experimental data independent from the data used to fit model parameters. Table 4.5 summarises the expected behaviour for a knockout of each gene in *Xenopus* and axolotl, as predicted by the mathematical models. If the model predictions are not consistent with the independently obtained knockout data, this can lead to the refinement of the model or the selection of a more suitable parameter set.

	<i>Xenopus</i>	axolotl
Mix Knockout	low Activin: mesoderm high Activin: mesoderm	<b>low Activin: ectoderm</b> high Activin: ectoderm
Brachyury Knockout	low Activin: ** high Activin: endoderm	low Activin: ** high Activin: endoderm
Goosecoid Knockout	low Activin: mesoderm high Activin: endoderm	low Activin: mesoderm high Activin: mesoderm

**Table 4.5:** Model prediction of phenotypes of Morphant Activin injected animal caps. Samples marked \*\* show no change in the levels of *Mix* and *Goosecoid* but do not express *Brachyury*, so it is not clear what the resulting phenotype will be.

The model fits produced do not perfectly reproduce the experimental data. There are several explanations for this outlined below.

1. The model could be 'wrong'. For example, the connections between existing genes may be incorrect or genes (either known or unknown) may be missing from the model. The axolotl mesendoderm network given in figure 3.8 was inferred using a variety of experimental methods such as knock down and overexpression of genes and inferring the re-

maintaining connections from knowledge of the mesendoderm network in *Xenopus*. The gene interactions between most of the genes in the network are therefore likely to be correct.

2. The data used for fitting the mathematical model could be too sparse or too noisy. Only a limited number of data points are available for fitting the model, but in general the more data available the more accurate the fit. Since the data we use in the chapter are obtained in animal caps consisting of a uniform population of many cells, our data are unlikely to be too noisy.
3. Our mathematical models are an over-simplified representation of the mechanisms occurring in the biological system. Some details of the regulation of transcription by transcription factors are not included in our model: for example, we assume that for each gene its protein levels are proportional to the levels of mRNA.

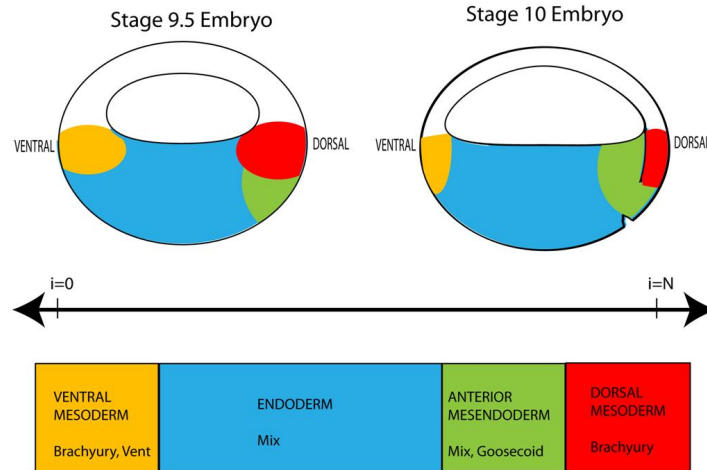
Although the model does not reproduce the experimental data completely, it is more important for a model to be able to make predictions on the behaviour of the network under experimental perturbations.

The gene expression data obtained in this chapter shows that, in animal caps that have an endodermal phenotype, Goosecoid and Mix are coexpressed. In whole embryos, Goosecoid and Mix are coexpressed in anterior mesendoderm and Mix (but not Goosecoid) is expressed in endoderm. In the next chapter, the mechanisms involved in the differentiation of endoderm and anterior mesendoderm are explored using mathematical models.

# Dorsal-Ventral Patterning in a Single-cell Model of Mesendoderm Specification in *Xenopus*

## 5.1 Introduction

During the early stages of embryo development several distinct regions form: these include dorsal mesoderm (expressing Brachyury), ventral mesoderm (expressing Vent and Brachyury), endoderm (expressing Mix) and anterior mesendoderm (expressing Mix and Goosecoid). The location of these regions in stage 9.5 and 10 embryos are illustrated in figure 5.1. Mesoderm is located in the marginal zone, anterior mesendoderm is on the dorsal side, and endoderm is found throughout the vegetal hemisphere. The mathematical models of the *Xenopus* mesendoderm network formulated in [95] can only account for the formation of mesoderm and anterior mesendoderm. Goosecoid is absent from ventral regions of the embryo, where it is repressed by transcription factors such as Vent1 and Vent2 [124]. This evidence suggests that by including Vent1/2 in a model of the *Xenopus* mesendoderm network we may be able to account for the formation of mesoderm and endoderm on the ventral side of the embryo. Vent1/2 and Goosecoid are part of the GRN regulating the patterning of the dorsal-ventral (DV) axis. TFs and proteins involved in patterning the DV axis were introduced in section 1.9. In this chapter, we formulate two models which include the negative regulation of Goosecoid by Vent1/2 in a single cell. The first model (the ‘DV only’ model) focuses on the mutual negative regulation of Goosecoid by a single representative Vent gene, with the resulting mathematical model being bistable with stable steady states corresponding to dorsal and ventral fates. In the second model (the ‘DV and mesendoderm model’), Vent and BMP are added to the *Xenopus in vivo* model showing that, by including Vent, the model can account for the formation of endoderm as well as anterior mesendoderm and mesoderm. First we review existing mathematical models of DV patterning.



**Figure 5.1:** Cartoon showing the spatial organisation of mesoderm, endoderm and anterior mesendoderm in stage 9.5 and 10 *Xenopus* embryos. These regions are as interpreted by the regions where Mix, Brachyury and Goosecoid are expressed.

### 5.1.1 Mathematical models of DV patterning

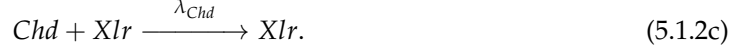
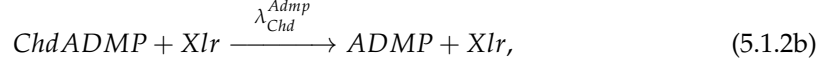
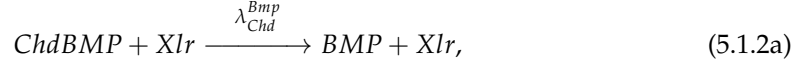
Several mathematical models of DV patterning in Zebrafish [156], *Drosophila* [33, 146] and *Xenopus* [7] are available in the literature. All these models consist of systems of reaction diffusion equations representing the interactions between various extracellular signals. Zhang et al [156] formulate a model of DV patterning using a 3D geometry to capture the shape of a Zebrafish embryo. The interactions of BMP and Chordin are modelled along with BMP-receptor and BMP-Chordin complexes, with the BMP-Chordin complex being degraded via the action of Tolloid. The model reproduces key experimental observations, showing that both Chordin and Tolloid are required to form a sharp BMP gradient. Positive BMP feedback and negative Chordin feedback are also shown to regulate the BMP gradient. Models of DV patterning in *Drosophila* [33, 146] also use reaction diffusion models to capture key interactions. Eldar et al [33] show that the conditions needed for robustness of DV patterning are restricted diffusion of the free BMP ligand, and that Sog (analogous to Chordin in *Xenopus*) is only cleaved efficiently when in complex with BMP.

#### A continuous model of DV patterning in *Xenopus*

Ben-Zvi et al [7] use a model of DV patterning to explore the scaling of the BMP gradient with embryo size. The model includes two BMP ligands, BMP (representing the combined inputs of BMP2, BMP4 and BMP7) and ADMP, Chordin (an inhibitor of BMP signalling) and Xlr (a protease which cleaves Chordin). BMP and ADMP ligands bind to Chordin to give Chordin-ligand complexes



Chordin can be cleaved by Xlr, either when in complex (releasing BMP/ADMP) or as a single ligand



All species in the model can diffuse and the production of BMP/ADMP are defined using Hill functions of the total signalling level ( $S(x, t) = \text{ADMP}(x, t) + \text{BMP}(x, t)$ ). ADMP is produced in regions with a low signal, such that  $\alpha_{\text{ADMP}}(S(x, t)) = 10^{-3} \frac{T_{\text{ADMP}}^4}{S(x, t)^4 + T_{\text{ADMP}}^4}$ , and BMP is produced in regions with high signalling, such that  $\alpha_{\text{BMP}}(S(x, t)) = 10^{-3} \frac{S(x, t)^4}{S(x, t)^4 + T_{\text{BMP}}^4}$ . ADMP and BMP are assumed to turnover at constant rates,  $\beta_{\text{ADMP}}$  and  $\beta_{\text{BMP}}$ , respectively. The model then consists of the following system of reaction-diffusion equations

$$\frac{\partial[\text{Chd}]}{\partial t} = D_{\text{Chd}} \nabla^2[\text{Chd}] - [\text{Chd}] \left( k_{\text{Admp}}[\text{ADMP}] + k_{\text{Bmp}}[\text{BMP}] + \lambda_{\text{Chd}}[\text{Xlr}] \right), \quad (5.1.3a)$$

$$\begin{aligned} \frac{\partial[\text{ADMP}]}{\partial t} &= D_{\text{Admp}} \nabla^2[\text{ADMP}] - k_{\text{Admp}}[\text{ADMP}][\text{Chd}] + \lambda_{\text{Chd}}^{\text{admp}}[\text{Xlr}][\text{ChdADMP}] \\ &+ \alpha_{\text{ADMP}}(S) - \beta_{\text{ADMP}}[\text{ADMP}], \end{aligned} \quad (5.1.3b)$$

$$\begin{aligned} \frac{\partial[\text{BMP}]}{\partial t} &= D_{\text{Bmp}} \nabla^2[\text{BMP}] - k_{\text{Bmp}}[\text{BMP}][\text{Chd}] + \lambda_{\text{Chd}}^{\text{Bmp}}[\text{Xlr}][\text{ChdBMP}] \\ &+ \alpha_{\text{BMP}}(S) - \beta_{\text{BMP}}[\text{BMP}], \end{aligned} \quad (5.1.3c)$$

$$\frac{\partial[\text{ChdADMP}]}{\partial t} = D_{\text{ChdAdmp}} \nabla^2[\text{ChdADMP}] + k_{\text{Admp}}[\text{ADMP}][\text{Chd}] - \lambda_{\text{Chd}}^{\text{admp}}[\text{Xlr}][\text{ChdADMP}], \quad (5.1.3d)$$

$$\frac{\partial[\text{ChdBMP}]}{\partial t} = D_{\text{ChdBmp}} \nabla^2[\text{ChdBMP}] - k_{\text{Bmp}}[\text{BMP}][\text{Chd}] + \lambda_{\text{Chd}}^{\text{Bmp}}[\text{Xlr}][\text{ChdBMP}]. \quad (5.1.3e)$$

Boundary conditions are defined such that all fluxes are zero at the ventral pole. At the dorsal pole the flux of Chordin is given by  $D_{\text{Chd}} \nabla[\text{Chd}] = \eta_{\text{Chd}}$ , where  $\eta_{\text{Chd}}$  is a constant and the flux of Admp is given by  $D_{\text{Admp}} \nabla[\text{Admp}] = \alpha_{\text{Admp}}$ , where  $\alpha_{\text{Admp}}$  is a constant. All proteins and complexes are initially absent, except for BMP, which is uniformly distributed.

A systematical screen of model parameters in [7] reveals that two possible mechanisms involved in the formation of BMP gradients emerge: shuttling-based and inhibition-based. In a shuttling based mechanism, the activator (BMP) is physically translocated to ventral regions of the embryo, facilitated by its binding to the inhibitor (Chordin), followed by the activator being released from the inhibitor by a protease (Xlr) that degrades Chordin. In this model, BMP and ADMP diffuse at a faster rate once in complex with Chordin, and cleavage by Xlr is also more effective when Chordin is in a complex. The inhibition based mechanism does not require the physical translocation of the activator; instead the BMP gradient reflects the gradient of Chordin. Here all the proteins diffuse at the same rate and Chordin and its complexes

model	parameter	value	model	parameter	value
both	$[Xlr]$	$10^{-2}$	both	$\lambda_{Chd}^{Admp}$	1
both	$\lambda_{Chd}^{Bmp}$	1	both	$k_{Admp}$	$10^{-2}$
both	$k_{Bmp}$	1	both	$T_{Admp}$	$10^{-4}$
both	$D_{Chd}$	10	both	$D_{Comp}$	10
Shuttling	$D_{Lig}$	$10^{-1}$	Shuttling	$\lambda_{Chd}$	$10^{-2}$
Shuttling	$\eta_{Chd}$	1	Inhibition	$D_{Lig}$	10
Inhibition	$\lambda_{Chd}$	1	Inhibition	$\eta_{Chd}$	$10^3$

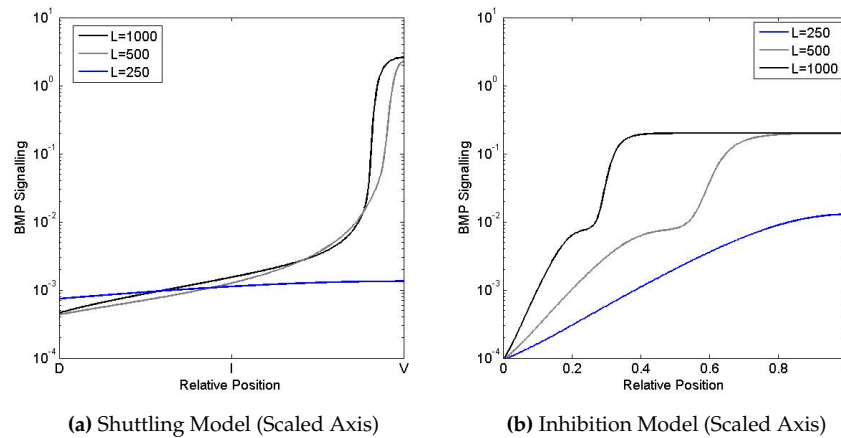
**Table 5.1:** Parameters used to solve (5.1.3)

are all cleaved by  $Xlr$  at the same rate. Ben-Zvi et al [7] propose that a shuttling mechanism is required for the scaling of a dorsal half *Xenopus* embryos, by showing that the scaling of dorsal half embryos only occurs when parameters corresponding to a shuttling mechanism are used.

Ben-Zvi et al [7] then explore the scaling of the BMP gradient in a dorsal half embryos, built around the assumption that *Xenopus* embryos scale with size. However the evidence used to make this assumption is misinterpreted [35]. In particular, Spemann's experiments are quoted as being evidence that scaling occurs in dorsal half embryos. Spemann [29] divided cleaving salamander eggs (i.e. a urodele amphibian) into two halves: the half containing the future dorsal lip produces a well proportioned embryo, and a belly piece is formed from a ventral half. Ben-Zvi et al [7] take this to be evidence that *Xenopus* (an anuran amphibian) also exhibit scaling in dorsal halves. Ben-Zvi et al [7] also quote a paper by Cooke [23] to be evidence that dorsal half embryos produce well proportioned embryos, when in fact the quoted paper only stated that mesoderm patterning scales in transverse sections of tailbud embryos. There is evidence that dorsal halves from the 8-cell *Xenopus* blastula develop into tadpoles with normal heads and a small body and ventral halves develop into belly pieces [67]. Taken together, these papers suggest that, while dorsal halves from urodeles scale with embryo size, dorsal halves from anurans (such as *Xenopus*) do not.

A signalling profile is said to scale with embryo size if for the activation thresholds  $S = 10^{-2}$  and  $S = 10^{-1}$ , the relative position, scaled by embryo length, shifts by less than 20%. This is quite a large shift in the position of an activation threshold. To produce an in-proportion embryo, the shift in position may need to be much less than 20%. We now reproduce the numerical results given in [7] using a modified version of MATLAB's PDE solver, as provided by Danny Ben-Zvi, which runs faster than the standard MATLAB PDE solver. Unless otherwise stated the parameter values from table 5.1 are used. We attempt to reproduce the results of the model for both shuttling and inhibition parameters, but setting the ADMP and BMP degradation terms such that they are non-zero. For a wild type embryo, we set  $L = 1000\mu m$  and for a dorsal half  $L = 500\mu m$ ; we also plot results for  $L = 250\mu m$ . All results then are scaled by setting  $X = x/L$

In the shuttling mechanism (see figure 5.2(a)) BMP ligands are translocated to ventral regions of the embryo. Our results, like those given in Ben-Zvi et al [7], show that the BMP gradient scales with embryo length for a dorsal half embryo. In the inhibition based model, the BMP gradient does not scale with embryo length. Instead, the profile for a dorsal half embryo is the same as the profile for the dorsal half of a wild type embryo.



**Figure 5.2:** Solutions to (5.1.3), using the parameters given in table 5.1. **(a)** The BMP signalling profile for the shuttling based mechanism, for a wild type embryo (black line) and a dorsal half (grey line), with the dorsal half scaled to full length. **(b)** The BMP signalling profile for the inhibition based mechanism, for a wild type embryo (black line) and a dorsal half (grey line), with the dorsal half scaled to full length.  $\beta_{Admp} = 0.01$

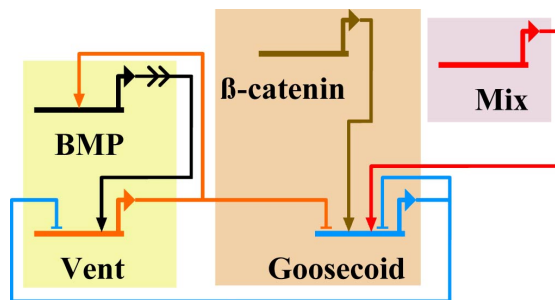
### Summary

In this subsection the mathematical model of BMP gradient formation given in *Xenopus* was reviewed. To reproduce the numerical results of the model given in [7], several modifications need to be made. Firstly, Ben-Zvi et al [7] state that the BMP activation profiles are plotted at their steady state. However, they set the ADMP degradation term to zero, meaning that due to the mathematical properties of the Hill function used for the rate of ADMP production, ADMP never reaches a steady state concentration. Either a non-trivial rate of ADMP degradation or using a Heaviside function, whereby for concentrations of BMP above a threshold level ADMP stops accumulating, need to be used to allow ADMP to reach a steady state value and to reproduce plots similar to those in [7]. Secondly, in the parameter screen, ADMP production only enters the model via a flux term on the dorsal side of the embryo. However, to reproduce the model results of [7] the ADMP production term is included across the whole embryo. Another issue was experienced whilst attempting to reproduce the BMP activation profiles in the inhibition-based model. The profiles plotted for a wild-type embryo ( $L = 1000$ ) and a dorsal-half embryo ( $L = 500$ ) are not the same as those given in [7], while plotting for a wild-type embryo with  $L = 500$  and  $L = 250$  for a dorsal-half produces profiles similar to those in [7].

The model of [7] considers the extracellular protein interactions of BMP, ADMP and Chordin, showing that a gradient of BMP can form by two different mechanisms. In this chapter we are concerned with adding Vent (a downstream target of BMP signaling), rather than on the mechanisms of BMP gradient formation. As such we proceed to formulate a single cell model of DV patterning, noting that this model could eventually be combined with a model of extracellular components of DV patterning as introduced in this section.

## 5.2 Simple 'DV only' model in a single cell

In this section, we develop a simplified model of DV patterning in a single cell. The model includes BMP4, a single representative Vent, Goosecoid, Mix and  $\beta$ -catenin. We neglect details of the BMP signalling pathway and its extracellular regulation by factors such as Chordin, instead assuming that BMP acts in the same way as a transcription factor (i.e. directly on its downstream targets). The interactions we include in our mathematical model are shown in figure 5.3 and discussed in what follows. The notation used for the concentration of each species in the model is given in table 5.2.



**Figure 5.3:** Network diagram showing the interactions between Vent, BMP and Goosecoid in a single cell.

Protein	Signal or TF	Protein Concentration
$\beta$ -catenin	signal	$C$
BMP	signal	$Bmp$
Vent	TF	$V$
Mix	TF	$M$
Goosecoid	TF	$G$

**Table 5.2:** Summary of genes present in the simplified DV network, with the notation used in the mathematical models.

### 5.2.1 Modelling the regulation of DV patterning

#### The time evolution of $\beta$ -catenin

$\beta$ -catenin is a maternal factor localised to dorsal regions of the embryo [126]. We therefore assume that in dorsal cells there exists an initial condition of  $\beta$ -catenin ( $C(0) > 0$ ) and that it turns over at a constant rate such that

$$\frac{dC}{dt} = -\mu_C C. \quad (5.2.1)$$

#### The time evolution of Goosecoid

It has been shown that *Goosecoid* is activated by Mix. *Goosecoid* is also activated by factors downstream of  $\beta$ -catenin (such as Lim1 and Siamois) [89]. For simplicity in our model we assume that  $\beta$ -catenin directly activates *Goosecoid*. Vent represses *Goosecoid* [124] and *Goosecoid* also negatively regulates its own expression [89]. The equation governing the concentration



of Goosecoid is then given by

$$\frac{dG}{dt} = \left\{ \lambda_{M,G} \mathcal{H} \left( \frac{M}{\theta_{M,G}} \right) + \lambda_{C,G} \mathcal{H} \left( \frac{C}{\theta_{C,G}} \right) \right\} \left\{ 1 - \mathcal{H} \left( \frac{V}{\theta_{V,G}} + \frac{G}{\theta_{G,G}} \right) \right\} - \mu_G G, \quad (5.2.2)$$

where  $\mathcal{H}(x)$  is the Hill function as defined in (1.11.2).

### The time evolution of Vent

In *Xenopus* there are two Vent genes, Vent1 and Vent2 [108]. In our model, we choose to model only a single Vent gene for simplicity. Note that there is only one Vent gene in humans [101, 114], so assuming a single Vent in our model is following a similar argument to that used to simplify the *Xenopus* mesendoderm GRN in [95]. We choose Vent2 to be this gene, since it is involved in the BMP4 positive feedback loop [54], in addition to its role repressing the transcription of Goosecoid [124]. The overexpression and knockdown of Vent2 also have more severe phenotypes than those for Vent1 [38, 107]. We should keep in mind that although we choose Vent2 to be the Vent gene, the effects of Vent in our model most likely represents the combined effects of the two Vent genes. Vent is activated by BMP signalling and is repressed by Goosecoid, such that

$$\frac{dV}{dt} = \lambda_{Bmp,V} \mathcal{H} \left( \frac{Bmp}{\theta_{Bmp,V}} \right) \left\{ 1 - \mathcal{H} \left( \frac{G}{\theta_{G,V}} \right) \right\} - \mu_V V. \quad (5.2.3)$$

### The time evolution of BMP

The transcription of BMP4 can be activated by its own signalling pathway, either with Vent2 as a cofactor or by P-Smad1 alone [54]. Since we want to consider a rather simplified model of the feedback loop we assume that Vent acts to activate BMP. The equation defining the concentration of BMP is therefore given by

$$\frac{dBmp}{dt} = \lambda_{V,Bmp} \mathcal{H} \left( \frac{V}{\theta_{V,Bmp}} \right) - \mu_{Bmp} Bmp. \quad (5.2.4)$$

### The time evolution of Mix

Mix is expressed in endoderm and anterior mesendoderm. In our model we assume that Mix is maintained at a steady state value, and as such Mix enters the model as a constant parameter.

## 5.2.2 Model equations

The equations governing the concentrations of  $\beta$ -catenin ( $C$ ), Goosecoid ( $G$ ), Vent ( $V$ ) and BMP4 ( $Bmp$ ) in a single cell, based on the network in figure 5.3, are given by the following system of

ODEs

$$\frac{dC}{dt} = -\mu_C C, \quad (5.2.5a)$$

$$\frac{dG}{dt} = \left\{ \lambda_{M,G} \mathcal{H} \left( \frac{M}{\theta_{M,G}} \right) + \lambda_{C,G} \mathcal{H} \left( \frac{C}{\theta_{C,G}} \right) \right\} \left\{ 1 - \mathcal{H} \left( \frac{V}{\theta_{V,G}} + \frac{G}{\theta_{G,G}} \right) \right\} - \mu_G G, \quad (5.2.5b)$$

$$\frac{dV}{dt} = \lambda_{Bmp,V} \mathcal{H} \left( \frac{Bmp}{\theta_{Bmp,V}} \right) \left\{ 1 - \mathcal{H} \left( \frac{G}{\theta_{G,V}} \right) \right\} - \mu_V V, \quad (5.2.5c)$$

$$\frac{dBmp}{dt} = \lambda_{V,Bmp} \mathcal{H} \left( \frac{V}{\theta_{V,Bmp}} \right) - \mu_{Bmp} Bmp. \quad (5.2.5d)$$

In this single cell model different regions of the embryo can be distinguished by choosing different initial conditions for  $\beta$ -catenin, i.e.  $C(0) = C_0$ , where  $C_0 \geq 0$ . Since P-Smad1, a downstream factor involved in the BMP signalling pathway, is expressed ubiquitously in early blastula embryos, we assume that a low level of BMP is initially expressed in all cells [126], such that  $Bmp(0) = Bmp_0$ , where  $Bmp_0$  is a positive constant, and that Goosecoid and Vent are not initially expressed in any cell. The initial conditions are then defined by

$$C(0) = C_0, \quad Bmp(0) = Bmp_0, \quad G(0) = 0, \quad V(0) = 0. \quad (5.2.6)$$

### 5.2.3 Non-dimensional model

To reduce the number of parameters in the model, it is nondimensionalised using the timescale of Goosecoid turnover,  $\tau = \mu_G t$ . Concentrations ( $Z$ ) are scaled  $\hat{Z} = Z/\theta_Z$ , where the following are defined for notational simplicity  $\theta_M \equiv \theta_{M,G}$ ,  $\theta_C \equiv \theta_{C,G}$ ,  $\theta_V \equiv \theta_{V,G}$ ,  $\theta_G \equiv \theta_{G,V}$ ,  $\theta_{Bmp} \equiv \theta_{Bmp,V}$ . Dimensionless parameters are defined as

$$\hat{\theta}_{Z,X} \equiv \theta_{Z,X}/\theta_Z, \quad \hat{\lambda}_{Y,Z} \equiv \lambda_{Y,Z}/\theta_Z \mu_G, \quad \hat{\mu}_Z \equiv \mu_Z/\mu_G.$$

After applying these scalings and dropping the hats for ease of notation the non-dimensional model is

$$\frac{dC}{d\tau} = -\mu_C C, \quad (5.2.7a)$$

$$\frac{dG}{d\tau} = \left\{ \lambda_{M,G} \mathcal{H}(M) + \lambda_{C,G} \mathcal{H}(C) \right\} \left\{ 1 - \mathcal{H} \left( V + \frac{G}{\theta_{G,G}} \right) \right\} - G, \quad (5.2.7b)$$

$$\frac{dV}{d\tau} = \lambda_{Bmp,V} \mathcal{H}(Bmp) \left\{ 1 - \mathcal{H}(G) \right\} - \mu_V V, \quad (5.2.7c)$$

$$\frac{dBmp}{d\tau} = \lambda_{V,Bmp} \mathcal{H} \left( \frac{V}{\theta_{V,Bmp}} \right) - \mu_{Bmp} Bmp. \quad (5.2.7d)$$

We hope to find that (5.2.7) has two stable steady states representing dorsal and ventral fates, with the dorsal fate corresponding to Goosecoid being expressed in the absence of Vent and BMP4 and the ventral fate corresponding to Vent and BMP4 being expressed in the absence of

Variable	Parameter	Value	Variable	Parameter	Value
C	$\mu_C$	0.1	V	$\lambda_{Bmp,V}$	5
G	$\lambda_{M,G}$	10		$\mu_V$	1
	$\lambda_{C,G}$	50	Bmp	$\lambda_{V,Bmp}$	1
	$\theta_{G,G}$	1		$\theta_{V,Bmp}$	1
	M	10		$\mu_{Bmp}$	0.1

**Table 5.3:** Dimensionless parameter values used to obtain numerical results for the system given in (5.2.7). Parameters were selected such that (5.2.7) is bistable with steady states corresponding to dorsal and ventral cell states, and so that the system evolves to these steady states dependent on the initial concentration of  $\beta$ -catenin in the cell.

Goosecoid. We seek solutions to (5.2.7) such that both dorsal and ventral fates are available. The model consists of a positive feedback loop between Vent and BMP, and mutual inhibition between Vent and Goosecoid. It has been shown that GRNs consisting of mutual inhibiting factors [37, 95] can be bistable provided that the cooperativity of binding is greater than unity. As a consequence of these observations we proceed to consider the case where the condition is satisfied, i.e.  $m > 1$ .

## 5.2.4 Steady-state analysis

In this section, we consider the steady states of the system (5.2.7), satisfying the coupled system of equations

$$C^* = 0, \quad (5.2.8a)$$

$$G^* = \lambda_{M,G} \mathcal{H}(M) \left\{ 1 - \mathcal{H} \left( V^* + \frac{G^*}{\theta_{G,G}} \right) \right\}, \quad (5.2.8b)$$

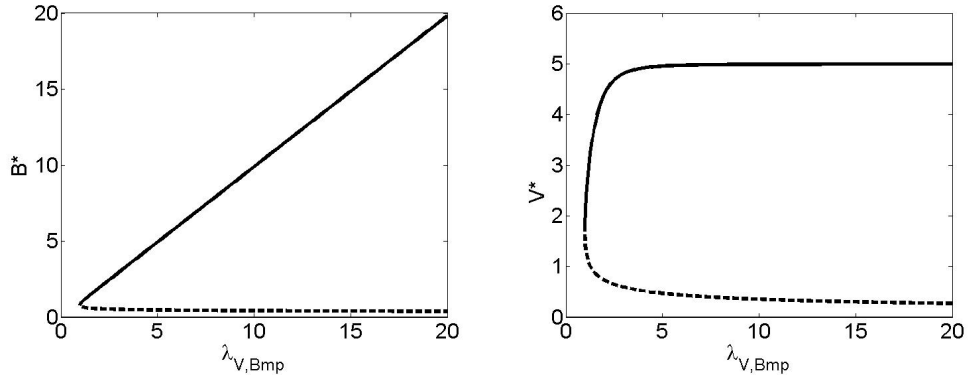
$$V^* = \frac{\lambda_{Bmp,V}}{\mu_V} \mathcal{H}(Bmp^*) \{ 1 - \mathcal{H}(G^*) \}, \quad (5.2.8c)$$

$$Bmp^* = \frac{\lambda_{V,Bmp}}{\mu_{Bmp}} \mathcal{H} \left( \frac{V^*}{\theta_{V,Bmp}} \right). \quad (5.2.8d)$$

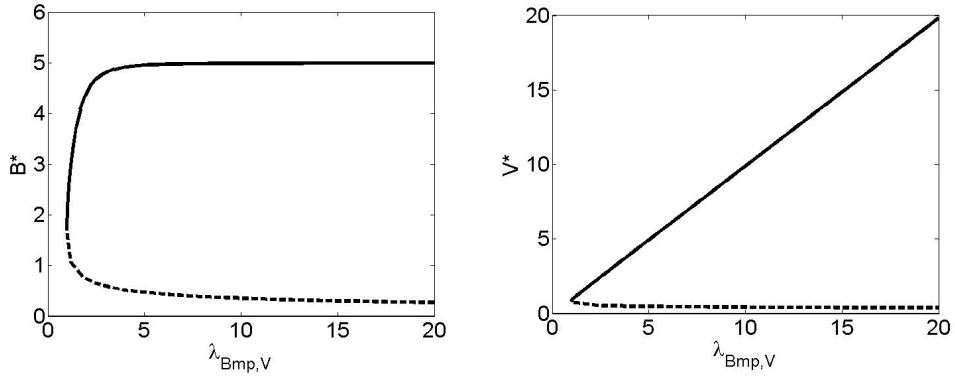
Note that the steady state values of  $G^*$ ,  $V^*$  and  $Bmp^*$  are independent of the concentration of  $\beta$ -catenin ( $C$ ) since this decays to zero as the steady state is approached. However in section 5.2.5 we show that the system can evolve to the dorsal or the ventral steady state dependent on the initial condition of  $\beta$ -catenin.

### Steady state solutions in the absence of Goosecoid ( $G^* = 0$ )

In the absence of any factors to activate Goosecoid ( $M = 0$  and  $C = 0$ ), we expect that BMP and Vent can maintain themselves via mutual positive regulation and evolve to a non-trivial stable steady state. Figure 5.4 shows plots of the steady-state values of BMP and Vent for a range of  $\lambda_{V,Bmp}$ . The trivial steady state, where Vent and BMP are not expressed, is available for all values of  $\lambda_{V,Bmp}$ . As  $\lambda_{V,Bmp}$  increases a saddle-node bifurcation marks the appearance of a two non-trivial steady states. The non-trivial stable steady state represents a cell adopting a ventral fate, with upregulated Vent and BMP. As the value of  $\lambda_{V,Bmp}$  increases, the steady state concentration of BMP increases, while the steady state value of Vent is rather insensitive to



**Figure 5.4:** Numerical investigation of the Vent and BMP positive feedback loop, as described by (5.2.7c) and (5.2.7d) with  $G = 0$ . The trivial steady state ( $V^* = 0, Bmp^* = 0$ ) is available for all values of  $\lambda_{V,Bmp}$ . As  $\lambda_{V,Bmp}$  increases a saddle node bifurcation occurs at  $\lambda_{V,Bmp} \approx 0.96$ , marking the appearance of a non trivial stable steady state and an unstable steady state. Parameters other than  $\lambda_{V,Bmp}$  are as in table 5.3.

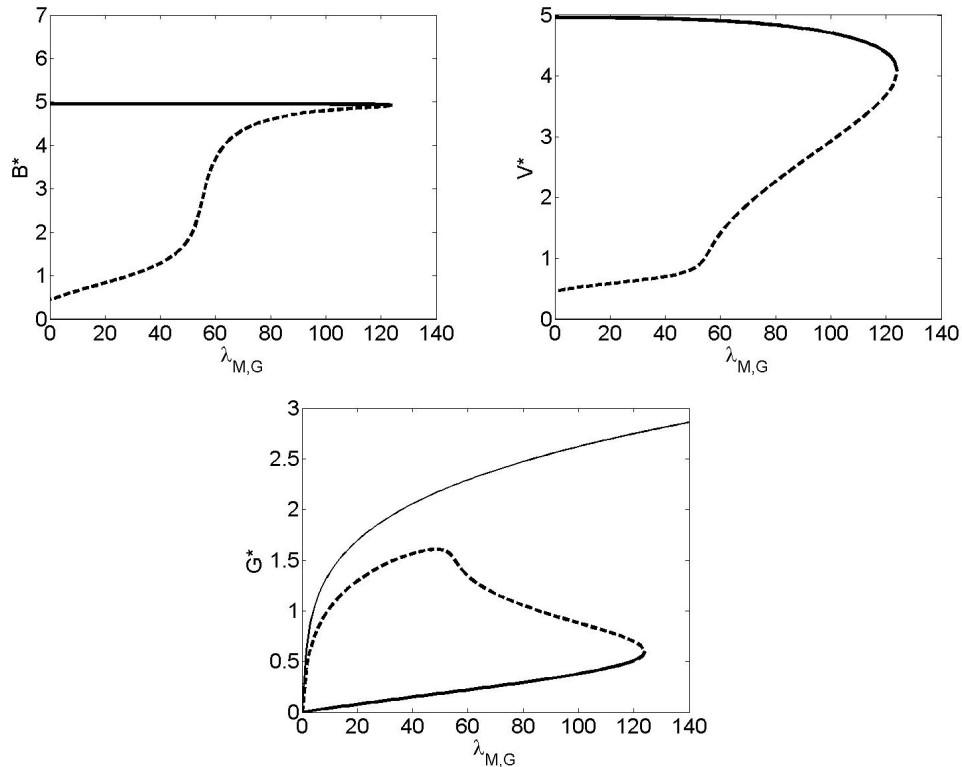


**Figure 5.5:** Numerical investigation of the Vent and BMP positive feedback loop, as described by (5.2.7c) and (5.2.7d) with  $G = 0$ . The trivial steady state ( $V^* = 0, Bmp^* = 0$ ) is available for all values of  $\lambda_{Bmp,V}$ . As  $\lambda_{Bmp,V}$  increases a saddle node bifurcation occurs at  $\lambda_{Bmp,V} \approx 0.96$ , marking the appearance of a non trivial stable steady state (thick solid line) and an unstable steady state (thick dashed line). Parameters other than  $\lambda_{Bmp,V}$  are as in table 5.3.

changes in  $\lambda_{V,Bmp}$ . Plotted in figure 5.5 are the steady-state values of BMP and Vent for various values of  $\lambda_{Bmp,V}$ . As  $\lambda_{Bmp,V}$  increases a saddle-node bifurcation marks the appearance of the non-trivial steady states.

### Steady state solutions for fixed Mix ( $M$ ) concentration

We now investigate steady-state solutions of (5.2.7) in the presence of a fixed concentration of Mix ( $M > 0$ ). Steady-state concentrations of Vent, BMP and Goosecoid are plotted as functions of  $\lambda_{M,G}$  in figure 5.6. When  $\lambda_{M,G} = 0$ , there are three steady states for the concentration of BMP and Vent: the trivial stable steady state, a (non-trivial) unstable steady state and a (non-trivial) stable steady state. At  $\lambda_{M,G} = 0$ , the only steady state for Goosecoid is the trivial steady state, as  $\lambda_{M,G}$  increases Goosecoid becomes bistable, with stable steady states corresponding to up-regulated and downregulated levels. For further increases in  $\lambda_{M,G}$ , the downregulated steady

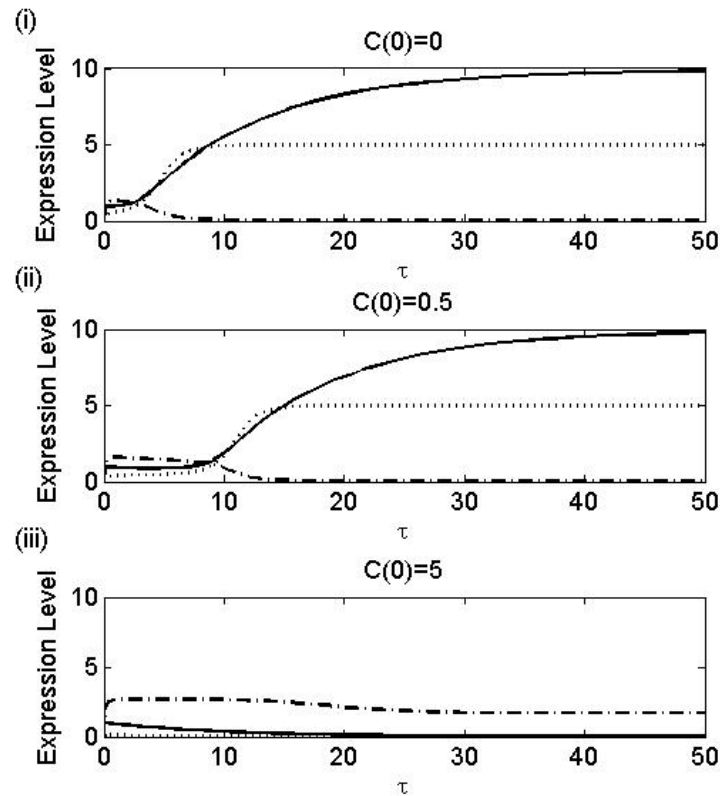


**Figure 5.6:** Steady state concentrations of BMP ( $Bmp^*$ ), Vent ( $V^*$ ) and Goosecoid ( $G^*$ ) as functions of  $\lambda_{M,G}$ . As  $\lambda_{M,G}$  increases a fold bifurcation marks the disappearance of the stable steady state representing ventral fates (thin solid line) and the unstable steady state (thick dashed line). The stable steady state representing dorsal fates (thin solid line) is present for all non-negative values of  $\lambda_{M,G}$ .

state disappears via a fold bifurcation, leaving a monostable steady state with upregulated Goosecoid.

## 5.2.5 Time-dependent solutions

In this section we explore the time-dependent behaviour of our model in different conditions and compare these with the experimental results of [124]. Figure 5.7 shows how the initial condition of  $\beta$ -catenin,  $C(0) = C_0$ , (i.e. the strength of the dorsalisng signal a cell is subjected to) determines the fate of a cell. In the absence of  $\beta$ -catenin (figure 5.7(i)), the Vent/BMP positive feedback loop becomes established and the activation of Goosecoid by Mix is suppressed by Vent, meaning the system evolves to the ventral steady state. For  $C_0$  less than a critical value ( $C_0^C$ ) the solutions will evolve to the ventral steady state as shown in figures 5.7(i) and (ii). In figure 5.7(ii), where  $C_0$  is close to the critical value, there exists a phase where Goosecoid, BMP and Vent are coexpressed at non-negligible levels before the Vent/BMP feedback loop becomes established and the system evolves to the ventral steady state. This co-expression of all three factors corresponds to the solution passing close to the unstable steady state. For  $C_0$  greater than the critical value ( $C_0 > C_0^C$ ), the concentration of Goosecoid in the system grows rapidly, leading to the repression of Vent, with the BMP initially present decaying to negligible levels.



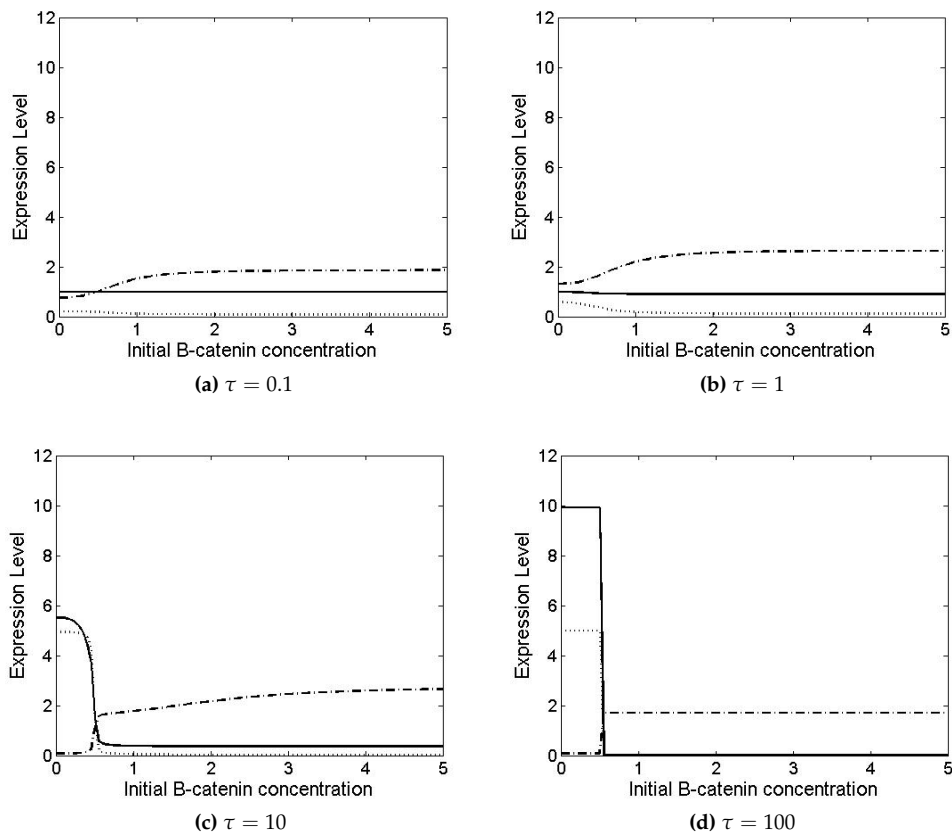
**Figure 5.7:** Time evolution of (5.2.7) for various initial conditions of  $\beta$ -catenin, showing Vent (dotted line), BMP (solid line) and Goosecoid (dot-dashed line). (i) In the absence of  $\beta$ -catenin ( $C(0) = 0$ ) the system evolves to the ventral steady state branch. (ii) For value of  $\beta$ -catenin close to some critical value, the solution passed close to the unstable steady state. (iii) For a larger value of  $\beta$ -catenin ( $C(0) = 5$ ) the cell evolves to the dorsal steady state branch.

In this case the system has evolved to the dorsal steady state (see figure 5.7(iii)).

### $\beta$ -catenin dose response

As shown in figure 5.7 the initial dose of  $\beta$ -catenin can determine whether solutions to (5.2.7) evolve to the ventral or dorsal steady state. Solutions are shown in figure 5.8 as functions of the initial concentration of  $\beta$ -catenin. Initially both BMP and Goosecoid are expressed for all concentrations of  $\beta$ -catenin. At later times the expression becomes more refined, and Vent/BMP are expressed at low concentrations and Goosecoid is expressed at high concentrations.

In figure 5.9 the effect of varying the concentration of Mix ( $M$ ) in the system is shown in the absence (figure 5.9(i)) and presence (figure 5.9(ii)) of  $\beta$ -catenin. In the absence of  $\beta$ -catenin the system shows the same qualitative behaviour for all values of  $M$ , with Vent and BMP reaching an upregulated steady state and any initial expression of Goosecoid becomes repressed. In the presence of  $\beta$ -catenin, Vent and BMP are repressed by Goosecoid and reach the trivial steady state for all values of  $M$ . The steady state value of Goosecoid ( $G^*$ ) is dependent on the value of



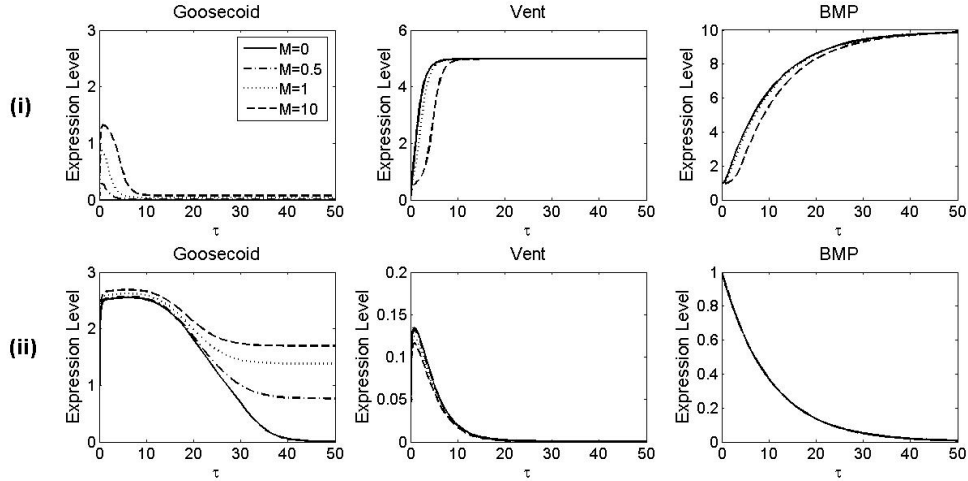
**Figure 5.8:** Numerical solutions to (5.2.7) plotted against initial  $\beta$ -catenin concentration ( $C_0$ ) at time  $\tau = T$ .  $\beta$ -catenin can induce Goosecoid (dot-dashed line) at high concentration, but at low concentrations Goosecoid becomes repressed by Vent (dotted line) and BMP (solid line).

$M$ : as  $M$  increases  $G^*$  also increases (see equation (5.2.8)). However the qualitative behaviour is similar for all  $M$ .

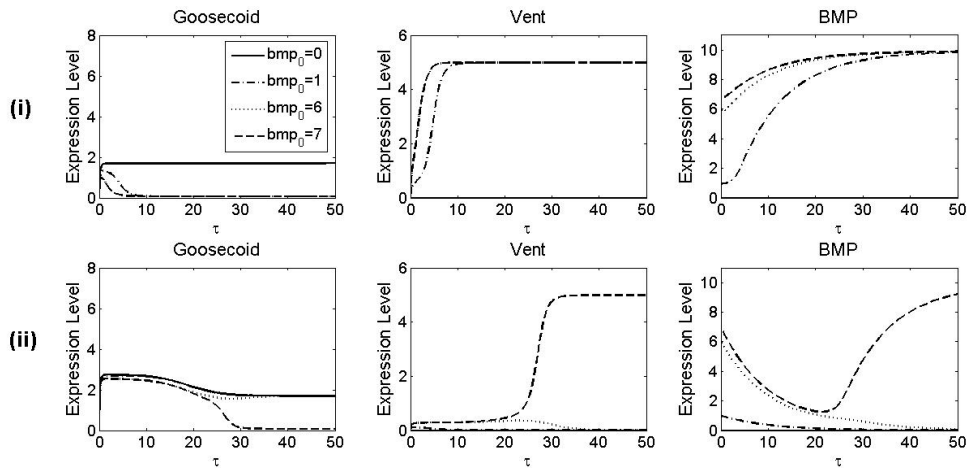
Figure 5.10 plots the time evolution of Vent, BMP and Goosecoid for several initial values of BMP. In the absence of BMP, the system evolves to the dorsal steady state independent of the initial concentration of  $\beta$ -catenin.

### Goosecoid and Vent knockouts

By setting parameters on the right hand side of (5.2.7b) to be zero, so that  $dG/dt = 0$ , we investigate the effect of a Goosecoid knockout on our system. Experimental observations in [124] state that in animal caps (consisting of a uniform population of cells) treated with Activin and a Goosecoid MO, the expression of Vent1 and Vent2 are upregulated. In our model the knockout of Goosecoid results in the system evolving to the ventral steady state (figure 5.11 (iv)-(vi)), which is consistent with experimental observations. Conversely a knockout of Vent results in the system evolving to the dorsal steady state for all values of  $C_0$  (figure 5.11 (i)-(iii)), consistent with experimental data showing that the double knockdown of Vent1/Vent2 results in dorsalised embryos [124].



**Figure 5.9:** Numerical solutions to (5.2.7) for various values of  $M$  (concentration of Mix) for two cases: (i)  $C(0) = 0$  and (ii)  $C(0) = 5$ . (i) The qualitative behaviour is the same for all values of  $M$ , with the system evolving to a state with upregulated Vent and BMP. (ii) In the presence of  $\beta$ -catenin the qualitative behaviour is the same for all values of  $M$ , with the system evolving to a state with no Vent and BMP, and the steady state value of Goosecoid dependent on the value of  $M$ .

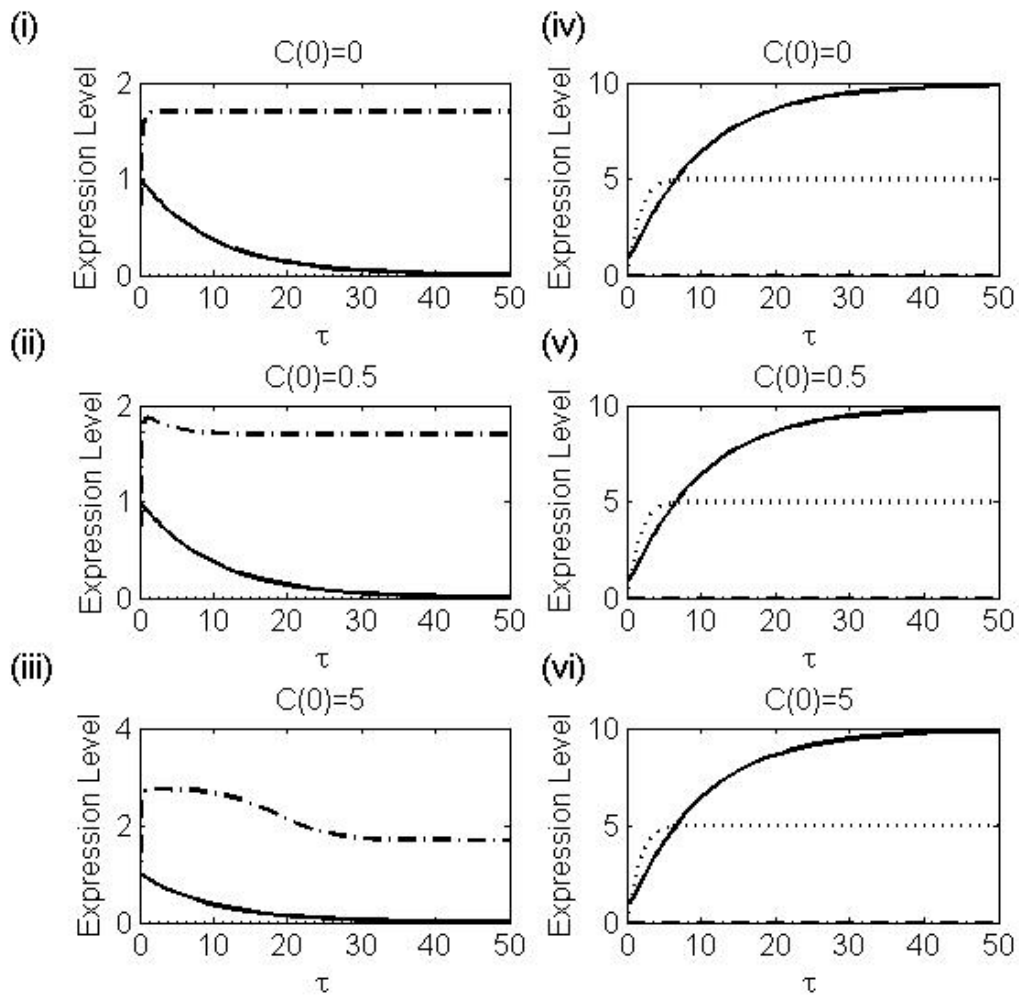


**Figure 5.10:** Numerical solutions to (5.2.7) for various values of initial BMP concentration ( $Bmp(0) = Bmp_0$ ) for two cases: (i)  $C(0) = 0$  and (ii)  $C(0) = 5$ . (i) For all  $Bmp_0 \geq 1$  the system evolves to the ventral steady state. When  $Bmp_0 = 0$  the system evolves to the dorsal steady state. (ii) When  $\beta$ -catenin is present the system evolves to the dorsal state for all  $Bmp_0 \leq 6$ . For large  $Bmp_0$ , the system evolves to a ventral fate.

## 5.2.6 Summary

In this section, we introduced a simplified version of the *Xenopus* dorsal-ventral patterning GRN, where the two Vent genes are treated as a single gene in the network. The network does not include the extracellular repression of the BMP signalling pathway by Chordin; however, it is thought that this may act to reinforce the repression of Vent by Goosecoid. A mathematical model based on the GRN, giving the time evolution of each transcription factor in a single



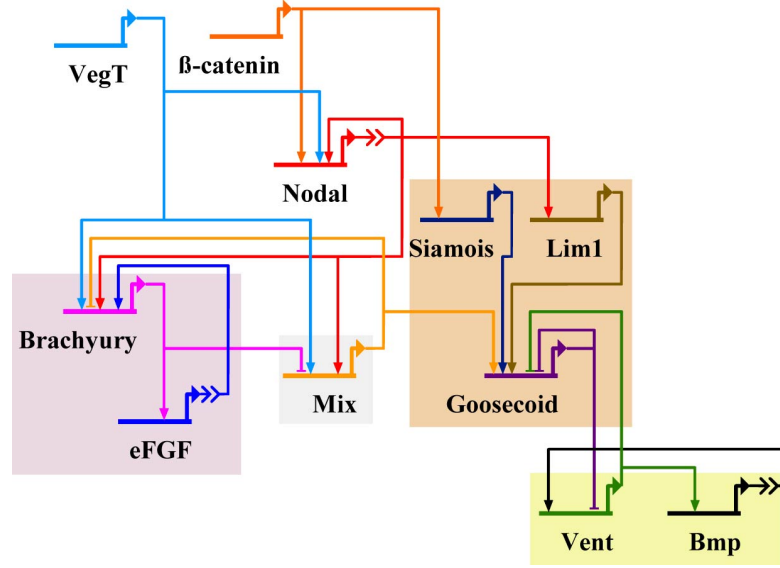


**Figure 5.11:** (i)-(iii) Time evolution of (5.2.7) for various initial conditions of  $\beta$ -catenin in the absence of Vent, showing BMP (solid line) and Goosecoid (dot-dashed line). (iv)-(vi) Time evolution of (5.2.7) for various initial conditions of  $\beta$ -catenin in the absence of Goosecoid, showing Vent (dotted line) and BMP (solid line).

cell, is formulated. The model is bistable with stable steady states corresponding to dorsal and ventral fates. The model reproduces qualitatively the experimental data of [124].

### 5.3 A 'DV and mesendoderm' model in a single cell

We now proceed to couple this model to the *Xenopus* mesendoderm model formulated in [95] to enable the model to account for the formation of endoderm, as well as anterior mesendoderm and mesoderm.



**Figure 5.12:** Network diagram of a simplified version of the *Xenopus* mesendoderm network including Vent and BMP. Nodal, BMP and eFGF encode signals and all other genes encode transcription factors.

### 5.3.1 Model formulation

The network upon which we base our model is shown in figure 5.12. Note that this is identical to the simplified (*in vivo*) mesendoderm network presented in figure 3.4, with the addition of Vent and BMP, with Vent also acting to repress Goosecoid. All equations are the same as in the *Xenopus in vivo* model of [95], except for the following.

#### The time evolution of Goosecoid

Recall from section 5.2.1 that Goosecoid expression can be activated by either Lim.1 and Siamois, or by Mix. Goosecoid can be repressed by both Vent and itself. This leads to the following equation governing the time evolution of Goosecoid

$$\frac{dG}{dt} = \left\{ \lambda_{LI,G} \mathcal{H} \left( \frac{L}{\theta_{L,G}} \right) \mathcal{H} \left( \frac{I}{\theta_{I,G}} \right) + \lambda_{M,G} \mathcal{H} \left( \frac{M}{\theta_{M,G}} \right) \right\} \left\{ 1 - \mathcal{H} \left( \frac{G}{\theta_{G,G}} + \frac{Vent}{\theta_{V,G}} \right) \right\} - \mu_G G. \quad (5.3.1)$$

Note that this is the same as the equation for Goosecoid in the *in vivo* model of [95], except for the addition of the term for the repression of Goosecoid by Vent.

#### The time evolution of BMP and Vent

The equations for the time evolution of BMP and Vent are as described in section 5.2.1.

### 5.3.2 Model equations

The equations governing the time evolution of VegT ( $V$ ),  $\beta$ -catenin ( $C$ ), Nodal ( $N$ ), Lim1 ( $L$ ), Siamois ( $I$ ), eFGF ( $E$ ), Brachyury ( $B$ ), Mix ( $M$ ), Goosecoid ( $G$ ), Vent ( $Vent$ ) and BMP ( $Bmp$ ) in a

single cell, based on the GRN given in figure 5.12, are

$$\frac{dV}{dt} = -\mu_V V, \quad (5.3.2a)$$

$$\frac{dC}{dt} = -\mu_C C, \quad (5.3.2b)$$

$$\frac{dN}{dt} = \left\{ \lambda_{V,N} \mathcal{H} \left( \frac{V}{\theta_{V,N}} \right) + \lambda_{N,N} \mathcal{H} \left( \frac{N}{\theta_{N,N}} \right) \left( 1 + \lambda_{C,N} \mathcal{H} \left( \frac{C}{\theta_{C,N2}} \right) \right) \right\} - \mu_N N, \quad (5.3.2c)$$

$$\frac{dL}{dt} = \lambda_{N,L} \mathcal{H} \left( \frac{N}{\theta_{N,L}} \right) - \mu_L L, \quad (5.3.2d)$$

$$\frac{dI}{dt} = \lambda_{C,I} \mathcal{H} \left( \frac{C}{\theta_{C,I}} \right) - \mu_I I, \quad (5.3.2e)$$

$$\frac{dE}{dt} = \lambda_{B,E} \mathcal{H} \left( \frac{B}{\theta_{B,E}} \right) - \mu_E E, \quad (5.3.2f)$$

$$\begin{aligned} \frac{dB}{dt} = & \left\{ \lambda_{V,B} \mathcal{H} \left( \frac{V}{\theta_{V,B}} \right) + \lambda_{E,B} \mathcal{H} \left( \frac{E}{\theta_{E,B}} \right) + \lambda_{N,B} \mathcal{H} \left( \frac{N}{\theta_{N,B}} \right) \right\} \left\{ 1 - \mathcal{H} \left( \frac{G}{\theta_{G,B}} + \frac{M}{\theta_{M,B}} \right) \right\} \\ & - \mu_B B, \end{aligned} \quad (5.3.2g)$$

$$\begin{aligned} \frac{dG}{dt} = & \left\{ \lambda_{L,I} \mathcal{H} \left( \frac{L}{\theta_{L,G}} \right) \mathcal{H} \left( \frac{I}{\theta_{I,G}} \right) + \lambda_{M,G} \mathcal{H} \left( \frac{M}{\theta_{M,G}} \right) \right\} \left\{ 1 - \mathcal{H} \left( \frac{G}{\theta_{G,G}} + \frac{Vent}{\theta_{V,G}} \right) \right\} \\ & - \mu_G G, \end{aligned} \quad (5.3.2h)$$

$$\frac{dM}{dt} = \left\{ \lambda_{V,M} \mathcal{H} \left( \frac{V}{\theta_{V,M}} \right) + \lambda_{N,M} \mathcal{H} \left( \frac{N}{\theta_{N,M}} \right) \right\} \left\{ 1 - \mathcal{H} \left( \frac{B}{\theta_{B,M}} \right) \right\} - \mu_M M, \quad (5.3.2i)$$

$$\frac{dVent}{dt} = \lambda_{Bmp,V} \mathcal{H} \left( \frac{Bmp}{\theta_{Bmp,V}} \right) \left\{ 1 - \mathcal{H} \left( \frac{G}{\theta_{G,V}} \right) \right\} - \mu_{Vent} Vent, \quad (5.3.2j)$$

$$\frac{dBmp}{dt} = \lambda_{V,Bmp} \mathcal{H} \left( \frac{Vent}{\theta_{V,Bmp}} \right) - \mu_{Bmp} Bmp. \quad (5.3.2k)$$

Initial conditions are selected such that different regions of the embryo can be distinguished. VegI,  $\beta$ -catenin and BMP are all maternal factors found in the embryo, with figure 5.13 illustrating the spatial localisation of these factors in stage 1 embryos. Selecting different values of  $V_0$ ,  $C_0$  and  $Bmp_0$  can be used to represent cells in different regions of the embryo. The initial conditions are

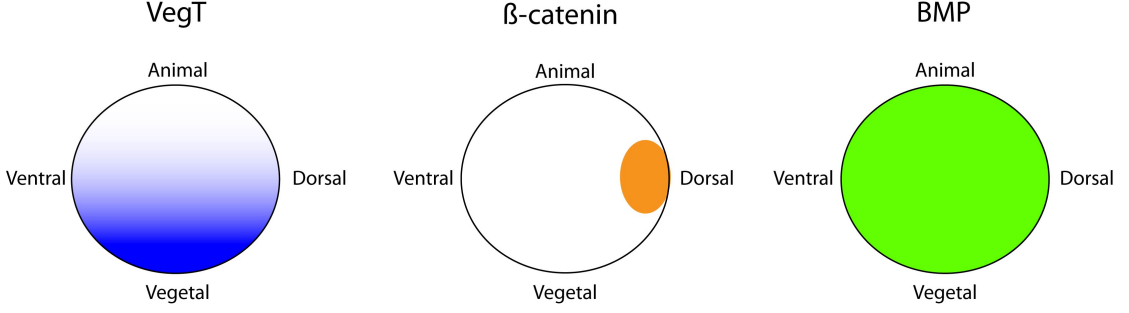
$$V(0) = V_0, \quad C(0) = C_0, \quad N(0) = 0, \quad L(0) = 0, \quad I(0) = 0, \quad E(0) = 0, \quad B(0) = 0,$$

$$G(0) = 0, \quad M(0) = 0, \quad Vent(0) = 0, \quad Bmp(0) = Bmp_0,$$

where  $V_0$ ,  $C_0$  and  $Bmp_0$  are positive constants.

### 5.3.3 Non-dimensional model

Choosing the same non-dimensional timescale as [95], we rescale by the timescale of Brachyury turnover, defining nondimensional time by  $\tau = \mu_B t$ . After defining the following for notational simplicity  $\theta_V \equiv \theta_{V,N}$ ,  $\theta_C \equiv \theta_{C,N}$ ,  $\theta_B \equiv \theta_{B,E}$ ,  $\theta_E \equiv \theta_{E,B}$ ,  $\theta_N \equiv \theta_{N,B}$ ,  $\theta_G \equiv \theta_{G,B}$ ,  $\theta_M \equiv \theta_{M,B}$ ,  $\theta_L \equiv \theta_{L,G}$ ,  $\theta_I \equiv \theta_{I,G}$ ,  $\theta_{Bmp} \equiv \theta_{Bmp,Vent}$  and  $\theta_{Vent} \equiv \theta_{Vent,Bmp}$ , dimensionless concentrations are



**Figure 5.13:** Cartoon showing the spatial localisation of VegT [155],  $\beta$ -catenin [126] and BMP2 [20] in stage 1 embryos.

given by  $\hat{Z} = Z/\theta_Z$ . Dimensionless parameters are then defined as follows

$$\hat{\theta}_{Z,X} \equiv \theta_{Z,X}/\theta_Z, \quad \hat{\lambda}_{Y,Z} \equiv \lambda_{Y,Z}/\theta_Z\mu_G, \quad \hat{\mu}_Z \equiv \mu_Z/\mu_G.$$

After applying the scalings above to (5.3.2), dropping the hats for ease of notation, the non-dimensional model is as follows

$$\frac{dV}{dt} = -\mu_V V, \tag{5.3.3a}$$

$$\frac{dC}{dt} = -\mu_C C, \tag{5.3.3b}$$

$$\frac{dN}{dt} = \left\{ \lambda_{V,N} \mathcal{H}(V) + \lambda_{N,N} \mathcal{H}\left(\frac{N}{\theta_{N,N}}\right) (1 + \lambda_{C,N} \mathcal{H}(C)) \right\} - \mu_N N, \tag{5.3.3c}$$

$$\frac{dL}{dt} = \lambda_{N,L} \mathcal{H}\left(\frac{N}{\theta_{N,L}}\right) - \mu_L L, \tag{5.3.3d}$$

$$\frac{dI}{dt} = \lambda_{C,I} \mathcal{H}\left(\frac{C}{\theta_{C,I}}\right) - \mu_I I, \tag{5.3.3e}$$

$$\frac{dE}{dt} = \lambda_{B,E} \mathcal{H}(B) - \mu_E E, \tag{5.3.3f}$$

$$\frac{dB}{dt} = \left\{ \lambda_{V,B} \mathcal{H}\left(\frac{V}{\theta_{V,B}}\right) + \lambda_{E,B} \mathcal{H}(E) + \lambda_{N,B} \mathcal{H}(N) \right\} \{1 - \mathcal{H}(G + M)\} - B, \tag{5.3.3g}$$

$$\frac{dG}{dt} = \left\{ \lambda_{L,G} \mathcal{H}(L) \mathcal{H}(I) + \lambda_{M,G} \mathcal{H}\left(\frac{M}{\theta_{M,G}}\right) \right\} \left\{ 1 - \mathcal{H}\left(\frac{G}{\theta_{G,G}} + \frac{Vent}{\theta_{V,G}}\right) \right\} - \mu_G G, \tag{5.3.3h}$$

$$\frac{dM}{dt} = \left\{ \lambda_{V,M} \mathcal{H}\left(\frac{V}{\theta_{V,M}}\right) + \lambda_{N,M} \mathcal{H}\left(\frac{N}{\theta_{N,M}}\right) \right\} \left\{ 1 - \mathcal{H}\left(\frac{B}{\theta_{B,M}}\right) \right\} - \mu_M M, \tag{5.3.3i}$$

$$\frac{dVent}{dt} = \lambda_{Bmp,V} \mathcal{H}(Bmp) \left\{ 1 - \mathcal{H}\left(\frac{G}{\theta_{G,V}}\right) \right\} - \mu_{Vent} Vent, \tag{5.3.3j}$$

$$\frac{dBmp}{dt} = \lambda_{V,Bmp} \mathcal{H}(Vent) - \mu_{Bmp} Bmp. \tag{5.3.3k}$$

Subject to initial conditions

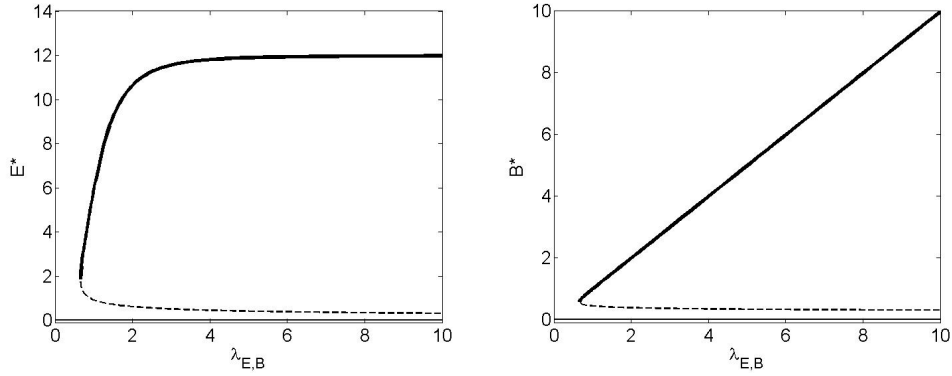
$$V(0) = V_0, \quad C(0) = C_0, \quad N(0) = 0, \quad L(0) = 0, \quad I(0) = 0, \quad E(0) = 0, \quad B(0) = 0,$$

$$G(0) = 0, \quad M(0) = 0, \quad Vent(0) = 0, \quad Bmp(0) = Bmp_0,$$

Variable	Parameter	Value	Variable	Parameter	Value
V	$\mu_V$	0.01	C	$\mu_C$	0.01
N	$\lambda_{V,N}$	1	B	$\lambda_{E,B}$	12
	$\lambda_{N,N}$	3		$\lambda_{V,B}$	2
	$\lambda_{C,N}$	1		$\lambda_{X,B}$	10
	$\theta_{N,N}$	1		$\theta_{V,B}$	1
M	$\lambda_{V,M}$	10	G	$\lambda_{LI,G}$	300
	$\lambda_{X,M}$	12		$\lambda_{M,G}$	5
	$\theta_{V,M}$	4		$\theta_{M,G}$	1
	$\theta_{X,M}$	3		$\theta_{G,G}$	1
	$\theta_{B,M}$	1		L	$\lambda_{N,L}$
I	$\lambda_{C,I}$	1	$\theta_{N,L}$		1
	$\theta_{C,I}$	1	Bmp	$\lambda_{V,Bmp}$	5
E	$\lambda_{B,E}$	12		$\theta_{V,Bmp}$	1
V	$\lambda_{Bmp,V}$	2		$\mu_{Bmp}$	0.1
	$\theta_{Bmp,V}$	1	all other $\mu$	1	
	$\theta_{G,V}$	1			

**Table 5.4:** Dimensionless parameter values used to obtain numerical results for the system given in (5.3.3). Parameters were selected such that stable steady states corresponding to mesoderm, endoderm and anterior mesoderm are solutions to (5.3.3) and that the system can evolve to these steady states dependent on initial concentrations of VegT,  $\beta$ -catenin and BMP.

where  $V_0$ ,  $C_0$  and  $Bmp_0$  are positive constants.



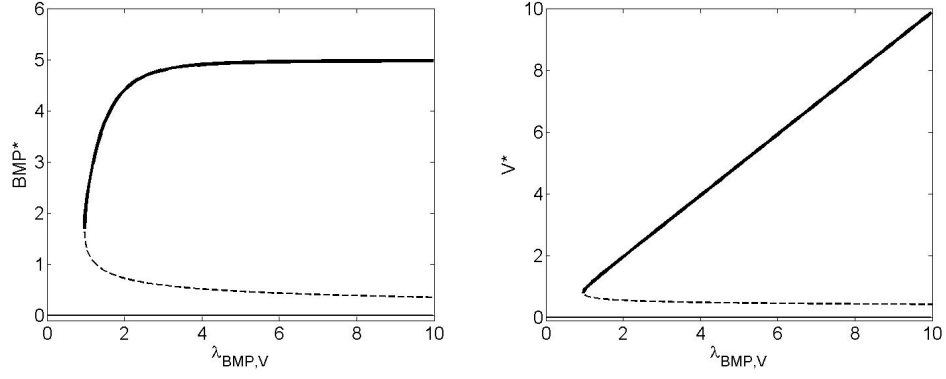
**Figure 5.14:** Steady state concentrations of Brachyury ( $B^*$ ) and eFGF ( $E^*$ ) as functions of  $\lambda_{E,B}$ . As  $\lambda_{E,B}$  increases a fold bifurcation marks the disappearance of the stable steady state representing the mesoderm fate (thick solid line) and the unstable steady state (dashed line). The trivial steady state (thin solid line) is present for all non-negative values of  $\lambda_{E,B}$ .

### 5.3.4 Steady states

The steady states of (5.3.3) are determined by the solutions to the following equations. First the steady state for  $N^*$  is found by solving

$$V^* = 0, \quad C^* = 0, \quad N^* = \frac{\lambda_{N,N}}{\mu_N} \mathcal{H} \left( \frac{N^*}{\theta_{N,N}} \right). \quad (5.3.4)$$

Note that (5.3.4) is the same as the steady state equation for Nodal in [95], where it was found that for  $m > 1$  the system is bistable, with stable steady states corresponding to the trivial



**Figure 5.15:** Steady state concentrations of BMP ( $BMP^*$ ) and Vent ( $Vent^*$ ) as functions of  $\lambda_{BMP,V}$ . As  $\lambda_{BMP,V}$  increases a fold bifurcation marks the disappearance of the stable steady state representing the ventral fate (thick solid line) and the unstable steady state (dashed line). The trivial steady state (thin solid line) is present for all non-negative values of  $\lambda_{BMP,V}$ .

steady state ( $N^* = 0$ ) and a positive steady state ( $N^* = N_S > 0$ ).  $L^*$  is then determined by

$$L^* = \frac{\lambda_{N,L}}{\mu_L} \mathcal{H}\left(\frac{N^*}{\theta_{N,L}}\right), \quad I^* = 0. \quad (5.3.5)$$

The coupled system in (5.3.3) can be solved for  $E^*$ ,  $B^*$ ,  $G^*$ ,  $M^*$ ,  $Vent^*$  and  $Bmp^*$

$$E^* = \frac{\lambda_{B,E}}{\mu_E} \mathcal{H}(B^*), \quad (5.3.6a)$$

$$B^* = \{\lambda_{E,B} \mathcal{H}(E^*) + \lambda_{N,B} \mathcal{H}(N^*)\} \{1 - \mathcal{H}(G^* + M^*)\}, \quad (5.3.6b)$$

$$G^* = \frac{\lambda_{M,G}}{\mu_G} \mathcal{H}\left(\frac{M^*}{\theta_{M,G}}\right) \left\{1 - \mathcal{H}\left(\frac{G^*}{\theta_{G,G}} + \frac{Vent^*}{\theta_{V,G}}\right)\right\}, \quad (5.3.6c)$$

$$M^* = \frac{\lambda_{N,M}}{\mu_M} \mathcal{H}\left(\frac{N^*}{\theta_{N,M}}\right) \left\{1 - \mathcal{H}\left(\frac{B^*}{\theta_{B,M}}\right)\right\}, \quad (5.3.6d)$$

$$Vent^* = \frac{\lambda_{Bmp,V}}{\mu_{Vent}} \mathcal{H}(Bmp^*) \left\{1 - \mathcal{H}\left(\frac{G^*}{\theta_{G,V}}\right)\right\}, \quad (5.3.6e)$$

$$Bmp^* = \frac{\lambda_{V,Bmp}}{\mu_{Bmp}} \mathcal{H}(Vent^*). \quad (5.3.6f)$$

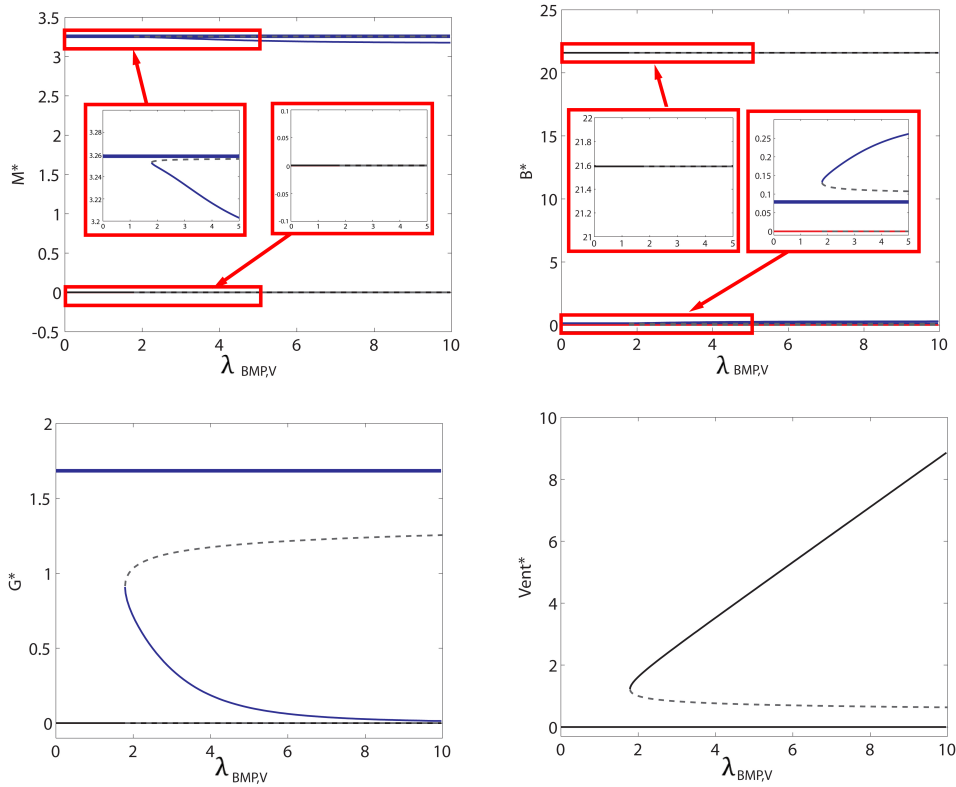
We consider solutions to (5.3.6) in two cases,  $N^* = 0$  and  $N^* = N_S > 0$ , corresponding to upregulated *Nodal* and downregulated *Nodal*, respectively.

### Steady-state solutions in the absence of Nodal

When  $N^* = 0$ , it follows from (5.3.6) that  $M^* = 0$ ,  $G^* = 0$  and

$$E^* = \frac{\lambda_{B,E}}{\mu_E} \mathcal{H}(B^*), \quad B^* = \lambda_{E,B} \mathcal{H}(E^*), \quad (5.3.7a)$$

$$Vent^* = \frac{\lambda_{Bmp,V}}{\mu_{Vent}} \mathcal{H}(Bmp^*), \quad Bmp^* = \frac{\lambda_{V,Bmp}}{\mu_{Bmp}} \mathcal{H}(Vent^*). \quad (5.3.7b)$$



**Figure 5.16:** Steady state solutions of Mix ( $M^*$ ), Brachyury ( $B^*$ ), Goosecoid ( $G^*$ ) and Vent ( $Vent^*$ ) plotted as functions of  $\lambda_{BMP,V}$ . There are six stable steady states of the system in total. The steady state branches for anterior mesoderm (thick blue line), endoderm (thin blue line), dorsal and ventral mesoderm (black lines) and dorsal and ventral ectoderm (red lines) and unstable branches (dashed grey lines) are shown.

Note that the steady states of Brachyury ( $B^*$ ) and eFGF ( $E^*$ ) are independent of solutions to Vent ( $Vent^*$ ) and Bmp ( $Bmp^*$ ). For sufficiently large  $\lambda_{B,E}$  and  $\lambda_{E,B}$ , (5.3.7a) has two non-trivial steady states [95] (see figure 5.14). Similarly, for sufficiently large  $\lambda_{Bmp,V}$  and  $\lambda_{V,Bmp}$ , (5.3.7b) has two non-trivial steady states, with the stable steady state corresponding to a ventral steady state (see figure 5.15). Since the equations for the steady states of Brachyury/eFGF (5.3.7b) and Vent/BMP (5.3.7a) are independent of each other, there are four possible states of the system: (1) the trivial steady state (see figure 5.17A), (2) Vent/BMP upregulated with no Brachyury/eFGF expression (see figure 5.17B), (3) Bra/eFGF upregulated with no Vent/BMP expression (see figure 5.17C) and (4) both Vent/BMP and Brachyury/eFGF upregulated (see figure 5.17D).

### Steady-state solutions in the presence of Nodal

When  $N^* = N_S > 0$  (where  $N_S$  is the non-trivial steady state solution to equation (5.3.4)), the steady state solutions for Mix, Brachyury, Goosecoid, eFGF, Vent and BMP are found by solving (5.3.6). Figure 5.16 shows steady state solutions as functions of the parameter  $\lambda_{BMP,V}$ . For small  $\lambda_{BMP,V}$ , only the trivial steady state of Vent is a solution to the system ( $V^* = 0$ ). In this case the steady states are identical to those given in [95], with non-trivial steady states corresponding

to mesoderm and anterior mesendoderm. As  $\lambda_{BMP,V}$  increases a fold bifurcation marks the appearance of ventral fates (characterised by a non-trivial steady state value of Vent) including endoderm and ventral mesoderm. An illustration of the non-trivial stable steady states is given in figure 5.17(E-F) with steady states representative of dorsal mesoderm (E), ventral mesoderm (F), anterior mesendoderm (G) and endoderm (H).

### 5.3.5 Time-dependent solutions

#### VegT dose response

To study the effect of VegT,  $\beta$ -catenin and BMP on the dynamics of our model, we solve (5.3.3) for various initial conditions each representative of different regions of the embryo. Initial conditions are set such that in cells with low concentrations of VegT ( $V_0 \leq 5$ )  $\beta$ -catenin is expressed at a non-trivial level ( $C_0 > 0$ ) and BMP is expressed at a low level in all cells. Thus, we define initial conditions with  $0 \leq V_0 \leq 10$

$$V(0) = V_0, \quad (5.3.8a)$$

$$C(0) = \begin{cases} V_0 & \text{if } V_0 \leq 5, \\ 0 & \text{otherwise,} \end{cases} \quad (5.3.8b)$$

$$Bmp_0 = 2. \quad (5.3.8c)$$

Solutions are plotted against  $V_0$  in figure 5.18. As in the *in vivo* mesendoderm model of [95], VegT activates the expression of Brachyury and Mix, with  $\theta_{V,M}$  set such that the concentration of VegT required to activate Brachyury is lower than that required to activate Mix. BMP is initially expressed at a level much lower than its steady state value. For  $V_0$  sufficiently small the system evolves to a mesoderm steady state, with Vent and BMP also expressed. When  $V_0$  increases past a critical value the system evolves to the anterior mesendoderm steady state. For further increases in  $V_0$ , such that  $\beta$ -catenin is not expressed, the system evolves to the endoderm steady state.

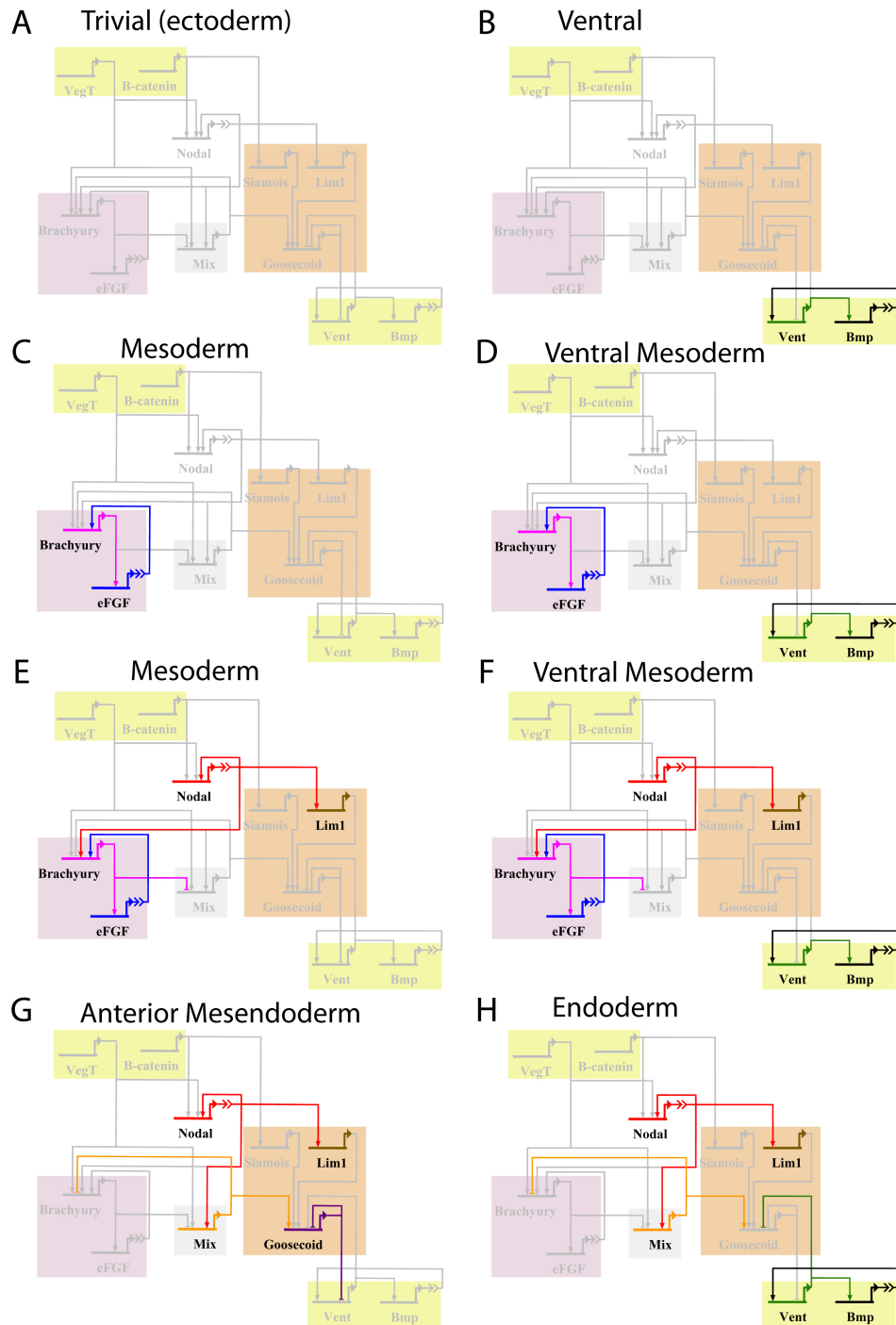
#### VegT dose response with no $\beta$ -catenin

In the absence of a dorsalisating signal (i.e. the case where  $\beta$ -catenin is not present), we find that the system does not evolve to the anterior mesendoderm for any value of  $V_0$  (see figure 5.19). We find that for small  $V_0$  the system evolves to the mesoderm steady state and for  $V_0$  greater than some critical value the system evolves to the endoderm steady state. For all values of  $V_0$ , BMP and Vent evolve to the upregulated steady state.

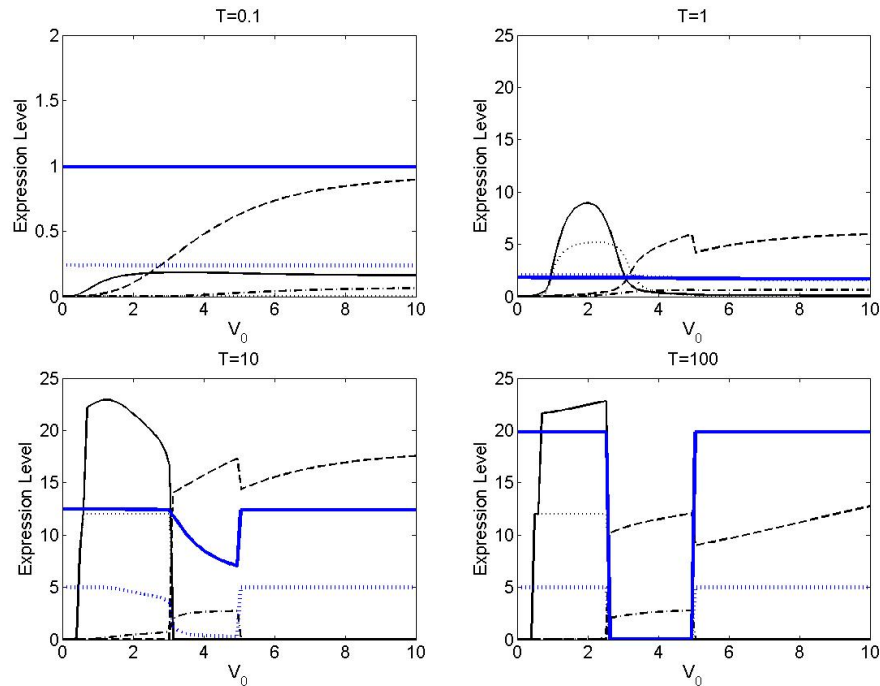
#### VegT dose response with no BMP

In the absence of an initial concentration of BMP, the system evolves to the mesoderm steady state for small  $V_0$  and to the anterior mesendoderm steady state for all  $V_0$  greater than some





**Figure 5.17:** Network diagrams illustrating the stable steady states obtainable for the system of equations defined in (5.3.3). (A-D) Steady states in the absence of Nodal. (A) shows the trivial steady state. In (B) Vent and BMP are maintained via mutual positive regulation. In (C) Brachyury and eFGF are part of a positive feedback loop. The two steady states in (B) and (C) can be combined to give the state shown in (D). (E-H) Steady states in the presence of Nodal. (E) Brachyury and eFGF the steady state representing mesoderm (F) when Vent and BMP are also expressed the steady state represents ventral mesoderm. (G) when Mix and Goosecoid are co-expressed the steady state represents anterior mesendoderm. (H) If Mix is expressed, but Vent represses Goosecoid, the steady state represents endoderm.



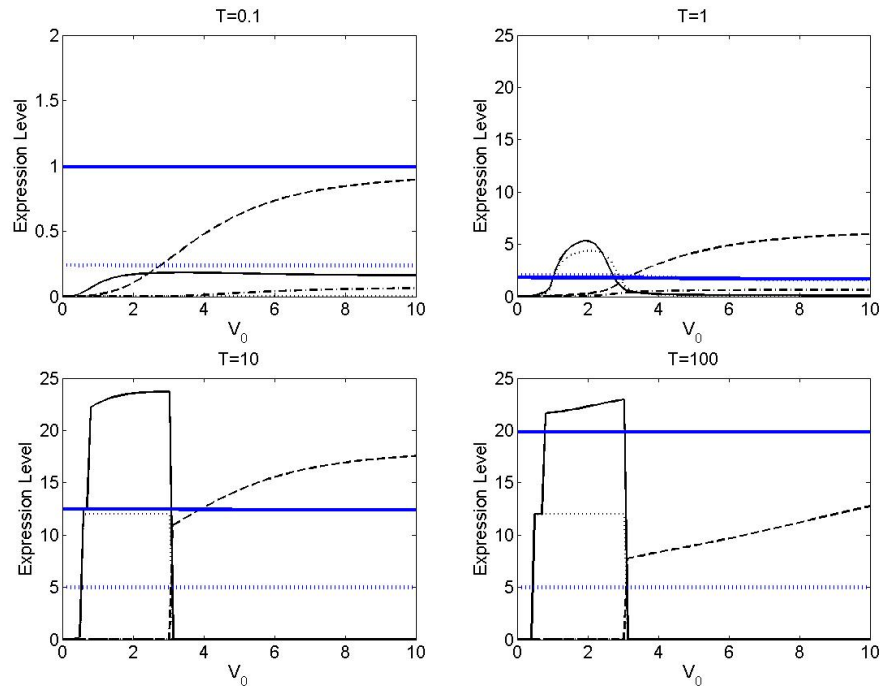
**Figure 5.18:** Numerical solutions to (5.3.3) plotted against initial VegT concentration ( $V_0$ ) for various  $\tau = T$ . Initial conditions are as defined in (5.3.8). The concentrations of BMP (thick blue solid line), Vent (thick blue dotted line), Mix (dashed line), Goosecoid (dot-dashed line), Brachyury (solid line) and eFGF (dotted line) are shown. Parameters are as chosen in table 5.4.

critical value ( see figure 5.20). Note that here we see that the range of values of  $V_0$  for which the system evolves to the mesoderm steady state is reduced compared with in figures 5.18 and 5.19. When both BMP and  $\beta$ -catenin are simultaneously removed from the system (figure 5.21), the system behaves in a similar way to when BMP alone is removed, except we find that the system evolves to the mesoderm steady state for a larger range of  $V_0$ .

### VegT dose response with pre-established BMP gradient

The investigation of the time-dependent behaviour of (5.3.3) has found that including Vent and BMP in a model of the mesendoderm network can account for the formation of mesoderm, endoderm and anterior mesendoderm. Recall that a model of the mesendoderm network without these two factors can only account for the formation of mesoderm and anterior mesendoderm. However we find that Vent and BMP are upregulated in cells we expect to form dorsal mesoderm.

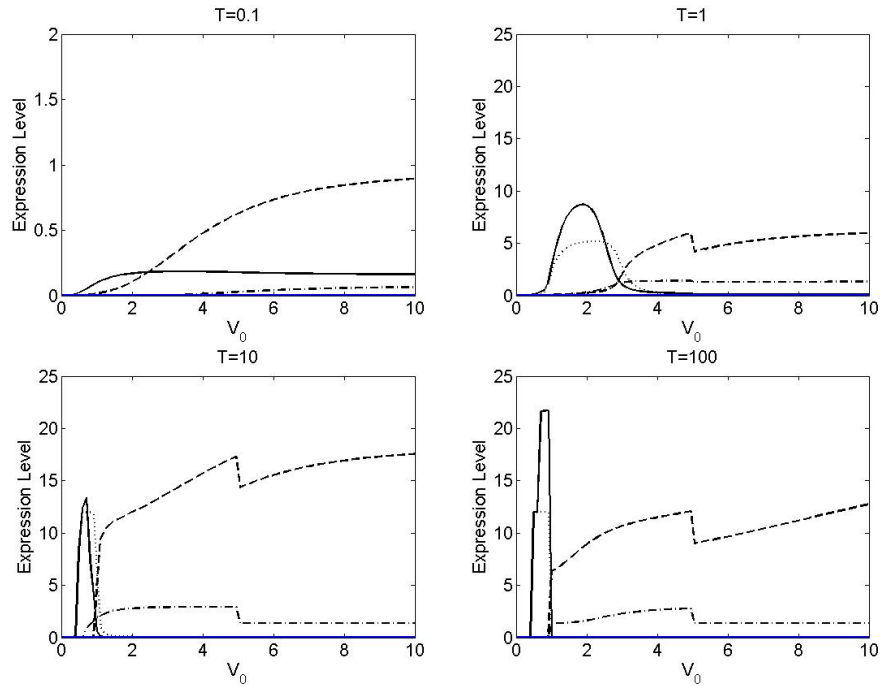
The formation of a BMP gradient along the dorsal-ventral axis is known to be regulated (in part) by extracellular interactions. By setting the initial conditions of BMP such that  $B(0) = 0.15 * V_0$  i.e. a gradient such that BMP levels are low in dorsal cells and higher in ventral cells, we obtain the results given in figure 5.22, such that Vent and BMP are not expressed at the mesoderm steady state (i.e. dorsal mesoderm)



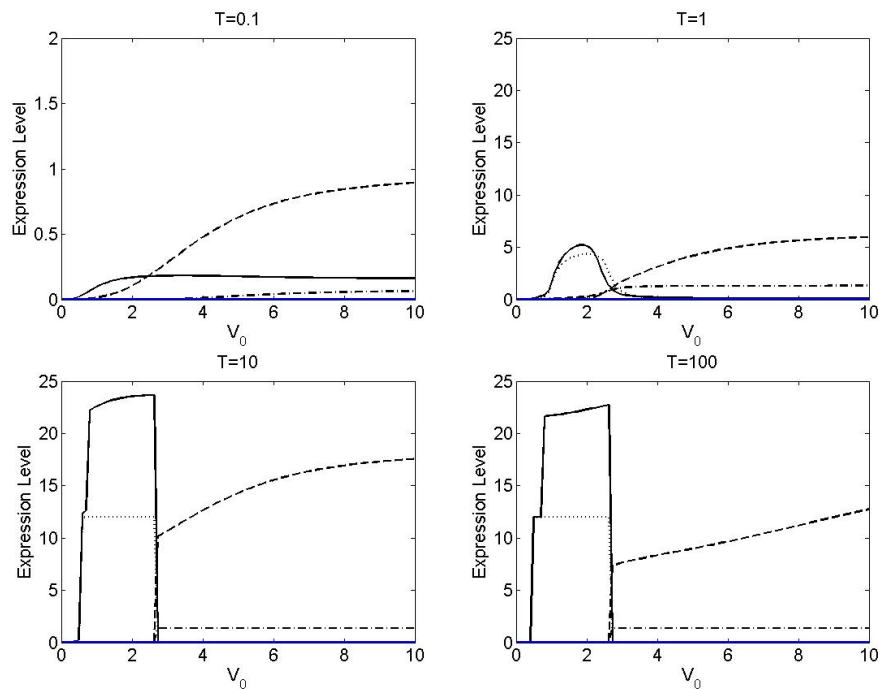
**Figure 5.19:** Numerical solutions to (5.3.3) in the absence of  $\beta$ -catenin plotted against initial VegT concentration ( $V_0$ ) for various  $\tau = T$ . Initial conditions are as defined in (5.3.8), except  $C_0 = 0$ . The concentrations of BMP (thick blue solid line), Vent (thick blue dotted line), Mix (dashed line), Goosecoid (dot-dashed line), Brachyury (solid line) and eFGF (dotted line) are shown. Parameters are as chosen in table 5.4.

### Experimental observations

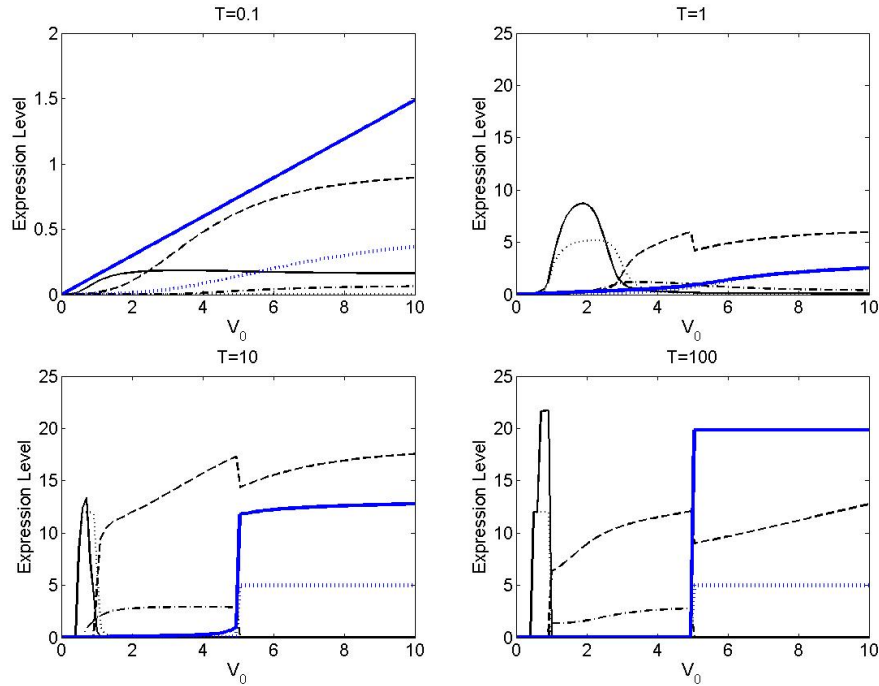
Our numerical investigation of the mathematical model given in (5.3.3) provides predictions for the behaviour of the network in the cases of BMP and  $\beta$ -catenin depletion. The model compares favourably with observations in embryos treated with  $\beta$ -catenin MO and BMP2/4/7 MOs [115]. Embryos depleted of  $\beta$ -catenin are ventralised, forming a ‘belly piece’ [115]. The mathematical model qualitatively reproduces this behaviour, with anterior mesendoderm (i.e. head forming regions) not forming in the absence of  $\beta$ -catenin (figure 5.19). Embryos depleted of BMP2/4/7 form tail-less embryos [115], with DV patterning maintained in the absence of ventral BMP signals. The mathematical model suggests that in the absence of BMP, that the embryo would form a head piece (consisting of mesoderm and anterior mesendoderm only) rather than a tail-less embryo (figure 5.20). ADMP, a candidate for maintaining DV patterning in the absence of ventral BMP signals [116], is not included in our models. Finally a double knockout of  $\beta$ -catenin and BMP2/4/7 results in a head-like embryo. The model qualitatively reproduces this observation, with only mesoderm and anterior mesendoderm forming in the absence of  $\beta$ -catenin and BMP (figure 5.21).



**Figure 5.20:** Numerical solutions to (5.3.3) in the absence of BMP, plotted against initial VegT concentration ( $V_0$ ) for various  $\tau = T$ . Initial conditions are as defined in (5.3.8), except  $Bmp_0 = 0$ . The concentrations of BMP (thick blue solid line), Vent (thick blue dotted line), Mix (dashed line), Goosecoid (dot-dashed line), Brachyury (solid line) and eFGF (dotted line) are shown. Parameters are as chosen in table 5.4.



**Figure 5.21:** Numerical solutions to (5.3.3) in the absence of  $\beta$ -catenin and BMP plotted against initial VegT concentration ( $V_0$ ) for various  $\tau = T$ . Initial conditions are as defined in (5.3.8), except  $C_0 = 0$  and  $Bmp_0 = 0$ . The concentrations of BMP (thick blue solid line), Vent (thick blue dotted line), Mix (dashed line), Goosecoid (dot-dashed line), Brachyury (solid line) and eFGF (dotted line) are shown. Parameters are as chosen in table 5.4.

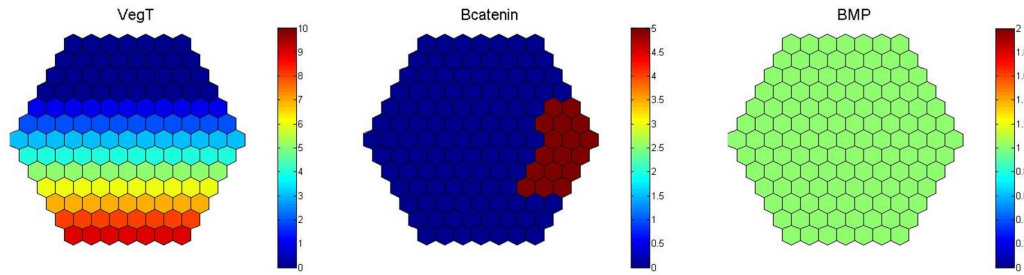


**Figure 5.22:** Numerical solutions to (5.3.3) plotted against initial VegT concentration ( $V_0$ ) for various  $\tau = T$ . Initial conditions are as defined in (5.3.8). The concentrations of BMP (thick blue solid line), Vent (thick blue dotted line), Mix (dashed line), Goosecoid (dot-dashed line), Brachyury (solid line) and eFGF (dotted line) are shown. Parameters are as chosen in table 5.4.

### 5.3.6 2D plots of the single cell model

In the previous section we explored numerical solutions to (5.3.3) subject to initial conditions representative of different regions of the embryo. To visualise how these initial conditions and resulting gene expression patterns correspond to regions of the embryo, we show results in two dimension domains. Each hexagon represents a single cell. Note that as we are solving a single-cell mathematical model, the solution in each cell is independent of its neighbours as there is no signalling between cells.

Figure 5.23 shows initial conditions of VegT,  $\beta$ -catenin and BMP as well as a cartoon of the expression of these factors in stage 1 embryos. All other transcription factors are assumed not to be expressed at  $t = 0$ . The solutions showing concentrations of Brachyury, Mix, Goosecoid and Vent subject to these initial conditions are shown in figure 5.24. At  $\tau = 1$  (figure 5.24(i)), Brachyury is expressed in cells which are subjected to a low initial dose of VegT (the equatorial region of the embryo), with expression levels being highest in dorsal regions where  $\beta$ -catenin is expressed. Mix is expressed in cells subjected to high levels of VegT with strongest levels in cells also expressing  $\beta$ -catenin. Goosecoid is expressed in Mix positive cells at this early time point and Vent is uniformly expressed throughout the embryo. By  $\tau = 10$  (figure 5.24(ii)), Goosecoid is restricted to dorsal cells which also express  $\beta$ -catenin. Within this region, Goosecoid levels are highest in cells which also express Mix, and lower in cells which also co-express Brachyury and Vent. At  $\tau = 100$  (figure 5.24(iii)), all  $\beta$ -catenin positive cells now co-express Mix and



**Figure 5.23:** Initial conditions used to solve (5.3.3). Solutions showing concentrations of Mix, Brachyury, Goosecoid and Vent at later times are shown in figure 5.24. VegT is in a gradient running from vegetal pole to animal pole,  $\beta$ -catenin is expressed in dorsal cells only and BMP is expressed at a low uniform level.

Goosecoid. In other regions, cells with high levels of VegT express Mix and cells with low levels of VegT express Brachyury.

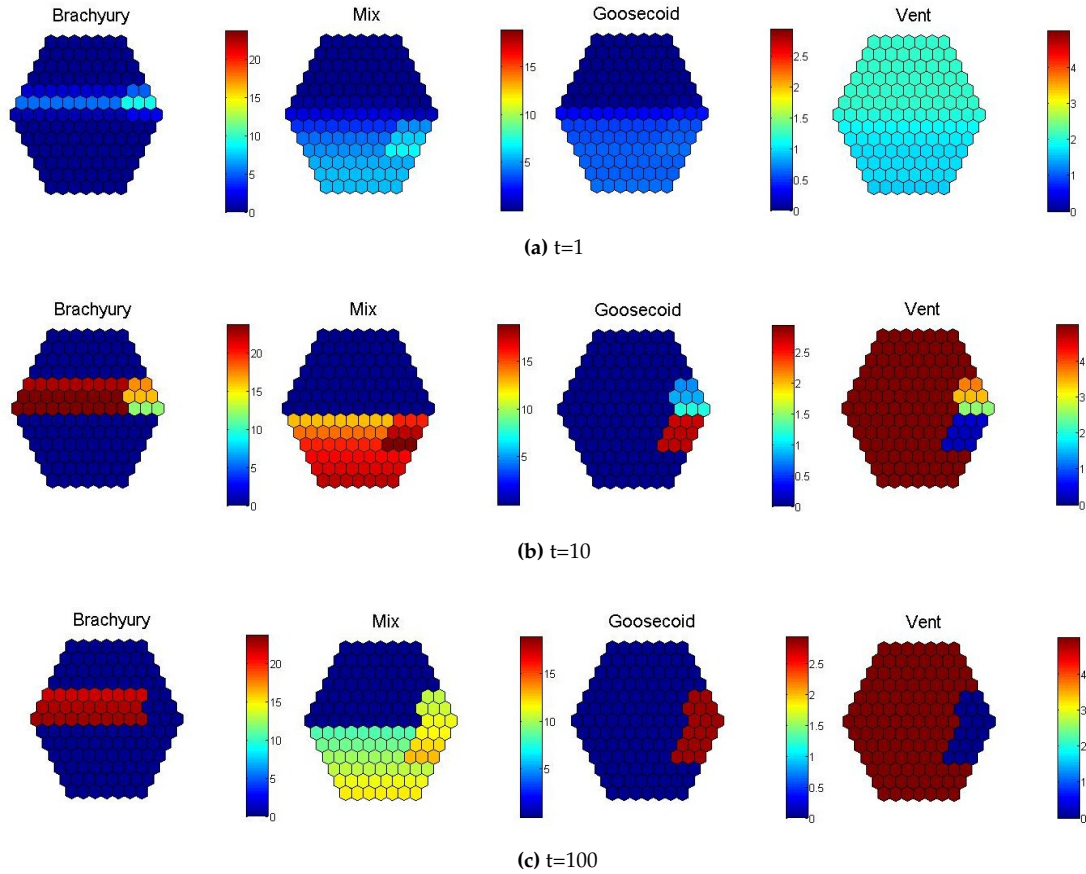
The initial conditions shown in figure 5.25 are identical to those in figure 5.23, except that  $\beta$ -catenin concentration is higher in the vegetal-most part of the dorsal marginal zone than it is in the part closest to the animal pole. Figure 5.26 shows concentrations of Brachyury, Mix, Goosecoid and Vent subject to these initial conditions. The resulting behaviour is similar to that found in the previous case, with Brachyury expressed in cells with a low initial concentration of VegT and Mix expressed in cells with a high concentration of VegT. However, the behaviour in the dorsal marginal zone differs between the two solutions. In figure 5.26, Brachyury expression extends across the whole marginal zone (compared to in figure 5.24, where Brachyury is not found in the dorsal region).

### 5.3.7 Summary

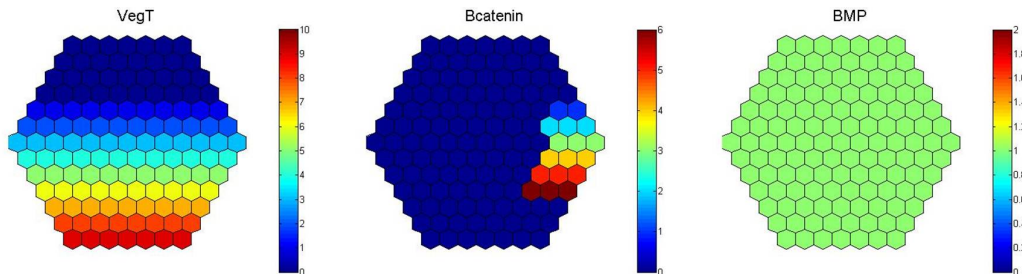
In this section, a mathematical model of the simplified *Xenopus* mesendoderm network including Vent and BMP is formulated and analysed. Steady state analysis shows that stable steady states corresponding to mesoderm, endoderm and anterior mesendoderm are solutions to the model. By contrast, a mesendoderm model which does not include Vent and BMP does not have a stable steady state corresponding to endoderm. Time-dependent solutions of this model suggest that initial concentrations of VegT,  $\beta$ -catenin and BMP can pattern mesoderm, endoderm and anterior mesendoderm, consistent with experimental observations of [115].

## 5.4 Discussion

In this chapter we introduced simplified models of the *Xenopus* dorsal-ventral (DV) patterning network. The simplifications applied to the full network include representing the two Vents, multiple Nodals and multiple Mix genes by a single node for each gene family. Using a single node for each of the Mix and Nodal gene families is motivated by the fact that humans and mice have a single gene in each family, and the hypothesis that the *Xenopus* mesendoderm net-

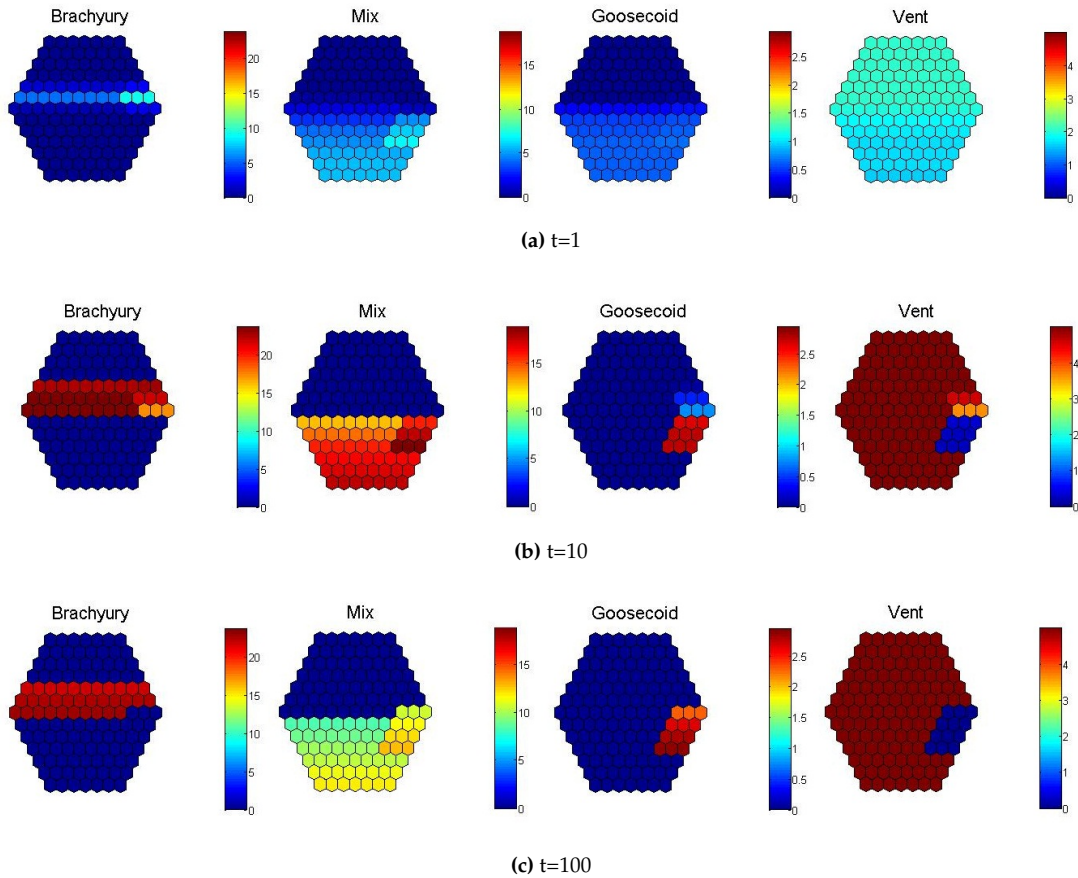


**Figure 5.24:** Solutions to (5.3.3), subject to initial conditions given in figure 5.23, showing concentrations of Mix, Brachyury, Goosecoid and Vent.



**Figure 5.25:** Initial conditions used to solve (5.3.3). Solutions showing concentrations of Mix, Brachyury, Goosecoid and Vent at later times are shown in figure 5.26. VegT is in a gradient running from vegetal pole to animal pole,  $\beta$ -catenin is expressed in dorsal cells only and BMP is expressed at a low uniform level.

work is overly complex [95]. The two vent genes in *Xenopus* have similar expression patterns, except that Vent2 extends further towards the organiser than Vent1. The fate of cells in the ventral mesoderm to become blood or muscle is determined by the combination of Vent genes present. In developing our models, we were interested in the formation of dorsal and ventral fates rather than the subsequent differentiation of ventral mesoderm into blood and muscle. Thus, to simplify the models, we use a single node representing the two Vent genes.



**Figure 5.26:** Solutions to (5.3.3), subject to initial conditions given in figure 5.25, showing concentrations of Mix, Brachyury, Goosecoid and Vent.

For the simplified network given in figure 5.12, two versions of the mathematical models were developed; the ‘DV only’ version considered the mutual negative regulation of Goosecoid and Vent and positive feedback between Vent and BMP, while the ‘DV and mesoderm’ model extended the first model to include the dynamics of the mesoderm network. Each model comprises the time evolution of transcription factor concentrations in a single cell, with signals (i.e. Nodal, eFGF and BMP) assumed to act as transcription factors.

The ‘DV only’ model was found to be bistable with stable steady states corresponding to dorsal and ventral fates. The model is able to reproduce qualitatively observations from whole embryos that cells where  $\beta$ -catenin is present become dorsal and in the absence of  $\beta$ -catenin cells become ventral. In the case of a Vent or Goosecoid knockout the model also reproduces qualitatively experimental behaviour [124]. The ‘DV and mesoderm’ model has eight stable steady states, two of which correspond to dorsal mesoderm, two to ventral mesoderm, one to anterior mesoderm, one to endoderm, one to ventral ectoderm and one to the trivial steady state (which corresponds to dorsal ectoderm). Numerical investigations of the second model suggest that the initial conditions of VegT,  $\beta$ -catenin and BMP can pattern mesoderm, endoderm and anterior mesoderm.

The models presented in this chapter are relatively simple compared with the full mesendo-



derm network in [89] and the interactions of DV patterning. Despite this, our models can reproduce qualitatively several experimental observations. This leads to the suggestion that complexity in the GRN makes it robust, giving the correct patterning in a number of different conditions. For example, a Goosecoid depleted embryo has a dorsalised phenotype, a Vent1/Vent2 depleted embryo has a dorsalised phenotype, but a triple depletion of Goosecoid/Vent1/Vent2 restores normal DV patterning [124]. A possible explanation for this is that, in the triple knockout case, extracellular dorsal and ventral molecules (such as BMP, ADMP and Chordin) can regulate DV patterning independently of Vent and Goosecoid [124].

Recall that the models developed in this chapter are for a single cell and do not include cell to cell communication. Regulation of DV patterning by extracellular molecules (for example the repression of BMP signalling by Chordin and the translocation of ADMP from dorsal to ventral regions) might be important in establishing the initial DV gradient and maintaining patterning in the absence of Goosecoid and Vent. A model of the extracellular components of DV patterning in *Xenopus* has been developed in [7]. This model could be used as a starting point in developing a DV model which incorporates the extracellular and intracellular components of the GRN.

In the next chapter we extend models of Nodal signalling and the *Xenopus* mesendoderm network (as developed in [94]) into a grid of cells representing the embryo.

# Multicellular Models of Mesendoderm Specification

In this chapter we develop multicellular models of mesendoderm formation, in both a line of cells and in a two-dimensional grid of cells. We adopt a two-dimensional grid approach rather than a more realistic three-dimensional approach because patterns in mesendodermal gene expression occur primarily along the animal-vegetal axes and dorsal-ventral axes, while patterns are uniform along the anterior-posterior axes. Thus a model on a two-dimensional template will be suitable to studying the formation of the primary germ layers. In section 6.1 we give an overview of a mathematical model of the *Xenopus* mesendoderm GRN in a line of cells as formulated in [94]. In section 6.1.2 we develop a mathematical model of the axolotl mesendoderm GRN in a line of cells. This model is an extension of the single cell models presented in chapters 3 and 4, as we include the diffusion of extracellular ligands between cells and also include the Nodal signalling pathway rather than treating Nodal as a transcription factor as in chapter 3. In section 6.3 we present work carried out to clone axolotl Antivin, an important component of the Nodal signalling pathway, and measure its expression in response to the overexpression of Nodal1. For the remainder of the chapter we extend the mesendoderm models from a line to a grid of cells and explore its behaviour in response to different modes of Nodal regulation in response to maternal factors.

## 6.1 A multicellular model of the *Xenopus* mesendoderm GRN

In [94] multicellular models of the simplified *Xenopus* mesendoderm GRN were developed and analysed in a line of cells running from the animal cap to the vegetal pole, via the marginal zone. The model consists of two main parts: the Nodal signalling pathway and the network downstream of Nodal. An analysis of the Nodal signalling pathway explored how Antivin antagonises the spread of Nodal throughout the line of cells, while the network downstream of Nodal explored the conditions under which mesoderm and anterior mesendoderm form. In this section we introduce the governing equations for this model and give a summary of the

important findings of the model.

### 6.1.1 A model of Nodal signalling

Middleton [94] developed a model of Nodal signalling, which included the antagonism of Nodal by Antivin. In the model Nodal can induce the expression of both *Nodal* and *Antivin*, with extracellular Antivin able to antagonise extracellular Nodal [142]. The model included a single Nodal gene rather than the multiple Nodal genes present in the *Xenopus* genome. We give an overview of the model formulation in what follows.

Nodal ligands ( $N^o$ ) bind to free receptors ( $R$ ) to become Nodal-bound receptors ( $R^\diamond$ ) in a reversible reaction where  $k_N$  and  $k_{-N}$  are the rates of association and dissociation of Nodal to its receptor



Following the binding of Nodal to its receptor, Smad2 ( $S$ ) becomes phosphorylated to form phosphorylated Smad2, or P-Smad2 ( $P$ ). It is assumed that this occurs via the formation of an intermediate complex ( $R^{\diamond\diamond}$ )



P-Smad2 then regulates downstream targets of the pathway, including Nodal itself and Antivin, where the activation of downstream targets is modelled using a Hill function.

Antivin is a downstream target of Nodal signalling, which acts to antagonise Nodal signalling. This is modelled using two different mechanisms: receptor mediated repression [17] and heterodimer mediated repression [15]. In receptor mediated repression, Antivin ligands ( $T^o$ ) bind to a free receptor to form an Antivin-bound receptor ( $R^\ddagger$ ) which is inactive, the rate of association and dissociation of Antivin to free receptors are  $k_T$  and  $k_{-T}$



In heterodimer mediated repression an Antivin ligand binds directly to a Nodal ligand to form a Nodal-Antivin heterodimer ( $T^\ddagger$ ) which is inactive, the rate of association and dissociation of Antivin to Nodal are  $l_T$  and  $l_{-T}$



Extracellular Nodal, extracellular Antivin and Nodal-Antivin heterodimer can move between neighbouring cells with rates of transmission  $\sigma_N$ ,  $\sigma_T$  and  $\sigma_{T^\ddagger}$ , respectively. All other species do not move between cells. It is likely that the rate of change of intracellular *Antivin* and *Nodal* occur on a slower timescale than other processes [94]. Thus, processes which occur on a fast timescale compared with the rate of change of intracellular *Antivin* and *Nodal* are scaled by a small parameter ( $\epsilon \ll 1$ ). Equations are formulated using the law of mass action, and after applying non-dimensional scalings as detailed in [94], the equations governing Nodal

signalling in cell  $i$  are given by

$$\frac{dV_i}{d\tau} = -\mu_V V_i, \quad (6.1.5a)$$

$$\frac{dC_i}{d\tau} = -\mu_C C_i, \quad (6.1.5b)$$

$$\epsilon \frac{dT_i^o}{dt} = \sigma_T \Delta T_i^o + \underbrace{\nu (k_{-T} R_i^\ddagger - k_T T_i^o R_i)}_{\text{receptor mediated repression}} + \frac{\delta_T}{\rho} T_i \underbrace{-l_T N_i^o T_i^o + l_{-T} T_i^\ddagger}_{\text{heterodimer mediated repression}} - \mu_{T^o} T_i^o, \quad (6.1.5c)$$

$$\epsilon \frac{dN_i^o}{dt} = \sigma_N \Delta N_i^o + \frac{\nu}{\rho} (k_{-N} R_i^\diamond - k_N N_i^o R_i) \underbrace{-l_T N_i^o T_i^o + l_{-T} T_i^\ddagger}_{\text{heterodimer mediated repression}} + \frac{\delta_N}{\rho} N_i - \mu_{N^o} N_i^o, \quad (6.1.5d)$$

$$\epsilon \frac{dT_i^\ddagger}{dt} = \sigma_{T^\ddagger} \Delta T_i^\ddagger + \underbrace{l_T N_i^o T_i^o - l_{-T} T_i^\ddagger}_{\text{heterodimer mediated repression}} - \mu_{T^\ddagger} T_i^\ddagger, \quad (6.1.5e)$$

$$\frac{dT_i}{dt} = \lambda_{P,T} \mathcal{H} \left( \frac{P_i}{\theta_{P,T}} \right) - (\mu_T + \delta_T) T_i, \quad (6.1.5f)$$

$$\frac{dN_i}{dt} = \lambda_{V,N} \mathcal{H} \left( \frac{V_i}{\theta_{V,N}} \right) + \lambda_{P,N} \mathcal{H} \left( \frac{P_i}{\theta_{P,N}} \right) \left\{ 1 + \lambda_{C,N} \mathcal{H} \left( \frac{C_i}{\theta_{C,N}} \right) - \right\} - (\mu_N + \delta_N) N_i, \quad (6.1.5g)$$

$$\epsilon \frac{dP_i}{dt} = k_p \nu R_i^{\diamond\diamond} - \mu_P P_i, \quad (6.1.5h)$$

$$\epsilon \frac{dR_i}{dt} = k_{-N} R_i^\diamond - k_N N_i^o R_i + \underbrace{k_{-T} R_i^\ddagger - k_T T_i^o R_i}_{\text{receptor mediated repression}}, \quad (6.1.5i)$$

$$\epsilon \frac{dR_i^\diamond}{dt} = -k_{-N} R_i^\diamond + k_N N_i^o R_i - k_s R_i^\diamond S_i + (k_{-s} + k_p) R_i^{\diamond\diamond}, \quad (6.1.5j)$$

$$\epsilon \frac{dR_i^{\diamond\diamond}}{dt} = - (k_{-s} + k_p) R_i^{\diamond\diamond} + k_s R_i^\diamond S_i, \quad (6.1.5k)$$

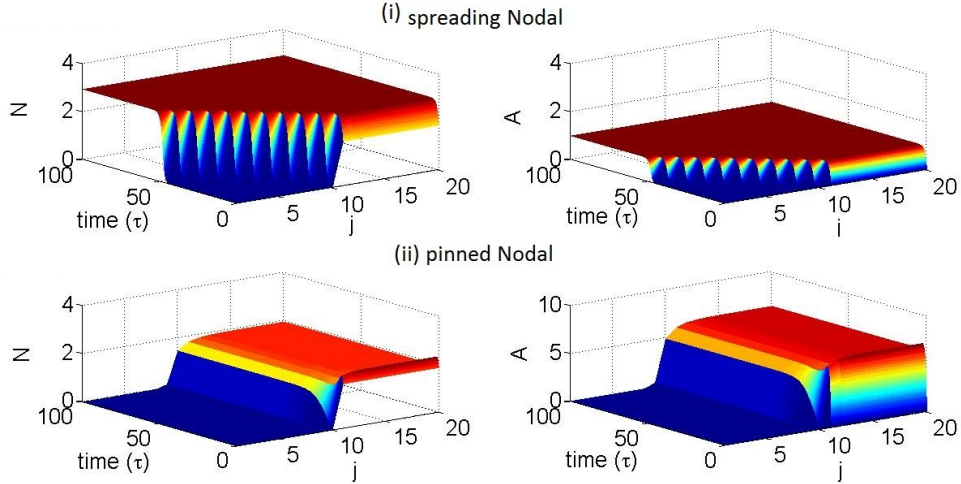
$$\epsilon \frac{dR_i^\ddagger}{dt} = -k_{-T} R_i^\ddagger + k_T T_i^o R_i, \quad (6.1.5l)$$

where terms of the form  $\Delta X_i$  are as defined in (1.12.3) and  $\nu$  and  $\rho$  are the membrane and extracellular volume fractions  $\rho = v_E/v_I$  and  $\nu = v_M/v_I$  where  $v_E$ ,  $v_I$  and  $v_M$  are the local extracellular, intracellular and membrane volumes, respectively. Initial conditions were selected such that all factors except intracellular Nodal are absent and all receptors are initially unbound, such that

$$\begin{aligned} V_i(0) = 0, \quad C_i(0) = 0, \quad T_i^o(0) = 0, \quad T_i^\ddagger(0) = 0, \quad T_i(0) = 0, \\ N_i(0) = N_0, \quad P_i(0) = 0, \quad R_i(0) = 1, \quad R_i^\diamond(0) = 0, \quad R_i^{\diamond\diamond}(0) = 0, \quad R_i^\ddagger(0) = 0, \end{aligned} \quad (6.1.6)$$

where  $N_0$  is a positive constant.

Middleton [94] explored the above model both in a single cell and in a line of cells. The single cell model was found to have stable steady states corresponding to upregulated Nodal and Antivin and the trivial steady state. In a line of cells, dependent on the choice of parameters, solutions either form traveling waves corresponding to Antivin spreading throughout the line of cells, or to 'pinned' waves corresponding to Antivin preventing the spread of Nodal. To



**Figure 6.1:** Solutions to (6.1.5), showing the resulting concentration of intracellular Nodal and Antivin in a line of twenty cells. (i) When  $\lambda_{P,A} = 1$ , Nodal becomes expressed in all cells. (ii) When  $\lambda_{P,A} = 50$ , Antivin pins Nodal, preventing the spread of Nodal throughout the line of cells. All other parameters as as defined in table 6.4.

illustrate these two types of behaviour, we solve (6.1.5), using the stiff ODE solve `ode15s` in MATLAB, and plot the resulting concentrations of intracellular Nodal and Antivin in a line of 20 cells (figure 6.1), where we set initial conditions such that Nodal is not initially expressed in cells 1 to 10 ( $N_0 = 0$ ) and is expressed close to its upregulated steady state value in cells 11 to 20 ( $N_0 = 2$ ). In figure 6.1(i), the rate of production of Antivin in response to P-Smad2 was set to  $\lambda_{P,A} = 1$ , such that Nodal is still able to spread throughout the line of cells. In figure 6.1(ii), where  $\lambda_{P,A} = 50$ , high levels of Antivin ‘pins’ Nodal such that it does not spread throughout the line of cells. Experimental evidence suggests that the pinning of Nodal by Antivin occurs *in vivo* since, in the presence of Antivin, Nodal is only expressed one or two cells from its source, while in Antivin knockout experiments the Nodal signal propagates throughout the field of cells [14].

### 6.1.2 The mesendoderm GRN downstream of Nodal

Middleton [94] then proceeds to formulate a model of the *Xenopus* mesendoderm GRN downstream of Nodal in a line of cells. This model includes a simplified version of the FGF signalling pathway which we give summary of here. Extracellular FGF ligands ( $E^o$ ) bind to free FGF receptors ( $F$ ) to give FGF bound receptors ( $F^\circ$ )



MAP kinases ( $K$ ) then bind to the activated receptor complex and MAP kinase becomes phospho-

orylated ( $K^*$ ) via the formation of an intermediate MAP kinase bound receptor ( $F^{\diamond\diamond}$ )



It is assumed that certain processes, such as the binding of extracellular eFGF to its receptor, occur on a fast timescale compared with the rate of change of intracellular eFGF, and these processes are scaled by a small parameter ( $\epsilon \ll 1$ ). The equations governing the mesendoderm GRN downstream of Nodal (figure 1.7A) in cell  $i$  are then given by

$$\epsilon \frac{dE_i^o}{d\tau} = \sigma_E \Delta E_i + \delta_E E_i - \bar{v} (k_E E_i^o - k_{-E} F_i^\diamond) - \mu_{E^o} E_i^o, \quad (6.1.9a)$$

$$\frac{dE_i}{d\tau} = \lambda_{B,E} \mathcal{H}(B_i) - \mu_E E_i, \quad (6.1.9b)$$

$$\epsilon \frac{dK_i^*}{d\tau} = \nu k_{K^*} F_i^{\diamond\diamond} - \mu_{K^*} K_i^*, \quad (6.1.9c)$$

$$\epsilon \frac{dF_i^\diamond}{d\tau} = k_E E_i^o F_i - k_{-E} F_i^\diamond - k_K F_i^\diamond + (k_{-K} + k_{K^*}) F_i^{\diamond\diamond}, \quad (6.1.9d)$$

$$\epsilon \frac{dF_i^{\diamond\diamond}}{d\tau} = k_K F_i^\diamond - (k_{-K} + k_{K^*}) F_i^{\diamond\diamond}, \quad (6.1.9e)$$

$$\epsilon \frac{dF_i}{d\tau} = -k_E E_i^o F_i + k_{-E} F_i^\diamond, \quad (6.1.9f)$$

$$\frac{dI_i}{d\tau} = \lambda_{C,I} \mathcal{H}\left(\frac{C_i}{\theta_{C,I}}\right) - \mu_I I_i, \quad (6.1.9g)$$

$$\frac{dL_i}{d\tau} = \lambda_{P,L} \mathcal{H}\left(\frac{P_i}{\theta_{P,L}}\right) - \mu_L L_i, \quad (6.1.9h)$$

$$\frac{dB_i}{d\tau} = \left\{ \lambda_{K^*,B} \mathcal{H}(K_i^*) + \lambda_{V,B} \mathcal{H}\left(\frac{V_i}{\theta_{V,B}}\right) + \lambda_{P,B} \mathcal{H}(P_i) \right\} \{1 - \mathcal{H}(G_i + M_i)\} - B_i, \quad (6.1.9i)$$

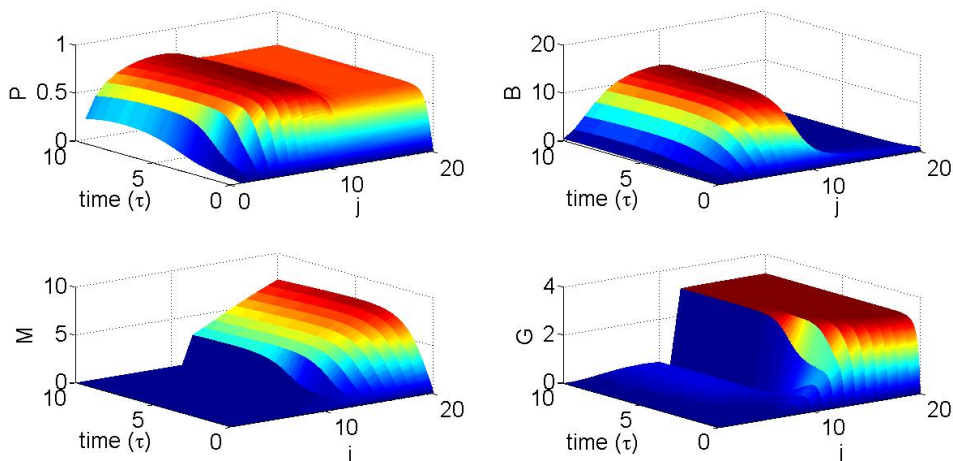
$$\frac{dG_i}{d\tau} = \left\{ \lambda_{L,I,G} \mathcal{H}(L_i) \mathcal{H}(I_i) + \lambda_{M,G} \mathcal{H}\left(\frac{M_i}{\theta_{M,G}}\right) \right\} \left\{ 1 - \mathcal{H}\left(\frac{G_i}{\theta_{G,G}}\right) \right\} - \mu_G G_i, \quad (6.1.9j)$$

$$\frac{dM_i}{d\tau} = \left\{ \lambda_{V,M} \mathcal{H}\left(\frac{V_i}{\theta_{C,M}}\right) + \lambda_{P,M} \mathcal{H}\left(\frac{P_i}{\theta_{P,M}}\right) \right\} \left\{ 1 - \mathcal{H}\left(\frac{B_i}{\theta_{B,M}}\right) \right\} - \mu_M M_i. \quad (6.1.9k)$$

$V_i, C_i, P_i$  are defined by solutions to equation (6.1.5), and the above model is the non-dimensional version obtained after applying the scalings given in [94]. Initial conditions are selected such that all factors in (6.2.5) are initially absent and all FGF receptors are free, such that

$$\begin{aligned} E_i^o(0) = 0, \quad K_i^*(0) = 0, \quad F_i^\diamond(0) = 0, \quad F_i^{\diamond\diamond}(0) = 0, \quad F_i(0) = 1, \\ I_i(0) = 0, \quad L_i(0) = 0, \quad B_i(0) = 0, \quad G_i(0) = 0, \quad M_i(0) = 0. \end{aligned} \quad (6.1.10)$$

Representative solutions of (6.1.5)-(6.2.5) are given in figure 6.2. Initial conditions of (6.1.5) are selected such that  $V_i(0) = 0$  and  $C_i(0) = C_0$ , where  $V_0, C_0$  are positive constants selected such that cells 1 to 10 represent the marginal zone where the expression of  $\beta$ -catenin overlaps with the expression of VegT and cells 11 to 20 represent the Vegetal region where VegT is expressed. Solutions to the model find that Brachyury is expressed in cells with a low level of VegT, whilst Mix and Goosecoid are expressed in cells with a high level of VegT. Further investigations in [94] show that the steepness of the VegT gradient determines the size



**Figure 6.2:** Solutions to (6.1.5) and (6.2.5) in a line of twenty cells. Brachyury is expressed in cells  $j = 1$  to  $j = 10$ , where VegT concentrations are low and Mix/Goosecoid are expressed in cells  $j = 11$  to  $j = 20$  where VegT concentration are high. Parameters as as defined in table 6.5.

of the regions expressing Mix and Brachyury. In the remainder of this chapter we will build on existing results presented in this section by formulating a mathematical model of the axolotl mesendoderm network in a line of cells and then extend both the *Xenopus* and axolotl models from a line of cells into a two dimensional grid of cells. In the next section, we formulate a mathematical model of the axolotl mesendoderm GRN, and explore how regions of cells corresponding to mesoderm and anterior mesendoderm form and compare these results with current experimental understanding.

## 6.2 Multicellular models of the axolotl mesendoderm GRN

Recall that in chapter 3 we developed mathematical models based on the axolotl mesendoderm GRN in a single cell. Two versions of the model were explored, the *in vitro* version giving the GRN downstream of Activin and the *in vivo* version giving the GRN downstream of  $\beta$ -catenin. We showed that both versions of the model were bistable with stable steady states corresponding to mesoderm and anterior mesendoderm, with the *in vivo* model reaching the steady states dependent on the initial dose of  $\beta$ -catenin. In this section we extend the single cell *in vivo* model into a line of cells. First we give a summary of experimental observations which are important while considering the model.

### 6.2.1 Experimental observations

The expression of Mix and Brachyury are illustrated in figure 6.3. At stage 10 Mix is detected in the mesoderm at the blastopore lip and Brachyury is not detectable [139]. Both Mix and Brachyury are detected at stage 10.75, where Mix expression is retained in the involuted meso-

derm and Brachyury is detected in the mesoderm and in a fraction of the dorsal mesoderm previously marked by Mix. By stage 12 Mix is found in the ventral mesoderm and the endoderm and Brachyury is found in the dorsal mesoderm [139]. Thus, Mix and Brachyury are expressed in distinct regions of the embryo, with the expression of Mix preceding that of Brachyury.

Brachyury and Mix are regulated by Nodal1 in axolotl [16]. At stage 9 Nodal1 expression is strongest on the dorsal side of the embryo. At stage 10 Nodal1 is detected in the dorsal lip and at stage 12 Nodal1 is mainly found in the mesoderm with weak expression in the endoderm. Thus it is thought that Nodal1 overlaps with  $\beta$ -catenin expressing region on the dorsal side of the embryo [16].

## 6.2.2 Governing equations

We formulate a model of the axolotl mesendoderm GRN (figure 1.7) in a line of cells, similar to the *Xenopus* models given in section 6.1.1, and explore its behaviour. The dynamics of the Nodal signalling pathway are assumed to be identical to those given in (6.1.5), except that  $\beta$ -catenin and not VegT can initiate the expression of intracellular Nodal, whereby, dependent on the parameter values selected, Nodal can either spread throughout the line of cells or be pinned by Antivin. The equations governing Nodal signalling downstream of  $\beta$ -catenin in axolotl are given by

$$\frac{dC_i}{dt} = -\mu_C C_i \quad (6.2.1a)$$

$$\frac{dT_i^o}{dt} = \sigma_T \Delta T_i^o + \nu \left( k_{-T} R_i^\ddagger - k_T T_i^o R_i \right) - l_T N_i^o T_i^o + l_{-T} T_i^\ddagger + \frac{\delta_T}{\rho} T_i - \mu_{T^o} T_i^o, \quad (6.2.1b)$$

$$\frac{dN_i^o}{dt} = \sigma_N \Delta N_i^o + \frac{\nu}{\rho} \left( k_{-N} R_i^\diamond - k_N N_i^o R_i \right) - l_T N_i^o T_i^o + l_{-T} T_i^\ddagger + \frac{\delta_N}{\rho} N_i - \mu_{N^o} N_i^o, \quad (6.2.1c)$$

$$\frac{dT_{i,j}^\ddagger}{dt} = \sigma_{T^\ddagger} \Delta T_{i,j}^\ddagger + l_T N_{i,j}^o T_{i,j}^\ddagger - l_{-T} T_{i,j}^\ddagger - \mu_{T^\ddagger} T_{i,j}^\ddagger, \quad (6.2.1d)$$

$$\frac{dT_i}{dt} = \lambda_{P,T} \mathcal{H} \left( \frac{P_i}{\theta_{P,T}} \right) - (\mu_T + \delta_T) T_i, \quad (6.2.1e)$$

$$\frac{dP_i}{dt} = k_p \nu R_i^{\diamond\diamond} - \mu_P P_i, \quad (6.2.1f)$$

$$\frac{dN_i}{dt} = \lambda_{C,N} \mathcal{H} \left( \frac{C_i}{\theta_{C,N_1}} \right) + \lambda_{P,N} \mathcal{H} \left( \frac{P_i}{\theta_{P,N}} \right) \left\{ 1 + \lambda_{C,N} \mathcal{H} \left( \frac{C_i}{\theta_{C,N_2}} \right) \right\} - (\mu_N + \delta_N) N_i, \quad (6.2.1g)$$

$$\frac{dR_i}{dt} = k_{-N} R_i^\diamond - k_N N_i^o R_i + k_{-T} R_i^\ddagger - k_T T_i^o R_i, \quad (6.2.1h)$$

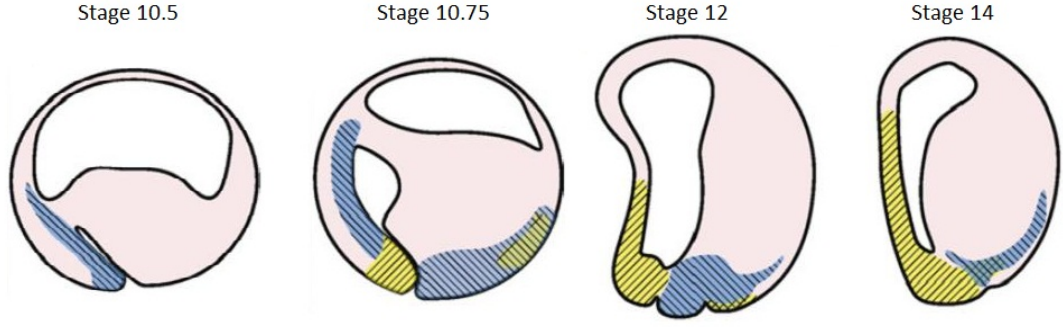
$$\frac{dR_i^\diamond}{dt} = k_N N_i^o R_i - k_{-N} R_i^\diamond - k_s R_i^\diamond S_i + (k_{-s} + k_p) R_i^{\diamond\diamond}, \quad (6.2.1i)$$

$$\frac{dR_i^{\diamond\diamond}}{dt} = k_s R_i^\diamond S_i - (k_{-s} + k_p) R_i^{\diamond\diamond}, \quad (6.2.1j)$$

$$\frac{dR_i^\ddagger}{dt} = -k_{-T} R_i^\ddagger + k_T T_i^o R_i, \quad (6.2.1k)$$

where terms of the form  $\Delta X_i$  are as defined in (1.12.3) and  $\nu$  and  $\rho$  are the membrane and extracellular volume fractions  $\rho = v_E/v_I$  and  $\nu = v_M/v_I$  where  $v_E$ ,  $v_I$  and  $v_M$  are the local





**Figure 6.3:** Cartoon showing the expression of Mix (blue) and Brachyury (yellow) during axolotl early development. Dorsal = left, vegetal = bottom. Figure modified from [139].

extracellular, intracellular and membrane volumes, respectively. To investigate a multicellular model of the network downstream of Nodal, we formulate the following system of equations based on the GRN given in figure 1.7B

$$\frac{dE_i^0}{dt} = \sigma_E \Delta E_i + \delta_E E_i - \bar{v} (k_E E_i^0 - k_{-E} F_i^\diamond) - \mu_{E^0} E_i^0, \quad (6.2.2a)$$

$$\frac{dE_i}{dt} = \lambda_{B,E} \mathcal{H}(B_i) - \mu_E E_i, \quad (6.2.2b)$$

$$\frac{dK_i^*}{dt} = \nu k_{K^*} F_i^{\diamond\diamond} - \mu_{K^*} K_i^*, \quad (6.2.2c)$$

$$\frac{dF_i^\diamond}{dt} = k_E E_i^0 F_i - k_{-E} F_i^\diamond - k_K F_i^\diamond + (k_{-K} + k_{K^*}) F_i^{\diamond\diamond}, \quad (6.2.2d)$$

$$\frac{dF_i^{\diamond\diamond}}{dt} = k_K F_i^\diamond - (k_{-K} + k_{K^*}) F_i^{\diamond\diamond}, \quad (6.2.2e)$$

$$\frac{dF_i}{dt} = -k_E E_i^0 F_i + k_{-E} F_i^\diamond, \quad (6.2.2f)$$

$$\frac{dL_i}{dt} = \lambda_{P,L} \mathcal{H}\left(\frac{P_i}{\theta_{P,L}}\right) - \mu_L L_i, \quad (6.2.2g)$$

$$\frac{dB_i}{dt} = \{\lambda_{K^*,B} \mathcal{H}(K_i^*) + \lambda_{P,B} \mathcal{H}(P_i) \mathcal{H}(M_i)\} \{1 - \mathcal{H}(G_i)\} - B_i, \quad (6.2.2h)$$

$$\frac{dG_i}{dt} = \left\{ \lambda_{L,G} \mathcal{H}(L_i) + \lambda_{M,G} \mathcal{H}\left(\frac{M_i}{\theta_{M,G}}\right) \right\} \left\{ 1 - \mathcal{H}\left(\frac{G_i}{\theta_{G,G}}\right) \right\} - \mu_G G_i, \quad (6.2.2i)$$

$$\frac{dM_i}{dt} = \lambda_{P,M} \mathcal{H}\left(\frac{P_i}{\theta_{P,M}}\right) \left\{ 1 - \mathcal{H}\left(\frac{B_i}{\theta_{B,M}}\right) \right\} - \mu_M M_i. \quad (6.2.2j)$$

Note that by summing (6.2.1h)-(6.2.1k) we find that the total number of Nodal receptors is conserved

$$\frac{d}{dt} (R + R^\diamond + R^{\diamond\diamond} + R^\ddagger) = 0 \quad \Rightarrow \quad R + R^\diamond + R^{\diamond\diamond} + R^\ddagger = R^\bullet,$$

where  $R^\bullet$  is the total number of Nodal receptors. Similarly, by summing (6.2.2d)-(6.2.2f), we find that the total number of FGF receptors ( $F^\bullet$ ) is conserved, such that

$$\frac{d}{dt} (F + F^\diamond + F^{\diamond\diamond}) = 0 \quad \Rightarrow \quad F + F^\diamond + F^{\diamond\diamond} = F^\bullet,$$

### 6.2.3 Non-dimensionalisation and parameter sizes

#### Nondimensional Scalings

We proceed by non-dimensionalising (6.2.1)-(6.2.2) following the scalings used in [94] which we give a summary of here. We base dimensionless time ( $\tau$ ) on the rate of turnover and secretion of intracellular Antivin, such that  $\tau \equiv (\mu_N + \delta_N) t$ . The dimensionless rates of signalling ( $\sigma_X$ ), turnover ( $\mu_Y$ ) and dissociation of receptors ( $k_{-Z}$ ) are based on the rate of nodal turnover and secretion such that  $\hat{\sigma}_X \equiv \sigma_X / (\mu_N \delta_N)$  for  $X \in \{N, T, T^\ddagger, E\}$ ,  $\hat{\mu}_Y \equiv \mu_Y / (\mu_N + \delta_N)$  for  $Y \in \{N, T, E\}$  and  $\hat{k}_{-Z} \equiv k_{-Z} / (\mu_N + \delta_N)$  for  $Z \in \{N, T, T^\ddagger, E, S, K\}$ . Dimensionless rates of secretion of Nodal, Antivin and FGF are given by  $\hat{\delta}_N \equiv \delta_N / \mu_N$  and  $\hat{\delta}_X \equiv \delta_X / (\mu_N + \delta_N)$  for  $X \in \{T, E\}$ . Dimensionless association rates are defined by  $\hat{k}_s \equiv k_s S / (\mu_N + \delta_N)$ ,  $\hat{k}_K \equiv k_K K / (\mu_N + \delta_N)$ ,  $\hat{k}_Y \equiv k_Y R^\bullet / (\mu_N + \delta_N)$  for  $Y \in \{N, T\}$  and  $\hat{k}_E \equiv k_E F^\bullet / (\mu_N + \delta_N)$ . The association and dissociation rates of the Nodal-Antivin complex are scaled by  $\hat{l}_T \equiv l_T R^\bullet / (\mu_N + \delta_N)$  and  $\hat{l}_{-T} \equiv l_{-T} / (\mu_N + \delta_N)$ . The nondimensional phosphorylation rate of Smad2 is  $\hat{k}_P \equiv k_P / k_{-S}$  and the nondimensional phosphorylation rate of MAPK is  $\hat{k}_{K^*} \equiv k_{K^*} / (\mu_N + \delta_N)$ . We define the following nondimensional rates of production:  $\hat{\lambda}_{P,N} \equiv \lambda_{P,N} / (\mu_N + \delta_N) R^\bullet$ ,  $\hat{\lambda}_{P,T} \equiv \lambda_{P,T} / (\mu_N + \delta_N) R^\bullet$  and  $\hat{\lambda}_{C,N} \equiv \lambda_{C,N} / (\mu_N + \delta_N) R^\bullet$ . The following dimensionless concentrations are based on the total number of receptors, such that for  $X \in \{N, N^\circ, R^\circ, R^{\circ\circ}, R\}$  we have  $\hat{X} = X / R^\bullet$  and for  $Y \in \{E^\circ, K^*, F, F^\circ, F^{\circ\circ}\}$  we have  $\hat{Y} = Y / F^\bullet$ . The dimensionless concentration of P-Smad2 is  $\hat{P} \equiv k_s P / k_{-S}$  and remaining concentrations are given by  $\hat{Z} \equiv Z / \theta_Z$ , where the following are written for notational simplicity:

$$\theta_G \equiv \theta_{G,B}, \quad \theta_B \equiv \theta_{B,E}, \quad \theta_E \equiv \theta_{E,B}, \quad \theta_L \equiv \theta_{L,G}, \quad \theta_M \equiv \theta_{M,B}.$$

We define the following dimensionless thresholds:  $\hat{\theta}_{P,N} \equiv k_s \theta_{P,N} / k_{-S}$ ,  $\hat{\theta}_{P,T} \equiv \theta_{P,T} / R^\bullet$ ,  $\hat{\theta}_{K^*,B} \equiv \theta_{K^*,B} / F^\bullet$ ,  $\hat{\theta}_{P,B} \equiv k_s \theta_{P,B} / k_{-S}$  and  $\hat{\theta}_{P,M} \equiv k_s \theta_{P,M} / k_{-S}$ . Remaining dimensionless rates of production, turnover and thresholds are defined by  $\hat{\lambda}_{Y,Z} \equiv \lambda_{Y,Z} / \theta_Z (\mu_N + \delta_N)$ ,  $\hat{\mu}_Z \equiv \mu_Z / (\mu_N + \delta_N)$  and  $\hat{\theta}_{X,Z} \equiv \theta_{X,Z} / \theta_Z$ .

#### Parameter Sizes

We again follow the work of Middleton et al [94] in making the following assumptions about the rate at which certain processes occur, based on the fact that intracellular Nodal is turned over at a faster rate than extracellular Nodal (i.e.  $\mu_N \ll \mu_{N^\circ}$ ). It is assumed that other processes occur on a similarly fast timescale and we make the following rescalings

$$\begin{aligned} \hat{k}_{-N} &\rightarrow \epsilon^{-1} \hat{k}_{-N}, & \hat{k}_N &\rightarrow \epsilon^{-1} \hat{k}_N, & \hat{k}_P &\rightarrow \epsilon^{-1} \hat{k}_P, & \hat{\mu}_P &\rightarrow \epsilon^{-1} \hat{\mu}_P, & \hat{k}_S &\rightarrow \epsilon^{-1} \hat{k}_S, \\ \hat{k}_{-S} &\rightarrow \epsilon^{-1} \hat{k}_{-S}, & \hat{\delta}_T &\rightarrow \epsilon^{-1} \hat{\delta}_T, & \hat{k}_T &\rightarrow \epsilon^{-1} \hat{k}_T, & \hat{k}_{-T} &\rightarrow \epsilon^{-1} \hat{k}_{-T}, & \hat{l}_T &\rightarrow \epsilon^{-1} \hat{l}_T, \\ \hat{l}_{-T} &\rightarrow \epsilon^{-1} \hat{l}_{-T}, & \hat{\mu}_{T^\circ} &\rightarrow \epsilon^{-1} \hat{\mu}_{T^\circ}, & \hat{k}_{-E} &\rightarrow \epsilon^{-1} \hat{k}_{-E}, & \hat{k}_E &\rightarrow \epsilon^{-1} \hat{k}_E, & \hat{\mu}_{K^*} &\rightarrow \epsilon^{-1} \hat{\mu}_{K^*}, \\ & & & & \hat{k}_K &\rightarrow \epsilon^{-1} \hat{k}_K, & \hat{k}_{-K} &\rightarrow \epsilon^{-1} \hat{k}_{-K}. \end{aligned} \quad (6.2.3)$$

where  $\epsilon = (\mu_N + \delta_N) / \mu_{N^\circ} \ll 1$ . After applying the scalings described in this section and

defining the following for notational simplicity:  $\bar{\delta}_N = \delta_N / (\delta_N + 1)\rho$ ,  $\bar{k}_P = \rho\hat{k}_P\hat{k}_S S^{-1}$ ,  $\bar{k}_{-S} = \hat{k}_S(1 + \hat{k}_P) - \bar{k}_P$  and  $\hat{v} = \nu/\rho$ , the equations governing Nodal signalling downstream of  $\beta$ -catenin are given by

$$\frac{dC_i}{d\tau} = -\mu_C C_i \quad (6.2.4a)$$

$$\epsilon \frac{dT_i^0}{d\tau} = \sigma_T \Delta T_i^0 + \nu \left( k_{-T} R_i^\ddagger - k_T T_i^0 R_i \right) - l_T N_i^0 T_i^0 + l_{-T} T_i^\ddagger + \frac{\delta_T}{\rho} T_i - \mu_{T^0} T_i^0, \quad (6.2.4b)$$

$$\epsilon \frac{dN_i^0}{d\tau} = \sigma_N \Delta N_i^0 + \frac{\nu}{\rho} \left( k_{-N} R_i^\diamond - k_N N_i^0 R_i \right) - l_T N_i^0 T_i^0 + l_{-T} T_i^\ddagger + \frac{\delta_N}{\rho} N_i - \mu_{N^0} N_i^0, \quad (6.2.4c)$$

$$\epsilon \frac{dT_{i,j}^\ddagger}{d\tau} = \sigma_{T^\ddagger} \Delta T_{i,j}^\ddagger + l_T N_{i,j}^0 T_{i,j}^0 - l_{-T} T_{i,j}^\ddagger - \mu_{T^\ddagger} T_{i,j}^\ddagger, \quad (6.2.4d)$$

$$\frac{dT_i}{d\tau} = \lambda_{P,T} \mathcal{H} \left( \frac{P_i}{\theta_{P,T}} \right) - (\mu_T + \delta_T) T_i, \quad (6.2.4e)$$

$$\epsilon \frac{dP_i}{d\tau} = k_p \nu R_i^{\diamond\diamond} - \mu_P P_i, \quad (6.2.4f)$$

$$\frac{dN_i}{d\tau} = \lambda_{C,N} \mathcal{H} \left( \frac{C_i}{\theta_{C,N_1}} \right) + \lambda_{P,N} \mathcal{H} \left( \frac{P_i}{\theta_{P,N}} \right) \left\{ 1 + \lambda_{C,N} \mathcal{H} \left( \frac{C_i}{\theta_{C,N_2}} \right) \right\} - (\mu_N + \delta_N) N_i, \quad (6.2.4g)$$

$$\epsilon \frac{dR_i}{d\tau} = k_{-N} R_i^\diamond - k_N N_i^0 R_i + k_{-T} R_i^\ddagger - k_T T_i^0 R_i, \quad (6.2.4h)$$

$$\epsilon \frac{dR_i^\diamond}{d\tau} = -k_{-N} R_i^\diamond + k_N N_i^0 R_i - k_S R_i^\diamond S_i + (k_{-s} + k_p) R_i^{\diamond\diamond}, \quad (6.2.4i)$$

$$\epsilon \frac{dR_i^{\diamond\diamond}}{d\tau} = k_S R_i^\diamond S_i - (k_{-s} + k_p) R_i^{\diamond\diamond}, \quad (6.2.4j)$$

$$\epsilon \frac{dR_i^\ddagger}{d\tau} = -k_{-T} R_i^\ddagger + k_T T_i^0 R_i, \quad (6.2.4k)$$

and the governing equations downstream of Nodal are

$$\epsilon \frac{dE_i^0}{d\tau} = \sigma_E \Delta E_i - \bar{v} (k_E E_i^0 - k_{-E} F_i^\diamond) + \delta_E E_i - \mu_{E^0} E_i^0, \quad (6.2.5a)$$

$$\frac{dE_i}{d\tau} = \lambda_{B,E} \mathcal{H} \left( \frac{B_i}{\theta_{B,E}} \right) - (\delta_E + \mu_E) E_i, \quad (6.2.5b)$$

$$\epsilon \frac{dK_i^*}{d\tau} = \nu k_{K^*} F_i^{\diamond\diamond} - \mu_{K^*} K_i^*, \quad (6.2.5c)$$

$$\epsilon \frac{dF_i^\diamond}{d\tau} = k_E E_i^0 F_i - k_{-E} F_i^\diamond - k_K F_i^\diamond + (k_{-K} + k_{K^*}) F_i^{\diamond\diamond}, \quad (6.2.5d)$$

$$\epsilon \frac{dF_i^{\diamond\diamond}}{d\tau} = k_K F_i^\diamond - (k_{-K} + k_{K^*}) F_i^{\diamond\diamond}, \quad (6.2.5e)$$

$$\epsilon \frac{dF_i}{d\tau} = -k_E E_i^0 F_i + k_{-E} F_i^\diamond, \quad (6.2.5f)$$

$$\frac{dL_i}{d\tau} = \lambda_{P,L} \mathcal{H} \left( \frac{P_i}{\theta_{P,L}} \right) - \mu_L L_i, \quad (6.2.5g)$$

$$\frac{dB_i}{d\tau} = \left\{ \lambda_{K^*,B} \mathcal{H} \left( \frac{K_i^*}{\theta_{K^*,B}} \right) + \lambda_{P,B} \mathcal{H} \left( \frac{P_i}{\theta_{P,B}} \right) \mathcal{H} \left( \frac{M_i}{\theta_{M,B}} \right) \right\} \left\{ 1 - \mathcal{H} \left( \frac{G_i}{\theta_{G,B}} \right) \right\} - \mu_B B_i, \quad (6.2.5h)$$

$$\frac{dG_i}{d\tau} = \left\{ \lambda_{L,G} \mathcal{H} \left( \frac{L_i}{\theta_{L,G}} \right) + \lambda_{M,G} \mathcal{H} \left( \frac{M_i}{\theta_{M,G}} \right) \right\} \left\{ 1 - \mathcal{H} \left( \frac{G_i}{\theta_{G,G}} \right) \right\} - \mu_G G_i, \quad (6.2.5i)$$

$$\frac{dM_i}{d\tau} = \lambda_{P,M} \mathcal{H} \left( \frac{P_i}{\theta_{P,M}} \right) \left\{ 1 - \mathcal{H} \left( \frac{B_i}{\theta_{B,M}} \right) \right\} - \mu_M M_i. \quad (6.2.5j)$$

Initial conditions are selected such that all Nodal and eFGF receptors are free  $R_i(0) = 1$ ,  $R_i^\diamond(0) = 0$ ,  $R_i^{\diamond\diamond}(0) = 0$ ,  $R_i^\ddagger(0) = 0$ ,  $F_i(0) = 1$ ,  $F_i^\diamond(0) = 0$ ,  $F_i^{\diamond\diamond}(0) = 0$ . There is an initial concentration of  $\beta$ -catenin,  $C_i(0) = C_0$ , where  $C_0 \geq 0$  and all other factors are initially absent  $T_i^o(0)=0$ ,  $T_i(0) = 0$ ,  $N_i^o(0) = 0$ ,  $N_i(0) = 0$ ,  $T_i^\ddagger(0) = 0$ ,  $E_i^o(0) = 0$ ,  $E_i(0) = 0$ ,  $L_i(0) = 0$ ,  $B_i(0) = 0$ ,  $G_i(0) = 0$  and  $M_i(0) = 0$ .

#### 6.2.4 Numerical solutions

We now solve equations (6.2.4) and (6.2.5) in a line of 50 cells, selecting initial conditions such that it represents a line running from a region where  $\beta$ -catenin is not expressed to the dorsal region where  $\beta$ -catenin is expressed. This may represent a line of cells running from the ventral region to the dorsal region, although since gastrulation occurs as the stages when mesendoderm forms, it is not clear where our line of cells corresponds to once this rearrangement of cells has occurred. Recall that in axolotl the only maternal factor involved in mesendoderm induction in our model is  $\beta$ -catenin, since VegT is not involved in the axolotl mesendoderm GRN. Initial conditions are chosen such that the first  $\lfloor n/3 \rfloor$  cells represent a region where  $\beta$ -catenin is absent and in the remaining  $\lfloor 2n/3 \rfloor$  we consider two different cases. In the first case we assume that a gradient of  $\beta$ -catenin runs from cell  $j = n/3 + 1$  to cell  $j = n$ , such that

$$C_i(0) = \begin{cases} 0 & \text{for } i \leq \lfloor n/3 \rfloor \\ a(i - \lfloor n/3 \rfloor) & \text{for } \lfloor n/3 \rfloor < i \leq \lfloor n \rfloor, \end{cases} \quad (6.2.6)$$

where  $a$  is a positive constant. We chose this gradient of  $\beta$ -catenin based on experimental evidence that  $\beta$ -catenin can induce mesoderm and endoderm in a dose dependent manner in axolotl animal caps [16]. However,  $\beta$ -catenin is deposited maternally and localised with cortical rotation [98], and there is currently no evidence that a gradient of  $\beta$ -catenin exists in the embryo. Thus we consider a second case where a constant level of  $\beta$ -catenin is found in the last  $\lfloor n/3 \rfloor$  cells but is not expressed elsewhere, such that

$$C_i(0) = \begin{cases} 0 & \text{for } i < \lfloor 2n/3 \rfloor \\ b & \text{for } i \geq \lfloor 2n/3 \rfloor, \end{cases} \quad (6.2.7)$$

where  $b$  is a positive constant. We now proceed investigate time-dependent solutions to (6.2.4) and (6.2.5) subject to these two sets of initial conditions using the Matlab solver for stiff ODEs, `ode15s`.

#### Gradient of $\beta$ -catenin

Plotted in figure 6.4 are solutions to (6.2.4)-(6.2.5) subject to the initial concentration of  $\beta$ -catenin defined by (6.2.6) such that a gradient of  $\beta$ -catenin levels is found in cells 16 to 50 and absent elsewhere. Parameter values (given in tables 6.1 and 6.2) were selected such that (6.2.4) is consistent with experimental observations in *Xenopus* where Nodal is pinned by Antivin [95].

Variable	Parameter	Value	Variable	Parameter	Value
N	$\lambda_{P,N}$	3	T	$\lambda_{P,T}$	12
	$\theta_{P,N}$	0.666		$\theta_{P,T}$	0.999
	$\lambda_{C,N}$	1		$\delta_T$	20
	$\theta_{C,N}$	1		$\mu_T$	1
	$\lambda_{C_2,N}$	1		$\sigma_T$	0.125
	$\theta_{C_2,N}$	1		$T^0$	$k_T$
$N^0$	$k_N$	1	$k_{-T}$		100
	$k_{-N}$	100	$\mu_{T^0}$		1
	$\mu_{N^0}$	1	P	$k_P$	10
$T^\ddagger$	$l_T$	1		$\mu_P$	0.01
	$l_{-T}$	100	S	$S$	1
	$\mu_{T^\ddagger}$	0		$k_S$	1
	$\bar{v}$	1		$k_{-S}$	0.01
C	$\mu_C$	0.01			

**Table 6.1:** Dimensionless parameters used to solve (6.2.4). Parameters are selected such that in a single cell case (6.2.4) is bistable.

Variable	Parameter	Value	Variable	Parameter	Value
M	$\lambda_{P,M}$	12	B	$\lambda_{K^*,B}$	12
	$\theta_{P,M}$	3		$\lambda_{P,B}$	20
	$\theta_{B,M}$	1		$\theta_{P,B}$	1
L	$\lambda_{P,L}$	1	G	$\lambda_{LI,G}$	1
	$\theta_{P,L}$	1		$\lambda_{M,G}$	8
E	$\lambda_{B,E}$	5		$\theta_{M,G}$	1
	$k_{K^*}$	10		$\theta_{G,G}$	3
$K^*$	$\mu_{K^*}$	0.01		$E^0$	$\sigma_E$
	$k_K$	1	$\delta_E$		1
K	$k_{-K}$	0.01	$k_E$		1
	all other $\mu$	1	$k_{-E}$		100

**Table 6.2:** Dimensionless parameters used to solve (6.2.5). Parameters are selected such that in a single cell case (6.2.5) is bistable with steady states corresponding to mesoderm and anterior mesendoderm.

We find that Nodal is restricted from spreading more than one or two cells away from the region where it is induced by  $\beta$ -catenin. There is a gradient of Nodal, Antivin and P-Smad2 which is similar to the gradient of  $\beta$ -catenin. Downstream of Nodal signalling we find that Mix and Goosecoid are co-expressed in regions with high levels of  $\beta$ -catenin and Brachyury and eFGF are expressed in regions with a lower level of  $\beta$ -catenin. These results are qualitatively similar to dose response data in axolotl animal caps [16] where mesoderm forms for a low level of  $\beta$ -catenin and anterior mesendoderm forms for a higher dose of  $\beta$ -catenin. We also observe that, in our model, Brachyury spreads into the region with no active Nodal signalling, this spread being due to the mutual positive regulation of eFGF and Brachyury. Figure 6.5 shows solutions to the model beyond  $t = 100$ . We find that levels of components of the Nodal signalling pathway decrease as time proceeds. As the levels of P-Smad2 decrease, Mix and Goosecoid become downregulated and Brachyury and FGF become upregulated in these cells. Thus at steady state Nodal is not maintained and eFGF and Brachyury are maintained via their mutual positive regulation.

In figures 6.6 and 6.7 solutions to (6.2.4)-(6.2.5) subject to the initial concentration of  $\beta$ -catenin defined by (6.2.6) are plotted for  $\lambda_{P,A} = 1$  and  $\lambda_{P,A} = 50$ , corresponding to the cases where Nodal can spread throughout the line of cells, and where Nodal is pinned by Antivin, respectively. When Nodal can spread throughout the line of cells we still observe regions correspond-

ing to mesoderm and anterior mesendoderm, but see that components of Nodal signalling spread into the region where  $\beta$ -catenin is not expressed (see figure 6.6). When  $\lambda_{P,A} = 50$ , the rate of production is high, which means that the level of P-Smad2 in response to Nodal signalling is low and Antivin pins Nodal to  $\beta$ -catenin expressing regions. Downstream of Nodal we see that a Brachyury region forms, but we do not see a region corresponding to anterior mesendoderm.

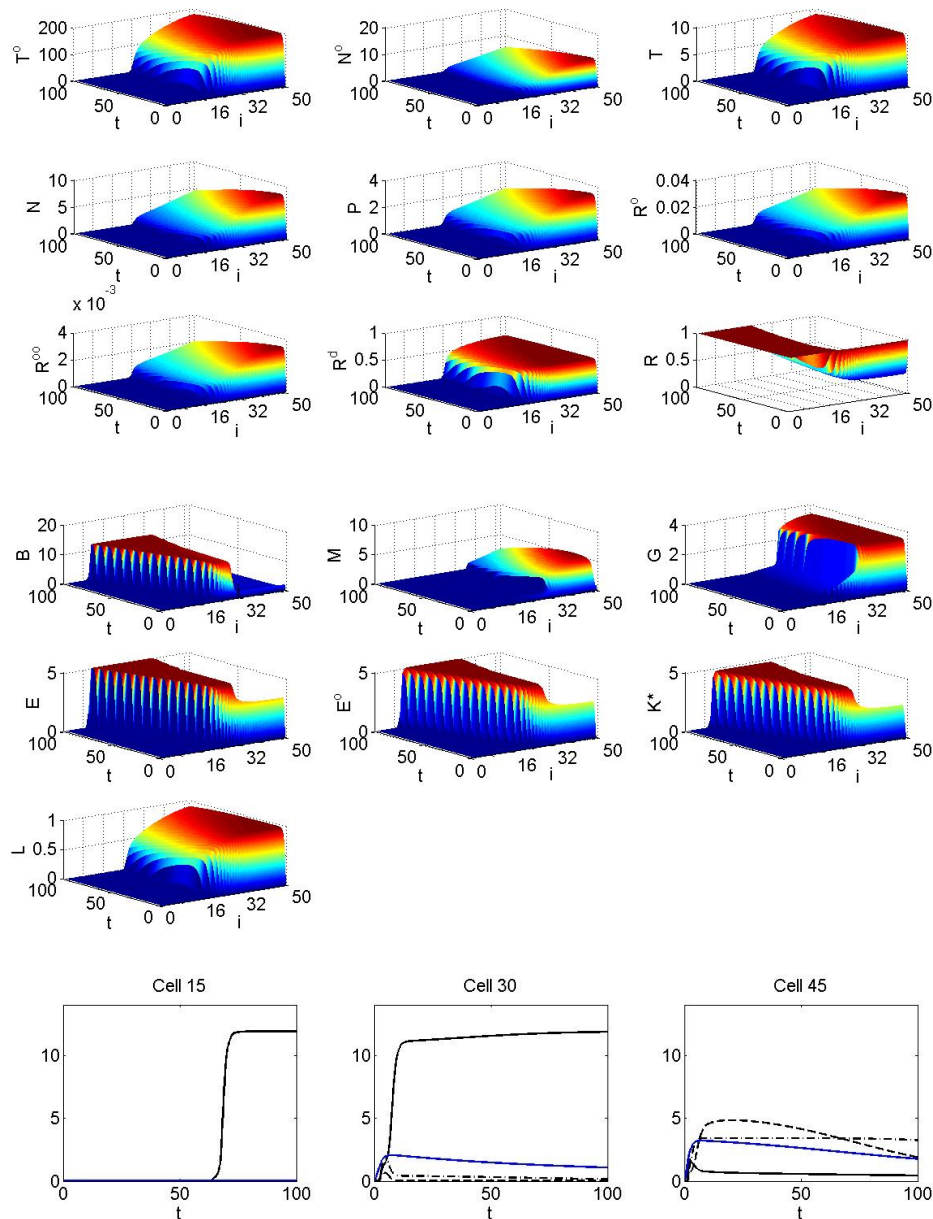
### Constant level of $\beta$ -catenin

Plotted in figure 6.8 are solutions to (6.2.4)-(6.2.5) subject to the initial concentration of  $\beta$ -catenin defined by (6.2.7) such that a uniform concentration of  $\beta$ -catenin is found in cells 33 to 50 and absent elsewhere. We set  $\lambda_{P,A} = 10$ , such that Antivin prevents Nodal from spreading more than one or two cells from its source, and investigate how cell to cell signalling results in the formation of regions corresponding to mesoderm and anterior mesendoderm. The solutions plotted in figure 6.8 show that cells 32 to 50, where  $\beta$ -catenin is expressed, correspond to anterior mesendoderm, while mesoderm forms on the boundary of the  $\beta$ -catenin expressing region. The solutions shown in figure 6.9 are for the same model as in figure 6.8, except we set  $\sigma_E = 0$ , such that there is no cell to cell communication via the FGF signalling pathway. We see that in this case only cells 30 and 31 express Brachyury and eFGF and does not spread throughout the line of cells. Thus eFGF signalling is essential for expanding the number of cells corresponding to mesoderm. Figure 6.10 shows solutions where  $\sigma_N = \sigma_T = \sigma_{T\dagger} = 0$ , such that there is no cell to cell communication via the Nodal signalling pathway. As before, we find that anterior mesendoderm forms in cells 32 to 50, but in the absence of Nodal spreading outside of this region.

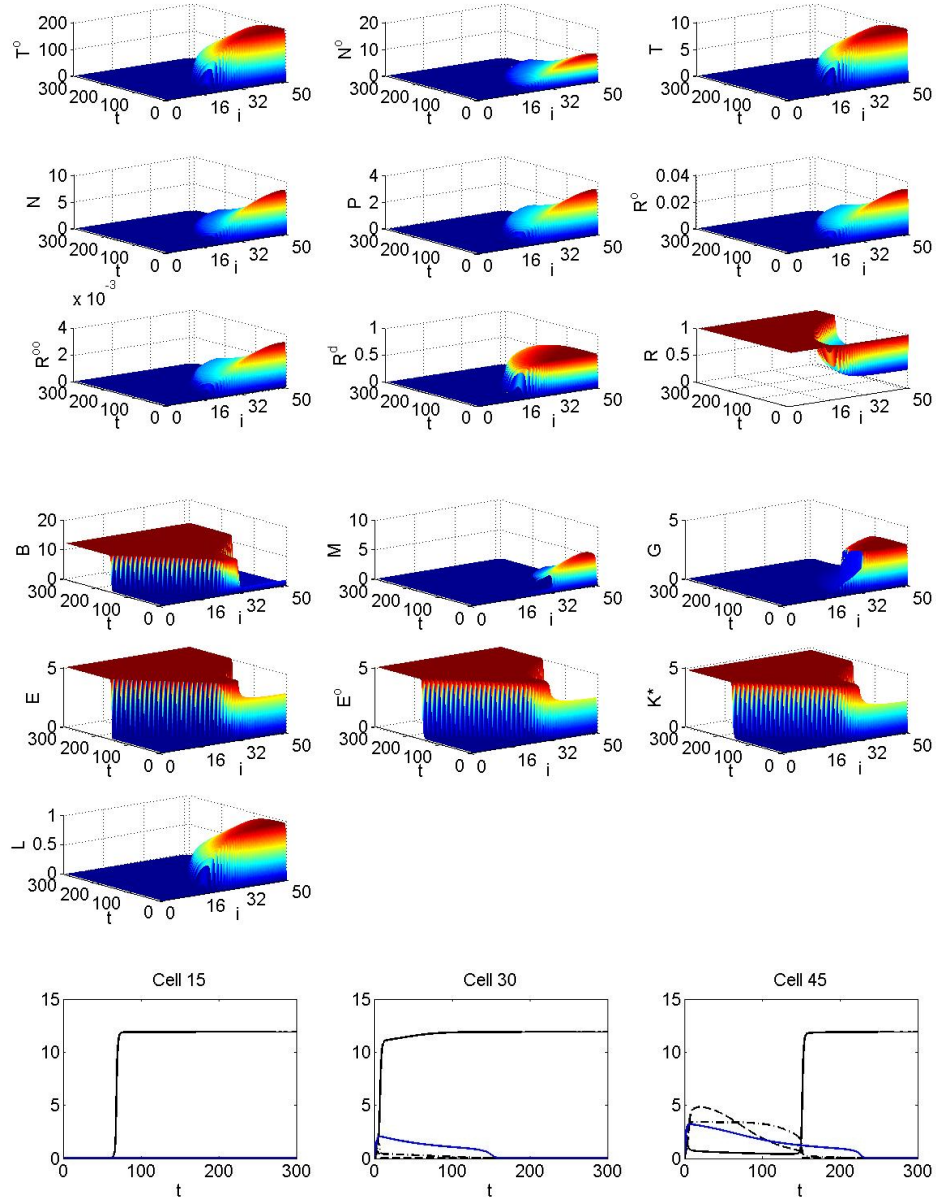
### 6.2.5 Discussion

In this section we developed mathematical models of the axolotl mesendoderm GRN in a line of cells. We found that Brachyury expressing (i.e. mesoderm) and Mix and Gooseoid expressing (i.e. anterior mesendoderm) populations of cells form for both an initial gradient of  $\beta$ -catenin and a uniform level of  $\beta$ -catenin in a selected number of cells. While experimental evidence shows that  $\beta$ -catenin can induce mesoderm and anterior mesendoderm in a dose dependent manner in axolotl animal caps [16], it is likely that a gradient of  $\beta$ -catenin does not exist *in vivo*. Our investigations show that regions corresponding to mesoderm and anterior mesendoderm can form when  $\beta$ -catenin is uniformly expressed in some cells and absent from others, and that the diffusion of Nodal is essential for the formation of these two distinct regions in this case.

To aid further development of multicellular models of the axolotl mesendoderm GRN, experimental data is required. A logical first step is to collect data for the expression of components of the Nodal signalling pathway to estimate model parameters, then extend the analysis to components downstream of Nodal. In the next section we clone Antivin, a gene involved in the regulation of Nodal signalling, which has not previously been identified in axolotl.

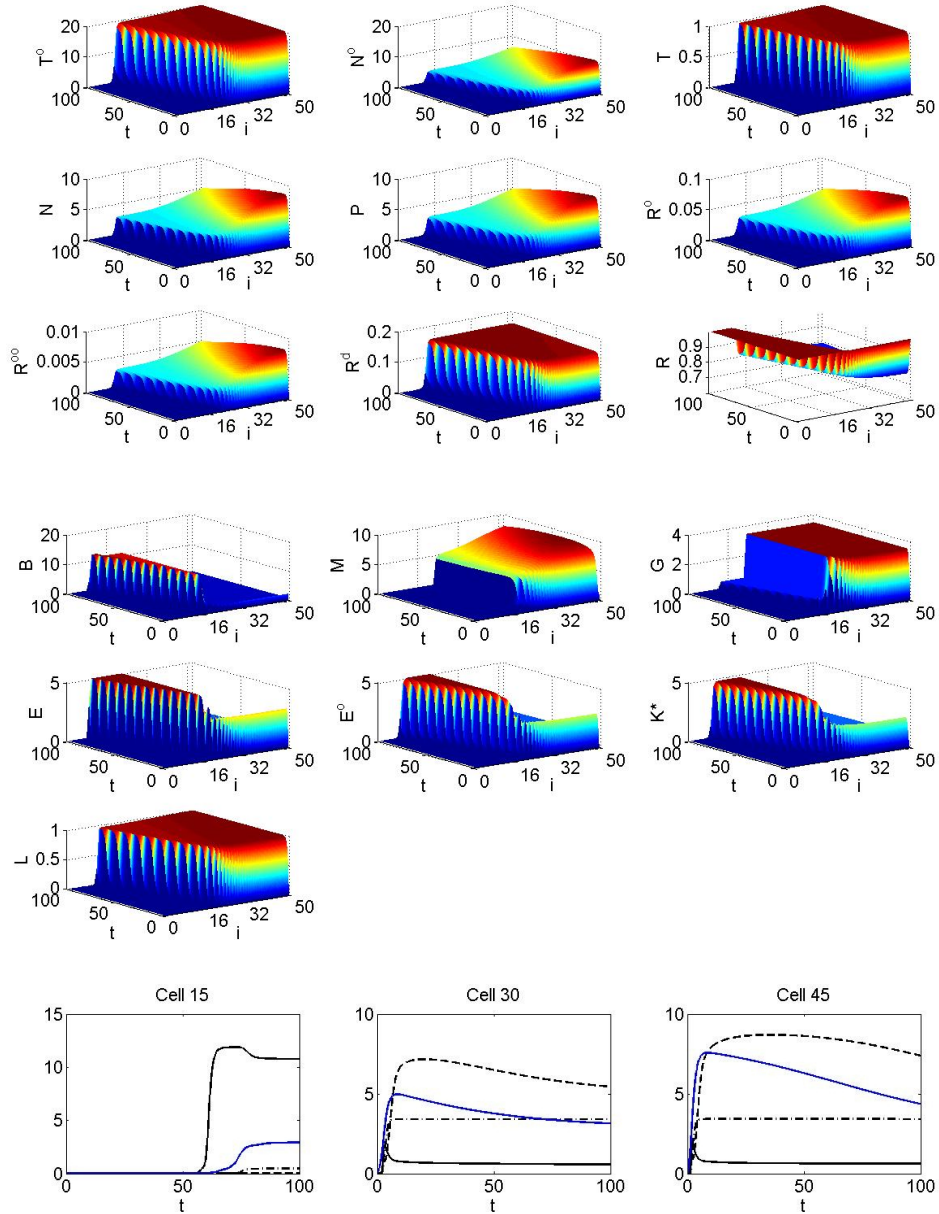


**Figure 6.4:** Numerical solutions for (6.2.4)-(6.2.5) subject to the initial condition of  $\beta$ -catenin given by (6.2.6) with  $a = 1/16$  for  $n = 50$  cells. No  $\beta$ -catenin is found in cells  $i = 1$  to 16, and a gradient of  $\beta$ -catenin exists in cells  $i = 17$  to 50. Nodal ( $N_i^o$ ) and its downstream component P-Smad2 ( $P_i$ ) are restricted to regions expressing  $\beta$ -catenin. Parameters are selected as in tables 6.1 and 6.2, with  $\lambda_{p,A} = 10$ , such that Antiviral pins Nodal expression. Downstream of P-Smad2, we find that Mix is expressed in regions with high  $\beta$ -catenin (cells 32 to 50) and Brachyury is initially expressed in regions with low  $\beta$ -catenin, but spreads into the region where  $\beta$ -catenin is absent.

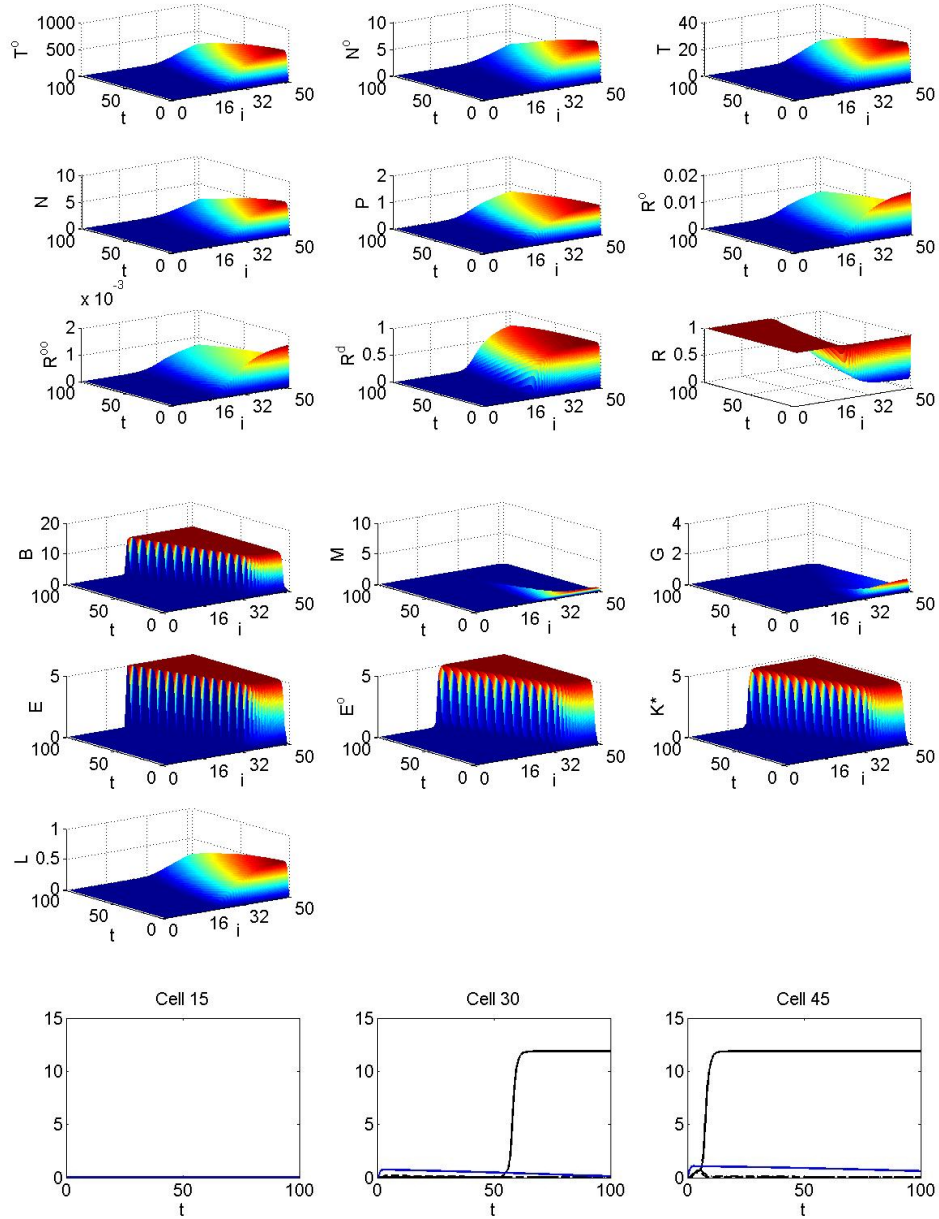


**Figure 6.5:** Numerical solutions for (6.2.4)-(6.2.5) subject to the initial condition of  $\beta$ -catenin given by (6.2.6) with  $a = 1/16$  for  $n = 50$  cells. No  $\beta$ -catenin is found in cells  $i = 1$  to 16, and a gradient of  $\beta$ -catenin exists in cells  $i = 17$  to 50. Nodal ( $N_i^o$ ) and its downstream component P-Smad2 ( $P_i$ ) are restricted to regions expressing  $\beta$ -catenin. Parameters are selected as in tables 6.1 and 6.2, with  $\lambda_{P,A} = 10$ , such that Antivin pins Nodal expression. Downstream of P-Smad2, we find that Mix is expressed in regions with high  $\beta$ -catenin (cells 32 to 50) and Brachyury is initially expressed in regions with low  $\beta$ -catenin, but spreads into the region where  $\beta$ -catenin is absent.

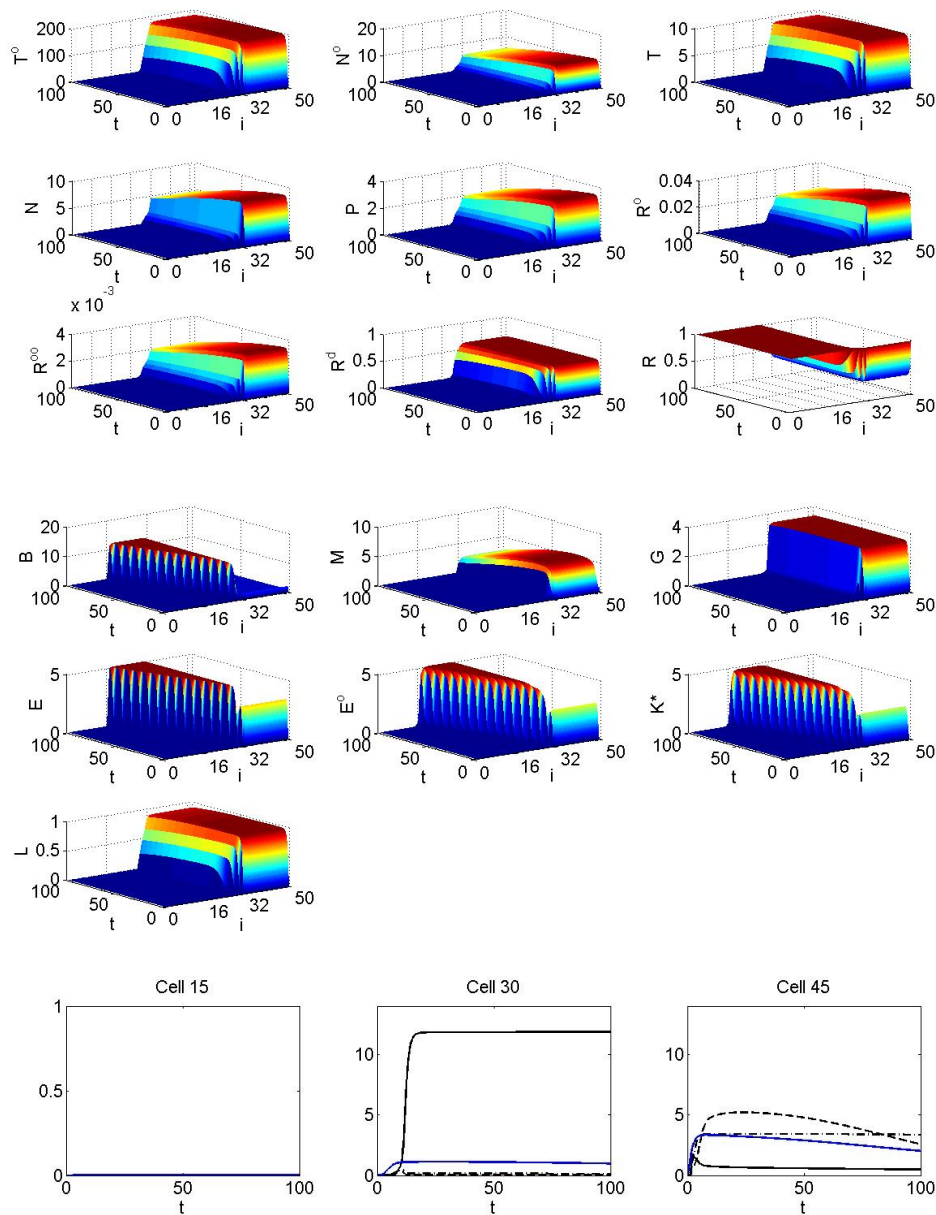




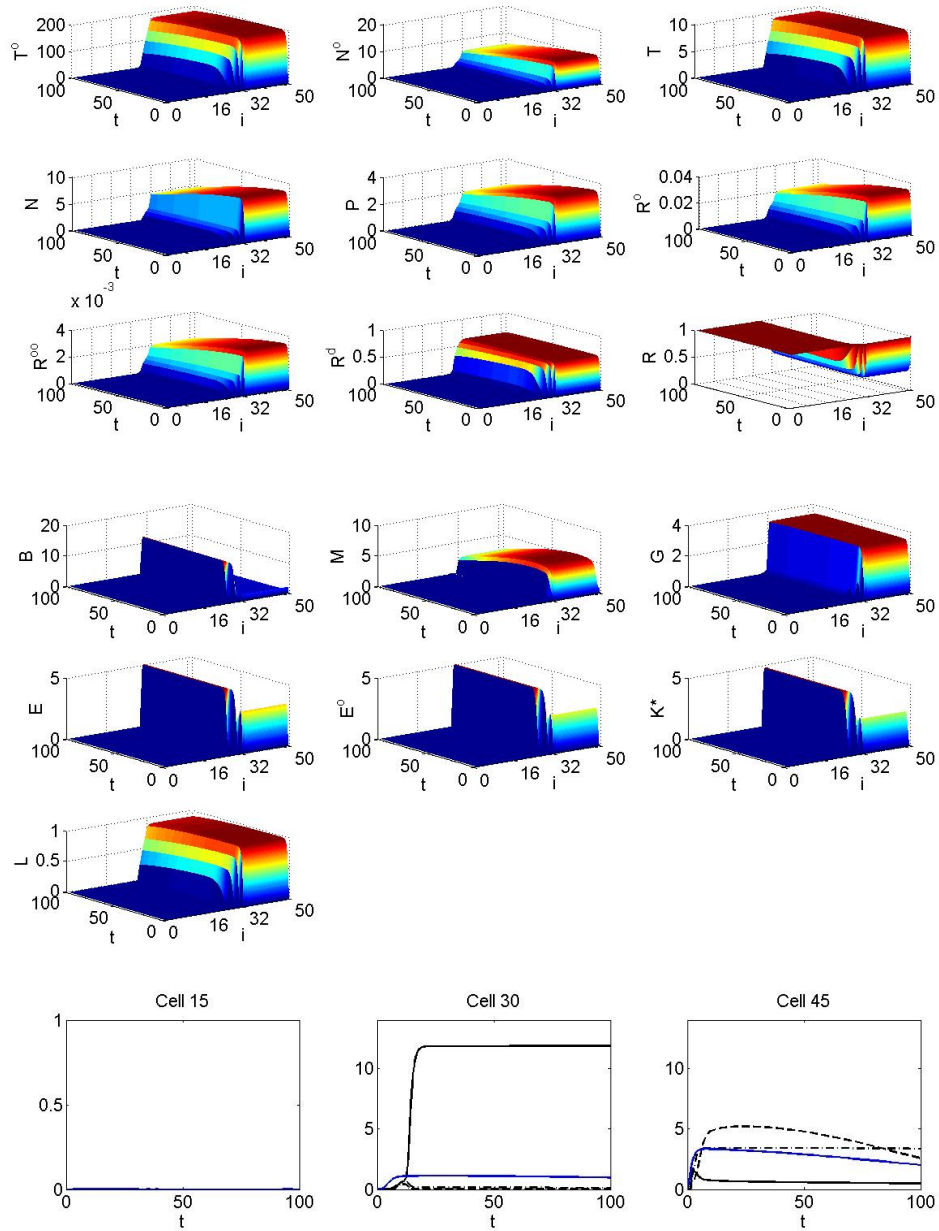
**Figure 6.6:** Numerical solutions for (6.2.4)-(6.2.5) subject to the initial condition of  $\beta$ -catenin given by (6.2.6) with  $a = 1/16$  for  $n = 50$  cells. No  $\beta$ -catenin is found in cells  $i = 1$  to 16, and a gradient of  $\beta$ -catenin exists in cells  $i = 17$  to 50. Nodal ( $N_i^o$ ) and its downstream component P-Smad2 ( $P_i$ ) are restricted to regions expressing  $\beta$ -catenin. Parameters are selected as in tables 6.1 and 6.2, with  $\lambda_{P,A} = 1$ , such that Nodal spreads throughout the line of cells. Downstream of P-Smad2, we find that Mix is expressed in regions with high  $\beta$ -catenin (cells 32 to 50) and Brachyury is initially expressed in regions with low  $\beta$ -catenin, but spreads into the region where  $\beta$ -catenin is absent.



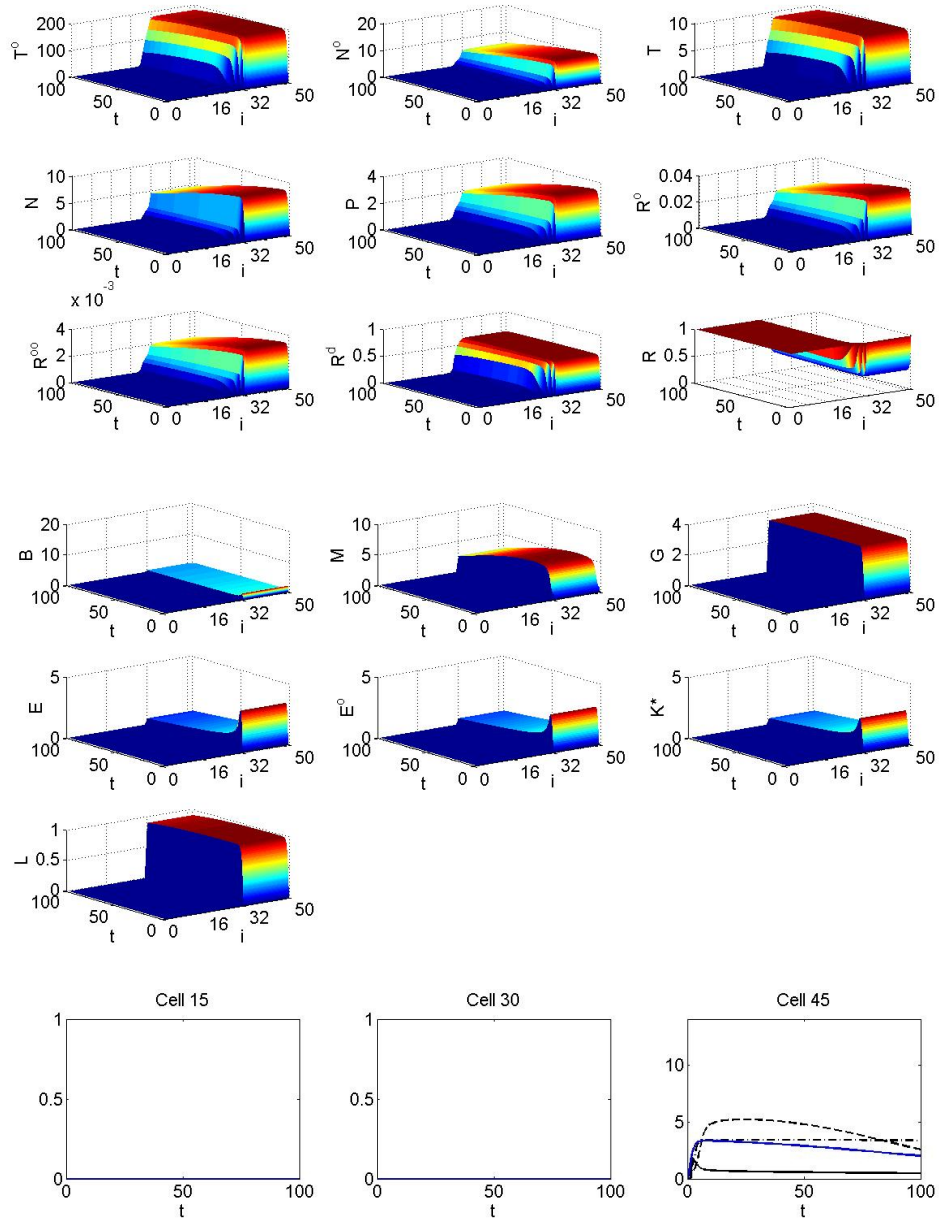
**Figure 6.7:** Numerical solutions for (6.2.4)-(6.2.5) subject to the initial condition of  $\beta$ -catenin given by (6.2.6) with  $a = 1/16$  for  $n = 50$  cells. No  $\beta$ -catenin is found in cells  $i = 1$  to 16, and a gradient of  $\beta$ -catenin exists in cells  $i = 17$  to 50. Nodal ( $N_i^o$ ) and its downstream component P-Smad2 ( $P_i$ ) are restricted to regions expressing  $\beta$ -catenin. Parameters are selected as in tables 6.1 and 6.2, with  $\lambda_{P,A} = 50$ , such that Nodal is pinned by Antivin. Downstream of P-Smad2, we find that Mix is expressed in regions with high  $\beta$ -catenin (cells 32 to 50) and Brachyury is initially expressed in regions with low  $\beta$ -catenin, but spreads into the region where  $\beta$ -catenin is absent.



**Figure 6.8:** Numerical solutions for (6.2.4)-(6.2.5) subject to the initial condition of  $\beta$ -catenin given by (6.2.7) with  $b = 50/16$  for  $n = 50$  cells. No  $\beta$ -catenin is found in cells  $i = 1$  to 32, and a uniform level  $\beta$ -catenin exists in cells  $i = 33$  to 50. Nodal ( $N_i^o$ ) and its downstream component P-Smad2 ( $P_i$ ) are restricted to regions expressing  $\beta$ -catenin. Parameters are selected as in tables 6.1 and 6.2, with  $\lambda_{P,A} = 10$ , such that Antiviral pins Nodal expression. Downstream of P-Smad2, we find that Mix is expressed in regions where  $\beta$ -catenin is expressed (cells 33 to 50) and Brachyury is initially expressed at the boundary of the  $\beta$ -catenin positive region, and then spreads into the region where  $\beta$ -catenin is absent.



**Figure 6.9:** Numerical solutions for (6.2.5) subject to the initial condition of  $\beta$ -catenin given by (6.2.7) with  $b = 50/16$  for  $n = 50$  cells. No  $\beta$ -catenin is found in cells  $i = 1$  to 32, and a uniform level  $\beta$ -catenin exists in cells  $i = 33$  to 50. Nodal ( $N_i^o$ ) and its downstream component P-Smad2 ( $P_i$ ) are restricted to regions expressing  $\beta$ -catenin. Parameters are selected as in tables 6.1 and 6.2, with  $\lambda_{P,A} = 10$ , such that Antiviral pins Nodal expression and  $\sigma_E = 0$  such that extracellular FGF does not spread from cell to cell. Downstream of P-Smad2, we find that Mix is expressed in regions where  $\beta$ -catenin is expressed (cells 33 to 50) and Brachyury is expressed at the boundary of the  $\beta$ -catenin positive region.



**Figure 6.10:** Numerical solutions for (6.2.5) subject to the initial condition of  $\beta$ -catenin given by (6.2.7) with  $b = 50/16$  for  $n = 50$  cells. No  $\beta$ -catenin is found in cells  $i = 1$  to 32, and a uniform level  $\beta$ -catenin exists in cells  $i = 33$  to 50. Nodal ( $N_i^o$ ) and its downstream component P-Smad2 ( $P_i$ ) are restricted to regions expressing  $\beta$ -catenin. Parameters are selected as in tables 6.1 and 6.2, with  $\lambda_{P,A} = 10$ , such that Antivin pins Nodal expression and terms of the form  $\sigma_X = 0$  such that there is no cell to cell communication via Nodal signalling. Downstream of P-Smad2, we find that Mix is expressed in regions where  $\beta$ -catenin is expressed (cells 33 to 50) and Brachyury is expressed at the boundary of the  $\beta$ -catenin positive region.

hit	species	gene	Accession number	identities	e value
1	Paralichthys olivaceus	lefty	AB232902.1	73%	2e-163
2	Oryzias latipes	lefty	NM_001163090.1	73%	1e-146
3	Xenopus (Silurana) tropicalis	lefty	NM_001130253.1	73%	4e-141
4	Oreochromis niloticus	left-right determination factor 2-like	XM_003440707.1	71%	4e-134
5	Xenopus laevis	Xantivin	AF209744.1	70%	8e-131

**Table 6.3:** NCBI BLAST results for the axolotl Antivin coding sequence. BLASTN 2.2.26+ is a nucleotide blast.

### 6.3 The cloning and expression of axolotl Antivin

Antivin (also known as Lefty) is an important component of the Nodal signalling pathway, which acts to inhibit Nodal signalling. In this section we clone and sequence a fragment of axolotl DNA which we identify as axolotl Antivin by comparing with Antivin sequences from other species. We then measure the expression of Antivin in axolotl embryos at various stages of development and presented initial data on the expression of Antivin in animal caps over expressing Nodal1.

#### 6.3.1 The axolotl *Antivin* sequence

A 98 base pair (bp) sequence of axolotl DNA, from a transcriptome project donated to us by Elly Tanaka, was shown to be similar to *Antivin* in other species, for example *Xenopus laevis*, using NCBI BLAST. This sequence included a stop codon, giving the 3' end of the axolotl *Antivin* coding sequence. To clone axolotl *Antivin* upstream of this 98bp, we used a genome walking technique (see materials and methods, chapter 2) and designed primers to 'walk' upstream of the fragment in libraries of axolotl genomic DNA. The resulting PCR fragments were cloned using T-vector and sequenced. NCBI BLAST was used to confirm that the resulting sequences corresponded to axolotl *Antivin*. After repeated rounds of genome walking, primers were designed against the resulting sequence, and PCR carried out against axolotl cDNA to give a 1041bp fragment of axolotl coding sequence (see figure 6.11(a)). To confirm that the sequence identified is an *Antivin* orthologue, databases were searched using NCBI BLAST. Top hits were all Antivin/Lefty orthologues (table 6.3) revealing that our cDNA sequence encodes axolotl *Antivin*. Furthermore, the conserved domain prediction in NCBI BLAST confirms that the sequence is a TGF- $\beta$  family member (figure 6.11(b)). The 1041bp of axolotl *Antivin* give a predicted polypeptide of 346 amino acids (figure 6.11(a)). Nucleotide alignments, comparing Antivin protein sequences from axolotl, *Xenopus*, human and mouse, are shown in figure 6.12. Axolotl Antivin contains two possible RXXR cleavage sites and 6 cysteine residues in the C-terminal region, which are conserved in all TGF- $\beta$  superfamily proteins [73]. Note that we have not yet cloned the 5' end of axolotl Antivin. From comparison with *Xenopus* Antivin sequences (figure 6.12), there is approximately 69bp (or 23 amino acids) of sequence required to reach the 5' end.

```

1   CGCCTTCCCCCAGACGAGGTCAGGGACGCCCTGCTGCACAAGCTGGGGCTGCCCGAGGTGCCCCCGATCC 70
   R L P P D E V R D A L L H K L G L P E V P P I

71  AGAAGAGGGACCTACAGCGCTGCTCATCCCGATCACATCAAGACCCAGTACCCGGACATGCTGCGGCG 140
   Q K R D L Q R L L I P D H I K T Q Y P D M L R R

141 GCACCAGCAGAGCCGGAGGCGGGGAGCGCACTGCCAGCCTGACGGGCATCCTCAGGGGCATTCCGGGC 210
   H Q Q S R R R R S A L P S L T G I L R G I P G
   ▼

211 AATGCAGACATCTCCGGGAGGTGCTGTACTCAGACGCCAGTCGCCAGACCCCTGGTCTTCGACATGGAGG 280
   N A D I S G E V L Y S D A S R Q T L V F D M E

281 CCCTCATCCCCGAGAACAGCGAGGTGACCATGGCCGAGCTCAAGCTCTTCAAGAAGCCGCCAACCGCCT 350
   A L I P E N S E V T M A E L K L F K K P P N R L

351 CAGCATGCCGGACCGGCGTACCACCGCATGGTGAACAATGCGCGCGTCAGCGTCTACTGGGTGGAGGTG 420
   S M P D R R Y H R M V N N A R V S V Y W V E V

421 CAGCAGGACGGGGCAACAAGACCTCGCTCATCGACTCCAGGCTGGTGCCCATCATGGAGTCCGGTTGGA 490
   Q Q D G G N K T S L I D S R L V P I M E S G W

491 AGAGCTTTGACGTCACACAGGCCGTGCACTACTGGCTAAAGAACAAGAAGCCCATGTCCATGCACCTGGA 560
   K S F D V T Q A V H Y W L K N K K P M S M H L E

561 GGTGAAGATTGAGGGGGAGCGGCATGGCAGCTACGCCCTCGGACATGGCCAAGTTTGTGCGCTTACCTCA 630
   V K I E G E R H G S Y A S D M A K F V R F T S

631 CAAGATCTATCGGACAAGGCCCTGGGGAGGCCCGAGCTGGTGCTTTACACCCTGAACCTGGAGGAACACG 700
   Q D L S D K A L G R P E L V L Y T L N L E E H
   ▼

701 GTGCACGCGGGGACTGCGAGGAGATATCCGCCAAACAGAGCAACGTCTGCTGCGAGGCAGGAGTACTTCAT 770
   G A R G D C E E I S A K Q S N V C C R Q E Y F I

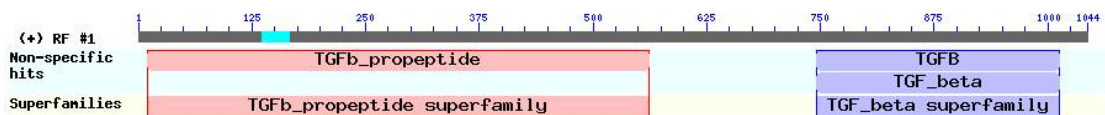
771 CAACTTCCGGGAGCTGACTTGGACCCAGTACTGGATCATAGAGCCGGCGGGCTACCAGGCCTTCCGGTGC 840
   N F R E L T W T Q Y W I I E P A G Y Q A F R C

841 GTGGGCGGCTGCAAGCAGCTCAAGAGCCCGTGCGGCACTTCGGCTACGGCGAGCGGACGTGCGCCGTGG 910
   V G G C K Q L K S P L R H F G Y G E R T C A V

911 TGGAGAGCGCGCCGCTCCCCATGATGTACCTGGTCAAGAAGGGCAACTACACGGAGATCGAGGTGGCCGA 980
   V E S A P L P M M Y L V K K G N Y T E I E V A E

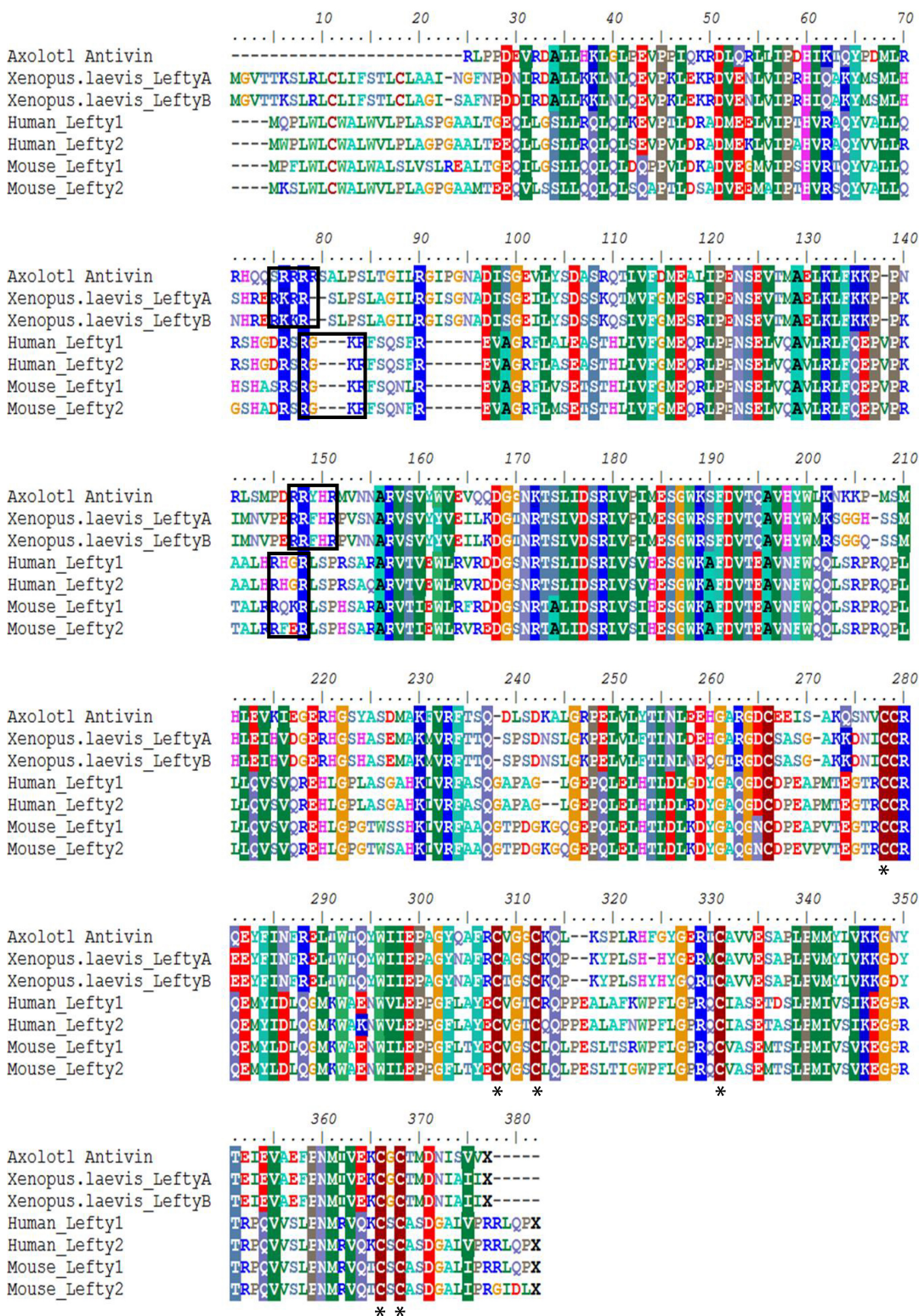
981 ATTCCCCAACATGATCGTGAGAAATGTGGCTGCACTATGGACAACATCTCCGTGGTGTGA 1041
   F P N M I V E K C G C T M D N I S V V *
    
```

(a)



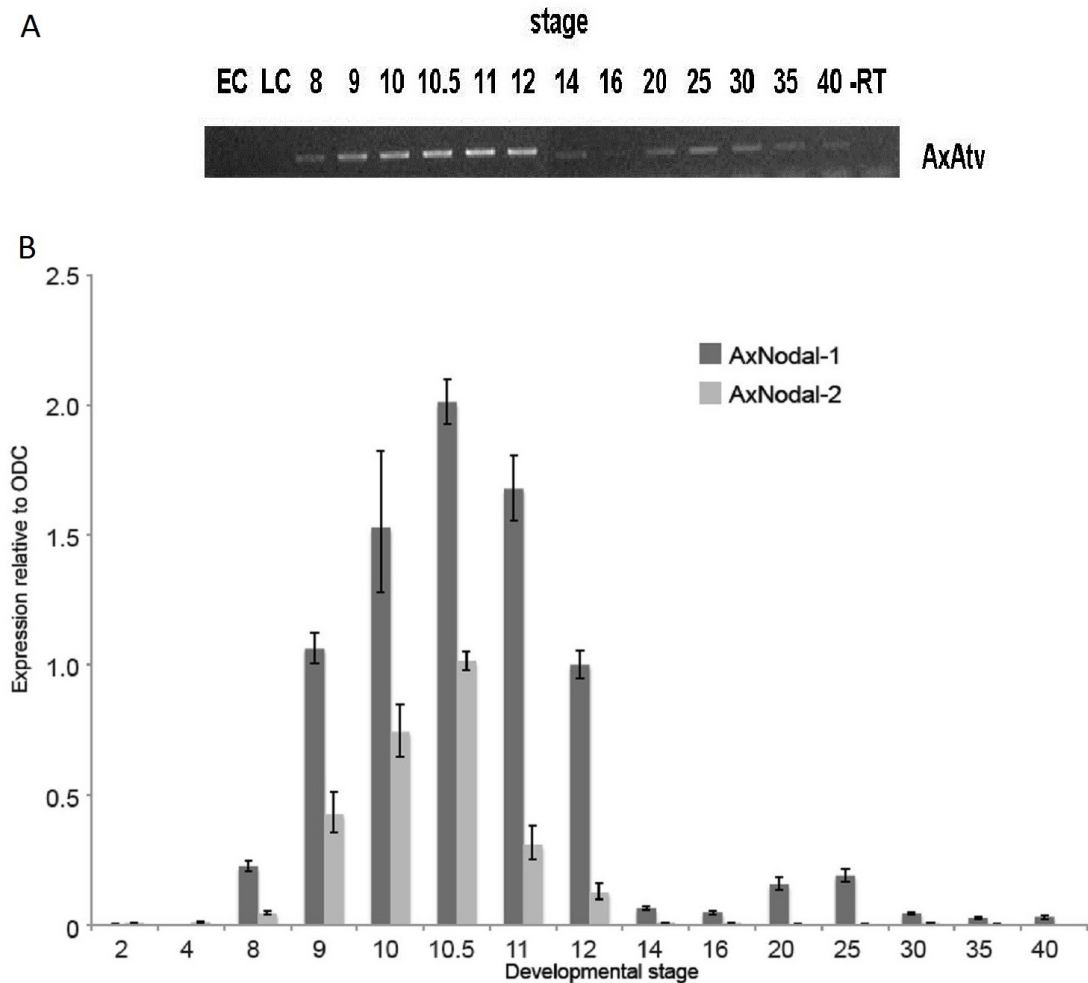
(b)

**Figure 6.11:** (a) The nucleotide sequence, and predicted translated sequence of our axolotl Antivn fragment. Numbers indicate the nucleotide position. \* marks the stop codon. Orange arrows indicate positions of introns, conserved cysteines are underlined and black boxes mark possible RXXR cleavage sites. (b) The conserved domain prediction using NCBI blast indicates that the sequence is a member of the TGF- $\beta$  superfamily.



**Figure 6.12:** Protein alignments of Antivin/Lefty sequences from axolotl, *Xenopus*, human and mouse. Coloured boxes highlight conserved amino acids. Black boxes indicate RXXR cleavage sites and asterisks (\*) mark conserved cysteines.

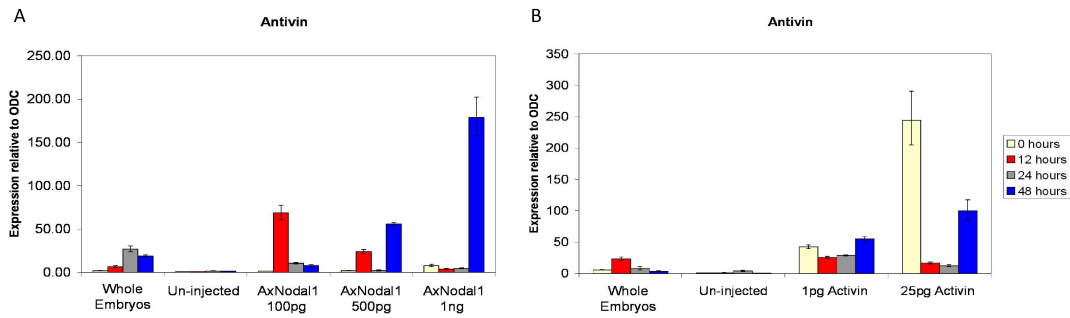




**Figure 6.13:** **A** Temporal expression pattern of AxAntivin. RT-PCR at various developmental stages, according to [8]. Transcripts are first expressed at stage 8 and peak at gastrula stages. RT-PCR primers were designed in predicted exon4 of AxAntivin. EC = early cleavage, LC = late cleavage. **B** The expression of AxNodal1 and AxNodal2 in axolotl at various developmental stages, taken from [139].

### 6.3.2 Expression of *Antivin*

To investigate the temporal expression of *Antivin* at stages of axolotl development, we designed primers and analysed expression using RT-PCR (figure 6.13A). *Antivin* is not detected during early cleavage or late cleavage, showing that it is not expressed maternally. *Antivin* is first detected at stage 8, when zygotic transcription commences, and is still expressed at stage 40. Expression levels peak at gastrula stages (stages 10-12), and a smaller peak in expression occurs at stages 20/25. The expression pattern of *Antivin* follow a similar pattern to qPCR data for the expression of *Nodal1* given in [139] (shown in figure 6.13B). In addition *Antivin* expression in axolotl is similar to the expression of *Antivin* in *Xenopus* [142]. The two peaks in the expression of *Antivin* and *Nodal* in axolotl embryos, with the peak at gastrula stages corresponding to the role of *Antivin* and *Nodal* in mesoderm induction and the peak at tailbud stages corresponding to the role in left-right axis determination.



**Figure 6.14: qPCR analysis of *Antivin* gene expression in response to (A) *AxNodal1* and (B) *Activin*.** Caps were collected at the equivalent to stage 9 (0 hours), then 12, 24 and 48 hours later. Gene expression levels are relative to ODC, then normalised to each gene in uninjected caps at 0 hours.

### 6.3.3 *Antivin* expression in *Nodal1* and *Activin* injected animal caps.

Recall that in chapter 4 we obtained quantitative gene expression data for important genes in the mesendoderm GRN in axolotl animal caps overexpressing *Nodal1* and *Activin*. We designed qPCR primers and a probe based on the axolotl *Antivin* sequence to measure relative expression of *Antivin* in these samples (figure 6.14). We find that in both the *Nodal*-injected and *Activin*-injected the expression of *Antivin* varies over time, with the highest levels of expression found in the caps treated with the highest dose of *Nodal1*/*Activin*. A possible reason for the variation in *Antivin* over time is that it is induced by *Nodal*, but also acts as a *Nodal* signalling agonist. To further explore the induction of *Antivin* by *Nodal* in axolotl, this data could be used to estimate parameters in a single cell model of *Nodal* signalling and the resulting model analysed. Preliminary results whereby we ran the parameter estimation algorithm (described in chapter 4) to fit the mathematical model of *Nodal* signalling to data for the expression of *Nodal* and *Antivin* in *Nodal*-injected caps were of limited success, as the resulting model could not fully reproduce experimental data (not shown). Since the expression of *Antivin* in *Nodal*-injected caps is rather dynamic, collected data on a more detailed timecourse may aid future work in estimating parameter values for *Nodal* signalling. Further experimental data would also elucidate how *Antivin* functions in axolotl and differences between *Activin* and *Nodal* signalling. This data will also aid further mathematical analysis.

## 6.4 Mathematical models of mesendoderm formation in a grid of cells

### 6.4.1 Motivation

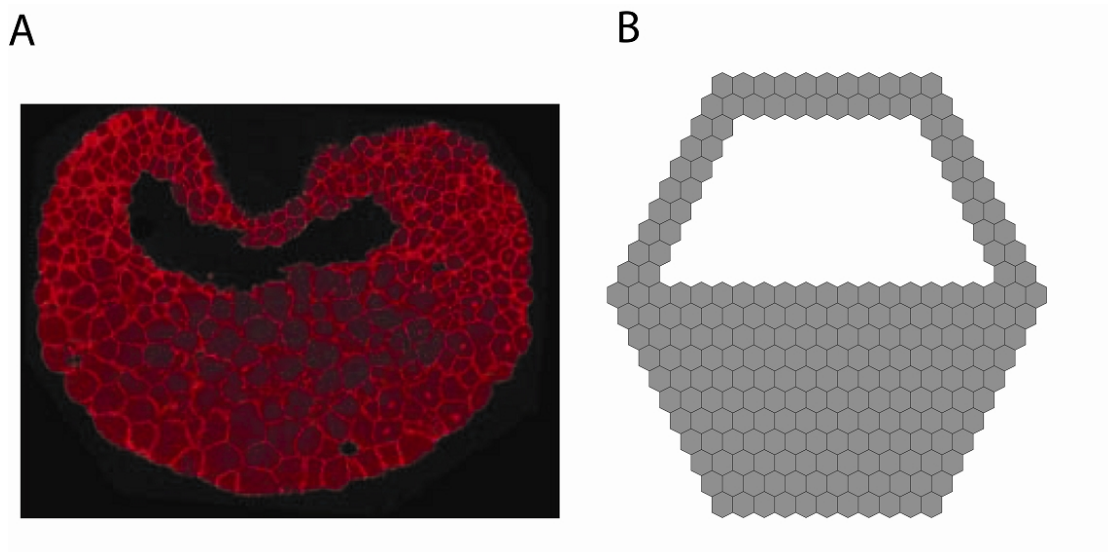
The models of the axolotl mesendoderm GRN explored in chapters 3 and 4, and the models of the simplified *Xenopus* mesendoderm GRN in [95] and chapter 5, represent the network within a single cell. These models do not consider the spread of signals throughout the embryo by cell

to cell communication, or the dynamics of the signalling pathway. Instead, in the single cell models, signals are assumed to act directly on their targets (in the same way as transcription factors). Mathematical models of the simplified *Xenopus* mesendoderm GRN in a line of cells are formulated in [94]. These models explore extracellular protein interactions and the spread of signals throughout a line of cells (see section 6.1 for more details).

Embryos are three dimensional structures, with cells differentiating along different axes, i.e. along the animal-vegetal and dorsal-ventral axes. Whilst mesoderm, endoderm and ectoderm form along the animal-vegetal axis of the embryo, on the dorsal side anterior mesendoderm lies between mesoderm and endoderm but is not found in ventral regions (see figure 5.1). In the previous chapter, it was shown that including dorsal-ventral patterning in a model of the *Xenopus* mesendoderm GRN can account for mesoderm and endoderm formation in both dorsal and ventral regions of the embryo. The models formulated in chapter 5 are in a single cell and do not include extracellular regulation, such as the binding of BMP to Chordin, which make the BMP ligand unable to bind to its receptors. With the overall aim of formulating a model of the *Xenopus* mesendoderm GRN including DV patterning and extracellular protein interactions in a two-dimensional grid of cells, we formulate and investigate models of the mesendoderm GRN in a grid of cells. These two-dimensional models are an immediate extension to the *Xenopus* and *axolotl* mesendoderm models in a line of cells, which are modified to allow for extracellular ligands diffusing within the grid of cells.

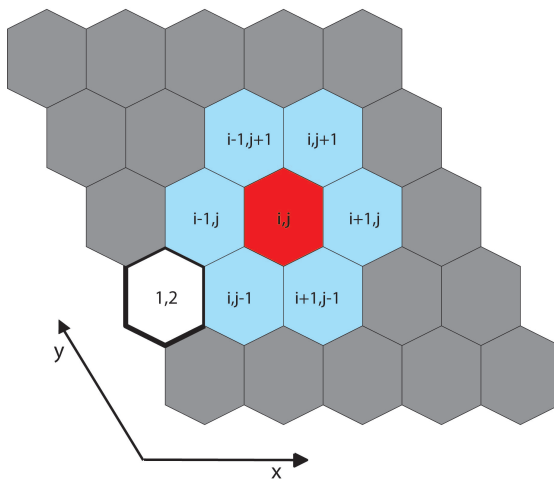
## 6.5 The *Xenopus* mesendoderm GRN in a two-dimensional grid of cells

During the development of a *Xenopus* embryo significant changes occur to its structure. An embryo starts as a single cell, which undergoes several rounds of cell division to become a multicellular organism. The morphogenic movements of gastrulation commence at stage 10.5. During gastrulation, epiboly occurs whereby cells of the prospective ectoderm move and expand to enclose the entire embryo and mesoderm becomes internalised [41]. The cell movements of gastrulation and epiboly may well be important for correct germ layer specification, as they occur at the same time as mesoderm and endoderm form. For simplicity we assume that cells do not move in our model of an embryo and base the spatial organisation on that of a stage 9 *Xenopus* embryo (see figure 6.15A). This is a reasonable assumption since, during the timescales during which mesendoderm forms, the neighbours of each cell are likely to not change significantly. The centre of the animal hemisphere consists of a fluid filled cavity known as the blastocoel. By definition, animal cap cells are found above the blastocoel, and vegetal cells are located below the blastocoel in the vegetal hemisphere. The blastocoel is known to have two functions; it allows the movements which occur at gastrulation and prevents signals from the vegetal hemisphere from reaching animal cap cells [41]. Note that there is a difference in size between the animal cap and vegetal cells with vegetal cells being larger. For simplicity, we will assume that all cells in the model embryo are the same size and shape. We choose to construct the model of the



**Figure 6.15:** (A) A cryosection of a stage 9 *Xenopus* embryo showing cellular organisation and geometry, taken from Schohl and Fagotto, *Development*, 2007 [126]. (B) A representation of the geometry of a stage 9 *Xenopus* embryo assuming uniformly sized cells represented by regular hexagons. The number of cells across the vegetal hemisphere in our representation is approximately the same as in the cryosection.

embryo using hexagonal cells rather than square cells since the cells of the *Xenopus* embryo can be well approximated using a hexagonal geometry. Based on these assumptions, we construct the ‘model embryo’ as shown in figure 6.15B, where the animal cap, which consists of a two cell thick layer, sits on top of the blastocoel (a region with no cells) and the bottom half of the embryo consists of vegetal cells.



**Figure 6.16:** The labeling system we use for a grid of hexagonal cells. Cell  $(i, j)$  is highlighted in red, with its six nearest neighbours highlighted in blue. The labelling we use is similar to that used to label a square lattice. Cell  $(i = 1, j = 2)$  is labelled for an illustration of boundary conditions (see main text).

Signalling molecules are secreted by cells, diffuse throughout the extracellular space and bind to membrane bound receptors. We introduce coupling between cells such that signals can dif-

**Figure 6.17:** A cartoon showing the spatial patterns of P-Smad2 in *Xenopus* embryos. Dorsal is on the right hand side of the sections. Red marks the strongest signal and pale yellow makes weak signal. Figure taken from [126].

fuse to a cells nearest neighbours (where each hexagon has six nearest neighbours as shown in figure 6.16). For a protein  $X$ , which diffuses throughout the domain, the concentration of  $X$  in cell  $(i, j)$  is given by

$$\frac{d\mathbf{X}_{i,j}}{dt} = \sigma_x \Delta \mathbf{X}_{i,j} \quad (6.5.1)$$

where

$$\Delta \mathbf{X}_{i,j} = -6\mathbf{X}_{i,j} + \mathbf{X}_{i-1,j} + \mathbf{X}_{i-1,j+1} + \mathbf{X}_{i,j+1} + \mathbf{X}_{i+1,j} + \mathbf{X}_{i+1,j-1} + \mathbf{X}_{i,j-1}, \quad (6.5.2)$$

and  $\sigma_x$  is the strength of coupling between cells. Boundary conditions are defined such that for cells on the edge of the grid extracellular molecules do not leave the embryo, i.e. there is no flux at the boundary. For example for cell  $(1, 2)$ , as labelled in figure 6.16, has four neighbouring cells and  $\Delta \mathbf{X}_{i,j}$  is given by

$$\Delta \mathbf{X}_{1,2} = -4\mathbf{X}_{1,2} + \mathbf{X}_{2,2} + \mathbf{X}_{1,1} + \mathbf{X}_{1,3} + \mathbf{X}_{2,3}. \quad (6.5.3)$$

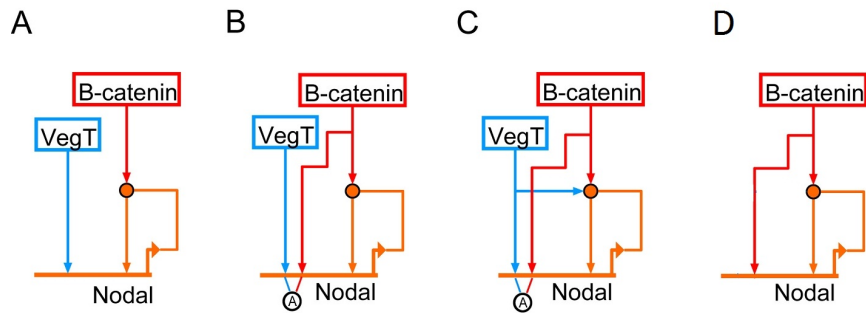
In this section we have introduced a grid of hexagonal cells as a suitable approximation for cells in a *Xenopus* embryo, and defined equations for the spread of a protein throughout the grid. We now proceed to extend the mesendoderm models given in a line of cells [94] and solve the resulting models in a grid of hexagonal cells. We start by considering a model of Nodal signalling.

## 6.6 The regulation of Nodal by VegT and $\beta$ -catenin

In this section we formulate and solve a model of Nodal signalling in a 2D grid of cells, to reproduce experimentally observed spatial patterns of P-Smad2. Figure 6.17 shows the spatial distribution of P-Smad2 in early stage *Xenopus* embryos between stages 8.5 and 10. At stage 8.5 P-Smad2 is expressed in a supraequatorial ring in a pattern similar to that of  $\beta$ -catenin. At stages 9 to 9.5, P-Smad2 expression is strongest dorsally, with activity throughout the vegetal hemisphere at stages 9.5/10. Note that this model is a two-dimensional generalisation of the one-dimensional model of Nodal signalling given in (6.2.4).

Recall that the Nodal genes are regulated by the maternal factors VegT and  $\beta$ -catenin in *Xenopus*. VegT induces the expression of Xnr1 and Xnr2 with the positive autoregulation of these Nodal genes enhanced by  $\beta$ -catenin. The induction of Xnr5 and Xnr6 requires both VegT and  $\beta$ -catenin. In axolotl, Nodal1 is induced by  $\beta$ -catenin alone. We explore different ways in which VegT and  $\beta$ -catenin regulate Nodal, and the resulting spatial patterns of P-Smad2. We choose four different ways of modelling the regulation of Nodal, as illustrated in figure 6.18:

1. VegT activates Nodal expression and  $\beta$ -catenin acts to enhance Nodal positive autoregu-



**Figure 6.18:** Methods by which VegT and  $\beta$ -catenin can regulate Nodal. **(A)** Nodal is activated by VegT alone, with  $\beta$ -catenin enhancing Nodal autoregulation. **(B)** Both VegT and  $\beta$ -catenin are required to activate Nodal, with  $\beta$ -catenin enhancing Nodal autoregulation. **(C)** Both VegT and  $\beta$ -catenin are required to activate Nodal, but either VegT and  $\beta$ -catenin can enhance Nodal autoregulation. **(D)**  $\beta$ -catenin are required is activate Nodal and also enhances Nodal autoregulation.

lation. This is how the *Xenopus* genes Xnr1 and Xnr2 are regulated.

2. Both VegT and  $\beta$ -catenin are required to activate Nodal and  $\beta$ -catenin or VegT can act to enhance Nodal positive autoregulation. This is similar to how Xnr5 and Xnr6 are regulated.
3. Both VegT and  $\beta$ -catenin are required to activate Nodal and  $\beta$ -catenin also acts to enhance Nodal positive autoregulation.
4.  $\beta$ -catenin activates Nodal and also acts to enhance Nodal positive autoregulation. This is how Nodal1 is regulated in axolotl.

The equations governing the concentrations of VegT and  $\beta$ -catenin ( $V_{i,j}$ ,  $C_{i,j}$ ), intracellular and extracellular Antivin ( $T_{i,j}^o$ ,  $T_{i,j}$ ), extracellular Nodal ( $N_{i,j}^o$ ), Antivin-Nodal heterodimer ( $T_{i,j}^\ddagger$ ), re-

ceptor complexes ( $R_{i,j}$ ,  $R_{i,j}^\circ$ ,  $R_{i,j}^{\circ\circ}$ ,  $R_{i,j}^\ddagger$ ) and P-Smad2 ( $P_{i,j}$ ) in cell ( $i, j$ ) are

$$\frac{dV_{i,j}}{dt} = -\mu_V V_{i,j}, \quad (6.6.1a)$$

$$\frac{dC_{i,j}}{dt} = -\mu_C C_{i,j}, \quad (6.6.1b)$$

$$\epsilon \frac{dT_{i,j}^o}{dt} = \sigma_T \Delta T_{i,j}^o + \nu \left( k_{-T} R_{i,j}^\ddagger - k_T T_{i,j}^o R_{i,j} \right) - l_T N_{i,j}^o T_{i,j}^o + l_{-T} T_{i,j}^\ddagger + \frac{\delta_T}{\rho} T_{i,j} - \mu_{T^o} T_{i,j}^o, \quad (6.6.1c)$$

$$\epsilon \frac{dN_{i,j}^o}{dt} = \sigma_N \Delta N_{i,j}^o + \frac{\nu}{\rho} \left( k_{-N} R_{i,j}^\circ - k_N N_{i,j}^o R_{i,j} \right) - l_T N_{i,j}^o T_{i,j}^o + l_{-T} T_{i,j}^\ddagger + \frac{\delta_N}{\rho} N_{i,j} - \mu_{N^o} N_{i,j}^o, \quad (6.6.1d)$$

$$\epsilon \frac{dT_{i,j}^\ddagger}{dt} = \sigma_{T^\ddagger} \Delta T_{i,j}^\ddagger + l_T N_{i,j}^o T_{i,j}^o - l_{-T} T_{i,j}^\ddagger - \mu_{T^\ddagger} T_{i,j}^\ddagger, \quad (6.6.1e)$$

$$\frac{dT_{i,j}}{dt} = \lambda_{P,T} \mathcal{H} \left( \frac{P_{i,j}}{\theta_{P,T}} \right) - (\mu_T + \delta_T) T_{i,j}, \quad (6.6.1f)$$

$$\epsilon \frac{dP_{i,j}}{dt} = k_p \nu R_{i,j}^{\circ\circ} - \mu_P P_{i,j}, \quad (6.6.1g)$$

$$\epsilon \frac{dR_{i,j}}{dt} = k_{-N} R_{i,j}^\circ - k_N N_{i,j}^o R_{i,j} + k_{-T} R_{i,j}^\ddagger - k_T T_{i,j}^o R_{i,j}, \quad (6.6.1h)$$

$$\epsilon \frac{dR_{i,j}^\circ}{dt} = k_N N_{i,j}^o R_{i,j} - k_{-N} R_{i,j}^\circ - k_s R_{i,j}^\circ S_{i,j} + (k_{-s} + k_p) R_{i,j}^{\circ\circ}, \quad (6.6.1i)$$

$$\epsilon \frac{dR_{i,j}^{\circ\circ}}{dt} = k_s R_{i,j}^\circ S_{i,j} - (k_{-s} + k_p) R_{i,j}^{\circ\circ}, \quad (6.6.1j)$$

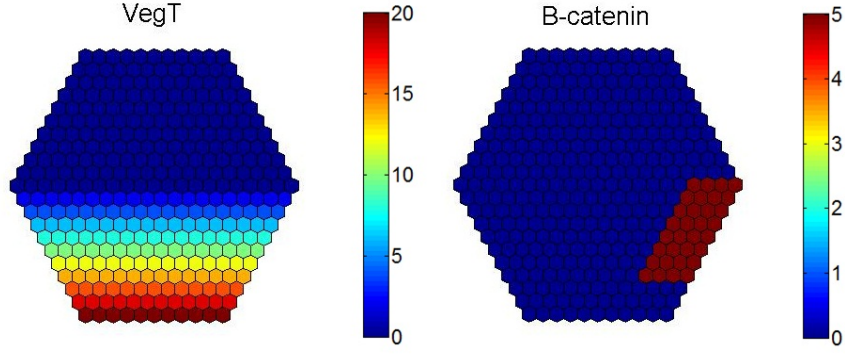
$$\epsilon \frac{dR_{i,j}^\ddagger}{dt} = -k_{-T} R_{i,j}^\ddagger + k_T T_{i,j}^o R_{i,j}. \quad (6.6.1k)$$

Terms of the form  $\Delta X_{i,j}$  are as defined in equation (6.5.2). The equation governing the concentration of intracellular Nodal ( $N_{i,j}$ ) in different cases is given in the next section. Note that the system given by (6.6.1) is identical to the model formulated in [94] (i.e. equation (6.1.5)) with variables  $X_i$  replaced by  $X_{i,j}$  and to allow movement of extracellular proteins and complexes in a 2D grid,  $\Delta X_i$  is replaced by  $\Delta X_{i,j}$ .

Initial conditions of VegT and  $\beta$ -catenin are defined to reproduce the experimentally observed localisation of VegT and  $\beta$ -catenin before zygotic transcription commences.  $\beta$ -catenin is found in dorsal regions at stages 8 to 8.5 [126] and maternal VegT is localised to the vegetal pole of developing embryos [138, 155]. We set the initial conditions of  $\beta$ -catenin such that it is expressed at a constant non-trivial level in dorsal marginal cells and absent from all other regions. VegT is set such that it is expressed in the vegetal hemisphere only, with its concentration highest at the vegetal pole. The initial conditions of VegT and  $\beta$ -catenin are illustrated in figure 6.19. All receptors are assumed to be free initially ( $R_{i,j}(0) = 1$ ,  $R_{i,j}^\circ(0) = 0$ ,  $R_{i,j}^{\circ\circ}(0) = 0$ ,  $R_{i,j}^\ddagger(0) = 0$ ), all Smad to be unphosphorylated ( $P_{i,j}(0) = 0$ ) and all other factors to be absent ( $T_{i,j}^o(0) = 0$ ,  $T_{i,j}(0) = 0$ ,  $N_{i,j}^o(0) = 0$ ,  $N_{i,j}(0) = 0$ ,  $T^\ddagger(0) = 0$ ).

### Equations for the time evolution of intracellular Nodal

For each mode of Nodal regulation by VegT and  $\beta$ -catenin described above, we introduce an



**Figure 6.19:** Plot of initial conditions of VegT and  $\beta$ -catenin used to solve (6.6.1). VegT is localised to the vegetal hemisphere and  $\beta$ -catenin is restricted to dorsal cells.

equation for the time evolution of intracellular Nodal. In figure 6.18A, VegT activates Nodal expression and  $\beta$ -catenin acts to enhance Nodal positive autoregulation

$$\frac{dN_{i,j}}{dt} = \lambda_{V,N} \mathcal{H} \left( \frac{V_{i,j}}{\theta_{V,N}} \right) + \lambda_{P,N} \mathcal{H} \left( \frac{P_{i,j}}{\theta_{P,N}} \right) \left\{ 1 + \lambda_{C,N} \mathcal{H} \left( \frac{C_{i,j}}{\theta_{C,N}} \right) \right\} - (\mu_N + \delta_N) N_{i,j}. \quad (6.6.2)$$

In figure 6.18B, both VegT and  $\beta$ -catenin are required to activate Nodal and  $\beta$ -catenin or VegT can act to enhance Nodal positive autoregulation

$$\frac{dN_{i,j}}{dt} = \lambda_{V,N} \mathcal{H} \left( \frac{V_{i,j}}{\theta_{V,N}} \right) \mathcal{H} \left( \frac{C_{i,j}}{\theta_{C_2,N}} \right) + \lambda_{P,N} \mathcal{H} \left( \frac{P_{i,j}}{\theta_{P,N}} \right) \left\{ 1 + \lambda_{C,N} \mathcal{H} \left( \frac{C_{i,j}}{\theta_{C,N}} \right) \right\} - (\mu_N + \delta_N) N_{i,j}. \quad (6.6.3)$$

In figure 6.18C, both VegT and  $\beta$ -catenin are required to activate Nodal and  $\beta$ -catenin also acts to enhance Nodal positive autoregulation

$$\begin{aligned} \frac{dN_{i,j}}{dt} = & \lambda_{V,N} \mathcal{H} \left( \frac{V_{i,j}}{\theta_{V,N}} \right) \mathcal{H} \left( \frac{C_{i,j}}{\theta_{C_2,N}} \right) \\ & + \lambda_{P,N} \mathcal{H} \left( \frac{P_{i,j}}{\theta_{P,N}} \right) \left\{ 1 + \lambda_{C,N} \mathcal{H} \left( \frac{C_{i,j}}{\theta_{C,N}} \right) + \lambda_{V_2,N} \mathcal{H} \left( \frac{V_{i,j}}{\theta_{V_2,N}} \right) \right\} - (\mu_N + \delta_N) N_{i,j}. \end{aligned} \quad (6.6.4)$$

In figure 6.18D,  $\beta$ -catenin activates Nodal and also acts to enhance Nodal positive autoregulation

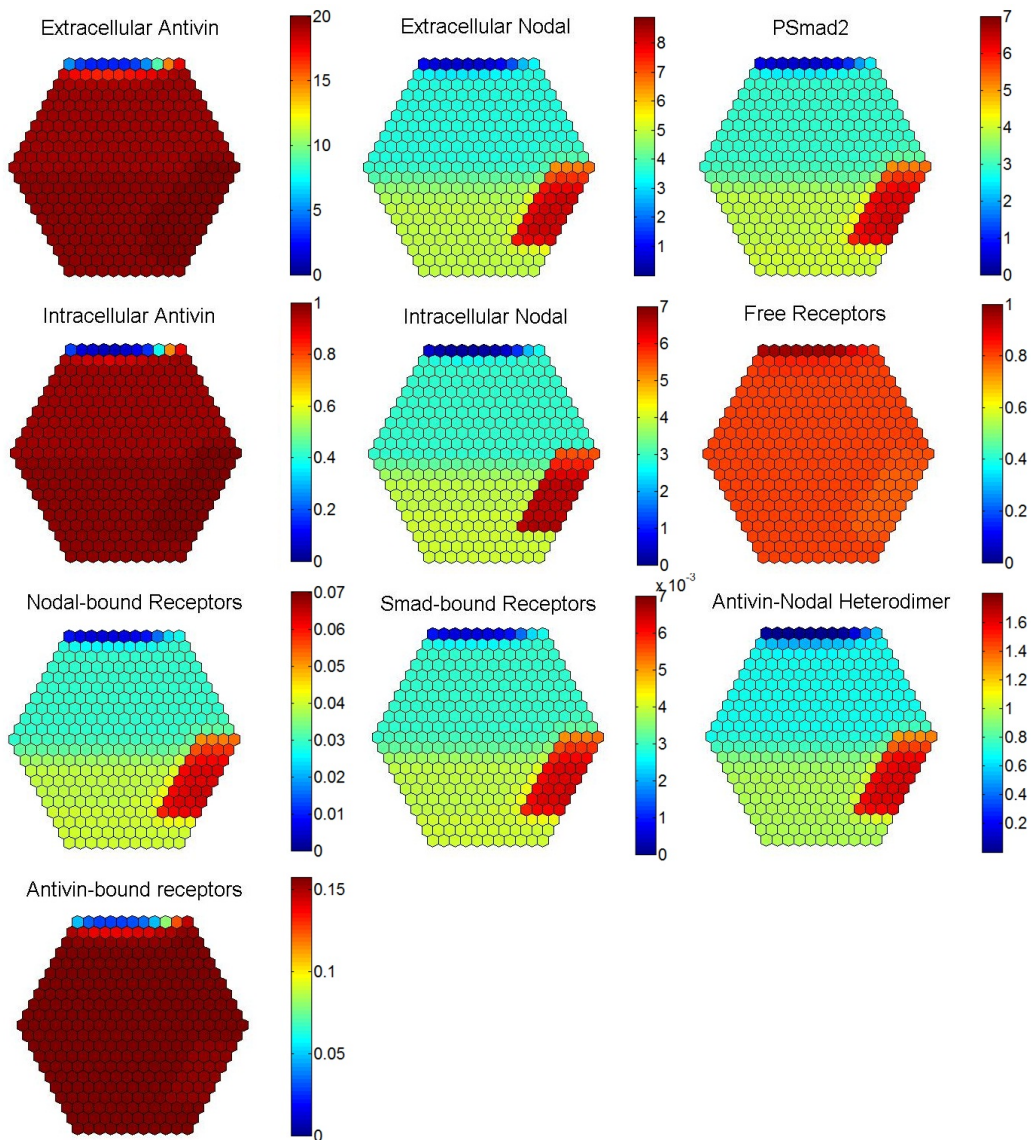
$$\frac{dN_{i,j}}{dt} = \lambda_{C,N} \mathcal{H} \left( \frac{C_{i,j}}{\theta_{P,N}} \right) + \lambda_{P,N} \mathcal{H} \left( \frac{P_{i,j}}{\theta_{P,N}} \right) \left\{ 1 + \lambda_{C,N} \mathcal{H} \left( \frac{C_{i,j}}{\theta_{C,N}} \right) \right\} - (\mu_N + \delta_N) N_{i,j}. \quad (6.6.5)$$

In equations (6.6.5)-(6.6.5),  $V_i$ ,  $C_i$  and  $P_i$  are defined by solutions to (6.6.1).

### 6.6.1 Numerical solutions

We seek solutions to the Nodal signalling model (equation (6.6.1)) for the different modes of Nodal regulation described above (equations (6.6.2)-(6.6.5)). The grid of cells represents cells on the outer surface of the embryo, rather than a cross section through the embryo, so there is no

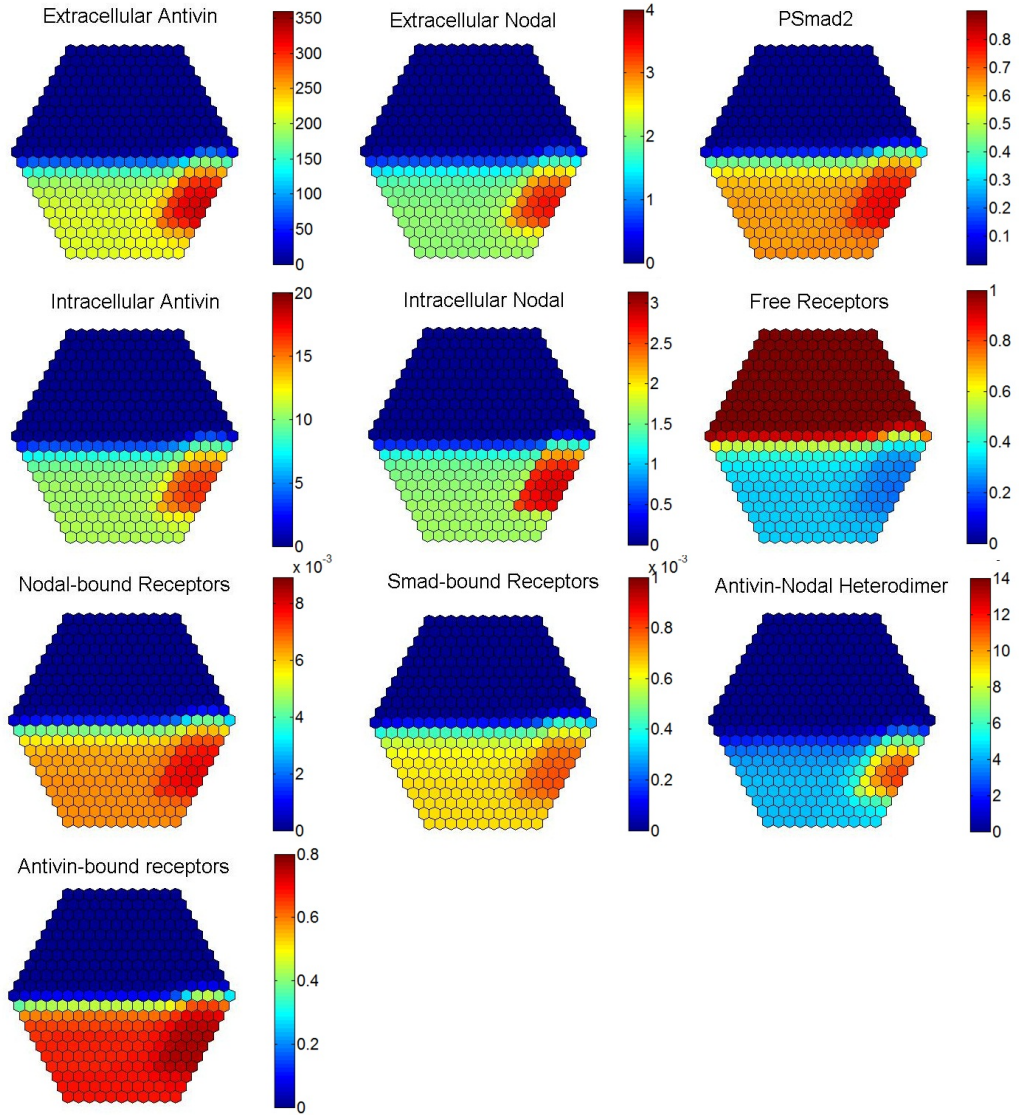




**Figure 6.20:** Numerical solutions to (6.6.1) and (6.6.2) at  $\tau = 100$ , subject to the initial conditions shown in figure 6.19. In this model VegT is required to activate the transcription of Nodal,  $\beta$ -catenin acts to enhance Nodal autoregulation and  $\lambda_{p,A} = 1$  such that Nodal can spread throughout the embryo. Antivin and Nodal have spread throughout the embryo, with levels of Nodal (and P-Smad1) highest in dorsal regions where  $\beta$ -catenin is expressed. Unless otherwise stated parameters used are as in table 6.4.

hole corresponding to the blastocoel. Each model is solved subject to two different parameter sets, one corresponding to the pinning of Nodal by Antivin (‘pinned case’) and the other where Nodal can spread (‘spreading case’).

Initial conditions used to solve (6.6.1) and (6.6.2)-(6.6.5) are shown in figure 6.19. VegT is expressed in the bottom half of the grid (representing the vegetal half of the embryo), in a gradient with expression highest in the vegetal most row of cells and lowest in the row of cells in the middle of the grid.  $\beta$ -catenin is expressed in a group of cells in the dorsal region of the embryo.



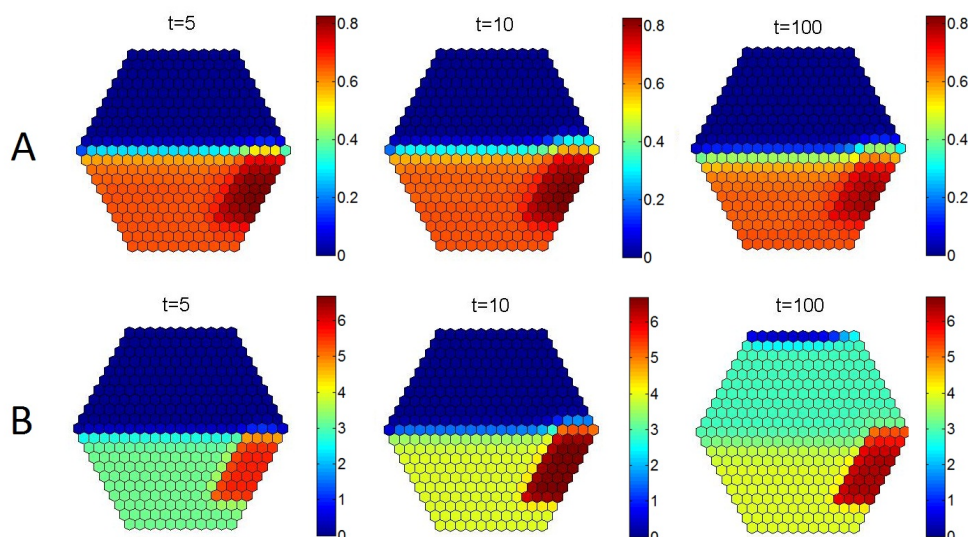
**Figure 6.21:** Numerical solutions to (6.6.1) and (6.6.2) at  $\tau = 100$ , subject to the initial conditions shown in figure 6.19. In this model VegT and is required to activate the transcription of Nodal,  $\beta$ -catenin acts to enhance Nodal autoregulation and  $\lambda_{P,A} = 50$  such that Antivin prevents the spread of Nodal throughout the embryo. Antivin and Nodal have spread throughout the embryo, with levels of Nodal (and P-Smad1) highest in dorsal regions where  $\beta$ -catenin is expressed. Unless otherwise stated parameters used are as in table 6.4.

Solutions to all variables of (6.6.1) and (6.6.2) are plotted in figures 6.20 and 6.21, for cases representing the spread and the pinning of Nodal, respectively. In the spreading case (figure 6.20), Nodal and Antivin are expressed throughout the embryo at  $\tau = 60$ , with Nodal levels highest in dorsal regions (i.e. regions where  $\beta$ -catenin is expressed) and lowest in the animal half of the embryo (i.e. regions where VegT is not expressed). In the pinned case (figure 6.21), Antivin prevents Nodal from spreading throughout the embryo, such that Nodal is not expressed in regions more than one cell away from a  $\beta$ -catenin or VegT expressing cell. Note that in both fig-

Variable	Parameter	Value	Variable	Parameter	Value
N	$\lambda_{P,N}$	3	T	$\lambda_{P,T}$	12
	$\theta_{P,N}$	0.666		$\theta_{P,T}$	0.999
	$\lambda_{V,N}$	1		$\delta_T$	20
	$\theta_{V,N}$	1		$\mu_T$	1
	$\lambda_{C,N}$	1		$\sigma_T$	0.125
			$T^0$	$k_T$	1
				$k_{-T}$	100
				$\mu_{T^0}$	1
$N^0$	$k_N$	1	P	$k_P$	10
	$k_{-N}$	100		$\mu_P$	0.01
	$\mu_{N^0}$	1		$\bar{v}$	1
$T^\ddagger$	$l_T$	1	S	S	1
	$l_{-T}$	100		$k_S$	1
	$\mu_{T^\ddagger}$	0		$k_{-S}$	0.01
V	$\mu_V$	0.01	C	$\mu_C$	0.01

**Table 6.4:** Dimensionless parameters used to solve (6.6.1) with (6.6.2)-(6.6.5). Parameter are as used in [94], selected such that in a single cell model (6.6.1) with (6.6.2)-(6.6.5) is bistable with steady states corresponding to mesoderm and anterior mesendoderm.

ures 6.20 and 6.21, the patterns of concentration of all variables are similar to that of the output for P-Smad2. Therefore in what follows we plot numerical results for P-Smad2 only.



**Figure 6.22:** Numerical solutions to (6.6.1) and (6.6.2) showing the spatial distribution of P-Smad2 at  $\tau = 5$ ,  $\tau = 10$ ,  $\tau = 100$ , subject to the initial conditions shown in figure 6.19. In this model VegT and is required to activate the transcription of Nodal,  $\beta$ -catenin acts to enhance Nodal autoregulation and **(A)**  $\lambda_{P,A} = 50$  such that Antivin prevents the spread of Nodal throughout the embryo and **(B)**  $\lambda_{P,A} = 1$  such that Nodal spreads throughout the embryo. Unless otherwise stated parameters used are as in table 6.4.

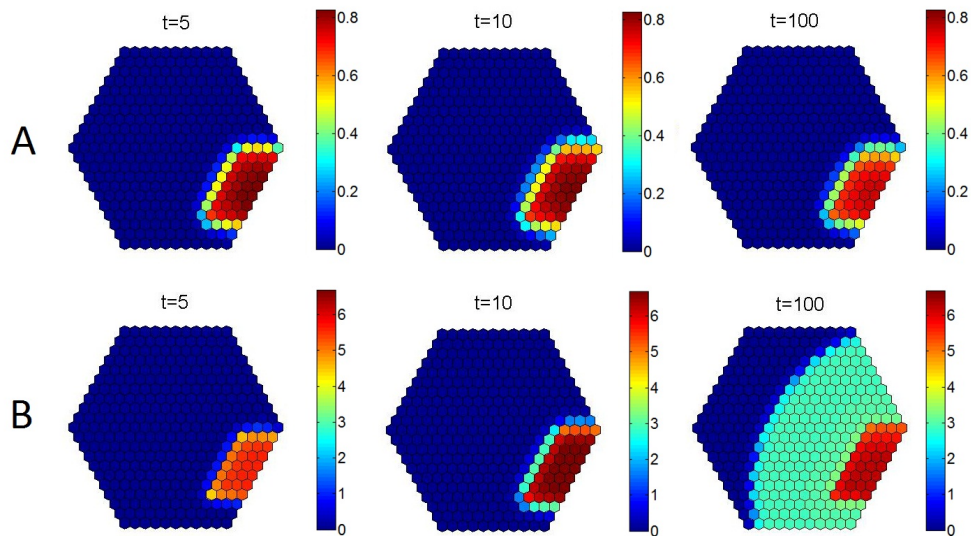
Figure 6.22 shows the spatial patterns of P-Smad2 in a model given by (6.6.1) and (6.6.2) where VegT activates Nodal and  $\beta$ -catenin enhances Nodal positive autoregulation. This regulation of Nodal is as occurs *in vivo* for Xnr1 and Xnr2 in *Xenopus*. In both cases P-Smad2 is not found in the embryo at  $t = 0$ , as defined by the initial conditions. In the ‘spreading case’ Smad2 becomes phosphorylated throughout the vegetal hemisphere (see  $t = 5$ ) with highest concen-

trations found in dorsal regions overlapping with the expression of  $\beta$ -catenin. At later times, as Nodal spreads into the animal cap, Smad2 becomes phosphorylated in this region. By  $t = 100$ , P-Smad2 is found throughout the embryo, with strongest levels found dorsally. In the ‘pinned case’ P-Smad2 is expressed throughout the vegetal hemisphere, with slightly stronger expression in the dorsal marginal zone. In this case P-Smad2 does not spread into the animal cap, consistent with the fact Antivin prevents the spread of extracellular Nodal. As the levels of VegT and  $\beta$ -catenin decay over time, the levels of P-Smad2 also decrease.

Figure 6.23 shows the spatial patterns of P-Smad2 in a model given by (6.6.1) and (6.6.3) where both VegT and  $\beta$ -catenin are required to activate Nodal, as is the case with Xnr5 and Xnr6 in *Xenopus*. In this model  $\beta$ -catenin also acts to enhance Nodal autoregulation. In the ‘spreading case’ Nodal is induced by  $\beta$ -catenin and VegT in dorsal regions, such that Smad2 becomes phosphorylated in this region. As Nodal spreads throughout the embryo, the number of cells where Smad2 is phosphorylated also increases until P-Smad2 is found in all cells of the embryo. In the ‘pinned case’ P-Smad2 is restricted to the dorsal cells where  $\beta$ -catenin is expressed, and is also found at low levels in the cells neighbouring this region. This is similar to the expression pattern of P-Smad2 seen in stage 9 *Xenopus* embryos. Recall from the timing of the expression of the Nodal genes in *Xenopus* (see figure 3.18) that Xnr5/6 are expressed from the MBT until stage 9 and Xnr1/2 expression commences at stage 9 and is maintained until stage 11. Therefore the expression of P-Smad2 at stage 9 is likely to be caused by Xnr5/6 signalling.

In figure 6.24 both VegT and  $\beta$ -catenin are required to induce the expression of Nodal and either VegT or  $\beta$ -catenin can enhance the positive autoregulation of Nodal as given by (6.6.1) and (6.6.4). In the ‘spreading case’ extracellular Nodal is secreted from cells in the dorsal marginal zone, and spreads from this region, as marked by P-Smad2. Note that, when compared with the case where only  $\beta$ -catenin can enhance Nodal autoregulation (figure 6.23), we find that Nodal spreads more rapidly throughout the vegetal hemisphere when VegT also enhances Nodal autoregulation. By  $t = 10$  P-Smad2 is found throughout the vegetal hemisphere but has yet to spread into the animal cap. At later times P-Smad2 is found in all cells. In the ‘pinned case’ P-Smad2 is highest in dorsal cells, and is found in cells neighbouring this region, but does not spread throughout the embryo.

Figure 6.25 shows the expression of P-Smad2 in a model given by (6.6.1) and (6.6.5) where  $\beta$ -catenin induces Nodal and also acts to enhance Nodal autoregulation. Note that in this model VegT does not act on Nodal signalling. This is what is thought to happen for Nodal1 in axolotl, where only  $\beta$ -catenin is required to induce Nodal1 for mesendoderm induction. In the ‘spreading case’ P-Smad2 is strongest in  $\beta$ -catenin expressing cells, and as time proceeds, Nodal spreads and Smad2 phosphorylation spreads throughout the embryo. In the ‘pinned case’ P-Smad2 is restricted to dorsal regions. The expression patterns for P-Smad2 have not been measured experimentally, meaning our models give predictions about the spatial pattern of P-Smad2 in axolotl embryos. Our attempts to measure the localisation of P-Smad2 in axolotl embryos, using immunohistochemistry following a protocol similar to that given in [83], have been unsuccessful so far.

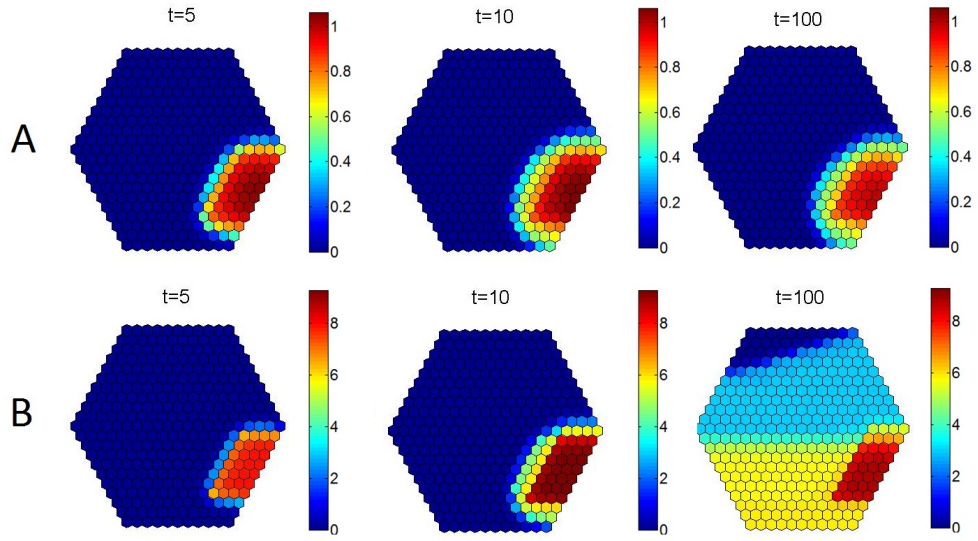


**Figure 6.23:** Numerical solutions to (6.6.1) and (6.6.3) showing the spatial distribution of P-Smad2 at  $\tau = 5$ ,  $\tau = 10$ ,  $\tau = 100$ , subject to the initial conditions shown in figure 6.19. In this model VegT and  $\beta$ -catenin are both required to activate the transcription of Nodal,  $\beta$ -catenin acts to enhance Nodal autoregulation and **(A)**  $\lambda_{P,A} = 50$  such that Antivin prevents the spread of Nodal throughout the embryo and **(B)**  $\lambda_{P,A} = 1$  such that Nodal spreads throughout the embryo. Unless otherwise stated parameters used are as in table 6.4.

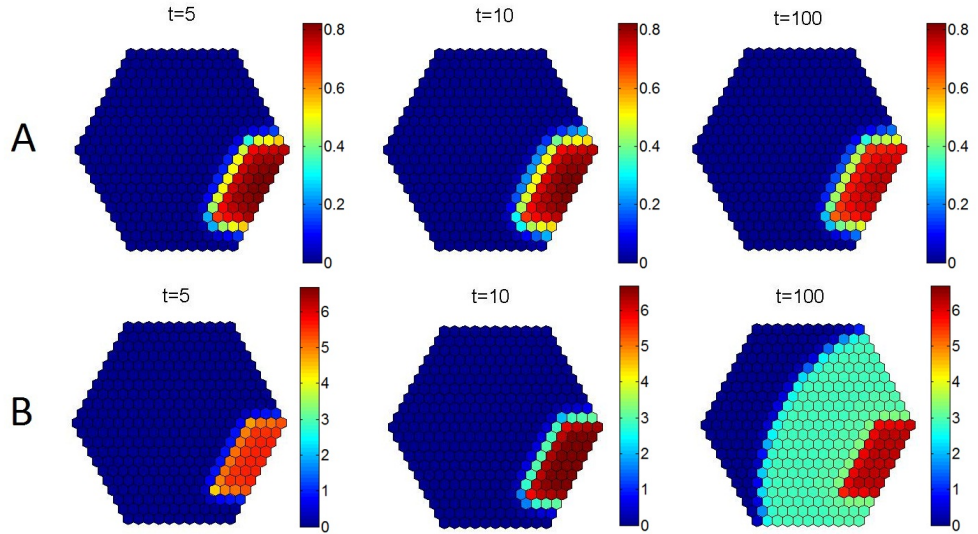
## 6.6.2 Summary

In this section mathematical models of Nodal signalling, and its induction by VegT and  $\beta$ -catenin, were explored in a two dimensional grid of hexagonal cells. Four different models were considered, based on how different Nodal genes are regulated in *Xenopus* and axolotl according to experimental evidence. Each model was solved in two cases; (1) where Nodal can spread throughout the embryo ('spreading') and (2) where Antivin restricts the spread of Nodal ('pinned'). In *Xenopus* Nodal is only expressed one or two cell diameters from its source, except when Antivin is knocked out and then Nodal spreads throughout the field of cells [14]. Therefore the solutions in the pinned case are likely to represent wild type behaviour, and solutions to the spreading case represent behaviour where expression of Antivin is reduced.

The model representing the regulation of Xnr5/6 is able to reproduce the pattern of P-Smad2 localisation in stage 9 *Xenopus* embryos where P-Smad2 is predominantly found in dorsal regions (compare figures 6.23 and 6.17). The pattern of P-Smad2 localisation in stage 9.5 *Xenopus* embryos where P-Smad2 is throughout the vegetal hemisphere with expression highest dorsally is reproduced by the model representing the regulation of Xnr1/2 (compare figures 6.22 and 6.17). These findings are expected when considering the timing of the expression of Nodal genes in *Xenopus*. Xnr5 and Xnr6 are the first Nodal genes involved in mesendoderm formation to be expressed, being present from stage 8 until just after stage 9. Xnr1 and Xnr2 expression commences at stage 9 and is maintained throughout gastrulation. Therefore we expect that the pattern of P-Smad2 found in stage 9 embryos is due to Xnr5/6 and the pattern of P-Smad2 in



**Figure 6.24:** Numerical solutions to (6.6.1) and (6.6.4) showing the spatial distribution of P-Smad2 at  $\tau = 5$ ,  $\tau = 10$ ,  $\tau = 60$ , subject to the initial conditions shown in figure 6.19. In this model VegT and  $\beta$ -catenin are both required to activate the transcription of Nodal,  $\beta$ -catenin or VegT can act to enhance Nodal autoregulation and **(A)**  $\lambda_{p,A} = 50$  such that Antivin prevents the spread of Nodal throughout the embryo and **(B)**  $\lambda_{p,A} = 1$  such that Nodal spreads throughout the embryo. Unless otherwise stated parameters used are as in table 6.4.



**Figure 6.25:** Numerical solutions to (6.6.1) and (6.6.5) showing the spatial distribution of P-Smad2 at  $\tau = 5$ ,  $\tau = 10$ ,  $\tau = 60$ , subject to the initial conditions shown in figure 6.19. In this model  $\beta$ -catenin is required to activate the transcription of Nodal,  $\beta$ -catenin also acts to enhance Nodal autoregulation and **(A)**  $\lambda_{p,A} = 50$  such that Antivin prevents the spread of Nodal throughout the embryo and **(B)**  $\lambda_{p,A} = 1$  such that Nodal spreads throughout the embryo. Unless otherwise stated parameters used are as in table 6.4.

stage 9.5 embryos is due to *Xnr1/2*, correlating to the timing of these signals in the embryo. Numerical solutions to the model representing the regulation of *Nodal1* in axolotl shows that P-Smad2 is present in  $\beta$ -catenin expressing cells, and cells within one or two cell diameters of a  $\beta$ -catenin expressing cell. The localisation of P-Smad2 has not been investigated successfully in axolotl embryos, meaning that the model gives a testable prediction for the pattern of P-Smad2 in hemisectioned axolotl embryos. In the next section, we extend the models of *Nodal* signalling to include factors downstream of P-Smad2, such as *Mix*, *Brachyury* and *Goosecoid*.

## 6.7 A multicellular model of the *Xenopus* mesendoderm GRN

The mathematical model of the mesendoderm GRN downstream of *Nodal* is also extended into a two-dimensional grid of cells. To do this, we take (6.2.5) and replace variables  $X_i$  with  $X_{i,j}$  and  $\Delta X_i$  with  $\Delta X_{i,j}$  to allow movement of extracellular proteins and complexes in a 2D grid. The non-dimensional equations governing the mesendoderm downstream of *Nodal* are then given by

$$\epsilon \frac{dE_{i,j}^o}{d\tau} = \sigma_E \Delta E_{i,j} + \delta_E E_{i,j} - \bar{v} \left( k_E E_{i,j}^o - k_{-E} F_{i,j}^\diamond \right) - \mu_{E^o} E_{i,j}^o, \quad (6.7.1a)$$

$$\frac{dE_{i,j}}{d\tau} = \lambda_{B,E} \mathcal{H}(B_{i,j}) - \mu_E E_{i,j}, \quad (6.7.1b)$$

$$\epsilon \frac{dK_{i,j}^*}{d\tau} = \nu k_{K^*} F_{i,j}^{\diamond\diamond} - \mu_{K^*} K_{i,j}^*, \quad (6.7.1c)$$

$$\epsilon \frac{dF_{i,j}^\diamond}{d\tau} = k_E E_{i,j}^o F_{i,j} - k_{-E} F_{i,j}^\diamond - k_K F_{i,j}^\diamond + (k_{-K} + k_{K^*}) F_{i,j}^{\diamond\diamond}, \quad (6.7.1d)$$

$$\epsilon \frac{dF_{i,j}^{\diamond\diamond}}{d\tau} = k_K F_{i,j}^\diamond - (k_{-K} + k_{K^*}) F_{i,j}^{\diamond\diamond}, \quad (6.7.1e)$$

$$\epsilon \frac{dF_{i,j}}{d\tau} = -k_E E_{i,j}^o F_{i,j} + k_{-E} F_{i,j}^\diamond, \quad (6.7.1f)$$

$$\frac{dI_{i,j}}{d\tau} = \lambda_{C,I} \mathcal{H} \left( \frac{C_{i,j}}{\theta_{C,I}} \right) - \mu_I I_{i,j}, \quad (6.7.1g)$$

$$\frac{dL_{i,j}}{d\tau} = \lambda_{P,L} \mathcal{H} \left( \frac{P_{i,j}}{\theta_{P,L}} \right) - \mu_L L_{i,j}, \quad (6.7.1h)$$

$$\frac{dB_{i,j}}{d\tau} = \left\{ \lambda_{K^*,B} \mathcal{H} \left( K_{i,j}^* \right) + \lambda_{V,B} \mathcal{H} \left( \frac{V_{i,j}}{\theta_{V,B}} \right) + \lambda_{P,B} \mathcal{H} \left( P_{i,j} \right) \right\} \left\{ 1 - \mathcal{H} \left( G_{i,j} + M_{i,j} \right) \right\} - B_{i,j}, \quad (6.7.1i)$$

$$\frac{dG_{i,j}}{d\tau} = \left\{ \lambda_{LI,G} \mathcal{H} \left( L_{i,j} \right) \mathcal{H} \left( I_{i,j} \right) + \lambda_{M,G} \mathcal{H} \left( \frac{M_{i,j}}{\theta_{M,G}} \right) \right\} \left\{ 1 - \mathcal{H} \left( \frac{G_{i,j}}{\theta_{G,G}} \right) \right\} - \mu_G G_{i,j}, \quad (6.7.1j)$$

$$\frac{dM_{i,j}}{d\tau} = \left\{ \lambda_{V,M} \mathcal{H} \left( \frac{V_{i,j}}{\theta_{C,M}} \right) + \lambda_{P,M} \mathcal{H} \left( \frac{P_{i,j}}{\theta_{P,M}} \right) \right\} \left\{ 1 - \mathcal{H} \left( \frac{B_{i,j}}{\theta_{B,M}} \right) \right\} - \mu_M M_{i,j}. \quad (6.7.1k)$$

Terms of the form  $\Delta X_{i,j}$  are as defined in equation (6.5.2). Initial conditions are set such that eFGF, *Siamois*, *Lim1*, *Brachyury*, *Goosecoid* and *Mix* are not expressed in any cells ( $E_{i,j}^o(0) = E_{i,j}(0) = I_{i,j}(0) = L_{i,j}(0) = B_{i,j}(0) = M_{i,j}(0) = G_{i,j}(0) = 0$  for all  $i, j$ ), all MAPK is unphosphorylated ( $K_{i,j}^*(0) = 0$  for all  $i, j$ ), and all receptors are free ( $F_{i,j}(0) = 1$ ,  $F^\diamond = F^{\diamond\diamond} = 0$  for all

Variable	Parameter	Value	Variable	Parameter	Value
$M$	$\lambda_{V,M}$	2	$B$	$\lambda_{K^*,B}$	12
	$\lambda_{P,M}$	12		$\lambda_{V,B}$	1
	$\theta_{V,M}$	4		$\lambda_{P,B}$	10
	$\theta_{P,M}$	3		$\theta_{V,B}$	1
	$\theta_{B,M}$	1		$\theta_{P,B}$	1
$I$	$\lambda_{C,I}$	1	$G$	$\lambda_{LI,G}$	1
	$\theta_{C,I}$	1		$\lambda_{M,G}$	100
$L$	$\lambda_{P,L}$	1		$\theta_{M,G}$	1
	$\theta_{P,L}$	1		$\theta_{G,G}$	1
$E$	$\lambda_{B,E}$	12	$E^o$	$\sigma_E$	0.06
$K^*$	$k_{K^*}$	1		$\delta_E$	1
	$\mu_{K^*}$	1		$k_E$	1
$R^{\infty}$	$k_K$	1		$k_{-E}$	100
	$k_{-K}$	1			

**Table 6.5:** Dimensionless parameters used to solve (6.7.1). Parameter are as used in [94], selected such that in a single cell case (6.7.1) is bistable with steady states corresponding to mesoderm and anterior mesendoderm.

$i, j$ ).

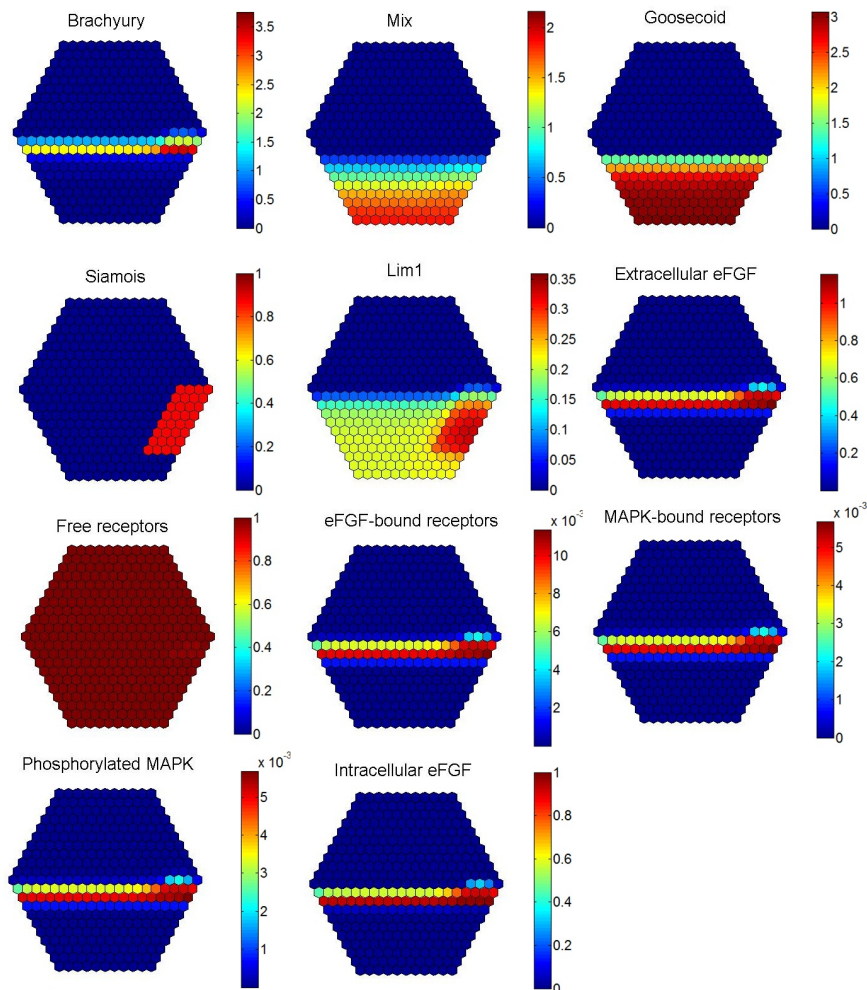
### 6.7.1 Numerical solutions

In this section we solve models of the *Xenopus* mesendoderm GRN to reproduce the spatial patterns of Mix and Brachyury found *in vivo*. The model given in equation (6.7.1) is solved subject to solutions for the localisation of P-Smad2 in the cases introduced in section 6.6.

Figure 6.26 plots the solutions to all variables of (6.7.1) in the case where the concentration of P-Smad2 is found by solutions to (6.6.1) and (6.6.2) (i.e. VegT alone activates transcription of Nodal and  $\beta$ -catenin enhances Nodal autoregulation). Brachyury is expressed in cells with low amounts of VegT whilst Mix and Goosecoid are expressed in cells with higher levels of VegT. Siamese is restricted to  $\beta$ -catenin expressing cells and the Lim1 expression pattern is similar to the of P-Smad2 in figure 6.21. eFGF and components of the eFGF signalling pathway show a similar expression pattern to that for Brachyury. In the following numerical results we plot only the solutions for Mix, Goosecoid and Brachyury, key genes in the formation of mesoderm, endoderm and anterior mesendoderm. Figure 6.27 shows numerical solutions to (6.6.1), (6.6.2) and (6.7.1) at three different time points. At  $t = 1$ , Brachyury is expressed at low levels uniformly along a row of cells representing the marginal zone and Mix and Goosecoid are expressed in vegetal cells. As time proceeds the levels of all three factors increases. At  $t = 10$ , Brachyury expression is highest on the dorsal side of the embryo.

Figure 6.28 shows numerical solutions to (6.6.1), (6.6.3) and (6.7.1), where VegT and  $\beta$ -catenin are required to activate Nodal and  $\beta$ -catenin enhances Nodal autoregulation. Figure 6.29 shows numerical solutions to (6.6.1), (6.6.4) and (6.7.1), where VegT and  $\beta$ -catenin are both required to activate Nodal and VegT or  $\beta$ -catenin can enhance Nodal autoregulation. Figure 6.30 shows numerical solutions to (6.6.1), (6.6.5) and (6.7.1), where  $\beta$ -catenin activates Nodal and acts to enhance Nodal autoregulation. The patterns of expression of Mix, Goosecoid and Brachyury are similar in figures 6.28-6.30: Three distinct regions of cells form, a region where Mix, Brachyury and Goosecoid are absent corresponding to ectoderm, a region where Brachyury is expressed

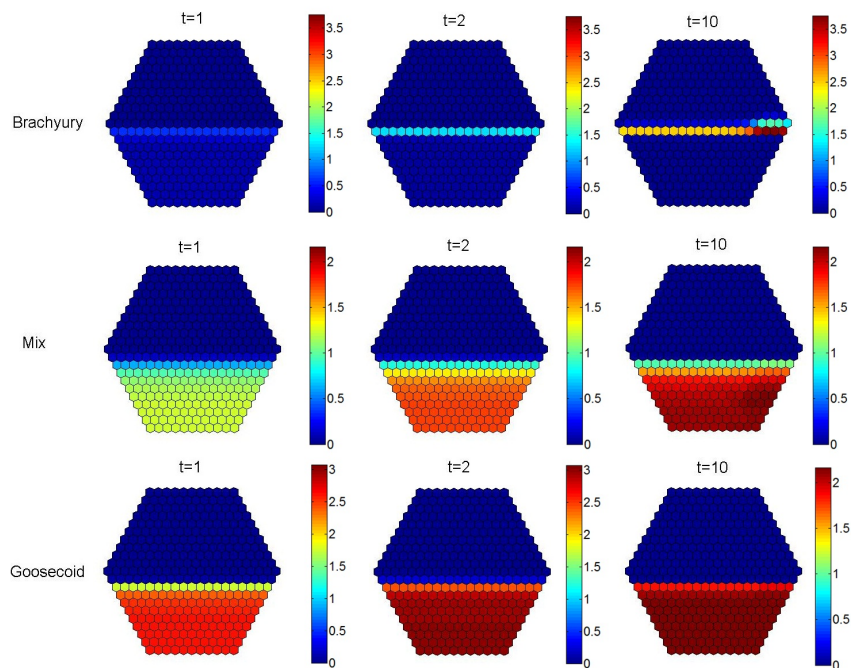




**Figure 6.26:** Numerical solutions to (6.6.1), (6.6.2) and (6.7.1) at  $\tau = 60$ , subject to the initial conditions shown in figure 6.19. In this model VegT is required to activate the transcription of Nodal,  $\beta$ -catenin acts to enhance Nodal autoregulation and  $\lambda_{P,A} = 50$  such that Nodal is pinned by Antivin. Unless otherwise stated parameters used are as in table 6.5.

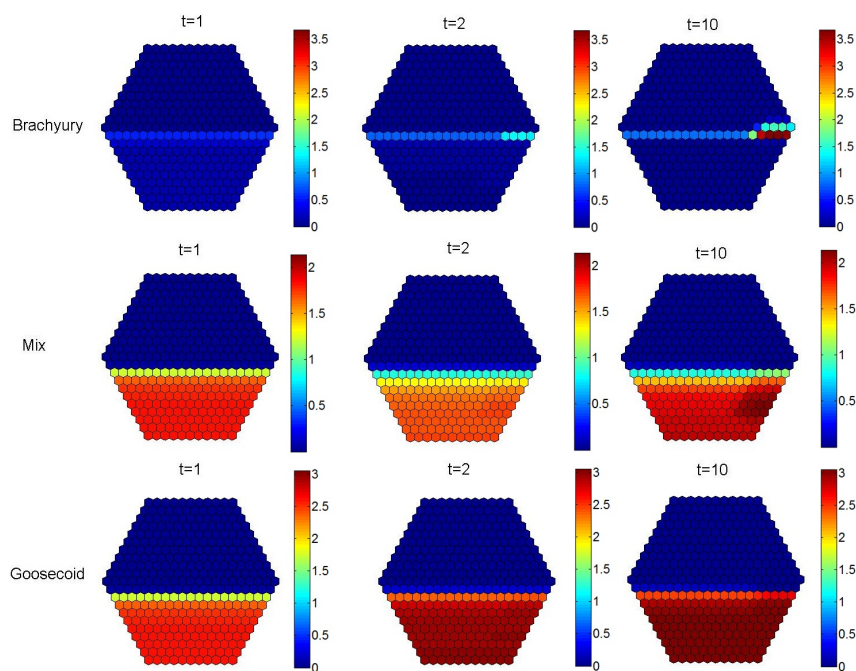
corresponding to mesoderm and a region where Mix and Goosecoid are co-expressed corresponding to anterior mesendoderm. In cells corresponding to mesoderm, Brachyury expression is strongest on the dorsal side of the embryo and weakest ventrally.

Numerical results of the mathematical models described above are consistent with experimental observations in *Xenopus*. Brachyury is first detected in cells of the prospective mesoderm on the dorsal side of the embryo [122]. This pattern of expression of Brachyury at early stages is similar to the patterns shown in figure 6.28. By early gastrulation Brachyury is found throughout the marginal zone [135], similar to the expression of Brachyury in figure 6.27. Note that both Mix and Goosecoid are co-expressed (corresponding to anterior mesendoderm) throughout the vegetal hemisphere in the model, whereas *in vivo* anterior mesendoderm is found only on the dorsal side of the embryo and Mix alone is expressed throughout the vegetal hemisphere. For

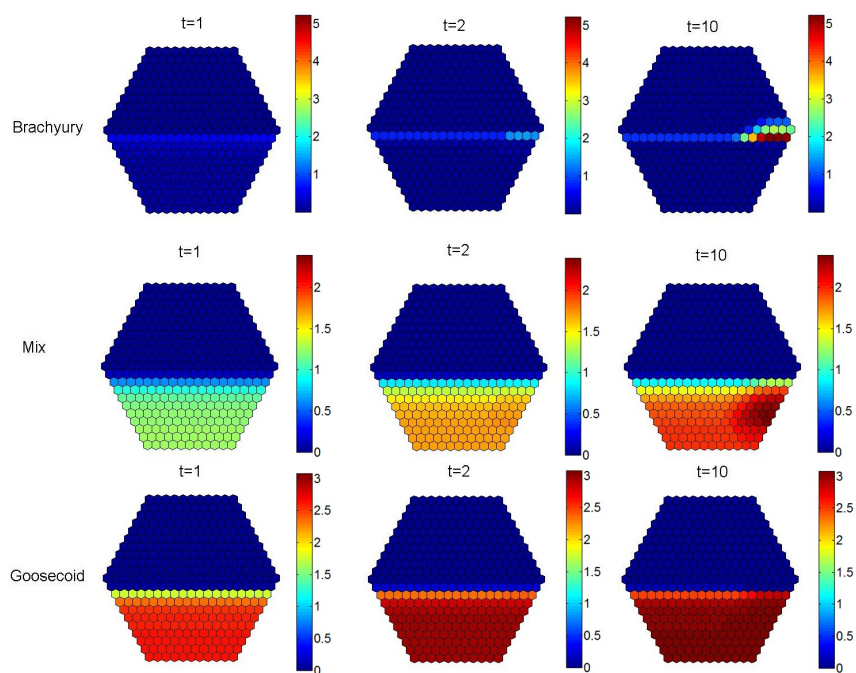


**Figure 6.27:** Numerical solutions to (6.6.1), (6.6.2) and (6.7.1) showing the spatial distribution of Brachyury, Mix and Goosecoid at  $\tau = 1$ ,  $\tau = 2$ ,  $\tau = 10$ , subject to the initial conditions shown in figure 6.19. In this model VegT is required to activate the transcription of Nodal,  $\beta$ -catenin can act to enhance Nodal autoregulation and  $\lambda_{P,A} = 50$  such that Antivin prevents the spread of Nodal throughout the embryo. Unless otherwise stated parameters used are as in table 6.5.

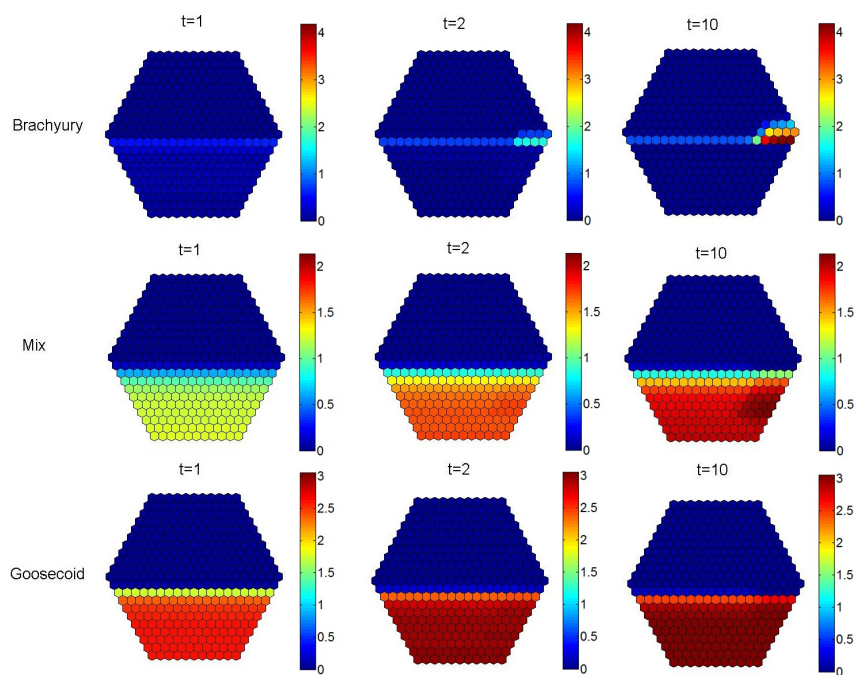
the model to be able to form endoderm, factors involved in dorsal-ventral patterning (as introduced in chapter 5.1) need to be included in the model. However, as already stated in this thesis, the axolotl gives a more suitable model system for building a quantitative mathematical model due to the presence of single Mix and Nodal genes in the axolotl. In the next section we solve a model of the axolotl mesendoderm GRN in a grid of cells.



**Figure 6.28:** Numerical solutions to (6.6.1), (6.6.3) and (6.7.1) showing the spatial distribution of Brachyury, Mix and Goosecoid at  $\tau = 1$ ,  $\tau = 2$ ,  $\tau = 10$ , subject to the initial conditions shown in figure 6.19. In this model VegT and  $\beta$ -catenin are required to activate the transcription of Nodal,  $\beta$ -catenin can act to enhance Nodal autoregulation and  $\lambda_{p,A} = 50$  such that Antivin prevents the spread of Nodal throughout the embryo. Unless otherwise stated parameters used are as in table 6.5.



**Figure 6.29:** Numerical solutions to (6.6.1), (6.6.4) and (6.7.1) showing the spatial distribution of Brachyury, Mix and Goosecoid at  $\tau = 1$ ,  $\tau = 2$ ,  $\tau = 10$ , subject to the initial conditions shown in figure 6.19. In this model VegT and  $\beta$ -catenin are required to activate the transcription of Nodal,  $\beta$ -catenin or VegT can act to enhance Nodal autoregulation and  $\lambda_{p,A} = 50$  such that Antivin prevents the spread of Nodal throughout the embryo. Parameters used are as in table 6.5.



**Figure 6.30:** Numerical solutions to (6.6.1), (6.6.5) and (6.7.1) showing the spatial distribution of Brachyury, Mix and Goosecoid at  $\tau = 1$ ,  $\tau = 2$ ,  $\tau = 10$ , subject to the initial conditions shown in figure 6.19. In this model  $\beta$ -catenin is required to activate the transcription of Nodal,  $\beta$ -catenin can act to enhance Nodal autoregulation and  $\lambda_{p,A} = 50$  such that Antivin prevents the spread of Nodal throughout the embryo. Parameters used are as in table 6.5.

## 6.8 A multicellular model of the axolotl mesendoderm GRN

In this section the mathematical model of the axolotl mesendoderm GRN downstream of Nodal is extended into a two-dimensional grid of cells. To do this, we take (6.2.2) and replace variables  $X_i$  with  $X_{i,j}$  and  $\Delta X_i$  with  $\Delta X_{i,j}$  to allow movement of extracellular proteins and complexes in a 2D grid. The non-dimensional equations governing the network downstream of Nodal are then given by

$$\epsilon \frac{dE_{i,j}^o}{d\tau} = \sigma_E \Delta E_{i,j} + \delta_E E_{i,j} - \bar{v} \left( k_E E_{i,j}^o - k_{-E} F_{i,j}^\diamond \right) - \mu_{E^o} E_{i,j}^o, \quad (6.8.1a)$$

$$\frac{dE_{i,j}}{d\tau} = \lambda_{B,E} \mathcal{H}(B_{i,j}) - \mu_E E_{i,j}, \quad (6.8.1b)$$

$$\epsilon \frac{dK_{i,j}^*}{d\tau} = \nu k_{K^*} F_{i,j}^{\diamond\diamond} - \mu_{K^*} K_{i,j}^*, \quad (6.8.1c)$$

$$\epsilon \frac{dF_{i,j}^\diamond}{d\tau} = k_E E_{i,j}^o F_{i,j} - k_{-E} F_{i,j}^\diamond - k_K F_{i,j}^\diamond + (k_{-K} + k_{K^*}) F_{i,j}^{\diamond\diamond}, \quad (6.8.1d)$$

$$\epsilon \frac{dF_{i,j}^{\diamond\diamond}}{d\tau} = k_K F_{i,j}^\diamond - (k_{-K} + k_{K^*}) F_{i,j}^{\diamond\diamond}, \quad (6.8.1e)$$

$$\epsilon \frac{dF_{i,j}}{d\tau} = -k_E E_{i,j}^o F_{i,j} + k_{-E} F_{i,j}^\diamond, \quad (6.8.1f)$$

$$\frac{dL_{i,j}}{d\tau} = \lambda_{P,L} \mathcal{H} \left( \frac{P_{i,j}}{\theta_{P,L}} \right) - \mu_L L_{i,j}, \quad (6.8.1g)$$

$$\frac{dB_{i,j}}{d\tau} = \left\{ \lambda_{K^*,B} \mathcal{H} \left( K_{i,j}^* \right) + \lambda_{P,B} \mathcal{H} \left( P_{i,j} \right) \mathcal{H} \left( M_{i,j} \right) \right\} \left\{ 1 - \mathcal{H} \left( G_{i,j} \right) \right\} - B_{i,j}, \quad (6.8.1h)$$

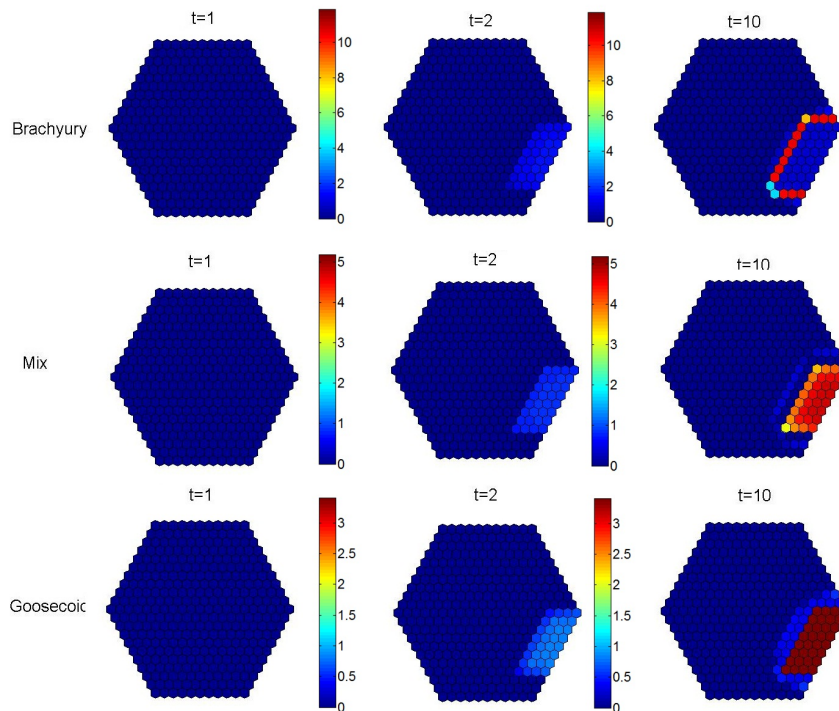
$$\frac{dG_{i,j}}{d\tau} = \left\{ \lambda_{L,G} \mathcal{H} \left( L_{i,j} \right) + \lambda_{M,G} \mathcal{H} \left( \frac{M_{i,j}}{\theta_{M,G}} \right) \right\} \left\{ 1 - \mathcal{H} \left( \frac{G_{i,j}}{\theta_{G,G}} \right) \right\} - \mu_G G_{i,j}, \quad (6.8.1i)$$

$$\frac{dM_{i,j}}{d\tau} = \lambda_{P,M} \mathcal{H} \left( \frac{P_{i,j}}{\theta_{P,M}} \right) \left\{ 1 - \mathcal{H} \left( \frac{B_{i,j}}{\theta_{B,M}} \right) \right\} - \mu_M M_{i,j}. \quad (6.8.1j)$$

Terms of the form  $\Delta X_{i,j}$  are as defined in equation (6.5.2) and  $P_{i,j}$  is determined by the solution to (6.6.5) and (6.7.1). Initial conditions are set such that eFGF, Lim1, Brachyury, Goosecoid and Mix are not expressed in any cells ( $E_{i,j}^o(0) = E_{i,j}(0) = L_{i,j}(0) = B_{i,j}(0) = M_{i,j}(0) = G_{i,j}(0) = 0$  for all  $i, j$ ), all MAPK is unphosphorylated ( $K_{i,j}^*(0) = 0$  for all  $i, j$ ), and all receptors are free ( $F_{i,j}(0) = 1, F^\diamond = F^{\diamond\diamond} = 0$  for all  $i, j$ ).

### 6.8.1 Numerical solutions

Figure 6.31 shows solutions to the axolotl mesendoderm model in a grid of cells for the localisation of Brachyury, Mix and Goosecoid, where  $\beta$ -catenin is localised to dorsal cells (as illustrated in figure 6.19). Mix and Goosecoid are co-expressed in cells which express  $\beta$ -catenin, while Brachyury is expressed in the cells bordering this region, where P-Smad2 is expressed at low levels as shown in figure 6.25A. We now compare the results of our model simulation with the spatial expression of Mix and Brachyury in axolotl embryos given in [139]. It is rather difficult to directly compare our model simulation with experimental data since morphogenic movements occur in the embryo, whilst our model considers a static group of cells. Despite this we



**Figure 6.31:** Numerical solutions to (6.6.1), (6.6.5) and (6.8.1) showing the spatial distribution of Brachyury, Mix and Goosecoid at  $\tau = 1$ ,  $\tau = 2$ ,  $\tau = 10$ , subject to the initial conditions shown in figure 6.19. In this model  $\beta$ -catenin are required to activate the transcription of Nodal and  $\beta$ -catenin acts to enhance Nodal autoregulation and  $\lambda_{p,A} = 50$  such that Antivin prevents the spread of Nodal throughout the embryo. Parameters used are as in tables 6.1 and 6.2.

can still extract important information on the validity of the model by comparing our model with experimental data. In [139], Mix and Brachyury are not co-expressed in the same cell, instead form two distinct neighbouring populations of cells. Our model reproduces this, with distinct populations of Brachyury-expressing cells and Mix-expressing cells neighbouring each other. By stage 12 Mix and Brachyury are also expressed in ventral regions of the embryo, which our model is unable to reproduce. We predict that, to allow for the expression of Mix and Brachyury in ventral regions, extra mechanisms need to be included such as the spread of  $\beta$ -catenin into ventral marginal zone. Including a more realistic geometry for the embryo which includes movements of cells would also aid further investigations.

## 6.9 Discussion

In this chapter we have developed and explored multicellular models of the mesendoderm GRN. First, we developed a multicellular model of the axolotl mesendoderm GRN in a line of cells. This model incorporated the Nodal and Antivin signalling model developed in [95] with the topology of the axolotl mesendoderm GRN downstream of Nodal. We explored two mechanisms via which distinct regions of Brachyury expressing cells (corresponding to mesoderm) and Mix and Goosecoid co-expressing cells (corresponding to anterior mesendoderm)

form. Obtaining experimental data about the spatial expression of key mesendodermal genes and development of the single cell quantitative model will aid further development of the multicellular model of mesendoderm formation in axolotl.

To aid studies of the Nodal signalling pathway in axolotl, we cloned axolotl Antivin. Antivin is a Nodal signalling agonist, which restricts the spread of Nodal ligands. We cloned a 1000bp fragment of axolotl cDNA which shows a high similarity to Antivin/Lefty sequences in other species. Axolotl Antivin is a zygotic transcription factor, whose expression in early development is similar to that of Nodal1. We measured Antivin expression in caps injected with Nodal1 and Antivin, finding that Antivin levels appear to significantly change over time in a non-uniform manner. To investigate further the regulation of Antivin and Nodal, more data is required to fit a mathematical model of Nodal signalling to the data. For example, Nodal and Antivin levels in Nodal1 injected caps could be measured every 4 hours instead of every 12 hours.

In the second half of this chapter we extended the mesendoderm GRN models for both *Xenopus* and axolotl from a line of cells into a grid of cells. Cells in the grid were chosen to be hexagonal rather than square, as hexagonal cells better represent the geometry of cells in an embryo. Solving models in a grid of cells allowed us to compare directly the spatial patterns formed by the mathematical model with spatial localisation of factors observed experimentally. Mathematical models of Nodal signalling were used to explore spatial patterns of P-Smad2 resulting from the induction and regulation of the Nodal signalling pathway by VegT and  $\beta$ -catenin. The mechanisms by which VegT and  $\beta$ -catenin induce Nodal in the models were based on experimental evidence on how Nodal genes are regulated in *Xenopus* and axolotl. The models based on the regulation of *Xenopus* Nodals by VegT and  $\beta$ -catenin can reproduce spatial patterns of P-Smad2 seen experimentally in [126]. Furthermore, the patterns of P-Smad2 which the models reproduce are consistent with the timing of Nodal gene expression and the mechanism of regulation for these genes. The expression of P-Smad2 has not been measured in axolotl embryos, thus the model based on the regulation of Nodal1 in axolotl gives a prediction for P-Smad2 expression in axolotl, which could be experimentally tested. The models of Nodal signalling were extended to include the *Xenopus* mesendoderm GRN downstream of Nodal. The numerical solutions obtained give expression patterns of Brachyury and Mix similar to those found experimentally. Goosecoid is expressed in all Mix expressing cells but, as discussed in [95] and chapter 5, for the mathematical model to be able to form endoderm the transcription factor Vent and DV patterning needs to be included. The model of the axolotl mesendoderm GRN in a 2D grid was able to account for some, but not all, experimental observations. Extensions to the model such as considering the spread of  $\beta$ -catenin and using a more realistic geometry of the embryo to include cell movement could be used to develop a more realistic model.

Extensions to the mathematical modelling work presented in this chapter are now discussed. To allow the model to reach a steady state representing endoderm, dorsal-ventral patterning needs to be included. An initial step in this process would be to extend the models of DV patterning formulated in chapter 5 to include extracellular regulation (such as BMP and Chordin). The models developed in this chapter qualitatively reproduce experimental observations in *Xeno-*



*pus*. Recall that the axolotl provides a more suitable model organism for quantifying mathematical models of the mesendoderm GRN than *Xenopus*. Once single cell models of the axolotl mesendoderm model (such as those in chapter 3) have been developed to reproduce quantitative experimental data fully, they can be extended into multicellular models such as those developed in this chapter.

# Discussion

In this thesis mathematical models of mesoderm and endoderm specification were developed using two amphibians, *Xenopus laevis* and axolotl, as model organisms. Mesoderm and endoderm are two distinct populations of cells which give rise to different cell types in the embryo. Important concepts in the specification of mesoderm and endoderm (‘mesendoderm’) were introduced in chapter 1, along with the gene regulatory networks (GRNs) involved in mesendoderm specification in axolotl and *Xenopus*. The presence of a single Mix and a single Nodal gene required for mesoderm in the axolotl leads to a mesendoderm GRN which is simpler than that found in *Xenopus*. Thus, in chapters 3 and 4, we focused on developing mathematical models of specification based on the axolotl mesendoderm GRN. In chapter 5, we modified an existing model of mesendoderm formation based on the *Xenopus* GRN to account for a wider set of experimental observations. Finally in chapter 6, we explored multicellular models of mesendoderm specification and made progress in obtaining experimental data for developing these models. In this chapter we give a summary of key findings from our work presented in chapters 3 to 6 and give directions for further work.

## 7.1 Single cell models of the axolotl mesendoderm GRN

In chapter 3 we developed mathematical models of specification based on current knowledge of the axolotl mesendoderm GRN as presented in [16, 139]. Whilst some interactions in the GRN have been tested experimentally, others are inferred from knowledge of mesendoderm specification in *Xenopus*. *In vitro* and *in vivo* versions of the model were developed, which encompass the time evolution of transcription factor concentrations in a single cell. The *in vitro* model, which gives the GRN downstream of Activin, is bistable with stable steady states corresponding to mesoderm (*Brachyury* upregulated) and anterior mesendoderm (*Mix* and *Goosecoild* upregulated) cell types. The steady state to which the model evolves was shown to depend on the dose of Activin a cell receives, and compares qualitatively with experimental data shown in section 4.1.1. The *in vivo* model gives the GRN downstream of  $\beta$ -catenin and has steady states corresponding to mesoderm and anterior mesendoderm cell types. The model solutions evolve

to these steady states dependent on the initial levels of  $\beta$ -catenin, consistent with experimental observations in [16]. Our qualitative analysis of the model of mesendoderm specification in axolotl provides evidence that the axolotl mesendoderm GRN can account for experimental observations. A key concept in developmental biology is that cells can determine their fate according to their position within the embryo, with this information given by a morphogen gradient [152]. The work of chapter 3 gives insight as to how a cell interprets positional information given by concentrations of Activin (*in vitro* case) and  $\beta$ -catenin (*in vivo* case).

In chapter 4 we developed a system for estimating parameter values for models of the axolotl mesendoderm GRN using gene expression data. Data obtained by quantitative PCR in Activin-injected animal caps was used to estimate parameters in the axolotl *in vitro* model using a computational algorithm consisting of the genetic algorithm and a local search method. The best fit of the model to the data was used to make predictions for the behaviour of the biological system when genes are knocked out. We tested experimentally the validity of the model prediction for the case of a Brachyury knockout, finding that the model prediction was not consistent with the *in vivo* behaviour of the GRN. Therefore we modified the parameter estimation algorithm to fit to both the ‘wild type’ model behaviour and to the behaviour in the case of the Brachyury knock out. Our findings in this chapter illustrate that the development of a mathematical model fully capable of reproducing experimental observations is an iterative process, requiring numerous rounds of model refinement, collection of experimental data, parameter estimation and validation of model predictions. Furthermore obtaining data over a more detailed time course will improve the likelihood that the algorithm is able to find biologically realistic parameter values for the mathematical model.

In chapter 4 we also investigated the ability of Activin, Nodal1 and Nodal2 to induce mesoderm and endoderm in axolotl animal caps. Differences were found in the mesendoderm-inducing ability of these three factors; Activin induced mesoderm and endoderm in a dose dependent manner, Nodal1 induced mesoderm but not endoderm and Nodal2 induced neither mesoderm nor endoderm. The differences in mesoderm induction warrants further investigation since, although it is thought that Activin and Nodal1 act via the same TGF- $\beta$  signalling pathway, our data suggests that different mechanisms are involved in response to the two ligands. In particular, we anticipate that Nanog, a gene found in axolotl but not *Xenopus*, may have a role in preventing Nodal1 inducing endoderm in animal caps, which requires further investigation both experimentally and using mathematical models.

## 7.2 Multicellular models of the axolotl mesendoderm GRN

In chapter 6 we developed multicellular models of the mesendoderm formation. We extended the single cell axolotl *in vivo* model introduced in chapter 3 into a line of cells. The multicellular model allows us to consider the spatial affects of mesendoderm patterning by including the diffusion of extracellular proteins (Nodal, Activin and eFGF). Our model incorporated the multicellular Nodal and Activin model developed in [95]. In axolotl embryos  $\beta$ -catenin is ex-

pressed non-uniformly. At early stages of development  $\beta$ -catenin is localised to dorsal regions during cortical rotation. Thus in our model we investigated a line of cells where  $\beta$ -catenin is present in dorsal cells and absent elsewhere. Two mechanisms were explored to account for the formation of populations of cells representing mesoderm and anterior mesendoderm. Further experimental evidence will test which of these mechanisms, or suggest an alternative mechanism, by which mesoderm and anterior mesendoderm form *in vivo*. To enable an investigation of the Nodal signalling pathway and to estimate parameter values in our mathematical model of Nodal and Antivin signalling, we cloned axolotl Antivin and measured its expression in Nodal and Antivin injected animal caps. Obtaining further data on the expression of Antivin in response to Nodal1 will aid further development of the mathematical model of Nodal signalling in axolotl.

### 7.3 Modifications to the mathematical models of mesendoderm formation in *Xenopus*

In chapter 5, we modified the single cell model of mesendoderm formation in *Xenopus* to include the ventrally expressed genes BMP and Vent, thus incorporating dorsal-ventral (DV) patterning. The model we developed was rather simple compared with the known regulation of BMP signalling, but can account for key experimental observations. Two versions of the model were developed: the ‘DV model’ and the ‘DV and mesendoderm model’. The mutual negative regulation of Vent and Goosecoid was explored in the ‘DV model’, which was found to be bistable with steady states corresponding to dorsal (*Goosecoid* expressing) and ventral (*Vent* expressing) cell fates. These results are consistent with experimental evidence where the antagonism between dorsal and ventral factors specifies cell fates along the dorsal-ventral axis [124]. The ‘DV and mesendoderm model’ was an extension the ‘DV model’ which included interactions of the simplified mesendoderm GRN given in [95]. The model was found to have stable steady states corresponding to mesoderm (*Brachyury* expressing), endoderm (*Mix* and *Vent* expressing) and anterior mesendoderm (*Mix* and *Goosecoid* expressing) cell fates. Thus, including ventral factors in a model of mesendoderm formation can account for the formation of mesendoderm in both dorsal and ventral regions of the embryo. A natural extension to this work is to extend the model to include the extracellular regulation of the BMP signalling pathway, both in a single cell and a multicellular model.

In the second part of chapter 6 we extended multicellular models of the mesendoderm GRN in *Xenopus* into a grid of cells. An advantage of solving the models in a grid of cells is that we can directly compare model simulations with *in situ* hybridisation images. We investigated the behaviour of the Nodal and Antivin signalling model in response to different modes of regulation by the maternal factors VegT and  $\beta$ -catenin. Our results showed that the patterns produced by the model were consistent with experimental observations for the localisation of PSmad2 and the timing and regulation of the multiple Nodal genes in *Xenopus*. Downstream of Nodal, we find that the models are capable of reproducing the expression patterns of *Mix* and

Brachyury, with Mix expressed throughout the vegetal hemisphere and Brachyury expressed in the marginal zone. However, the model shows Goosecoid expressed throughout the vegetal hemisphere, but in embryos it is found only in dorsal regions [124]. To obtain a model such that Goosecoid is restricted to dorsal regions, we would need to include BMP/Vent in the multicellular model.

## 7.4 Comparisons of mesendoderm formation in axolotl and *Xenopus*

The mesendoderm GRN was first studied in axolotl due to a prediction that it has a simpler structure than the mesendoderm GRN found in *Xenopus*, because of the presence of fewer *Mix* and *Nodal* genes. Several differences have emerged in the topology of the GRN in axolotl compared with *Xenopus*, which was initially surprising since it was thought that the mechanisms underlying mesendoderm formation in the two amphibians would be similar [139]. However, given the difference in Mix function in axolotl and *Xenopus*, studies were carried out to elucidate which mechanism was conserved in mammals. These studies found that Mix function in mouse is the same as that found in axolotl [139]. Thus, studying mesendoderm formation in axolotls may give insight into how mesendoderm is formed in mammals. Furthermore, Nanog, which has been found to have a role in mesendoderm formation in axolotl, is present in mammals but not in *Xenopus* suggesting that while axolotl development is like that of mammals, alternative mechanisms have evolved in *Xenopus*. The differences in the mechanisms of mesendoderm formation in axolotl and *Xenopus* become less surprising when considering other aspects of embryo development. For example, the mechanisms underlying the regulation of pluripotency, the method by which PGCs arise and the mechanisms of gastrulation are the same in axolotl and mammals, but different in *Xenopus* [64, 65, 68]. In fact, many of the differences in early development in amphibians can be thought of as arising due to a release of constraint arising due to a change in the location of PGC formation. In axolotl, PGCs are induced in the mesoderm where changes in the mesendoderm GRN would eliminate PGCs, but in *Xenopus* PGCs are predetermined in the endoderm such that changes in the mesendoderm GRN do not eliminate PGCs, thus mechanisms of mesendoderm formation are able to evolve in *Xenopus* but not in axolotl [65]. In this section we give a summary of some differences in mesendoderm formation in *Xenopus* and axolotl which have been explored in both species using mathematical models.

The first difference we explored was the regulation of *Brachyury* by Mix: in *Xenopus* Mix represses *Brachyury* and in axolotl Mix activates *Brachyury*. Both the *Xenopus* and axolotl mathematical models of the mesendoderm GRN have steady states corresponding to mesoderm and anterior mesendoderm, although different values of the model parameters are required to yield bistability in the two models and the levels of each of the transcription factors at these steady states also differs. The models also show differences in the requirement of Goosecoid. In the absence of *Goosecoid*, mesoderm and endoderm are steady states in the *Xenopus* model, while

only mesoderm forms in the absence of *Gooseoid* in the axolotl model. Thus while *Gooseoid* is dispensable for forming Mix expressing cells in *Xenopus*, it appears to be required to form this population of cells in axolotl. This is a consequence of the change in the Mix/*Brachyury* relationship: in *Xenopus* both Mix and *Gooseoid* can repress the expression of *Brachyury*, while in axolotl *Gooseoid* is the only factor that can repress *Brachyury* in the mesendoderm GRN. Previous studies have suggested that the mutual negative feedback between two transcription factors can account for the formation of two distinct cell types in response to a morphogen, as is shown for Mix and *Brachyury* in *Xenopus* [95, 123]. Our investigations show that two distinct cell types also form in response to a morphogen for a more complex network, whereby three factors (Mix, *Brachyury* and *Gooseoid*) are involved, where Mix activates *Brachyury* and *Gooseoid*, *Gooseoid* represses *Brachyury* and *Brachyury* represses Mix.

Another important aspect which we investigated was the function of maternal factors in inducing mesoderm and anterior mesendoderm. In *Xenopus* VegT is present in a gradient running from the vegetal to animal pole, while  $\beta$ -catenin is expressed dorsally and both of these factors have been shown to be important in mesendoderm formation. In *Xenopus* investigations of mathematical models of the mesendoderm GRN show that mesoderm and anterior mesendoderm form in regions as determined by the concentration of VegT and  $\beta$ -catenin [95]. In axolotl VegT is expressed uniformly and does not function in mesendoderm formation [16, 104] and  $\beta$ -catenin is expressed dorsally. We show in our mathematical model that mesoderm and anterior mesendoderm can form in the presence of  $\beta$ -catenin alone in axolotl. This is a surprising result since in *Xenopus* VegT rather than  $\beta$ -catenin provides the main initial positional information to drive mesendoderm formation. In our investigations of the multicellular models of mesendoderm formation we found differences in the requirement for cell to cell signalling in axolotl and *Xenopus*. In both organisms Nodal and FGF signals allow from cell to cell communication. However studies in *Xenopus* show that Antivin can restrict (or pin) the spread of Nodal throughout a line of cells [94]. In our investigations we found that although mesoderm and anterior mesendoderm can form when the diffusion of Nodal and FGF are set to zero in the *Xenopus* model, that the diffusion of Nodal one or two cells from its source and the establishment of the FGF and *Brachyury* positive feedback loop are required to form mesoderm in axolotl.

To summarise, whilst studying the differences in mesendoderm formation in *Xenopus* and axolotl, we found that several of the mechanisms thought to be central in driving mesendoderm formation in *Xenopus* are not present in axolotl (e.g. mutual inhibition of Mix/*Brachyury* and the graded distribution of VegT). By studying the axolotl mesendoderm GRN using mathematical models we have improved our understanding of the mechanisms via which mesendoderm is formed in axolotl. Despite these differences in the mechanisms via which mesendoderm forms, the primary germ layers form in the correct regions in both *Xenopus* and axolotl.

## 7.5 Conclusion

To conclude the work presented in this thesis has given insight into the mechanisms by which mesendoderm forms, identifying the axolotl as a suitable model organism for studying a simplified mesendoderm GRN and comparing the mechanisms of mesendoderm formation in axolotl with those in *Xenopus*. This work has given motivation for several directions for future studies both experimentally and theoretically, which we will now discuss.

The qualitative analysis of the axolotl mesendoderm GRN downstream of Activin provided several useful insights into the behaviour of the network. However, to develop a model with biologically valid parameter values, more experimental data is required to fit the model to. This data could be in the form of a more detailed time course or a detailed Activin dose response curve. Data on the behaviour of the network in response to perturbations would also aid the development of a model which is able to fully reproduce experimental observations. In addition to studying the mesendoderm GRN downstream of Activin, experimental investigations are required to elucidate the differences in the response of animal caps to Activin and Nodal1, including the role of Nanog and Antivin in Nodal/Activin signalling.

Once the axolotl mesendoderm GRN has been fully explored and quantified downstream of Activin, this knowledge would aid the study of the network in response to  $\beta$ -catenin. By collecting experimental data (either a detail time course or a dose response curve) downstream of  $\beta$ -catenin, parameter values of the axolotl *in vivo* model can be estimated. Furthermore experimental data on the distribution of maternal transcripts of  $\beta$ -catenin in whole embryos and how this overlaps with Mix, Brachyury and Goosecoid could be used in the multicellular mesendoderm models. Another future direction for developing multicellular models is to incorporate cell growth and the movements of gastrulation.

Another prospect for further study is how dorsal-ventral (DV) patterning overlaps with the formation of mesendoderm. In this thesis we developed a single cell model of mesendoderm formation with DV patterning in *Xenopus*. This work needs to be extended to include aspects of the signalling pathways involved in regulating DV patterning and our knowledge transferred in the axolotl, via experimental identification of these factors and their behaviour in axolotl and expanding the mathematical models in the axolotl to include these data.

Thus, there are several exciting directions that could aid further understanding of the mechanisms regulating the formation of the primary germ layers in axolotl. Furthermore, since many mechanisms of development in axolotl are the same as those in mammals, by gaining a better understanding of axolotl mesendoderm formation we may gain insights into mammalian development.

# References

- [1] E. Agius, M. Oelgeschlager, O. Wessely, C. Kemp, and E.M. De Robertis. Endodermal Nodal-related signals and mesoderm induction in *Xenopus*. *Development*, 127(6):1173–1183, 2000.
- [2] R. Albert and H.G. Othmer. The topology of the regulatory interactions predicts the expression pattern of the segment polarity genes in *Drosophila melanogaster*. *J. Theor. Biol.*, 223(1):1 – 18, 2003.
- [3] B. Alberts et al. *Molecular Biology of the Cell*. Garland publishing, Inc., 1994.
- [4] J.B. Armstrong and G.M. Malacinski. *Developmental biology of the axolotl*. Oxford University Press, 1989.
- [5] R.E. Baker, S. Schnell, and P.K. Maini. A clock and wavefront mechanism for somite formation. *Dev. Biol.*, 293(1):116 – 126, 2006.
- [6] R.E. Baker, S. Schnell, and P.K. Maini. Waves and patterning in developmental biology: vertebrate segmentation and feather bud formation as case studies. *Int. J. Dev. Biol.*, 53(5/6):783–794, 2009.
- [7] D. Ben-Zvi, A. Fainsod, B. Shilo, and N. Barkai. Scaling of the BMP activation gradient in *Xenopus* embryos. *Nature*, 453(2):1205–11., 2008.
- [8] N.P. Bordzilovskaya and T.A. Dettlaff. Table of stages of the normal development of axolotl embryos and the prognostication of timing of successive developmental stages at various temperatures. *Axolotl Newsletter*, 7:2–22, 1979.
- [9] R.T. Bottcher and C. Niehrs. Fibroblast growth factor signaling during early vertebrate development. *Endocr. Rev.*, 26(1):63–77, 2005.
- [10] P.Y. Bourillot, N. Garrett, and J.B. Gurdon. A changing morphogen gradient is interpreted by continuous transduction flow. *Development*, 129:2167–2180, 2002.
- [11] S. Brown, A. Teo, S. Pauklin, N. Hannan, et al. Activin/Nodal signaling controls divergent transcriptional networks in human embryonic stem cells and in endoderm progenitors. *Stem Cells*, 29(8):1176–1185, 2011.



## REFERENCES

- [12] W.W. Burggren and S. Warburton. Amphibians as animal models for laboratory research in physiology. *ILAR J.*, 48(3):260, 2007.
- [13] E.M. Callery. There's more than one frog in the pond: A survey of the amphibia and their contributions to developmental biology. *Seminars in Cell & Developmental Biology*, 17(1):80 – 92, 2006.
- [14] Y. Cha, S. Takahashi, and C.V.E. Wright. Cooperative non-cell and cell autonomous regulation of Nodal gene expression and signaling by Lefty/Antivin and Brachyury in *Xenopus*. *Dev. Biol.*, 290(2):246 – 264, 2006.
- [15] C. Chen and M.M. Shen. Two modes by which Lefty proteins inhibit Nodal signaling. *Curr. Biol.*, 14(7):618 – 624, 2004.
- [16] Y. Chen. *Mesoderm Induction in Ambystoma Mexicanum, a Urodele Amphibian*. PhD thesis, University of Nottingham, 2010.
- [17] S.K. Cheng, F. Olale, A.H. Brivanlou, and A.F. Schier. Lefty blocks a subset of TGF- $\beta$  signals by antagonizing EGF-CFC coreceptors. *PLoS Biol.*, 2(2):e30, 02 2004.
- [18] R.H. Chisholm, B.D. Hughes, and K.A. Landman. Building a morphogen gradient without diffusion in a growing tissue. *PLoS One*, 5(9):e12857, 09 2010.
- [19] K.W.Y. Cho, B. Blumberg, H. Steinbeisser, and E.M. De Robertis. Molecular nature of Spemann's organizer: the role of the *Xenopus* homeobox gene Goosecoid. *Cell*, 67(6):1111 – 1120, 1991.
- [20] J.H. Clement, P. Fettes, S. Knöchel, J. Lef, and Walter Knöchel. Bone morphogenetic protein 2 in the early development of *Xenopus laevis*. *Mech. Dev.*, 52(2-3):357 – 370, 1995.
- [21] D. Clements, R.V. Friday, and H.R. Woodland. Mode of action of VegT in mesoderm and endoderm formation. *Development*, 126:4903–4911, 1999.
- [22] F.L. Conlon, S.G. Sedgwick, K.M. Weston, and J.C. Smith. Inhibition of Xbra transcription activation causes defects in mesodermal patterning and reveals autoregulation of Xbra in dorsal mesoderm. *Development*, 122(8):2427–2435, 1996.
- [23] J. Cooke. Scale of body pattern adjusts to available cell number in amphibian embryos. *Dev. Biol.*, 290:775 – 778, 1981.
- [24] J. Cooke and E.C. Zeeman. A clock and wavefront model for control of the number of repeated structures during animal morphogenesis. *J. Theor. Biol.*, 58(2):455–476, 1976.
- [25] V. Cunliffe and J.C. Smith. Ectopic mesoderm formation in *Xenopus* embryos caused by widespread expression of a Brachyury homologue *cunliffe1992ectopic*. *Nature*, 1992.
- [26] L. Dale, W. Evans, and S.A. Goodman. Xolloid-related: a novel BMP1/Tolloid-related metalloprotease is expressed during early *Xenopus* development. *Mech. Dev.*, 119(2):177 – 190, 2002.

## REFERENCES

- [27] L. Dale and C.M. Jones. BMP signalling in early *Xenopus* development. *BioEssays*, 21:751–760, 1999.
- [28] S. Ben-Tabou de Leon and E.H. Davidson. Modeling the dynamics of transcriptional gene regulatory networks for animal development. *Dev. Biol.*, 325(2):317 – 328, 2009.
- [29] E.M. De Robertis. Spemann’s organizer and self-regulation in amphibian embryos. *Nat. Rev. Mol. Cell Biol.*, 7(4):296–302, 2006.
- [30] M.L. Dequéant and O. Pourquié. Segmental patterning of the vertebrate embryonic axis. *Nat. Rev. Genet.*, 9(5):370–382, 2008.
- [31] J.E. Dixon, C. Allegrucci, C. Redwood, et al. Axolotl Nanog activity in mouse embryonic stem cells demonstrates that ground state pluripotency is conserved from urodele amphibians to mammals. *Development*, 137(18):2973–2980, 2010.
- [32] K. Dorey and E. Amaya. FGF signalling: diverse roles during early vertebrate embryogenesis. *Development*, 137(22):3731–3742, 2010.
- [33] A. Eldar, R. Dorfman, D. Weiss, H. Ashe, B. Shilo, and N. Barkai. Robustness of the BMP morphogen gradient in *Drosophila* embryonic patterning. *Nature*, 419:261 – 262, 2002.
- [34] B. Ermentrout. *Simulating, analyzing, and animating dynamical systems: a guide to XPPAUT for researchers and students*, volume 14. Society for Industrial Mathematics, 2002.
- [35] P. Francois, A. Vonica, A.H. Brivanlou, and E.D. Siggia. Scaling of BMP gradients in *Xenopus* embryos. *Nature*, 461:E1, 2009.
- [36] G. Fáth. Propagation failure of traveling waves in a discrete bistable medium. *Physica D*, 116(1-2):176 – 190, 1998.
- [37] T.S. Gardner, C.R. Cantor, and J.J. Collins. Construction of a genetic toggle switch in *Escherichia coli*. *Nature*, 403:339–342, 2000.
- [38] V. Gawantka, H. Delius, K. Hirschfeld, C. Blumenstock, and C. Niehrs. Antagonizing the spemann organizer: role of the homeobox gene *Xvent-1*. *EMBO J.*, 14(24):6268 – 6279, 1995.
- [39] N. Geard and K. Willadsen. Dynamical approaches to modeling developmental gene regulatory networks. *Birth Defects Research Part C: Embryo Today: Reviews*, 87(2):131–142, 2009.
- [40] T. Gedeon, K. Mischaikow, K. Patterson, and E. Traldi. Binding cooperativity in Phage  $\lambda$  is not sufficient to produce an effective switch. *Biophys. J.*, 94(9):3384–3392, 2008.
- [41] S.F. Gilbert. *Developmental Biology*. Sinauer Associates, 9th edition, 2010.
- [42] J. Green. Morphogen gradients, positional information, and *Xenopus*: Interplay of theory and experiment. *Dev. Dyn.*, 225(4):392–408, 2002.

## REFERENCES

- [43] J.B.A. Green and J.C. Smith. Graded changes in dose of a *Xenopus* activin A homologue elicit stepwise transitions in embryonic cell fate. *Nature*, 1990.
- [44] O. Grimm, M. Coppey, and E. Wieschaus. Modelling the bicoid gradient. *Development*, 137(14):2253–2264, 2010.
- [45] W. Guo, A.P. Chan, H. Liang, E.D. Wieder, J.J. Molldrem, L.D. Etkin, and L. Nagarajan. A human Mix-like homeobox gene MIXL shows functional similarity to *Xenopus* Mix.1. *Blood*, 100:89–95, 2002.
- [46] J.B. Gurdon, P. Harger, A. Mitchell, and P. Lemaire. Activin signalling and response to a morphogen gradient. *Nature*, 371:487 – 492, 1994.
- [47] J.B. Gurdon, A. Mitchell, and K. Ryan. An experimental system for analyzing response to a morphogen gradient. *Proc. Natl Acad. Sci. USA*, 93(18):9334–9338, 1996.
- [48] J.B. Gurdon, H. Standley, S. Dyson, K. Butler, et al. Single cells can sense their position in a morphogen gradient. *Development*, 126(23):5309–5317, 1999.
- [49] T.A. Hall. BioEdit: a user-friendly biological sequence alignment editor and analysis program for Windows 95/98/NT. In *Nucleic acids symposium series*, volume 41, pages 95–98, 1999.
- [50] C.S. Hansen, C.D. Marion, K. Steele, S. George, and W.C. Smith. Direct neural induction and selective inhibition of mesoderm and epidermis inducers by Xnr3. *Development*, 124(2):483–492, 1997.
- [51] J. Heasman. Patterning the early *Xenopus* embryo. *Development*, 133(7):1205–1217, 2006.
- [52] C. Heisenberg and L. Solnica-Krezel. Back and forth between cell fate specification and movement during vertebrate gastrulation. *Curr. Opin. Genet. Dev.*, 18(4):311 – 316, 2008.
- [53] U. Hellsten, R.M. Harland, M.J. Gilchrist, D. Hendrix, et al. The genome of the Western clawed frog *Xenopus tropicalis*. *Science*, 328(5978):633–636, 2010.
- [54] K.A. Henningfeld, H. Friedle, S. Rastegar, and W. Knöchel. Autoregulation of Xvent-2B; direct interaction and functional cooperation of Xvent-2 and Smad1. *J. Biol. Chem.*, 277(3):2097, 2002.
- [55] K.A. Henningfeld, S. Rastegar, G. Adler, and W. Knöchel. Smad1 and Smad4 are components of the bone morphogenetic protein-4 (BMP-4)-induced transcription complex of the Xvent-2B promoter. *J. Biol. Chem.*, 275(29):21827, 2000.
- [56] G.L. Henry and D.A. Melton. Mixer, a homeobox gene required for endoderm development. *Science*, 281(5373):91–96, 1998.
- [57] B.G. Herrmann. Expression pattern of the Brachyury gene in whole-mount TWis/TWis mutant embryos. *Development*, 113(3):913–917, 1991.

## REFERENCES

- [58] C.S. Hill. TGF- $\beta$  signalling pathways in early *Xenopus* development. *Curr. Opin. Genet. Dev.*, 11:533–540, 2001.
- [59] J.H. Holland. Genetic algorithms. *Sci. Am.*, 267(1):66–72, 1992.
- [60] C. Hudson, D. Clements, R.V. Friday, D. Stott, and H.R. Woodland. *Xsox17- $\alpha$*  and - $\beta$  mediate endoderm formation in *Xenopus*. *Cell*, 91(3):397 – 405, 1997.
- [61] H.V. Isaacs, M.E. Pownall, and J.M. Slack. eFGF is expressed in the dorsal midline of *Xenopus laevis*. *Int. J. Dev. Biol.*, 39(4):575, 1995.
- [62] H.V. Isaacs, M.E. Pownall, and J.M.W. Slack. eFGF regulates *Xbra* expression during *Xenopus* gastrulation. *EMBO J.*, 13(19):4469, 1994.
- [63] A.D. Johnson, B. Crother, M.E. White, R. Patient, R. F. Bachvarova, M. Drum, and T. Masi. Regulative germ cell specification in axolotl embryos: a primitive trait conserved in the mammalian lineage. *Philos. T. Roy. Soc. B*, 358(1436):1371–1379, 2003.
- [64] A.D. Johnson, M. Drum, R.F. Bachvarova, T. Masi, M.E. White, and B.I. Crother. Evolution of predetermined germ cells in vertebrate embryos: implications for macroevolution. *Evol. Dev.*, 5(4):414–431, 2003.
- [65] A.D. Johnson, E. Richardson, R.F. Bachvarova, and B.I. Crother. Evolution of the germ line-soma relationship in vertebrate embryos. *Reproduction*, 141(3):291, 2011.
- [66] C.M. Jones, M.R. Kuehn, B.L. Hogan, J.C. Smith, and C.V. Wright. Nodal-related signals induce axial mesoderm and dorsalize mesoderm during gastrulation. *Development*, 121(11):3651, 1995.
- [67] H. Kageura and K. Yamana. Pattern regulation in defect embryos of *Xenopus laevis*. *Dev. Biol.*, 101(2):410 – 415, 1984.
- [68] T. Kaneda and J. Doi Motoki. Gastrulation and pre-gastrulation morphogenesis, inductions, and gene expression: Similarities and dissimilarities between urodelean and anuran embryos. *Developmental Biology*, 369(1):1 – 18, 2012.
- [69] G. Karlebach and R. Shamir. Modelling and analysis of gene regulatory networks. *Nat. Rev. Mol. Cell Biol.*, 9(10):770–780, 2008.
- [70] S. Kauffman. Homeostasis and differentiation in random genetic control networks. *Nature*, 224:177–178, 1969.
- [71] S.A. Kauffman. Metabolic stability and epigenesis in randomly constructed genetic nets. *J. Theor. Biol.*, 22(3):437–467, 1969.
- [72] M. Kerszberg and L. Wolpert. Mechanisms for positional signalling by morphogen transport: a theoretical study. *J. Theor. Biol.*, 191(1):103 – 114, 1998.
- [73] D.M. Kingsley. The TGF- $\beta$  superfamily: new members, new receptors, and new genetic tests of function in different organisms. *Genes & Development*, 8(2):133–146, 1994.

## REFERENCES

- [74] M. Kofron, T. Demel, J. Xanthos, J. Lohr, B. Sun, H. Sive, S. Osada, C. Wright, C. Wylie, and J. Heasman. Mesoderm induction in *Xenopus* is a zygotic event regulated by maternal VegT via TGF- $\beta$  growth factors. *Development*, 126(24):5759, 1999.
- [75] T. Koide, T. Hayata, and K.W.Y. Cho. *Xenopus* as a model system to study transcriptional regulatory networks. *Proc. Natl Acad. Sci. USA*, 102(14):4943, 2005.
- [76] C. Kühn, A. Kühn, A. Poustka, and E. Klipp. Modeling development: spikes of the sea urchin. *Genome Inform.*, 18:75–84, 2007.
- [77] C. Kühn, C. Wierling, A. Kühn, E. Klipp, et al. Monte carlo analysis of an ODE model of the sea urchin endomesoderm network. *BMC syst. biol.*, 3(1):83, 2009.
- [78] P.S. Kunwar, S. Zimmerman, J.T. Bennett, Y. Chen, M. Whitman, and A.F. Schier. Mixer/Bon and FoxH1/Sur have overlapping and divergent roles in Nodal signaling and mesendoderm induction. *Development*, 130(23):5589–5599, 2003.
- [79] C. LaBonne and M. Whitman. Mesoderm induction by activin requires FGF-mediated intracellular signals. *Development*, 120(2):463, 1994.
- [80] A.D. Lander, Q. Nie, and F. Wan. Do morphogen gradients arise by diffusion? *Dev. Cell*, 2(6):785 – 796, 2002.
- [81] A.D. Lander, Q. Nie, and F.Y.M. Wan. Internalization and end flux in morphogen gradient formation. *J. Comput. Appl. Math.*, 190(1-2):232 – 251, 2006.
- [82] B.V. Latinkic and J.C. Smith. Goosecoid and Mix.1 repress Brachyury expression and are required for head formation in *Xenopus*. *Development*, 126(8):1769–1779, 1999.
- [83] M.A. Lee, J. Heasman, and M. Whitman. Timing of endogenous activin-like signals and regional specification of the *Xenopus* embryo. *Development*, 128(15):2939–2952, 2001.
- [84] J. Leelawattanachai, C. Modchang, W. Triampo, D. Triampo, and Y. Lenbury. Modeling and genetic algorithm optimization of early events in signal transduction via dynamics of G-protein-coupled receptors: internalization consideration. *Appl. Math. Comput.*, 207(2):528 – 544, 2009.
- [85] P. Lemaire. A role for the vegetally expressed *Xenopus* gene Mix.1 in endoderm formation and in the restriction of mesoderm to the marginal zone. *Development*, 125:2371–2380, 1998.
- [86] P. Lemaire, N. Garrett, and J.B. Gurdon. Expression cloning of Siamois, a *xenopus* homeobox gene expressed in dorsal-vegetal cells of blastulae and able to induce a complete secondary axis. *Cell*, 81(1):85 – 94, 1995.
- [87] M. Leptin. Gastrulation movements: the logic and the nuts and bolts. *Developmental Cell*, 8(3):305 – 320, 2005.

## REFERENCES

- [88] K.J. Livak and T. D. Schmittgen. Analysis of relative gene expression data using real-time quantitative pcr and the  $2^{-\delta \delta c(t)}$  method. *Methods*, 25(4):402 – 408, 2001.
- [89] M. Loose and R. Patient. A gene regulatory network for *Xenopus* mesendoderm formation. *Dev. Biol.*, 271:467–478, 2004.
- [90] G. Luxardi, L. Marchal, V. Thome, and L. Kodjabachian. Distinct *Xenopus* Nodal ligands sequentially induce mesendoderm and control gastrulation movements in parallel to the Wnt/PCP pathway. *Development*, 137(3):417–426, 2010.
- [91] W. Ma, L. Lai, Q. Ouyang, and C. Tang. Robustness and modular design of the *Drosophila* segment polarity network. *Mol. Syst. Biol.*, 2(1), 2006.
- [92] H. Meinhardt and A. Gierer. Pattern formation by local self-activation and lateral inhibition. *BioEssays*, 22(8):753–760, 2000.
- [93] A. Mereau, C. Le Sommer, H. Lerivray, M. Lesimple, and S. Hardy. *Xenopus* as a model to study alternative splicing *in vivo*. *Biol. Cell*, 99:55–65, 2007.
- [94] A.M. Middleton. *Mathematical modelling of gene regulatory networks*. PhD thesis, University of Nottingham, 2007.
- [95] A.M. Middleton, J.R. King, and M. Loose. Bistability in a model of mesoderm and anterior mesendoderm specification in *Xenopus laevis*. *J. Theor. Biol.*, 260(1):41 – 55, 2009.
- [96] C. Modchang, W. Triampo, and Y. Lenbury. Mathematical modeling and application of genetic algorithm to parameter estimation in signal transduction: Trafficking and promiscuous coupling of G-protein coupled receptors. *Comput. Biol. Med.*, 38(5):574 – 582, 2008.
- [97] C.G. Moles, P. Mendes, and J.R. Banga. Parameter estimation in biochemical pathways: a comparison of global optimization methods. *Genome Res.*, 13:2467–2473, 2003.
- [98] R.T. Moon and D. Kimelman. From cortical rotation to organizer gene expression: toward a molecular explanation of axis specification in *Xenopus*. *BioEssays*, 20(7):536–546, 1998.
- [99] M. Moos, S. Wang, and M. Krinks. Anti-dorsalizing morphogenetic protein is a novel TGF- $\beta$  homolog expressed in the Spemann organizer. *Development*, 121(12):4293–4301, 1995.
- [100] U. Morbiducci, A. Tura, and M. Grigioni. Genetic algorithms for parameter estimation in mathematical modeling of glucose metabolism. *Comput. Biol. Med.*, 35(10):862 – 874, 2005.
- [101] P.A.B Moretti, A.J. Davidson, E. Baker, B. Lilley, L. I. Zon, and R.J. D’Andrea. Molecular cloning of a human vent-like homeobox gene. *Genomics*, 76:21 – 29, 2001.
- [102] A. Moustakas and C. Heldin. The regulation of TGF- $\beta$  signal transduction. *Development*, 136(22):3699–3714, 2009.
- [103] C.B. Muratov and S.Y. Shvartsman. Signal propagation and failure in discrete autocrine relays. *Phys. Rev. Lett.*, 93(11):118101, Sep 2004.

## REFERENCES

- [104] K. Nath and R.P. Ellison. RNA of AxVegT, the axolotl orthologue of the *Xenopus* meso-endoderm determinant is not localized in the oocytes. *Gene Expr. Patterns*, 7:197–201, 2007.
- [105] P.D. Nieuwkoop. The formation of the mesoderm in urodelean amphibians. *Dev. Genes Evol.*, 162(4):341–373, 1969.
- [106] P.D. Nieuwkoop. What are the key advantages and disadvantages of urodele species compared to anurans as a model system for experimental analysis of early development? *Int. J. Dev. Biol.*, 40(4):617–9., 1996.
- [107] D. Onichtchouk, V. Gawanka, R. Doschand H. Delius, K. Hirshfeld, C. Blumenstock, and C. Niehrs. The *Xvent-2* homeobox gene is part of the *BMP-4* signalling pathway controlling dorsoventral patterning of *Xenopus* mesoderm. *Development*, 122:3045 – 3053, 1996.
- [108] D. Onichtchouk, A. Glinka, and C. Niehrs. Requirement for *Xvent-1* and *Xvent-2* gene function in dorsoventral patterning of *Xenopus* mesoderm. *Development*, 125:1447 – 1456, 1998.
- [109] D.P. O'Rourke. Amphibians used in research and teaching. *ILAR J.*, 48(3):183, 2007.
- [110] K. M. Page, P.K. Maini, N. A.M. Monk, and C. D. Stern. A model of primitive streak initiation in the chick embryo. *J. Theor. Biol.*, 208(4):419 – 438, 2001.
- [111] D. Papatsenko and M. Levine. The drosophila gap gene network is composed of two parallel toggle switches. *PLoS One*, 6(7):e21145, 2011.
- [112] C. Papin and J.C. Smith. Gradual refinement of Activin-induced thresholds requires protein synthesis. *Dev. Biol.*, 217:166–172, 2000.
- [113] S. Piccolo, E. Agius, B. Lu, S. Goodman, L. Dale, and E.M. De Robertis. Cleavage of chordin by Xolloid metalloprotease Suggests a role for proteolytic processing in the regulation of Spemann organizer activity. *Cell*, 91(3):407 – 416, 1997.
- [114] V.P. S. Rawat, N. Arseni, F. Ahmed, M. A. Mulaw, et al. The vent-like homeobox gene ventx promotes human myeloid differentiation and is highly expressed in acute myeloid leukemia. *P. Natl Acad. of Sci. USA*, 107(39):16946–16951, 2010.
- [115] B. Reversade, H. Kuroda, H. Lee, A. Mays, and E.M. De Robertis. Depletion of *Bmp2*, *Bmp4* and *Bmp7* and Spemann organizer signals induces massive brain formation in *Xenopus* embryos. *Development*, 132(15):3381 – 3392, 2005.
- [116] B. Reversade and E.M. De Robertis. Regulation of ADMP and BMP2/4/7 at opposite embryonic poles generates a self-regulating morphogenetic field. *Cell*, 123(6):1147 – 1160, 2005.
- [117] M. Rex, E. Hilton, and R. Old. Multiple interactions between maternally-activated signalling pathways control *Xenopus* nodal-related genes. *Int. J. Dev. Biol.*, 46(2):217–226, 2002.

## REFERENCES

- [118] E.M. De Robertis and H. Kuroda. Dorsal-ventral patterning and neural induction in *Xenopus* embryos. *Annu. Rev. Cell Dev. Biol.*, 20(1):285–308, 2004.
- [119] A. Rodaway and R. Patient. Mesendoderm. an ancient germ layer? *Cell*, 105(2):169, 2001.
- [120] I. Roeder and I. Glauche. Towards an understanding of lineage specification in hematopoietic stem cells: A mathematical model for the interaction of transcription factors GATA-1 and PU.1. *J. Theor. Biol.*, 241(4):852 – 865, 2006.
- [121] F.M. Rosa. Mix.1, a homeobox mRNA inducible by mesoderm inducers, is expressed mostly in the presumptive endodermal cells of *Xenopus* embryos. *Cell*, 57(6):965 – 974, 1989.
- [122] A. Ruiz i Altaba and T.M. Jessell. Pintallavis, a gene expressed in the organizer and midline cells of frog embryos: involvement in the development of the neural axis. *Development*, 116(1):81–93, 1992.
- [123] Y. Saka and J.C. Smith. A mechanism for the sharp transition of morphogen gradient interpretation in *Xenopus*. *BMC Dev. Biol.*, 7:47, 2007.
- [124] V. Sander, B. Reversade, and E.M. De Robertis. The opposing homeobox genes Goosecoid and Vent1/2 self-regulate *Xenopus* patterning. *EMBO J.*, 26(12):2955–2965, 2007.
- [125] A.F. Schier. Nodal signalling in vertebrate development. *Annu. Rev. Cell Dev. Biol.*, 19:589–621, 2003.
- [126] A. Schohl and F. Fagotto.  $\beta$ -catenin, MAPK and Smad signalling during early *Xenopus* development. *Development*, 129:37–52, 2002.
- [127] A. Schohl and F. Fagotto. A role for maternal  $\beta$ -catenin in early mesoderm induction in *Xenopus*. *EMBO J.*, 22(13):3303–3313, 2003.
- [128] A. Schuler-Metz, S. Knöchel, E. Kaufmann, and W. Knöchel. The homeodomain transcription factor Xvent-2 mediates autocatalytic regulation of BMP-4 expression in *Xenopus* embryos. *J. Biol. Chem.*, 275(44):34365, 2000.
- [129] I. Shmulevich and J.D. Aitchison. Deterministic and stochastic models of genetic regulatory networks. *Methods Enzymol.*, 467:335–356, 2009.
- [130] D.R. Shook and R. Keller. Epithelial type, ingression, blastopore architecture and the evolution of chordate mesoderm morphogenesis. *J. Exp. Zool., Part B*, 310(1):85–110, 2008.
- [131] D.R. Shook and R. Keller. Morphogenic machines evolve more rapidly than the signals that pattern them: lessons from amphibians. *J. Exp. Zool., Part B*, 310B(1):111–135, 2008.
- [132] D.R. Shook, C. Majer, and R. Keller. Urodeles remove mesoderm from the superficial layer by subduction through a bilateral primitive streak. *Dev. Biol.*, 248(2):220–239, 2002.
- [133] J.C. Smith, A. Hagemann, Y. Saka, and P.H. Williams. Understanding how morphogens work. *Philos. Trans. R. Soc. London, Ser. B*, 363(1495):1387–1392, 2008.



## REFERENCES

- [134] J.C. Smith and G.M. Malacinski. The origin of the mesoderm in an anuran, *Xenopus laevis*, and a urodele, *Ambystoma mexicanum*. *Dev. Biol.*, 98(1):250–254, 1983.
- [135] J.C. Smith, B.M.J. Price, J.B.A. Green, D. Weigel, and B.G. Herrmann. Expression of a xenopus homolog of Brachyury (T) is an immediate-early response to mesoderm induction. *Cell*, 67(1):79 – 87, 1991.
- [136] J.C. Smith, B.M.J. Price, K. Van Nimmen, and D. Huylebroeck. Identification of a potent *Xenopus* mesoderm-inducing factor as a homologue of activin A. *Nature*, 345(6277):729–731, 1990.
- [137] P. Smolen, D.A. Baxter, and J.H. Byrne. Mathematical modeling of gene networks. *Neuron*, 26(3):567 – 580, 2000.
- [138] F. Stennard, G. Carnac, and J.B. Gurdon. The *Xenopus* T-box gene, Antipodean, encodes a vegetally localised maternal mRNA and can trigger mesoderm formation. *Development*, 122(12):4179–4188, 1996.
- [139] G. Swiers, Y. Chen, A.D. Johnson, and M. Loose. A conserved mechanism for vertebrate mesoderm specification in urodele amphibians and mammals. *Dev. Biol.*, 343(1-2):138 – 152, 2010.
- [140] S. Takahashi, Y. Onuma, C. Yokota, J.J. Westmoreland, M. Asashima, and C.V.E. Wright. Nodal-related gene *Xnr5* is amplified in the *Xenopus* genome. *genesis*, 44(7):309–321, 2006.
- [141] S. Takahashi, C. Yokota, K. Takano, K. Tanegashima, Y. Onuma, J. Goto, and M. Asashima. Two novel nodal-related genes initiate early inductive events in *Xenopus* Nieuwkoop center. *Development*, 127(24):5319–5329, 2000.
- [142] K. Tanegashima, C. Yokota, S. Takahashi, and M. Asashima. Expression cloning of *Xantivin*, a *Xenopus* lefty / *antivin*-related gene, involved in the regulation of activin signaling during mesoderm induction. *Mech. Dev.*, 99(1-2):3 – 14, 2000.
- [143] A.K.K. Teo, S.J. Arnold, M.W.B. Trotter, S. Brown, et al. Pluripotency factors regulate definitive endoderm specification through *omesodermin*. *Genes & development*, 25(3):238–250, 2011.
- [144] B. Thisse and C. Thisse. Functions and regulations of fibroblast growth factor signaling during embryonic development. *Dev. Biol.*, 287(2):390 – 402, 2005.
- [145] J.D. Thompson, D.G. Higgins, and T.J. Gibson. Clustal w: improving the sensitivity of progressive multiple sequence alignment through sequence weighting, position-specific gap penalties and weight matrix choice. *Nucleic acids res.*, 22(22):4673, 1994.
- [146] D. Umulis, M. Serpe, M.B. O'Connor, and H.G. Othmer. Robust, bistable patterning of the dorsal surface of the *Drosophila* embryo. *Proc. Natl Acad. Sci. USA*, 103(31):11613 – 11618, 2006.

## REFERENCES

- [147] L. Vallier, S. Mendjan, S. Brown, et al. Activin/Nodal signalling maintains pluripotency by controlling Nanog expression. *Development*, 136(8):1339–1349, 2009.
- [148] P. Venkataraman. *Applied optimization with MATLAB programming*. Wiley-Interscience, 2002.
- [149] F.C. Wardle and J.C. Smith. Transcriptional regulation of mesendoderm formation in *Xenopus*. *Semin. Cell Dev. Biol.*, 17(1):99 – 109, 2006.
- [150] O. Wartlick, A. Kicheva, and M. Gonzalez-Gaitan. Morphogen gradient formation. *Cold Spring Harbor Perspect. Biol.*, 1(3), 2009.
- [151] L. Wolpert. Positional information and the spatial pattern of cellular differentiation. *J. Theor. Biol.*, 25(1):1 – 47, 1969.
- [152] L. Wolpert. Positional information and patterning revisited. *J. Theor. Biol.*, 269(1):359 – 365, 2011.
- [153] R.-H. Xu, T.L. Sampsel-Barron, F. Gu, S. Root, et al. NANOG Is a direct target of TGF- $\beta$ /Activin-mediated SMAD signaling in human ESCs. *Cell Stem Cell*, 3(2):196 – 206, 2008.
- [154] J. Zhang, D.W. Houston, M.L. King, C. Payne, C. Wylie, and J. Heasman. The role of maternal VegT in establishing the primary germ layers in *Xenopus* embryos. *Cell*, 94(4):515–524, 1998.
- [155] J. Zhang and M.L. King. *Xenopus* VegT RNA is localized to the vegetal cortex during oogenesis and encodes a novel T-box transcription factor involved in mesodermal patterning. *Development*, 122(12):4119, 1996.
- [156] Y. Zhang, A.D. Lander, and Q. Nie. Computational analysis of BMP gradients in dorsal-ventral patterning of the zebrafish embryo. *J. Theor. Biol.*, 248(4):579 – 589, 2007.
- [157] X. Zhou, H. Sasaki, L. Lowe, B.L. Hogan, and M.R. Kuehn. Nodal is a novel TGF- $\beta$ -like gene expressed in the mouse node during gastrulation. *Nature*, 361:543–547, 1999.